PHASE FORMATION SEQUENCE AT METAL-GERMANIUM INTERFACES IN THIN FILM SYSTEMS.

BY

O.M. NDWANDWE

Dissertation presented in partial fullfilment of the requirements for the degree of

DOCTOR OF PHILOSOPHY

to the

DEPARTMENT OF PHYSICS
UNIVERSITY OF ZULULAND

Promoter: Dr. R. Pretorius, National Accelerator Centre, Faure
Co-promoter: Prof. B. Spoelstra, Department of Physics, University of Zululand

FEBRUARY 1996

ABSTRACT

Germanium thin films are used in integrated circuit electronic devices. Interest in germanium is due to the high mobility of its electrons and holes. It can therefore be used among other things as a high speed complementary transistor as well as in other devices. It is also used for making Ohmic contacts in GaAs devices. In strained layer (Ge,Si)/Si heterostructures, the band structure can be modified, which leads to interesting electronic properties. This thesis concerns itself mainly with phase formation in metal-germanium systems.

Characterisation of samples after heating in a vacuum furnace was done by Rutherford Backscattering Spectrometry (RBS) and X-Ray Diffraction (XRD). Ti-Ge, Pd-Ge, Zr-Ge, Fe-Ge and Cr-Ge thin film systems were investigated. First phases found in these systems were Ti_6Ge_5, Pd_2Ge, ZrGe, FeGe and $Cr_{11}Ge_8$ respectively. Subsequent phase formation was also investigated. Results obtained were compared to the predictions of the Effective Heat of Formation (EHF) model. Nucleation and phase skipping was also investigated. In germanides non-congruent phases with more negative effective heats of formation tend to form first in some systems (e.g. CoGe in the Co-Ge system). The two systems Ti-Ge and Ni-Ge were chosen for detailed investigation because they have non-congruent phases (viz. $TiGe_2$ and NiGe) with more negative effective heats of formation. An attempt is made to nucleatethese phases as first phases. A statistical view to phase formation is also introduced. In this model phase formation is described using elementary probability theory. Probabilities for atoms to meet in correct ratios to form phases are derived and used to predict first phases. Fractional heats which are closely related to effective heats of formation are also introduced. The model also makes use of diffusional and rotational activation energies to describe stability of phases against breaking into constituent parts. These activation energies are not readily available, which is a disadvantage of this model. Many models of phase prediction have been proposed in the past. Those of particular note are the Walser-Bene model, kinetic model of Gosele and Tu, the Zhang and Ivey model as well as the EHF model of Pretorius. These models as well as the statistical model developed as part of this work are described and compared to each other. The EHF model is found to be the most successful of the lot. It can predict phase formation in silicides, germanides and metal-metal systems. It can also predict phase formation sequence, phase decomposition, and the effect of impurities on phase formation. The success of this model is due to it's direct use of thermodynamic data, such as heats of formation ($\Delta H°$), and kinetics through the effective concentration of interacting species at the growth interface. It can also explain why different experiments produce different first phases in the same binary system at times.

ISINGENISO

Ijemani (Ge) isetshenziswa ezingcwecwaneni ezakha amasekhethe ezinto zikagesi. Okwenza kube khona uthando olungaka ku-jemani kungenxa yokuthi ama-elekhtroni ayo akwazi ukugijima ngesivinin esikhulu. Lokhu kwenza ukuthi isetshenziswe kuma thransista njengalawo asemishinini yokubala. Uma isetshenziswa ne GaAs, yenza ukuba lapho kuthintene khona izingcingo lungenzeki ushintsho ekugobhozeni kukagesi. Uma yenziwe yacinezelana ne Si, kwi-(Ge,Si)/Si, imihubhe lapho kuhamba khona ama elekthroni iyashintsheka. Ngenxa yalokhu ijemani iyasebenza ebunjiniyeleni obudinga ushinstho emihubheni yama elekthroni. Lomqulu umayelana nokwenzekayo lapho kuhlanganiswe khona izingcwecwe zalokho okusansimbi kanye ne-jemani.

Kudutshulwe ngezinhlayiyana ze-He (Rutherford Backscattering Spectrometry noma RBS) kwabuye kwasetshenziswa imisebe enamandla (X-ray Diffraction Spectroscopy noma XRD) ukuthola ukuthi yimaphi amafezi akhona kumasampula uma esefudunyezwe ngendlela efanele. Kuhlolwe ukwenzeka kwalamafezi ezingcwecweni eziyisiduli (solids) ze Ti-Ge, Pd-Ge, Zr-Ge, Fe-Ge kanye ne Cr-Ge. Kwatholakala ukuthi amafezi Ti_6Ge_5, Pd_2Ge, ZrGe, FeGe ne $Cr_{11}Ge_8$ enzeka kuqala kunamanye. Ukulandelana kwamafezi ngokuvela kwawo nako kuhloliwe. Okutholakele kuqhathaniswe nendlela yokubhula i-Effective Heat of Formation (EHF). Amanye amafezi ayaye angaveli, nakuba elindelekile, njenge CoGe kuma cwecwana ayisiduli enziwe nge Co ne Ge. Amacwecwe lapho kuhlolwe khona kabanzi ngokungaveli kwamafezi yilawa, Ti-Ge ne Ni-Ge. Bekufunwa ikakhulukazi i $TiGe_2$ ne NiGe. Kutholakala kulamacwecwe ukuthi ukushisa okuphumayo uma kubalwe ngendlela ye-EHF, kukhulu kunakwamanye amafezi, yingakho nje kulindeleke ukuba avele kuqala. Kubuye kwenziwa ngokokuqala indlela entsha yokubhula, esebenzisa amashansi okuhlangabezana kwama-atomu (Statistical Model of Phase Formation). Kulendlela amashansi okuxhumana kwama-atomu ngendlela efanele ukuze kwakheke amafezi ayabalwa. Ukushisa okuphumayo uma amafezi enzeka okubalwe ngalendlela kuqhathaniseka kahle naleyondlela ye-EHF. Lendlela entsha futhi isebenzisa amandla adingwa ama-atomu lapho ehamba esimweni esiyisiduli, nalapho ejikajika emi ndawonye, ukuthola ukuthi kulukhuni kangakanani ukuthi amafezi asenzekile abuye ashabalale futhi. Okungekuhle kahle ukuthi lamanani okuhamba nokujikeleza akatholakali kalula. Izindlela ezenziwa esikhathini esedlule ngabafokazi o- Walser-Bene, Gosele no Tu, kanye naleyo ka Zhang beno Ivey, ziye zahlolisiswa zaqhathaniswa naleyo ye-EHF. Kutholakale ukuthi indlela ye-EHF ibhula kangcono kunalezi ezinye. Lokhu kwenziwa ukuthi yona isebenzisa ulwazi olwakhiwa kudala olumayelana nokusebenza kwezinto uma zifudunyezwa. Ibuye futhi isebenzise ubungako be-elementi kwenye lapho zihlangana. Indleala ye-EHF, iyakwazi ukuchaza ukuthi kungani kuthi lapho kwenziwa ukuhlola ngezindlela ezahlukene kuvele imiphumela eyahlukene.

Acknowledgements.

I would like to extend my gratitude and sincere appreciation to the following group of people, without whose assistance and encouragement this work would not have been possible.

- Dr. R. Pretorius, Head, Van de Graaf Group, National Accelerator Center, Faure, for his guidance, encouragement and many stimulating discussions and insight throughout his supervision of this work.

- Prof. B. Spoelstra, Physics Department, University of Zululand, for his interest, advice and input into this work.

- Prof. J. Sharpey-Schafer, Director of the National Accelerator Centre, Faure, for his encouragement and use of facilities at the National Accelerator Centre.

- Dr. T. K. Marais for his friendship, expertise on all aspects of this work as well as for allowing me to use his LUKXRD software for X-ray analysis.

- Chris Theron, for his computer expertise, help during experimentation and fruitful discussions.

- Dr. Cecil Churms, for his useful X-ray analysis computer program, CCMILLER.

- Stanley Hendricks, for his useful common sense, encouragement, and friendship.

- Hendrik de Waal, for fruitful discussions, encouragement and help.

- Bill Schmitt, Gert Ackermann, Piet Groenewald, Tobie Swart, Karl Springhorn and Colin Doyle of the Van de Graaf Group for their assistance and efficient operation of the accelerator and maintenance of laboratory equipment.

- Stanley Hendricks, William Gordon, Cupido Cloete, Willem Cloete, Ginny Stone, and Fhatuwani Mundalamo for their friendship, help and constant encouragement.

- Ruben 'Sticker' Nzimakhwe of the Physics Department, University of Zululand, for his help and moral support.

- Thulane Jili of the Physics Department, University of Zululand, for his encouragement and moral support.

- Alpheus Zobolo of the Botany Department, University of Zululand, for his moral support and help.

- My mother and the rest of my family for their support.

- Bongani Linda, for his friendship moral support and help.

- My wife, Kate, for her patience, understanding and support during execution of this project.

- Lastly to my daughter Nonjabulo for constantly being by my side during typing, for whom without her 'help' this project would probably have been completed earlier.

Contents

CHAPTER 1

BACKGROUND AND SCOPE OF INVESTIGATION

1.1 Introduction

Silicide and germanide thin films find a broad application in integrated microelectronic devices. The electronic properties of these devices can be influenced by the chemical instability of the interfaces between different parts of the device. The study of interface composition and stability is therefore of utmost importance. Of special interest are reactions at metal-semiconductor interfaces. Though interfacial

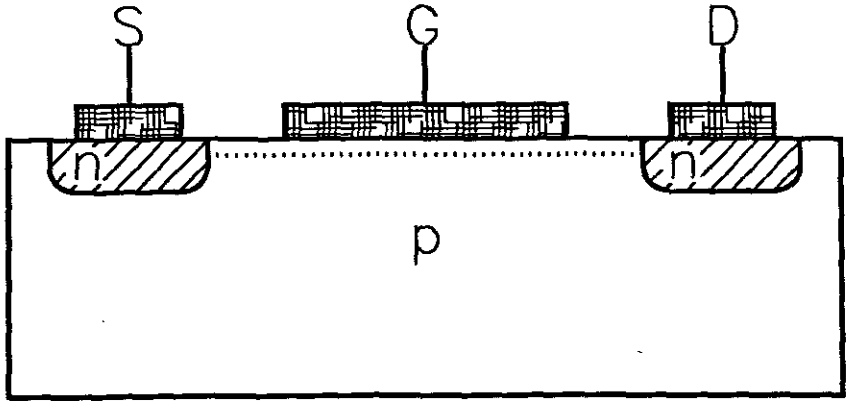

FIGURE 1.1: Schematic illustration of a simple semiconductor device e.g. an n-channel field effect transistor [1].

reactions have been studied for a long time; [2–6], there is still a limited understanding of which constraints favour initial phase formation of one reaction product over another. **Fig. 1.1** shows the structure of an n-channel FET. In this device the source and drain contacts to the two n-type regions in the p-type wafer must form ohmic contacts, while the gate contact should be rectifying in character. FETs are usually produced in both silicon and gallium arsenide and the choice of the material with which to form the Schottky contact depends on the relative stability of the metal and oxide contacts to the two semiconductors. **Fig. 1.2** shows the sequence of events required to fabricate a device e.g. a FET. The gate electrode is a SiO_2 polysilicon contact; while metal contacts are used for the source and drain electrodes. One may start with a p-type silicon wafer and proceed through two oxidations, four patterning steps (or lithography and etching processes), deposit from a vapour phase polysilicon, an oxide dielectric and a metal layer, and a doping operation to create the n-type source and drain regions in the wafer. The number of individual processing steps required in the fabrication of a typical microelectronic device is very large and each individual process must be controlled very precisely if the yield of correctly functioning devices is to be high.

The process of making electrical connections between the various devices inside a microelectronic chip and between the chip through package to the outside world is called metallization. This is done by means of thin films. Methods used to deposit these thin films include evaporation, sputtering and chemical vapour deposition. The resistivity of the thin films must be as low as possible ($\leq 50\Omega$.cm) [1]. The films should adhere strongly to both oxide and silicon surfaces. The electrical properties of the contact between the metal and the silicon should be carefully controlled (i.e. does one require an ohmic or rectifying contact ?). Additional technological requirements include easy patternability in a lithographic process and very low cost. Silicon is considered here as an example. An exposed silicon surface will quickly be covered by a thin native oxide layer. Bond formation with the oxide materials is necessary before satisfactory adhesion between the deposited metal and the substrate is obtained. Noble metals like gold and copper, form weak bonds with most oxides

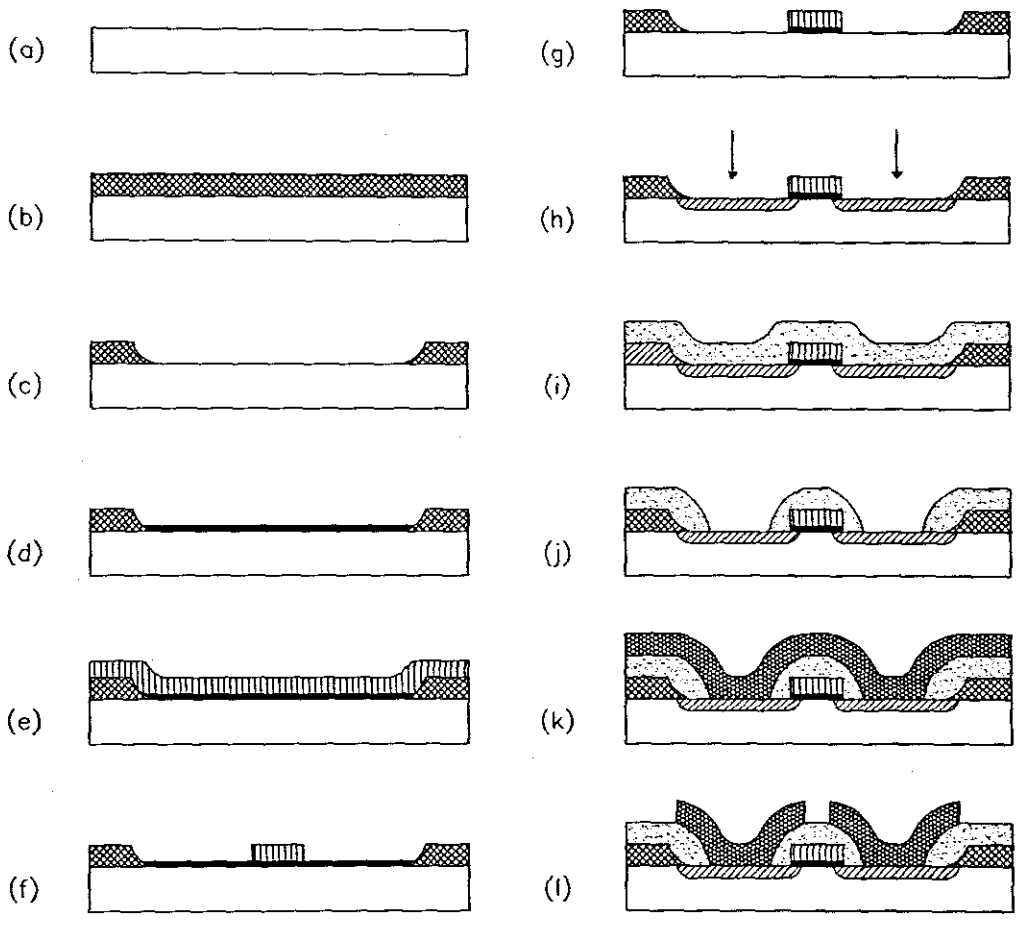

FIGURE 1.2: Sketch showing stages required to fabricate a simple field effect transistor (a) the starting material, a p-type silicon wafer; (b) the growth of a thick oxide layer which will be used to isolate the devices; (c) patterning of the oxide layer to define the area of the wafer in which the device is to be fabricated; (d) a thin gate oxide is grown over the exposed area of the silicon wafer; (e) deposition of polysilicon over the whole wafer; (f) patterning of gate contacts; (g) the gate oxide is removed in areas not protected by the polysilicon; (h) n-type contact regions are introduced by implantation or diffusion; (i) a second dielectric layer is deposited over the whole wafer surface, and is patterned in(j); (k) the contacting material is deposited; and patterned in (l) [1].

and an intermediate 'glue' layer of titanium or chromium is often used to improve the adhesion of gold conduction tracks. Aluminium on the other hand adheres strongly and is capable of reducing satisfactorily the oxide layer at temperatures above 450°C through the reaction

$$3SiO_2 + 4Al = 3Si + 2Al_2O_3 \tag{1.1}$$

Gold is preferred in devices which are not hermetically packaged and are therefore prone to atmospheric attacks. Unfortunately Al is soft and deforms easily under an applied stress. Because of the widely different thermal expansion coefficients between silicon and Al, a compressive stress is developed in Al films during heating and these stresses are relieved by grain boundary sliding. Grains are forced out of the film surface, and can in severe cases result in the formation of an open circuit in the metallization. The problem can be reduced by constraining the film under a glass layer.

In regions where the native oxide layer has been reduced by Al, Si will go into solution in the aluminium film. This process is rapid above 300°C and results in the transport of silicon away from the wafer surface. Voids will form in the silicon wafer and will fill with Al thus forming Al 'spikes' in the wafer surface. At the tip of these spikes the electric field across the contact will be greatly enhanced, and can alter the electrical properties of the contact region. The problem of spiking can be reduced by the introduction of a barrier layer between Si and Al such as a Ti film. Al thin films also suffer from electromigration failure. Electromigration is the transport of matter in response to the passage of an electric current. Diffusion in thin films is much faster than in the bulk material because thin films are usually crystalline and grain boundaries have a lower activation energy for diffusion than bulk material. The large surface area in thin films enhances diffusion because the activation energy for surface diffusion is usually smaller than the activation energy for grain boundary diffusion. Current densities carried by thin films can be very high (10^6 A.cm^{-2} or more). A simple method of increasing the resistance of thin film conductors to electromigration, is to remove the principal transport paths, the grain boundaries. Annealing will reduce the density of grain boundaries. One

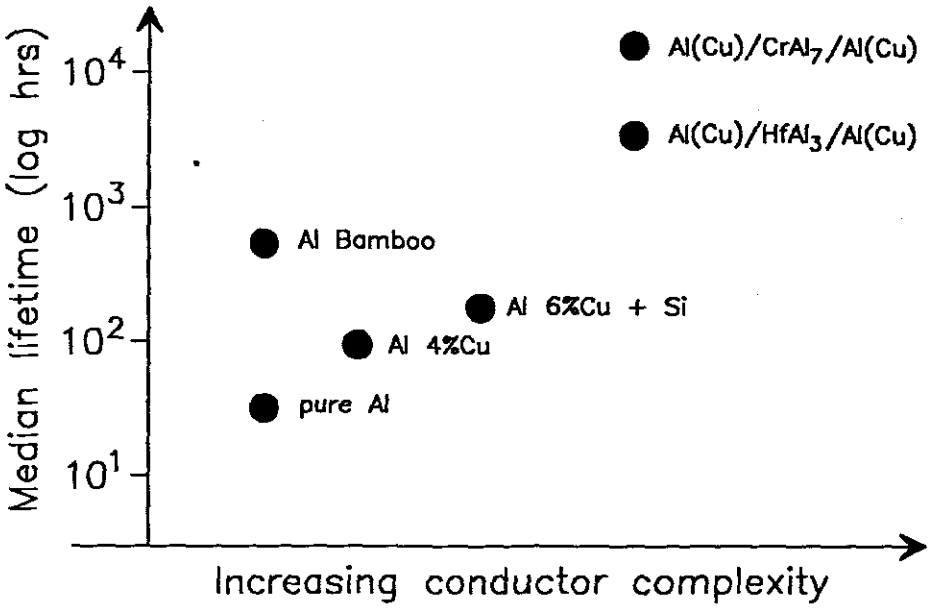

FIGURE 1.3: A comparison of the measured electromigration lifetime of a variety of aluminium-based conductor alloys tested under identical conditions [1].

may also reduce electromigration by adding a solute material e.g. the addition of a small concentration of tantalum to a gold film increases the activation energy for diffusion, while the addition of copper, magnesium and nickel to aluminium has a similar effect. **Fig. 1.3** shows a comparison of the measured electromigration lifetime versus complexity of the thin film. It is interesting to not that the more complex the thin film structure is the higher its resistance to electromigration. Most of the above mentioned problems (e.g. spiking, electromigration, corrosion etc.) can be reduced by the use of barrier layers. Necessary features of an ideal barrier layer are:

1. The barrier layer should be thermodynamically stable when in contact with the two materials which it separates.

2. There should be no rapid diffusion of any of the two materials it separates along the grain boundaries in the barrier film.

3. It should form low-resistance contacts with both materials.

4. The barrier must adhere well to all the materials with which it is in contact.

5. The material of the barrier layer should not have an electrochemical potential very different from that of the two materials it is separating, otherwise galvanic corrosion cells can be set up in the metallization layers.

Table 1.1 gives a comparison of the properties of a selection of barrier layers used at Al-Si contacts. The metallurgy of Al conductor on silicon technology has been looked at. A brief description of ways in which simple structures must be modified to give suitable electrical characteristics and long term stability is now looked into. **Fig. 1.4** shows a composite three layer metallization structure for the interconnection of devices on a silicon chip. Microelectronic semiconductor devices must be packaged properly. The following are the requirements expected of packaging materials.

1. to provide electrical contact from the devices on the chip to the outside world.

2. to provide a way of removing heat from active regions of devices and dumping it to heat sinks.

3. to protect the chip from chemical species which can attack the delicate connection paths on the surface of the chip.

TABLE 1.1: A comparison of the properties of a selection of barrier layers used at Al-Si contacts.

Metallization structure	Approx. maximum operating temp.	Observed mode of failure
Al/PtSi/Si	350°C	Compound formation
Al/$TiSi_2$/Si	400°C	Diffusion
Al/Cr/PtSi/Si	450°C	Compound formation
Al/Ti/PtSi/Si	450°C	Compound formation
Al/$Ti_{30}W_{70}$/PtSi/Si	500°C	Diffusion
Al/TiN/PtSi/Si	600°C	Compound formation
Al/TiC/PtSi/Si	600°C	Compound formation

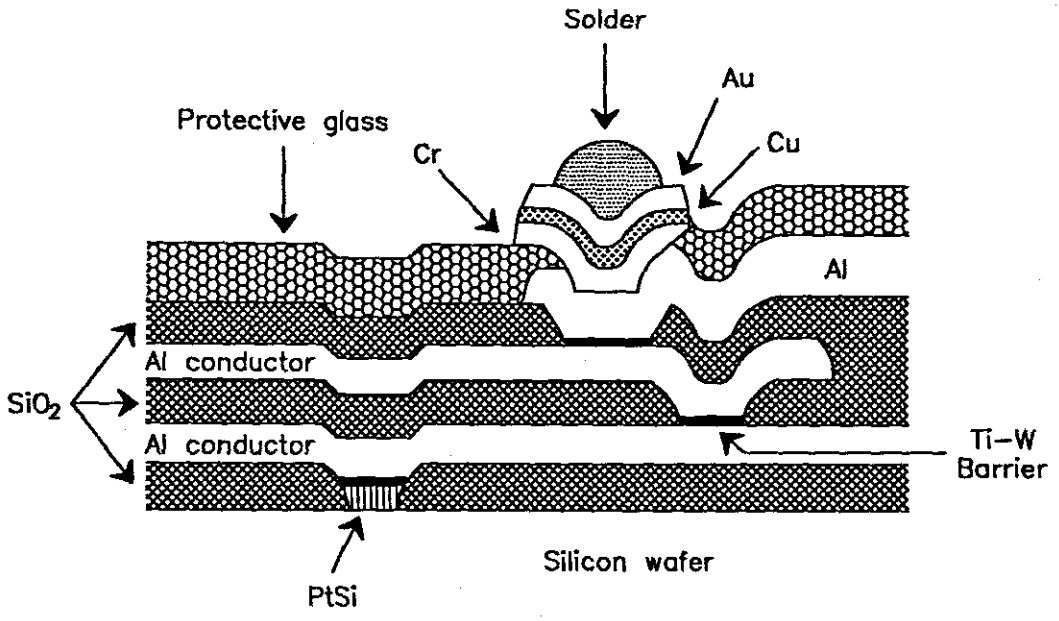

FIGURE 1.4: A sketch of a three layer aluminium-based metallization scheme, showing how the various thin film components can be brought together to form a set of stable interconnects for an integrated circuit [1].

4. to render the chip capable of being handled. Normal device chips are very small and fragile.

Table 1.2 lists some properties required from packaging and substrate materials. It is known that the computing power (or density of data storage) available on the surface of a chip increases greatly as the size of the individual device feature is reduced and the devices packed more closely together. The speed at which the devices operate is also increased as the lengths connecting the devices are shortened. The power dissipated in the device decreases with the size of the device. It is possible nowadays to pack together more than 1 million individual devices onto the surface of a silicon chip of about $1cm^2$ area (placing many devices together which may be different is called device integration). Problems encountered in the fabrication of these very small devices arise because the requirements for performance of components are stringent and it is not easy to find suitable materials to act as reliable conductors and insulators. The miniaturization of devices also increases the amount of waste heat generated per unit area of the chip, even though the heat lost by each device

TABLE 1.2: A table listing properties required from packaging and substrate materials.

Property	Importance
High strength High elastic modulus High thermal shock resistance	To support chip and metallization
High resistivity	For electrical isolation of chip
Chemical stability	To ensure no reactions with metal tracks or processing chemicals
High thermal conductivity	To remove waste heat
Thermal expansion coefficient	Should be matched to silicon to reduce stresses on chip
Low dielectric constant	To lower microwave losses
Surface smoothness	For ease of thin film deposition
Low porosity	Reduces outgassing after packaging
Low cost	To reduce the cost of complete device packages

is reduced. Packages (and materials used for packaging) must be well chosen and designed to provide good thermal contact between the chip surface and the external heat sinks. Chemical reactions which degrade the performance of metallization systems are much more rapid at higher temperatures.

1.2 Solid-Solid Interaction

Suppose two solid films, one made up of element A and the other made up of element B are deposited one after the other onto a non-reactive substrate as shown in **Fig. 1.5**. A could be a semiconductor or metal (e.g. Ge or Pt) while B could be

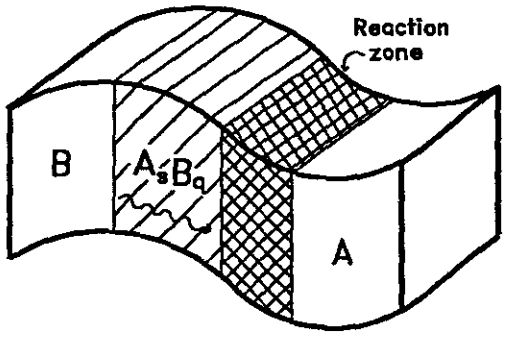

FIGURE 1.5: A sketch showing a binary thin film couple.

a metal (e.g. Pt). If the temperature at which the thin film couple is held is high enough a chemical reaction will take place at the interface joining the two films, thus producing new compound phases. Because of the increased interest in thin-film basic research and applications there has been many publications on aspects concerning compound phase formation at such an interface. In spite of these investigations many aspects of the processes responsible for compound formation are not yet fully understood.

1.2.1 Solid-state thermodynamics

Heats of formation ($\Delta H°$) and entropies ($\Delta S°$), can be calculated if the change in the heat capacities at constant pressure (ΔC_p) of the reactants and products is known. Heat capacities are however not generally available over the complete temperature range and are usually tabulated for temperatures above 298°K, and are used to calculate the variation of heats of formation ($\Delta H°$) and entropies ($\Delta S°$) as a function of temperature. When reactions occur in the solid state, the changes in heat capacities are nearly zero. This is due to the fact that the heat capacity of the product is approximately equal to the heat capacity of the reactants ($\Delta C_p \approx 0$). This is called the Neuman-Kopp rule [7]. The validity of this rule is demonstrated by **Table 1.3**. This table shows that the temperature dependence of the standard heats of formation is negligible and that ($\Delta\ H°_{298}$), can be used at any temperature of practical interest. $\Delta S°$ is also negligibly dependent on temperature.

TABLE 1.3: Calculated ΔH_T values from heat capacities given in ref [7] for some binary intermetallic compounds as a function of temperature.

Compound	ΔH_{298} kJ/(mole.at)	ΔH_{400} kJ/(mole.at)	ΔH_{500} kJ/(mole.at)	ΔH_{600} kJ/(mole.at)	ΔH_{1000} kJ/(mole.at)
$AuSb_2$	−6.5	−6.4	−6.4	−6.3	—
AuSn	−15.2	−15.3	−15.4	—	—
AuZn	−27.7	−27.6	−27.5	−27.4	−27.0
CoSi	−50.2	−50.2	−50.2	−50.1	—
$CoSi_2$	−34.3	−34.3	−34.2	−34.2	—
Cr_5Si_3	−35.0	−34.9	−34.9	−34.8	−34.9
CrSi	−30.2	−30.1	−30.0	−29.9	−29.8
$CrSi_2$	−25.8	−25.8	−25.9	−25.9	−25.9
Cu_2Mg	−11.7	−11.7	−11.8	−11.7	—
Mg_2Si	−26.4	−26.4	−26.5	−26.5	—
Mn_3Si	−31.1	−31.0	−30.9	−30.7	—
Mn_5Si_3	−41.6	−41.6	−41.6	−41.6	−42.0
MnSi	−41.5	−41.5	−41.5	−41.6	−41.9
$Mn_{11}Si_{19}$	−28.7	−28.2	−27.5	−26.8	−22.5
Ni_2Si	−46.9	−47.1	−47.4	−48.0	—
NiSi	−42.4	−42.6	−42.8	−43.2	—
$NiSi_2$	−29.2	−29.2	−29.3	−29.4	—
Re_5Si_3	−19.7	−19.7	−19.6	−19.5	−19.1
V_3Si	−45.2	−45.2	−45.3	−45.4	−44.5
VSi_2	−40.2	−40.2	−40.2	−40.2	−40.3

If, however any phase transition points are encountered, the corresponding heats of transformation, fusion or evaporation must be considered. For alloy phases and inter-metallic compounds no great error is made if the normal entropies of ordered alloys are taken additively. For disordered alloys a term proportional to the entropy of mixing must be added.

The change in Gibbs free energy at constant temperature is given by

$$\Delta G^{\circ}_{T} = \Delta H^{\circ}_{298} - T\Delta S^{\circ}_{298} \tag{1.2}$$

Using the heat capacities from reference [7], for compounds referred to in this work, the variation of the heat of formation ΔH° has been calculated at various temperatures and are shown in **Table 1.3**. The validity of the Neumann-Kopp rule is clearly demonstrated, showing that the temperature dependence of standard heats of formation is negligible and that ΔH°_{298}, can be used at any temperature of practical interest. Similar arguments show that ΔS° is also negligibly dependent on temperature.

The arguments presented above imply that the standard values (at $T = 298°\mathrm{K}$) of enthalpy and entropy can be used for thermodynamic calculations at any temperature. Furthermore, since all these reactions occur in the solid-state, the Gibbs free energy, can be approximated by the standard enthalpy of reaction alone, as the change in entropy may be considered to be zero for the majority of systems. To investigate the validity of this statement we note that equation

$$\Delta G^{\circ}_{T} \approx \Delta H^{\circ}_{298} \tag{1.3}$$

can be written only when the $T\Delta S^{\circ}_{298}$ term is small compared to ΔH°_{298}. In **Table 1.4** the contribution that the entropy term $T\Delta S^{\circ}_{298}$ makes to ΔG°_{T} is calculated as a percentage of the enthalpy ΔH°_{298} [8]. This is an upper limit imposed by assuming the temperature (°C) of practical interest to be $\frac{1}{3}$ of the liquidus minimum of the binary system. It can be seen that apart from the palladium silicides there are only six other compounds for which the entropy term contributes more than 10% of the enthalpy to the free energy change ΔG° (see **Table 1.4**). Furthermore, it should be pointed out that the relative ΔG° values should be compared for a certain binary system. For instance for all the palladium silicide phases the entropy terms are negative and ΔG° therefore changes in the same direction. As thermodynamic quantities are in any case not known with greater accuracy than about 10% [7], the change in enthalpy (ΔH°) is with a few exceptions a very good approximation for the free energy change (ΔG°) during solid state compound formation.

TABLE 1.4: The contribution of the entropy term $T\Delta S°$ to the Gibbs free energy change $\Delta G°$, as a percentage of the enthalpy $\Delta H°$ at a temperature $T = 273 + \frac{1}{3}t_{lm}$ where t_{lm} is the liquidus minimum (°C) of the binary phase diagram. Percentages greater than 10% are underlined[8].

Compound	$\Delta H°$ (kJ/mole.at)	$\Delta S°$ (J/deg.mole.at)	$\frac{1}{3}t_{lm}$ (°C)	$T\Delta S°$ (kJ/mole.at)	%
Metal-Metal					
Ag_2Te	−12.0	+6.23	117	+2.43	20.2
$AuPb_2$	−1.9	−0.77	71	−0.26	13.9
$AuSb_2$	−6.5	−6.40	120	−2.52	38.7
AuSn	−21.2	−0.25	72	−0.09	0.4
$CuMg_2$	−5.3	−2.07	162	−0.90	17.0
Cu_2Mg	−6.9	−0.33	162	−0.14	2.0
Cu_2Sb	−8.1	+4.93	175	+2.21	27.3
Ni_3Al	−41	−1.05	213	−0.51	1.2
NiAl	−59	−2.05	213	−1.00	1.7
Ni_2Al_3	−57	−1.66	213	−0.81	1.4
$NiAl_3$	−38	−1.03	213	−0.50	1.3
Ni_2Ge	−21.4	−0.03	254	−0.02	0.1
PbTe	−34.5	−2.30	109	−0.88	2.6
TiAl	−38	−3.30	220	−1.63	4.3
$TiAl_3$	−37	−5.23	220	−2.58	7.0
Metal-Silicon					
CoSi	−50.2	−3.10	398	−2.08	4.1
$CoSi_2$	−34.3	−1.23	398	−0.83	2.4
Cr_3Si	−34.4	−0.90	435	−0.64	1.9
Cr_5Si_3	−35.0	−0.70	435	−0.50	1.4
CrSi	−30.2	+0.80	435	+0.57	1.9
$CrSi_2$	−25.8	−0.90	435	−0.64	2.5
FeSi	−39.3	−2.15	400	−1.45	3.7
Mg_2Si	−26.4	−6.77	213	−3.29	12.5
Mn_3Si	−31.1	−2.80	347	−1.74	5.6
Mn_5Si_3	−41.6	+2.75	347	+1.71	4.1
MnSi	−41.5	−2.20	347	−1.36	3.3
$Mn_{11}Si_{19}$	−28.7	−2.94	347	−1.82	6.4

Cont...

Compound	$\Delta H°$ (kJ/mole.at)	$\Delta S°$ (J/deg.mole.at)	$\frac{1}{3}t_{lm}$ (°C)	$T\Delta S°$ (kJ/mole.at)	%
Mo_3Si	−29.1	+0.38	467	+0.28	1.0
Mo_5Si_3	−38.8	+1.01	467	+0.75	2.0
$MoSi_2$	−43.9	−0.40	467	−0.30	0.7
$NbSi_2$	−46.0	−1.40	434	−0.99	2.2
NiSi	−42.4	−2.15	321	−1.28	3.0
$NiSi_2$	−29.3	−0.70	321	−0.42	1.4
Pd_5Si	−29.2	−13.00	270	−7.06	24.2
Pd_9Si_2	−31.1	−13.80	270	−7.49	24.1
Pd_3Si	−38.5	−15.40	270	−8.36	21.7
Pd_2Si	−43.0	−15.90	270	−8.63	20.1
PdSi	−26.2	−5.00	270	−2.72	10.4
Re_5Si_3	−19.7	+2.14	375	+1.39	7.04
$ReSi_2$	−30.1	+0.01	375	+0.01	0.0
Sc_5Si_3	−69.0	−2.48	333	−1.50	2.2
Ta_2Si	−40.9	+1.17	462	+0.86	2.1
Ta_5Si_3	−41.8	+2.11	462	+1.55	3.7
$TaSi_2$	−32.4	−1.27	462	−0.93	2.9
Th_3Si_2	−55.9	−6.26	455	−4.56	8.2
ThSi	−63.0	−4.70	455	−3.42	5.4
Th_3Si_5	−59.7	−2.77	455	−2.02	3.4
$ThSi_2$	−56.9	−0.63	455	−0.46	0.8
Ti_5Si_3	−72.4	+1.03	443	+0.74	1.0
TiSi	−78.6	−0.20	443	−0.14	0.2
$TiSi_2$	−57.0	−2.33	443	−1.67	2.9
U_3Si	−23.0	−0.62	328	−0.37	1.6
U_3Si_2	−34.1	+1.80	328	+1.08	3.2
USi	−42.3	−1.25	328	−0.75	1.8
U_3Si_5	−44.3	−1.71	328	−1.03	2.3
USi_2	−43.2	−2.00	328	−1.20	2.8
USi_3	−32.6	−0.07	328	−0.04	0.1
V_3Si	−45.2	−1.05	467	−0.78	1.7
V_5Si_3	−58.0	+0.92	467	+0.68	1.2
VSi_2	−40.2	−2.70	467	−2.00	5.0
W_5Si_3	−16.9	+1.28	464	+0.94	5.6
WSi_2	−31.0	−2.10	464	−1.55	5.0
$ZrSi_2$	−53.1	−2.60	453	−1.89	3.6

1.2.2 Miedema model

The macroscopic atom model of Miedema [9] for calculating heats of formation is a semi-empirical model that relies on qualitative experimental information. Two constants which play a role in the cohesion of alloys are introduced into the model. It is assumed that the properties of the bulk metal can be assigned to macroscopic 'atoms' and that the heat of formation may be calculated as a function of concentration. Physical quantities of interest included in the model are the electron density at the surface of the Wigner-Seitz cell, n_{WS} and an adjusted value of the work function, ϕ^* . Two contributions to the enthalpy are introduced when considering the energetics of the contact interactions of dissimilar atoms. A positive contribution to ΔH° [9] results from the fact that the elimination of discontinuities in electron density when dissimilar atoms are in contact requires energy. One obtains a term,

$$\Delta H^{pos}_{A\,in\,B} \;\propto\; Q(\Delta n^{\frac{1}{3}}_{WS})^2$$

A negative term corresponding to stable alloys and inter-metallic compounds should exist. As the two cells are brought together there will not only be charge redistribution inside the cells, but there might also be a net transfer of charge. This transfer of charge corresponds to a negative ionic contribution to the heat of formation [9]:

$$\Delta H^{neg}_{A\,in\,B} \;\propto\; -P(\Delta\phi^*)^2$$

where P and Q are proportionality constants. For alloys of a transition metal and a polyvalent non-transition metal an additional negative term has to be included in the heat of formation. It is thought that hybridization effects, which occur when p-type and d-type wave functions are mixed, play a role. If A and B are both transition metals the heat effect for a dilute solution of A in B is given per mole of A by

$$\Delta H^{sol}_{A\,in\,B} = 2V_A^{\frac{2}{3}}\left[\frac{-P(\Delta\phi^*)^2 + Q(\Delta n^{\frac{1}{3}}_{WS})^2}{n^{-\frac{1}{3}}_{WS,A} + n^{-\frac{1}{3}}_{WS,B}}\right] \tag{1.4}$$

The degree f_B^A to which A atoms are surrounded by B atoms is

$$\Delta H^{for} = C_A f_B^A \Delta H^{sol}_{A\,in\,B}. \tag{1.5}$$

The atomic fraction of A (C_A) normalizes the units of the heat of solution in kJ per mole of A atoms to kJ per mole of atoms. For a random alloy, f_B^A is determined statistically by the fraction of the total atomic surface belonging to B, whereas in the case of ordered alloys (compounds) an empirical expression, accounting for the preference of atoms to be surrounded by dissimilar neighbours, is used. The average of A in B and B in A is taken to avoid discontinuities.

The Miedema model is for atoms in the metallic state. It can be extended to non-metallic atoms, such as Si and Ge, if a suitable "metallic" state of an atom is considered. Whenever a non-transition metal is a semiconductor in its reference state, which is taken to be at standard temperature and pressure, instead of metallic, and the heat of enthalpy is predicted with respect to its metallic state, a positive transformation enthalpy is required to account for this structural stability. An additional term, ΔH^{trans} is used to convert a semiconducting element into a hypothetical metallic one. It's value for Si is +34 kJ (mol at.)$^{-1}$. For Ge it is +25 kJ (mol at.)$^{-1}$.

1.3 Compound Phase Formation

The formation of compound phases in thin films has been the object of careful observation and study for a long time [10]. It has been found that in a binary thin film not all compound phases, as they appear in the equilibrium phase diagram, grow at the same time. In thin films one compound phase usually grows until one of the unreacted element has been consumed before the next phase begins to grow. It is not unusual to find many compound phases growing simultaneously in bulk couples($\leq 10\mu$m). One is not only interested in the first phase but also in the order in which the phases follow each other during growth.

1.3.1 Prediction of phase formation

The Walser–Bene Model

The model predicts the first phase that nucleates at subeutectic temperatures in a thin film reaction couple. It is for reactions that are carried out isothermally.

It is postulated that the interface consist of a 'metallic glass' whose concentration is near the lowest-temperature eutectic in the binary system under consideration. The interface region is increased by diffusion upon annealing, until the region is metastable, at which point the first phase begins to nucleate. Nucleation should favour congruently melting phases over noncongruent phases. This is due to the fact that there is an energy barrier associated with the large rearrangement in short range order (SRO) required to go from a liquidlike SRO to the crystalline SRO for noncongruent phases at the same concentration. For congruent phases there is a much smaller change in SRO when the phases go through at the freezing point. Taking these considerations into account, the model states that *the first compound nucleated in planar binary reaction couples is the most stable congruently melting compound adjacent to the lowest temperature eutectic on the bulk equilibrium phase diagram.* The most stable compound is indicated by a higher melting temperature. Tsaur *et al.* [3] extended the model to subsequent phase formation in metal silicon systems. According to them *the second phase formed is the compound with the smallest ΔT that exists in the phase diagram between the composition of the first phase and the unreacted element.* ΔT is defined as the temperature difference between the liquidus curve and the peritectic(or peritectoid) point. ΔT is zero for congruently melting compounds. The fact that this model did not work for metal-metal systems flew into the face of the explanation that non-congruent phases do not nucleate because of energy barriers due to SRO. The model was extended to metal-metal systems by relaxing the requirement of congruency. Also the existence of a glassy membrane could not be proved. In spite of these setbacks the model can predict phase formation in a significant number of systems.

The Effective Heat of Formation Model

Suppose a compound $A_{1-x}B_x$ is to be formed at an effective concentration x' of element B at the growth interface, then element B will be the limiting element if $x' < x$. If ΔH° is the heat of formation of the compound phase $A_{1-x}B_x$ with x the compound concentration of the limiting element B, then the heat released is dictated

by the effective concentration of the limiting element and the concentration of the limiting element in the compound to be formed. An effective heat of formation $\Delta H'$ can therefore be defined [11–15] as:

$$\Delta H' = \Delta H^\circ \times \left(\frac{\textit{effective concentration limiting element}}{\textit{compound concentration limiting element}} \right) = \Delta H^\circ \times \left(\frac{x'}{x} \right) \quad (1.6)$$

where $\Delta H'$ and ΔH° are expressed in kJ per mole of atoms. With eq. 1.6 the effective heat of formation of any compound can be calculated as a function of the concentration of the reacting species. This is shown graphically for the Pd-Si system [16] in **Fig. 1.6**. To facilitate identification, solid lines are used to indicate compounds that are congruently melting, while dashed lines are used for non-congruent compounds. To predict phase formation using the EHF model, it is however necessary to know the effective concentrations of the two reacting species at the growth interface, which is chosen to be at the liquidus minimum [11–15] of the binary system. The liquidus minimum for the Pd-Si binary system is at 15.5 at.% Si and 84.5 at.% Pd and it can be directly seen from **Fig. 1.6** (top) that the congruent phase Pd_2Si has the most negative $\Delta H'$ at this effective concentration and is thus predicted to form first, in agreement with experimental observations A rule for silicide and germanide first phase formation based on the EHF model [11, 15] states:

> *The first compound to form during metal-silicon or metal-germanium interaction is the congruent phase with the most negative effective heat of formation ($\Delta H'$) at the concentration of the liquidus minimum of the binary system.*

Table 1.5 gives a comparison between the observed first phase and the phase as predicted by the EHF model for metal-silicon interaction.

In cases where the binary system does not have congruent phases, the non-congruent phase with the most negative effective heat of formation forms first.

For metal-metal systems the phase found to form first is the phase with the most negative $\Delta H'$, irrespective of whether it is congruent or non-congruent [13–15].

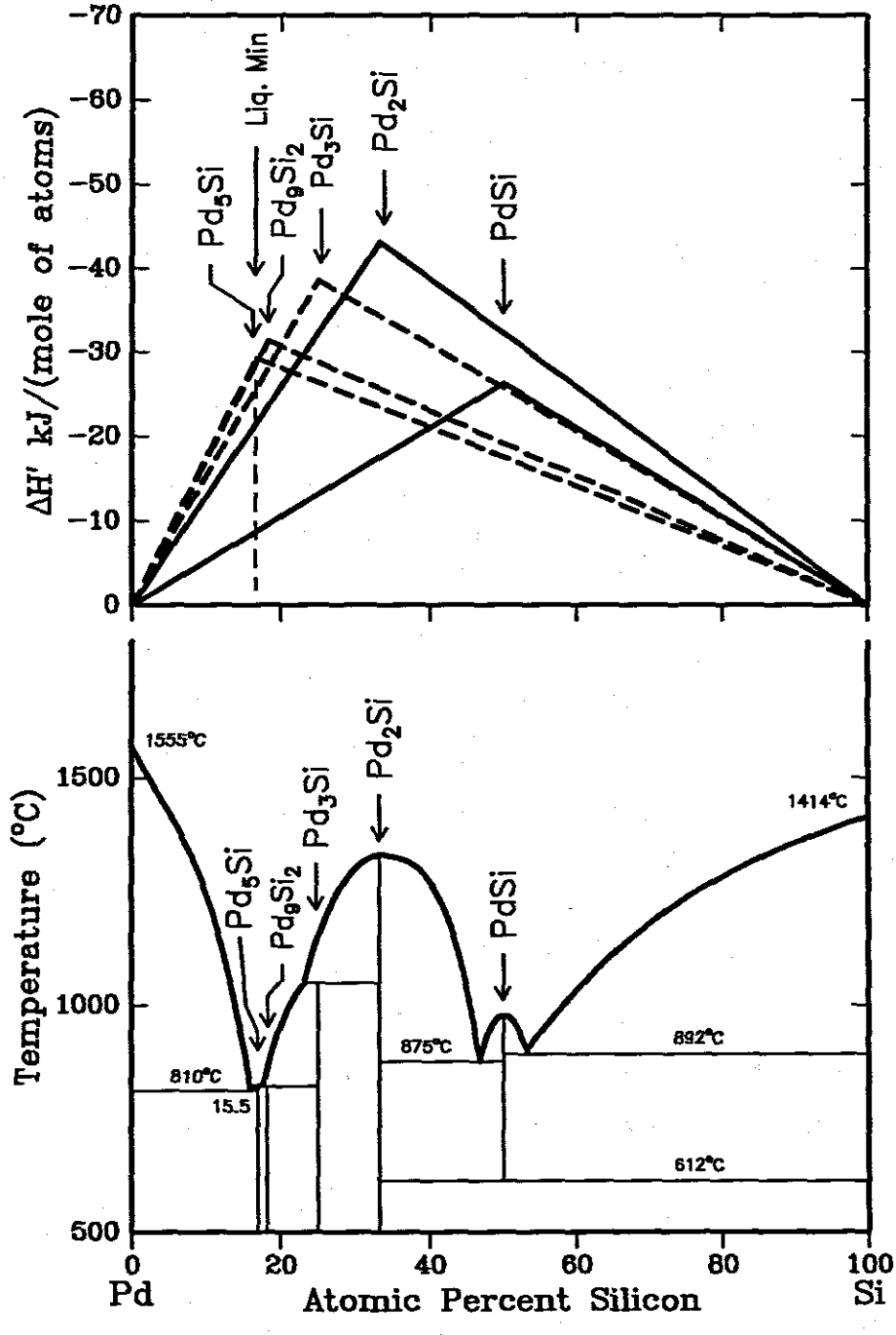

FIGURE 1.6: Effective heat of formation diagram (top) and the corresponding phase diagram (bottom) for the Pd-Si binary system. Each triangle of the top diagram represents the energy released as a function of concentration during formation of a particular silicide phase.

TABLE 1.5: Comparison of observed first phase formation and predicted first phase in silicides using the effective heat of formation ($\Delta H'$) model. The effective heat of formation is calculated at the concentration of the liquidus minimum of the binary phase diagram. The predicted compounds are those congruent phases with effective heats of formation ($\Delta H'$) within 5% of the congruent phase with the most negative $\Delta H'$. [8]

System	Liq. Min. (at.% Si)	Predicted Phases	Atoms per Unit Cell	Congruency	$\Delta H'$ kJ(mol.at.)$^{-1}$	Observed Phases	Ref.
Ca	5.6	Ca_2Si	12	C	−11.72	Ca_2Si	[17]
Co	22.5	Co_2Si	12	C	−26.01	Co_2Si	[18–23]
Cr	82	$CrSi_2$	9	C	−13.95	$CrSi_2$	[3, 18, 23–27]
Cu	30	$Cu_{19}Si_6$ [a]		C	−3.68	$Cu_{19}Si_6$	[18]
Er	85	Er_3Si_5 [b]		?	−29.80	Er_3Si_5	[18, 28]
		ErSi	8	?	−22.98		
		Er_5Si_3	16	C	−15.12		
Fe	33	FeSi	8	C	−25.94	FeSi	[18, 29]
Gd [c]	15.3	Gd_5Si_3	16	C	−25.05	—	
						$GdSi_2$	[30, 31]
Hf	92	HfSi	8	C	−14.42	HfSi	[18, 32, 33]
Mg	1.2	Mg_2Si	12	C	−0.95	Mg_2Si	[34]
Mn	21	Mn_5Si_3	16	C	−23.30	—	
						Mn_3Si [d]	[35]
						MnSi	[18, 36]
Mo	98.3	$MoSi_2$	6	C	−2.24	$MoSi_2$	[18, 37–40]
Nb	95	$NbSi_2$	9	C	−6.90	$NbSi_2$	[18, 39]
Ni	46.5	NiSi	8	C	−39.43	—	
		Ni_2Si	6 or 12	C	−37.64	Ni_2Si	[18, 41–49]
Os	88	Os_2Si_3	40	C	−6.81	Os_2Si_3	[18, 50]
Pd	15.5	Pd_2Si	9	C	−19.99	Pd_2Si	[18, 34, 39, 51, 52]
Pt	23	Pt_2Si	6	C	−32.91	Pt_2Si	[51, 53–55]
Rh	68.5	RhSi	8	C	−27.59	RhSi	[18, 56]
Ru	83	RuSi	8	C	−11.02		
		Ru_2Si_3	40	C	−10.88	Ru_2Si_3	[18, 50]
Ta	99	$TaSi_2$	9	C	−0.97	$TaSi_2$	[18, 39]
Ti	84 [e]	$TiSi_2$	24	C	−27.36	$TiSi_2$	[18, 57, 34, 58–67]
						Ti_5Si_3	[32, 58, 66–69]
						TiSi	[18, 32, 58, 63–65, 69–73]
V	97	VSi_2	9	C	−3.62	VSi_2	[18, 34, 39, 74]
W	99	WSi_2	6	C	−0.93	WSi_2	[18, 28, 39, 40, 75]

Agreement between predicted phases and experimentally observed first phases is in this case also good.

1.3.2 Phase formation sequence

An excellent review article [15] discusses how phase formation sequence may be predicted using the EHF model. The Cr-Si system is used here as an example. The first phase to form in this system is $CrSi_2$. If a thin layer of Cr (Cr<Si) is deposited on a thicker Si substrate, all the Cr will be consumed to form $CrSi_2$. There will be leftover Si. The effective concentration at the interface will move to values greater than the composition of $CrSi_2$ in Si. But there are no equilibrium phases corresponding to such compositions, thus no other new phase will form. If a thicker layer of Cr is deposited on a thinner layer of Si, $CrSi_2$ will as before be the first phase to form. This phase will grow until all Si is consumed. The effective concentration of the reactants at the Cr-$CrSi_2$ interface will become more Cr-rich until a concentration of about 60% Si, where CrSi is expected to form (CrSi has the most negative effective heat of formation at this concentration). This phase (CrSi) is however non-congruent and will be skipped. The congruent phase Cr_5Si_3 will form as a second phase. As the concentration at the interface changes further, the phase Cr_3Si will finally form. These predictions are consistent with what is found experimentally.

Each of these phases in the order predicted should form, provided factors such as non-congruency, nucleation barriers, etc. do not inhibit their formation. It was found that in the case of silicides, phases with a large ΔT, tend to be skipped in the sequence [15]. The above argument also holds for the germanides in general. A rule for phase formation sequence [15] could therefore be formulated which states:

> *'After first phase formation in metal-Si or metal-Ge systems the effective concentration moves in the direction of the remaining element and the next phase to form at the growth interface is the next phase richer in the unreacted element, which has the smallest temperature difference ΔT between the peritectic (or peritectoid) point and the liquidus. ($\Delta T = 0$*

for congruent phases.)'

As stated above, this rule holds in general for the germanides.

1.4 Importance of Germanides

Germanium crystals doped with either nickel or gold can be used as photoconductors in the near-infrared range of the electromagnetic spectrum. The dopants create acceptor states at 0.23 and 0.15eV above the valence band edge, respectively, and the electrons can be excited from the top of the valence band into these unoccupied states thus leaving holes in the valence band. Germanium devices must be cooled to about 77K to avoid thermal excitation of electrons to fill the acceptor states. Ge is therefore used in photon detection systems e.g. γ -ray detectors.

Germanium can also be used in GaAs solar cells. The GaAs homojunction solar cell is highly efficient and it can be built on a cheap substrate material like Si. Unfortunately, the large misfit at the heterojunction results in a solar efficiency of about half that achieved in homojunction GaAs substrates. One possible way of improving the performance of these devices is to include another layer between the silicon and the GaAs in an attempt to reduce the density of threading dislocations propagating into the active region of the solar cells. The lattice parameter of germanium is almost exactly the same as that of GaAs. Tsaur *et al.*[1] have demonstrated that an epitaxial germanium layer can be grown on the silicon substrate. When an epitaxial GaAs layer is grown on the germanium, the density of threading dislocations which propagates across the Ge/GaAs interface is relatively low (see **Fig. 1.7**). Optical fibres used in communication systems are made from silica 'doped' with germanium, or more properly germania, GeO_2 . The addition of germania alters the refractive index of the silica, and a fibre with a germanium-rich core region of higher refractive index than the outer cladding layers will act as a waveguide along which an optical beam will propagate by total internal reflection (see **Fig. 1.8**). The high mobility of both electrons and holes in germanium make it suitable for use in high speed devices(e.g. complementary transistor). It is also used in strained layer (Ge,Si)/Si heterostructures. These structures consists of thin, non-lattice matched layers,

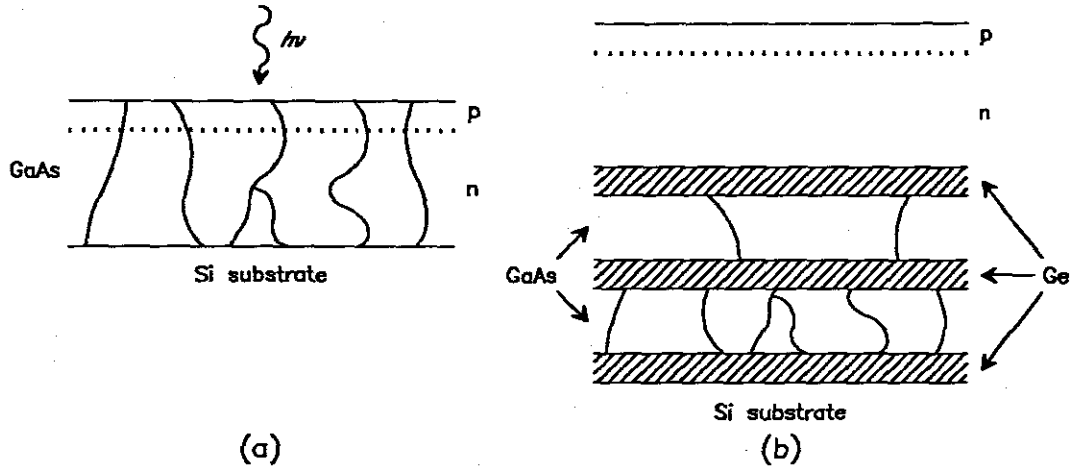

FIGURE 1.7: (a). A sketch of a GaAs homojunction solar cell in a thin epitaxial film grown on a silicon substrate. Threading dislocations are shown propagating up from the hetero-interface into the GaAs layer. (b). Shows a multilayered Ge/GaAs on silicon structure which can be used to reduce the dislocation content in the top GaAs layer which is where the homojunction solar cell is prepared [1].

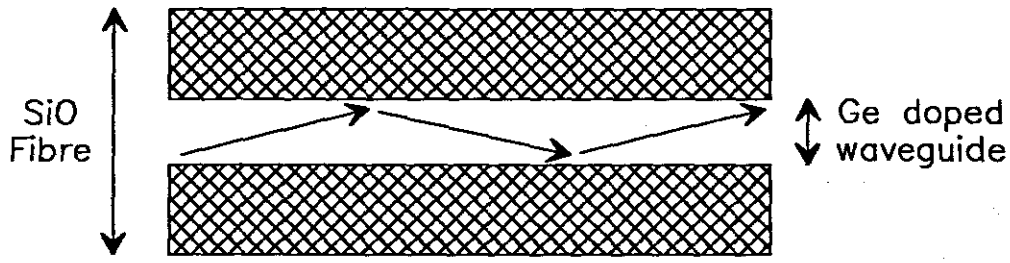

FIGURE 1.8: The structure of a germanium doped silica fibre, showing the core region along which the light propagates by total internal reflection [1].

grown epitaxially without generating misfit locations and has a variety of interesting properties which are attributed to band structure modification. Germanium make ohmic contacts on GaAS devices.

1.5 Scope of Investigation

The implementation of the germanium technology requires an understanding of the solid state interaction of germanium with other elements. This will lead to increased device reliability and better reproducibility. A study of germanides will lead to a

better understanding of the fundamental physics of solid-state interaction, when a comparison is made of germanides and other systems (e.g. silicides and metals) which have received extensive attention in the past. This study concerns itself with prediction of compound phase formation in germanides. Samples, which are first annealed in vacuum are characterised using RBS and XRD. These techniques as well as sample preparation methods are described in chapter 2. In chapter 3 phase formation sequence is investigated in the systems Ti-Ge, Pd-Ge, Zr-Ge, Fe-Ge and Cr-Ge. Results obtained after RBS and XRD analyses are then compared to the predictions of the EHF model. Chapter 4 deals with the question of nucleation and phase skipping in germanides. The systems Ni-Ge and Ti-Ge were chosen for detailed investigation because they have non-congruent phases with more negative effective heats of formation than congruent phases in the same system. An attempt is made to nucleate these non-congruent phases as first phases. Chapter 5 introduces a Statistical model of phase formation. In this model probabilities of atoms to meet in the correct ratio to form clusters that lead to phase formation are introduced. Stability of clusters against breaking into constituent parts through diffusion and rotations of atoms on site (where covalent bonding is involved) is also discussed. Fractional heats are defined and related to effective heats of formation. Chapter 6 compares the more popular models of phase formation to each other. These are the Walser-Bene, the kinetic model of Gosele and Tu, the Zhang and Ivey model, the Effective Heat of Formation model as well as the statistical model which forms part of this investigation. Chapter 7 summarises this investigation.

CHAPTER 2

EXPERIMENTAL METHODS

2.1 Sample Preparation

2.1.1 Substrate preparation and cleaning

Oxidized substrates of silicon which are about 280μm thick and 50mm in diameter were used. SiO_2 is known not to interact with most metals at moderate temperatures. The thickness of the silicon oxide layer was in all cases more than 3 000$\AA$ to prevent interaction between the deposited layers and the underlying silicon substrate. The substrates were cut to squares of edge 13 mm. The relatively large surface areas help one to obtain larger signals when compound phase identification is done using X-Ray Diffraction. The substrates were cleaned first in methanol, acetone, trichloroethylene, acetone, methanol and then distilled water in an ultrasonic bath. The resistivity of the distilled water was better than 10MΩ.cm. Wafers were then attached onto aluminium holders and loaded into a high vacuum chamber.

2.1.2 *Vacuum deposition*

The evaporator has three crucibles into which elements to be evaporated are loaded. The crucibles can be moved from the outside so that each of the three can be placed in the path of the electron beam in turn. The electron beam supplies the heating to the crucibles. Crucibles were cleaned before introducing the elements

to be evaporated. Each crucible is separated and shielded from that adjacent to it by partitions which are 20mm in height to prevent cross-contamination during depositions. Electrons are supplied by the electron gun. The filament current can be varied thus changing the electron beam current which in turn alters the rate of deposition. Sample holders, each of which can take up to seven samples, are loaded face down on a rotating platform which can take up to six sample holders. A quartz monitor was used to find the rate at which depositions were done as well as thicknesses of evaporated layers. All depositions were done in vacuum. Vacuum was maintained by means of ion pumps, sublimation pumps, cryopanel and a turbo-pump. The top part of the evaporator can be isolated from the bottom part by means of a baffle valve (see **Fig. 2.1**). This valve was kept closed during cleaning of crucibles and re-loading of samples, so that the bottom part was at a pressure of better than $\approx 10^{-8}$kPa. Pressure measurements were taken by means of a Penning

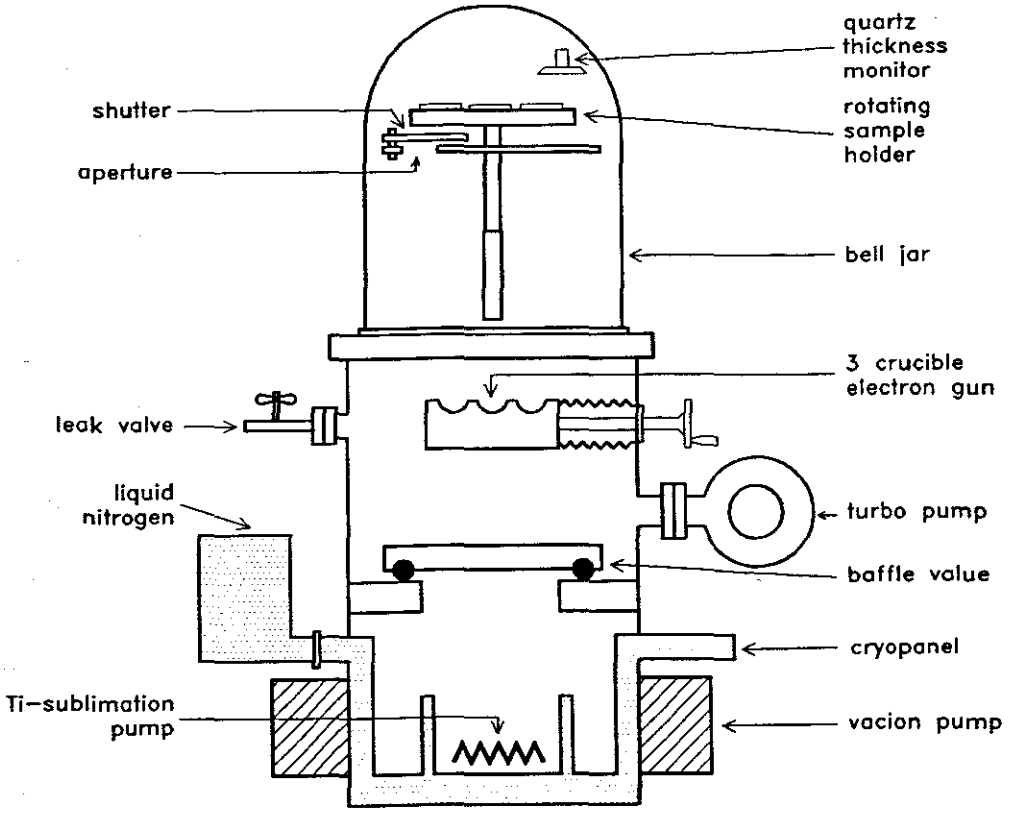

FIGURE 2.1: Sketch showing the high vacuum evaporation system

gauge in the range 10^{-3}kPa to 10^{-8}kPa.

The ion pump consists of pumping elements which are surrounded by a strong magnetic field. Each pumping element consists of a multi-cell anode structure between two titanium cathode plates. A voltage of about 6000V is maintained between the anode and cathode. Electrons moving from cathode to anode are forced by the magnetic field to spiral, thus increasing their path and probability of colliding with gas molecules. Collisions ionize the gas. Positively charged gas ions are accelerated by the electric field and move towards the titanium cathode. This effect sputters the titanium atoms. Titanium then getters the oxygen and nitrogen part of the gas. The gettering action of the ion pumps is increased by sublimation and cryopumping. The turbo pump on the top part of the evaporator can reduce the pressure to about 10^{-5} kPa if left to pump overnight. On opening the baffle valve and pouring liquid nitrogen vacuum is improved to about 10^{-9}kPa. Vapours such as H_2O and CO_2 are trapped on the cooled surface of the cryopanel. Non-condensable gases are then carried down by the condensable vapour and then trapped within the condensate. Sublimation pumps are also used to further decrease the pressure.

After evaporation samples were allowed to cool in vacuum for more than one hour to prevent oxidation of the samples. As a further precaution vacuum was broken by means of dry high grade nitrogen.

2.1.3 Vacuum annealing

After vacuum deposition had been done, the thin film couples need to be annealed to speed up interactions. Annealings were done in a vacuum furnace. Quartz boats onto which samples were to be placed were first pre-heated so as to drive out from them any gases. Samples were then loaded into the carousel of the tube furnace. This carousel can accommodate up to eight boats, each of which can hold up to four samples. Each boat could be individually slided in and out of the furnace. The furnace temperature could be monitored by means of a platinel $\prod$ thermocouple situated in the middle of the heating elements just above the boats with the samples.

An external microprocessor unit controlled the temperature and stabilized it to any desired preset value.

All anneals were done in vacuum. Vacuum was obtained by using a mechanical forepump together with a turbo-molecular pump. A cold trap filled with nitrogen also helped to reduce the pressure. Annealings were done at pressures of better than 10^{-7}kPa. After annealing was done samples were left in vacuum to allow them to cool for more than one hour. To prevent possible oxidation of the samples vacuum was broken by letting in dry nitrogen.

2.2 Sample Characterization

Various methods were used to find compound phases that grew during annealing as well as their thicknesses.

2.2.1 Rutherford backscattering

In Rutherford Backscattering (RBS) light ions having low energies, usually in the range 1–3 MeV, are scattered on solids to be investigated. At these low energies only elastic collisions occur, and this way nuclear reactions are avoided. A monoenergetic ion beam (H^+, He^+ or He^{++}) is directed to the sample, and then a solid state detector is used to analyze the backscattered particles. Samples are placed in vacuum ($\approx 10^{-6}$kPa) while being analyzed. The sample normal is usually tilted 10 degrees with respect to the ion beam, and only those particles backscattered at 165 degrees are analyzed by the detector. A permanent horseshoe magnet is used to prevent secondary electrons from escaping from the target.

The energy of the backscattered particle E_1 is determined by its mass m, the mass of the target M, the energy of the particle before collision E_0, and the scattering angle θ.

$$k = \frac{E_1}{E_0} = \frac{(M^2 - m^2 \sin^2\theta)^{\frac{1}{2}} + m\cos\theta}{m + M} \tag{2.1}$$

The constant k is known as the kinematic factor. If one knows the values of k, m and θ one can calculate the value of M, The target atom. This allows one to

analyze mass.

The type of scattering involved is Coulombic in nature, and the differential cross-section $\frac{d\sigma}{d\Omega}$ is the square of the scattering amplitude,

$$\frac{d\sigma}{d\Omega} = \left[\frac{zZe^2}{4E_0}\right]^2 \frac{4}{\sin^4\theta} \frac{\cos\theta + [1-(\frac{m}{M}\sin\theta)^2]^{\frac{1}{2}}}{[1-(\frac{m}{M}\sin\theta)^2]^{\frac{1}{2}}} \tag{2.2}$$

where z is the atomic number of the projectile atom of mass m, Z that of the target atom, and e is the electronic charge. It is clear from the expression of the differential cross-section that backscattering yields are proportional to the square of the atomic number of the target atom Z. Thus backscattering yields give quantitative analysis.

On entering the solid, the ion will lose energy to electrons of the target atom through ionization and electronic excitations. After collision with a host atom, the projectile atom will lose energy again on its backward outward path. One can do depth analysis based on this loss of energy. Energy loss can be expressed as dE/dx. The depth is measured as mass per unit area,ρdx, or number of atoms per unit area, Ndx, where ρ is the mass density and N the atomic density. The energy loss per unit area will therefore appear as dE/ρdx or dE/Ndx. The expression dE/Ndx is called the stopping cross section.

For small energy losses, the relation between energy loss ΔE and depth t is linear,

$$\Delta E = [S]\,t \tag{2.3}$$

where [S] is the backscattering energy loss factor. If values of [S] for a given θ are known, and values of ΔE obtained from the backscattering spectra, then the depth t can be calculated.

The number of counts per channel, or height H of the spectrum depends on the total number of incident ions, Q, the solid angle of the detector Ω, the average differential cross-section σ evaluated at E_0 and the total number of target atoms per unit area Ndx i.e.

$$H = Q\sigma\Omega N\delta x \tag{2.4}$$

or

$$H = \frac{Q\sigma\Omega N\delta E_1}{[S]} \tag{2.5}$$

where δE_1 is the energy width of a channel and δx is the layer thickness. The area A of an energy spectrum is the sum of the counts per channel of the spectrum. If the spectrum is rectangular in shape then area is given by

$$A = H\left(\frac{\Delta E}{\delta E_1}\right) \tag{2.6}$$

or

$$A = QNt\sigma\Omega \tag{2.7}$$

which shows that A is directly proportional to t. If a heavy impurity of mass m is on the surface of a light substrate of mass M,then from equation, the amount of impurity atoms per unit area is

$$(Nt)_i = \frac{A_i}{Q\Omega\sigma_i} \tag{2.8}$$

where i stands for the impurity atoms. The total number of incident particles and the solid angle of detection is

$$Q\Omega = \frac{H_m\,[S]_m^M}{\sigma_m N_m \delta E_1} \tag{2.9}$$

where the subscript and superscript on [S] denotes the scattering atom and stopping medium respectively. We therefore get

$$\frac{N_o.\text{ of impurity atoms}}{\text{cm}^2} = (Nt)_i = \frac{A_i N_m \sigma_m \delta E_1}{H_m \sigma_i\,[S]_m^M} \tag{2.10}$$

The concentration of Cr in Ge for example can be found from the peak height ratios. From equation 2.5 we get

$$H_{Cr} = \frac{Q\sigma_{Cr}\Omega N_{Cr}\sigma E_1}{[S]_{Cr}^{Ge}} \tag{2.11}$$

and

$$H_{Ge} = \frac{Q\sigma_{Ge}\Omega N_{Ge}\sigma E_1}{[S]_{Ge}^{Ge}} \tag{2.12}$$

The ratios give

$$\frac{H_{Cr}}{H_{Ge}} = \frac{\sigma_{Cr} N_{Cr}\,[S]_{Ge}^{Ge}}{\sigma_{Ge} N_{Ge}\,[S]_{Cr}^{Ge}} \tag{2.13}$$

or

$$\frac{N_{Cr}}{N_{Ge}} = \frac{\sigma_{Ge} H_{Cr} [S]_{Cr}^{Ge}}{\sigma_{Cr} H_{Ge} [S]_{Ge}^{Ge}} \tag{2.14}$$

from which not only the concentration of Cr in bulk Ge can be found but also the stoichiometric ratio of a compound of Cr and Ge can be deduced. Important points to note about RBS are that,

1. The energy of particles backscattered from heavy atoms is higher than that from lighter atoms.

2. The number of scattered particles is proportional to the square of the atomic number of the scatterer, Z^2.

3. The energy loss gives an indication of the depth scale.

One notices then that depositing a lighter element first and the heavier one on top helps to separate the spectra,and speeds up phase identification.

2.2.2 X-ray diffraction

Compound phase identification was done by means of a Phillips vertical diffractometer, employing the Bragg-Brentano geometry. In this configuration both sample and detector move, with the detector moving angle 2θ for each θ the sample moves. **Fig. 2.2** shows the x-ray diffraction setup.

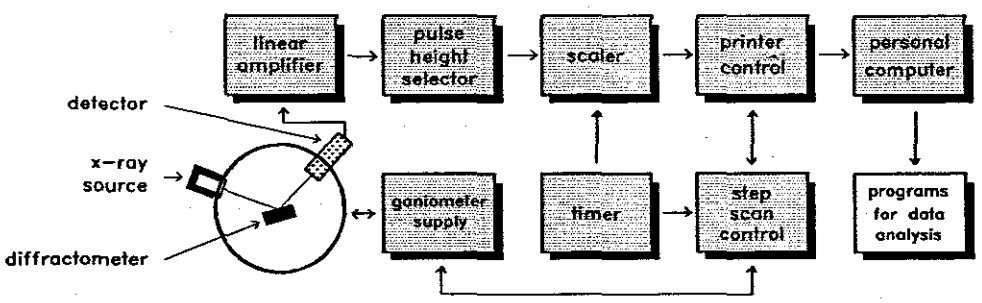

FIGURE 2.2: Sketch showing the essential features of the X-ray Diffractometer

Monochromatic x-rays were obtained from a Cu tube. The internal computer on the diffractometer controlled both sample and detector movements. Step size and duration of data acquisition on each step could be preset. Most of the spectra was accumulated for two seconds and each step was 0.2°.Data was routed to an external desk-top computer and stored on floppies for further analysis. A program was used to generate all possible reflections and their corresponding (hkl) values as a function of 2θ. This was compared by computer to experimental peaks, and thus compound phase identification was done.

CHAPTER 3

PHASE FORMATION AT METAL-Ge INTERFACES

3.1 Introduction

Germanium is a very important semiconductor. When doped with arsenic, gallium, or other elements, it is used in the electronic industry as a transistor element. Germanium and germanium oxide are transparent to the infrared and are used in optical equipment as well as extremely sensitive detectors. Germanium oxide's high index of refraction and dispersion has also made it useful as a component of glasses used in wide-angle camera lenses and microscope objectives. However, its application as a semiconductor element now provides the largest use of germanium. For device applications, it is of particular interest due to the high mobility of both the electrons and holes, making a high speed complementary transistor a possibility [76]. Strained layer (Ge,Si)/Si heterostructures have been shown to exhibit a wide variety of interesting properties attributed to band structure modifications [77]. Germanides are also used as ohmic contacts for GaAs devices, and it is commonly known that germanium detectors are used as radiation detectors. Successful implementation of germanium technology will however require an understanding of the solid-state interaction in metal-germanium systems. Such information will lead to increased device reliability and better reproducibility. Compared to the extensive studies

which have been carried out on the silicides, germanide formation has received little attention [78–85]. In this chapter we investigated first phase formation in Ge-metal binary systems and the predictions of the EHF model are tested against experimental data.

During the past few years there has been a marked decrease in device dimensions and an increase in the complexity of integrated circuits. This increase in the complexity of devices results in many different metals, semiconductors and insulators coming into contact with each other. Their interaction with one another therefore needs to be carefully studied and evaluated. Apart from a fundamental understanding of metal-semiconductor interaction, the special interest in germanides is due to their good characteristics, which amongst others include, a high electron mobility and very low carrier freeze-out temperatures. In this study the predictions of the Effective Heat of Formation Model are compared to experimentally obtained data in the five binary systems Ti-Ge, Pd-Ge, Zr-Ge, Fe-Ge and Cr-Ge.

3.2 Experimental

Thin layers of a metal (Ti, Pd, Zr, Fe, Cr) and Ge were deposited without breaking vacuum, on Si<100> covered with SiO_2. The thickness of the oxide layer was about 5000Å to prevent interaction of the evaporated layers with the substrate. Little interaction between the evaporated layers and the SiO_2 layer was observed for temperatures up to 600°C. Metal layers were in most cases deposited first in order to minimize possible oxidation of this layer when removed from the vacuum chamber. The SiO_2/Metal/Ge samples were annealed for various periods of time in an oil free vacuum system, with vacuum better than 10^{-8} kPa. All samples were analyzed by Rutherford Backscattering Spectrometry (RBS). The RUMP (Rutherford Backscattering Utilities and Manipulation Program) [86] computer program was used to determine the thicknesses of the Metal and Ge layers as well as the thicknesses of the compounds formed. Phase identification was done by means of X-ray diffraction (XRD) spectra. Computer programs were used to analyse some of the complex XRD spectra.

3.3 Results

3.3.1 Ti-Ge, Pd-Ge and Zr-Ge systems

Ti-Ge system

Crystallographic parameters for this system are shown in **Table 3.1.**

which was obtained from Pearson's Handbook of Crystallographic Data and Interrmetallic Phases. **Fig. 3.1** is the latest phase diagram of the Ge-Ti system. It shows that phases Ti_3Ge and TiGe previously thought to be equilibrium phases do not exist [88].

Layers of Ti followed by those of Ge were evaporated onto thermally oxidized Si substrates in vacuum. These were allowed to cool for more than an hour before transfering them to a furnace where they were annealed in vacuum.

A composition corresponding to $Ti_{0.32}Ge_{0.68}$ was made by evaporating a thin layer of Ti(1100Å) followed by a thicker layer of Ge(3000Å) onto oxidized Si substrates. Samples were annealed in vacuum of better than 10^{-7}kPa, for 20 minutes. Results of Rutherford Backscattering are shown in **Fig. 3.2.**

Signal heights are shown on both the Ti and Ge signals. The as deposited sample show no interaction. The spectrum of the sample annealed at 450°C shows that there has been interaction between Ti and Ge. The step on the signal height for the sample annealed at 500°C (not shown) indicate the presence of Ti_6Ge_5. The spectrum of the sample annealed at 550°C shows clearly the presence of this phase. At 600°C the heights on the Ge and Ti signals indicate the presence of $TiGe_2$.

X-ray diffraction results have shown that both Ti and Ge had already crystallized at 450°C (see **Fig. 3.3**). At 550°C, peaks corresponding to the phase Ti_6Ge_5 can be seen. No Ti peaks are shown by this spectrum, which means that Ti has been completely consumed. There are however peaks of Ge. An increase in temperature to the value 600°C results in the growth of $TiGe_2$, but peaks corresponding to Ti_6Ge_5 can still be seen.

An experiment was done where Ge(3000Å) was deposited on oxidized Si. A

TABLE 3.1: Parameters for the Ti-Ge binary system. The table was compiled from data given by references [87,16].

Phase	Composition at.% Zr	Pearson symbol	Space group	Prototype	$^{a}_{b}_{c}$ (Å)
αTi	0–2	hP2	$P6_3/mmc$	Mg	2.9508 — 4.6855
βTi	0–2	cI2	Im3m	W	3.3065
Ti_3Ge [a)]	25	tI43	I4	Ni_3P	10.29 — 5.14
Ti_5Ge_3	37.5	hP16	$P_3/Imcm$	Mn_5Si_3	7.537 — 5.223
TiGe [a)]	50	oP8	Pmm2	TiSi	3.809 6.834 5.235
Ti_6Ge_5	45.5	oI44	Ibam	Ti_6Ge_5	16.915 7.954 5.233
$TiGe_2$	66.7	oF24	Fddd	$TiSi_2$	8.864 5.030 8.594
Ge	100	cF8	Fd3m	C(diamond)	??

[a)] Phases not given as equilibruim phases on the latest phase diagram [88]

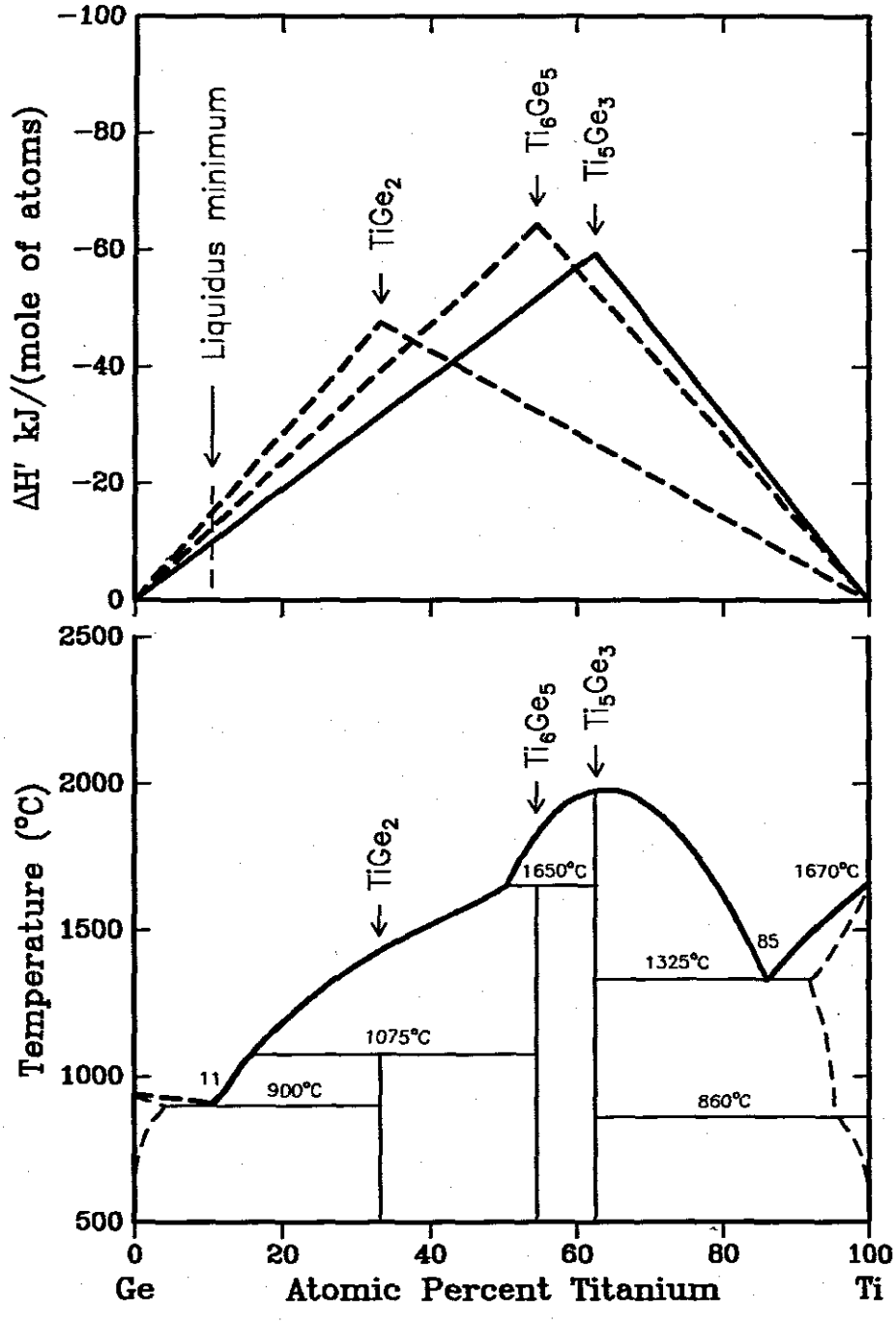

FIGURE 3.1: The phase diagram (bottom) and the EHF diagram (top) of the Ti-Ge system according to Moffat [88].

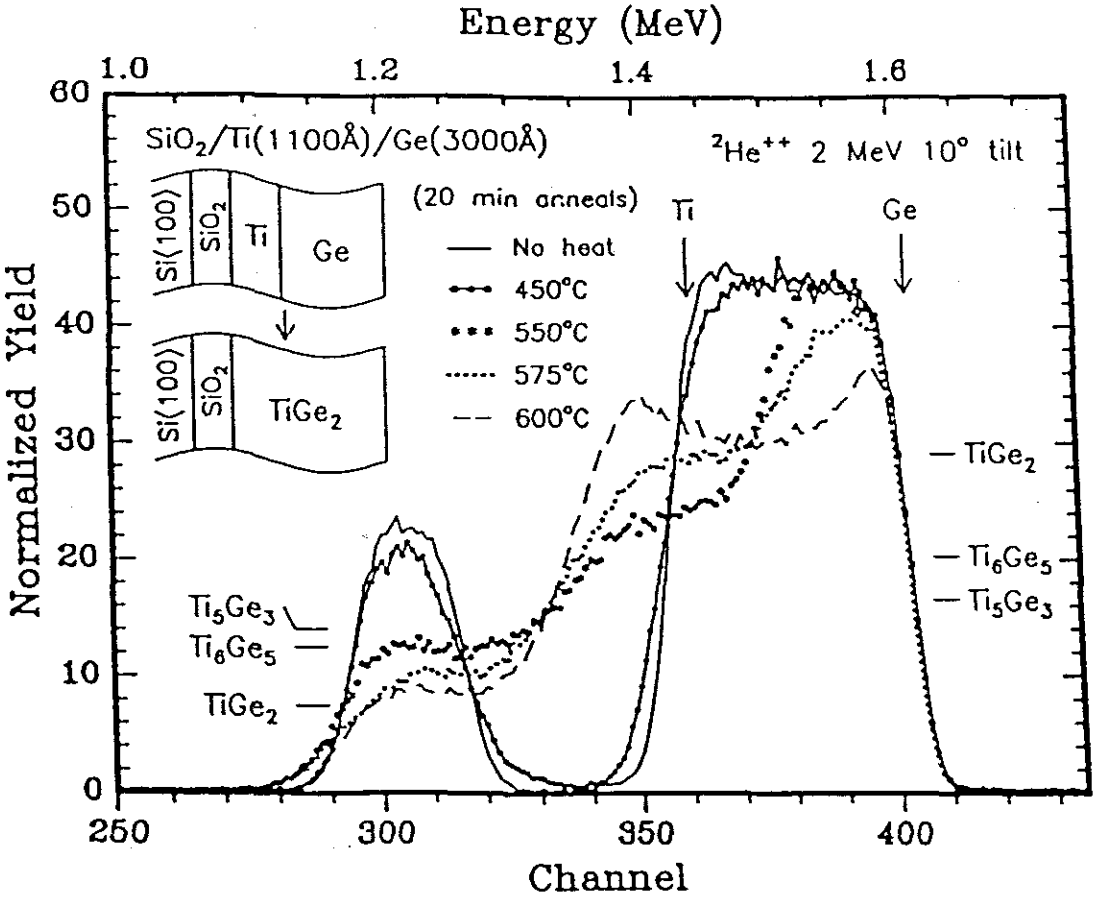

FIGURE 3.2: Backscattering diagram of samples made up of Si<>/SiO_2/Ti(1100Å)/Ge(3000Å). The step height on the Ge signal of the sample annealed at 550°C correspond to that of the phase Ti_6Ge_5. The 600°C shows the presence of $TiGe_2$.

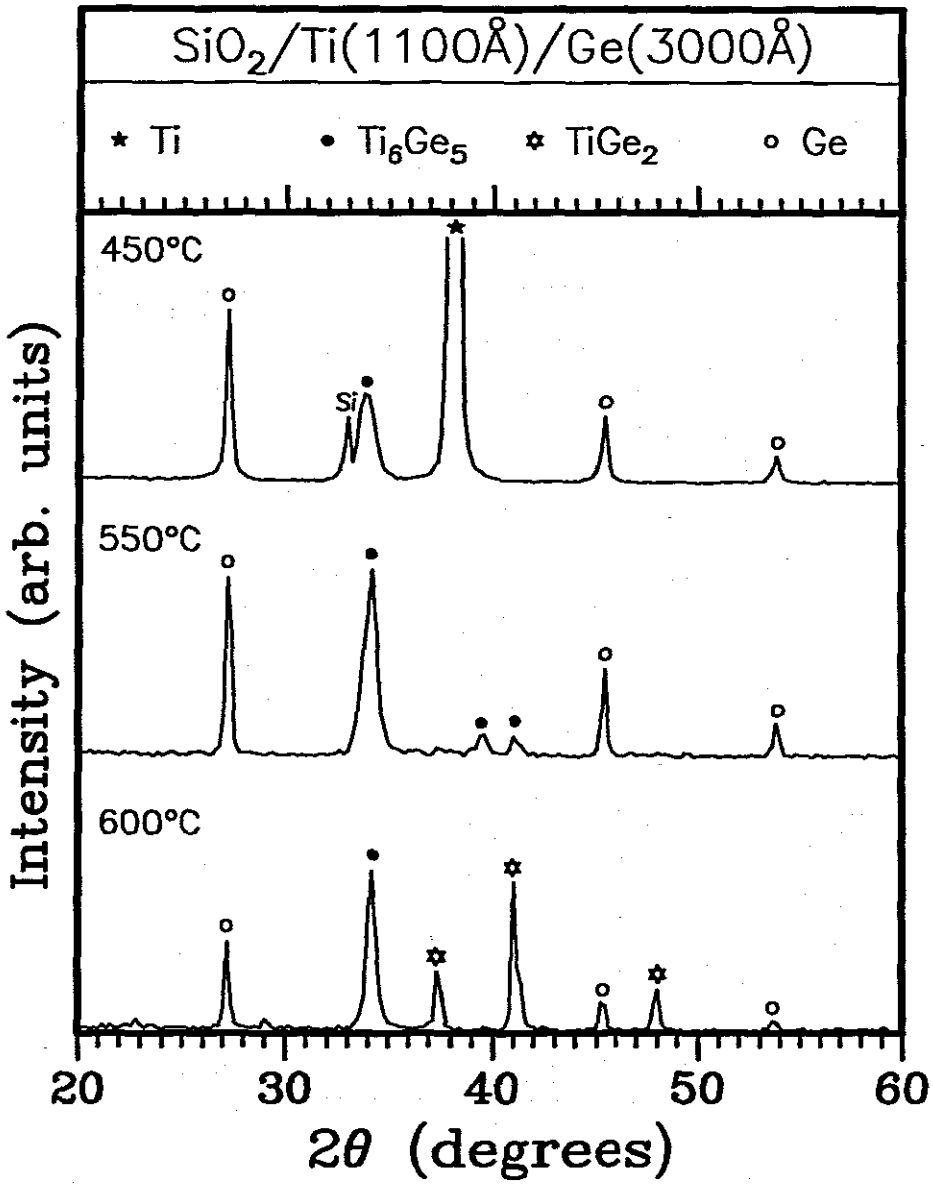

FIGURE 3.3: *The sample annealed at 450°C, shows that* Ti_6Ge_5 *is the first phase to form. At 550°C it is the only compound phase present together with free Ge. Ti has been used up at this stage. At 600°C peaks belonging to* $TiGe_2$ *appear.*

layer of Ti(1000Å) was deposited on top of the Ge layer. RBS results of this experiment are shown in **Fig. 3.4**.

Samples annealed at 500°C, showed that Ti_6Ge_5 had formed. This is confirmed by XRD results shown in **Fig. 3.5**.

The spectrum of the sample annealed at 450°C shows peaks corresponding to Ti_6Ge_5 as well as those of Ge. The RBS spectrum of the sample annealed at 600°C, shows the presence of $TiGe_2$.

The corresponding XRD results confirm this.

Pd-Ge system

Interaction in the Pd-Ge system was also studied. This system has six equilibrium phases. **Table 3.2** summarises their crystal parameters.

This system has been well studied **[80, 78, 83]**. The first phase found by these groups is Pd_2Ge. In this investigation the same phase, Pd_2Ge has also been found to form first. **Fig. 3.6** is an X-ray diagram showing interaction in this system. All samples were annealed for forty minutes in vacuum. The sample annealed at 200°C shows the presence of Pd_2Ge.

Zr-Ge system

Experiments were done to study solid state interaction in the Ge-Zr system, which has five equilibrium phases viz. $ZrGe_2$, ZrGe, Zr_5Ge_4, Zr_5Ge_3 and Zr_3Ge. There is uncertainty as to whether Zr_5Ge_4 is congruent or not. The temperature difference between the liquidus and the peritectic point for the ZrGe phase is small. Crystallographic parameters for the five phases were obtained from Pearson's Handbook of Crystallographic Data and Intermetallic Phases (see **Table 3.3**).

A composition corresponding to $Zr_{0.22}Ge_{0.78}$ was made by evaporating a thick layer of Ge(3100Å), onto oxidized Si wafers. This was followed by a thinner layer of Zr(910Å). Samples were then annealed in vacuum. Samples annealed at temperatures higher than 450°C peeled. The spectrum of the sample annealed at 325°

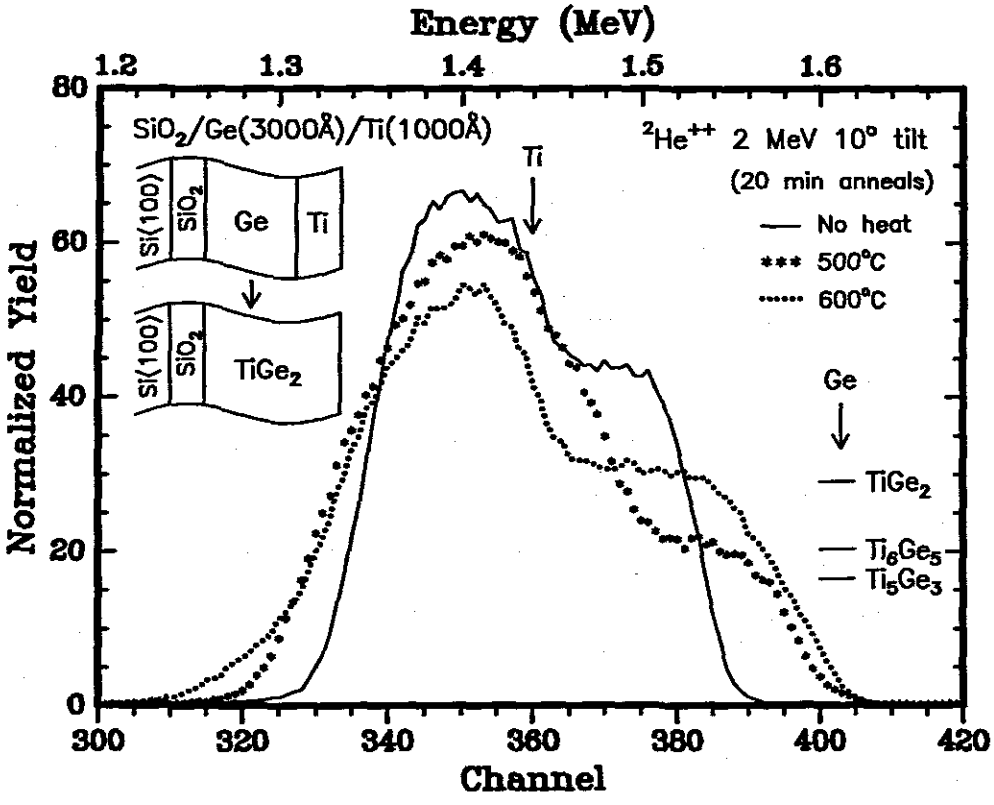

FIGURE 3.4: Backscattering spectra of Si<>/SiO_2/Ge(3000Å)/Ti(1000Å) samples as-deposited and annealed for 20 minutes at various temperatures. The sample annealed at 500°C shows the presence of Ti_6Ge_5. Sample thicknesses were chosen to have excess Ge thus $TiGe_2$ should be the final phase. This is indeed the case (see the 600°C spectrum).

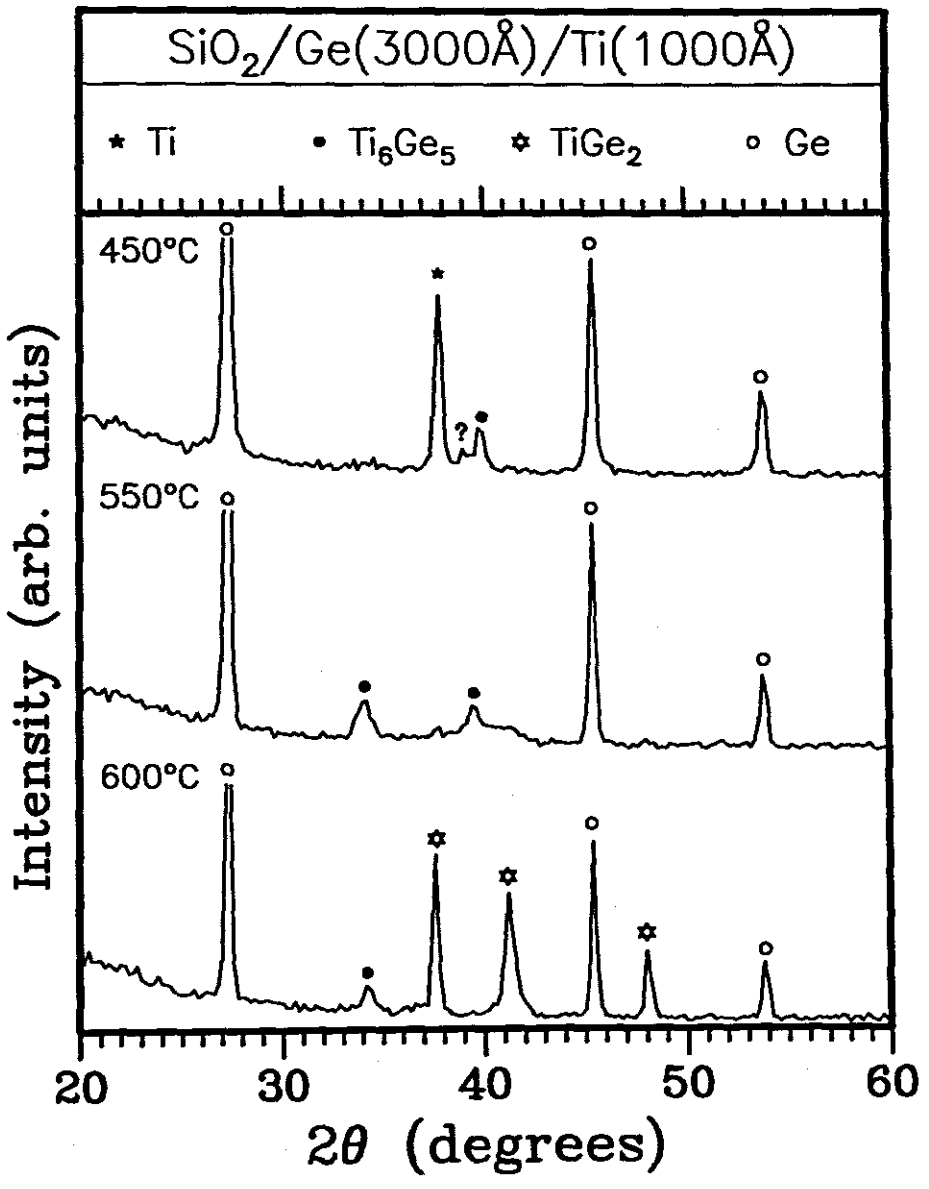

FIGURE 3.5: X-ray diffraction spectra of Si<>/SiO_2/Ge(3000Å)/Ti(1000Å) samples annealed at different temperatures for 20 minutes. The sample annealed at 450°C indicates the presence of Ti_6Ge_5. The latter phase grows with an increase in temperature. The sample annealed at 600°C shows the presence of both $TiGe_2$ and Ti_6Ge_5.

TABLE 3.2: *Crystallographic parameters for the Pd-Ge binary system. The table was compiled from data given by references [87, 16].*

Phase	Pearson symbol	Space group	Prototype	$^{a}_{b}_{c}$ (Å)
GePd	oP8	Pnma	MnP	5.782 3.481 6.259
$GePd_2$	hP9	$P\bar{6}2m$	Fe_2P	6.712 — 3.408
Ge_8Pd_{21}	tI116	$I4_1/a$	$Al_{21}Pt_8$	13.067 — 10.033
Ge_9Pd_{25}	hP34	$P\bar{3}$	Ge_9Pd_{25}	7.351 — 10.605
$GePd_5$	mC24	C2	$AsPd_5$	5.509 7.725 8.375
Ge_4Pd_{21}	cI2	$Im\bar{3}m$	W	3.085
Pd	cF4	$Fm\bar{3}m$	Cu	3.8874

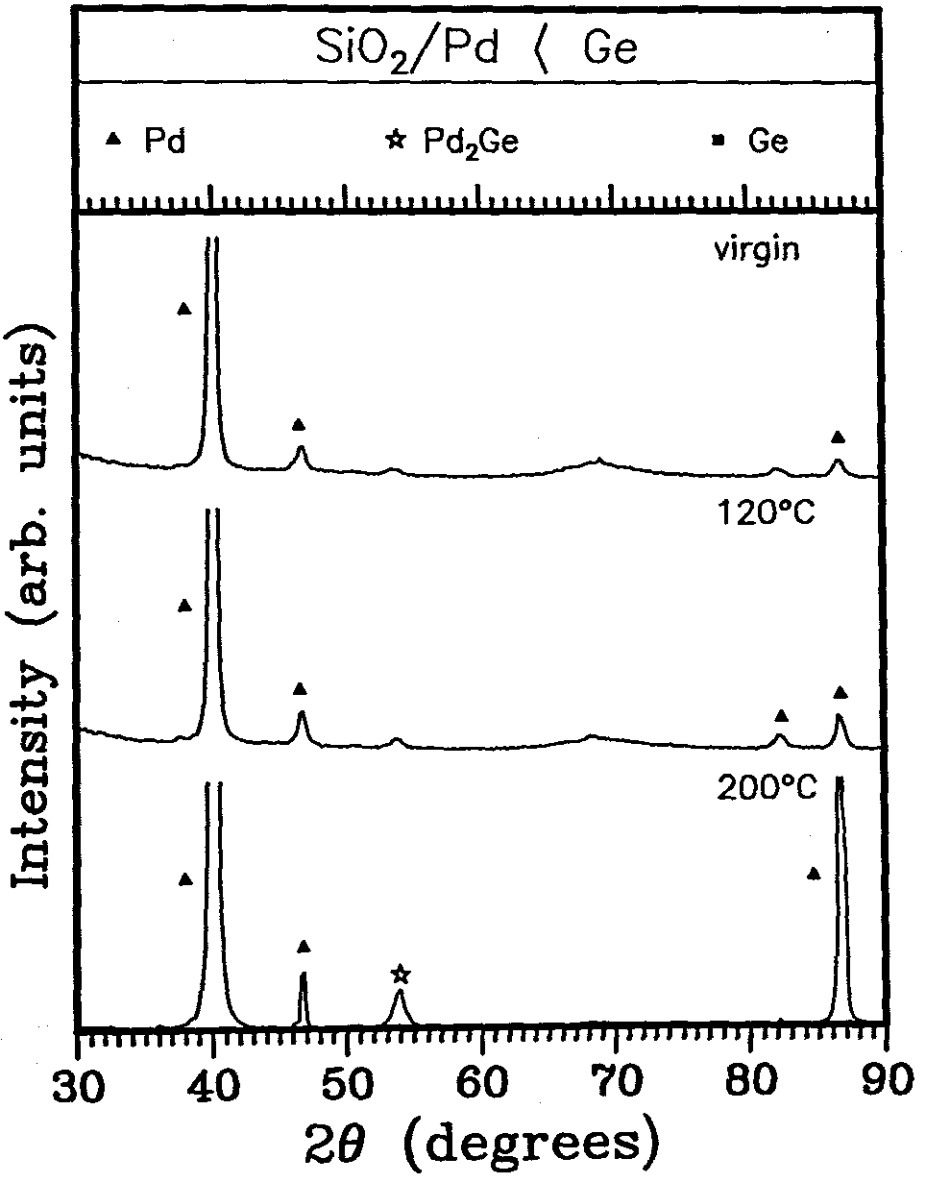

FIGURE 3.6: X-ray diffraction spectra of Si<>/SiO_2/Pd(1000Å)/Ge(2000Å) samples annealed at different temperatures. The sample annealed at 200°C indicates the presence of Pd_2Ge.

TABLE 3.3: Crystallographic parameters for the Zr-Ge binary system. The table was compiled from data given by references [87, 16].

Phase	Composition at.% Zr	Pearson symbol	Space group	Prototype	a b c (Å)
αZr	0–0.9	hP2	$P6_3/mmc$	Mg	3.232
					—
					5.147
βZr	0–1	cI2	Im3m	W	3.568
Zr_3Ge	25	tP32	$P4_2/n$	Ti_3P	11.08
					—
					5.48
Zr_5Ge_3	37.5	hP16	$P6_3/mcm$	Mn_5Si_3	7.993
					—
					5.597
Zr_5Ge_4	44.4	tP36	$P4_12_12_1$	Zr_5Si_4	7.243
					—
					13.162
ZrGe	50	oP8	Pnma	FeB	7.075
					3.904
					5.396
$ZrGe_2$	66.6	oC12	Cmcm	$ZrSi_2$	3.7893
					14.975
					3.7606
Ge	100	cF8	Fd3m	C(diamond)	5.658

[a] Phases not given as equilibruim phases on the latest phase diagram [88]

shows that interaction between Ge and Zr had begun. A RUMP fit to this spectrum showed that ZrGe had formed at the Zr and Ge interface. At higher temperature, a fit indicated the presence of both ZrGe and $ZrGe_2$. These fits showed that the two compounds grow simultaneously.

X-ray results on the samples showed that there is no interaction at 300°C. A peak identified as that of the phase ZrGe was found. At 350°C, a peak corresponding to $ZrGe_2$ appeared. The XRD results are shown in **Fig. 3.7**. They confirm RBS results.

3.3.2 Fe–Ge and Cr–Ge systems

Fe-Ge system

The Fe-Ge system has six equilibrium phases [87]. Data about the system was obtained from Massalski's book on Binary Alloy Phase Diagrams [16] and Pearson's Handbook of Crystallographic Data and Intermetallic Phases [87]. The Fe-Ge system has only one congruent phase viz. Fe_5Ge_3.

In the pure form iron exists in three allotropic modifications, each of which is stable over a certain range of temperatures. When it solidifies at 1540°C, the δ modification forms; this has a body centered cubic crystal lattice, and is stable down to 1400°C, when, at constant temperature, it alters to the γ modification, which has a face-centered cubic lattice structure. The γ iron is stable down to 910°C, when it alters to the α non-magnetic modification, which has a body-centered cubic lattice similar to that of δ iron. At 768°C (Curie point) the α iron becomes magnetic. This change from α non-magnetic to α magnetic is due to electron rearrangements in the outer shell of the iron atoms. The Fe-Ge system has five equilibrium phases (see **Table 3.4**).

Six different thin film sample configuration of Fe and Ge layers were prepared: SiO_2/Fe(280Å)/Ge(2150Å); SiO_2/Fe(840Å)/Ge(1750Å); SiO_2/Fe(800Å)/Ge(950Å); SiO_2/Fe(1925Å)/Ge(1050Å); SiO_2/Fe(850Å)/Ge(1300Å) and SiO_2/Fe(880Å)/Ge(1250Å). In the above configuration the first sample is Ge-rich enough to form $FeGe_2$ upon complete reaction. The next one should end as FeGe, while the remaining four

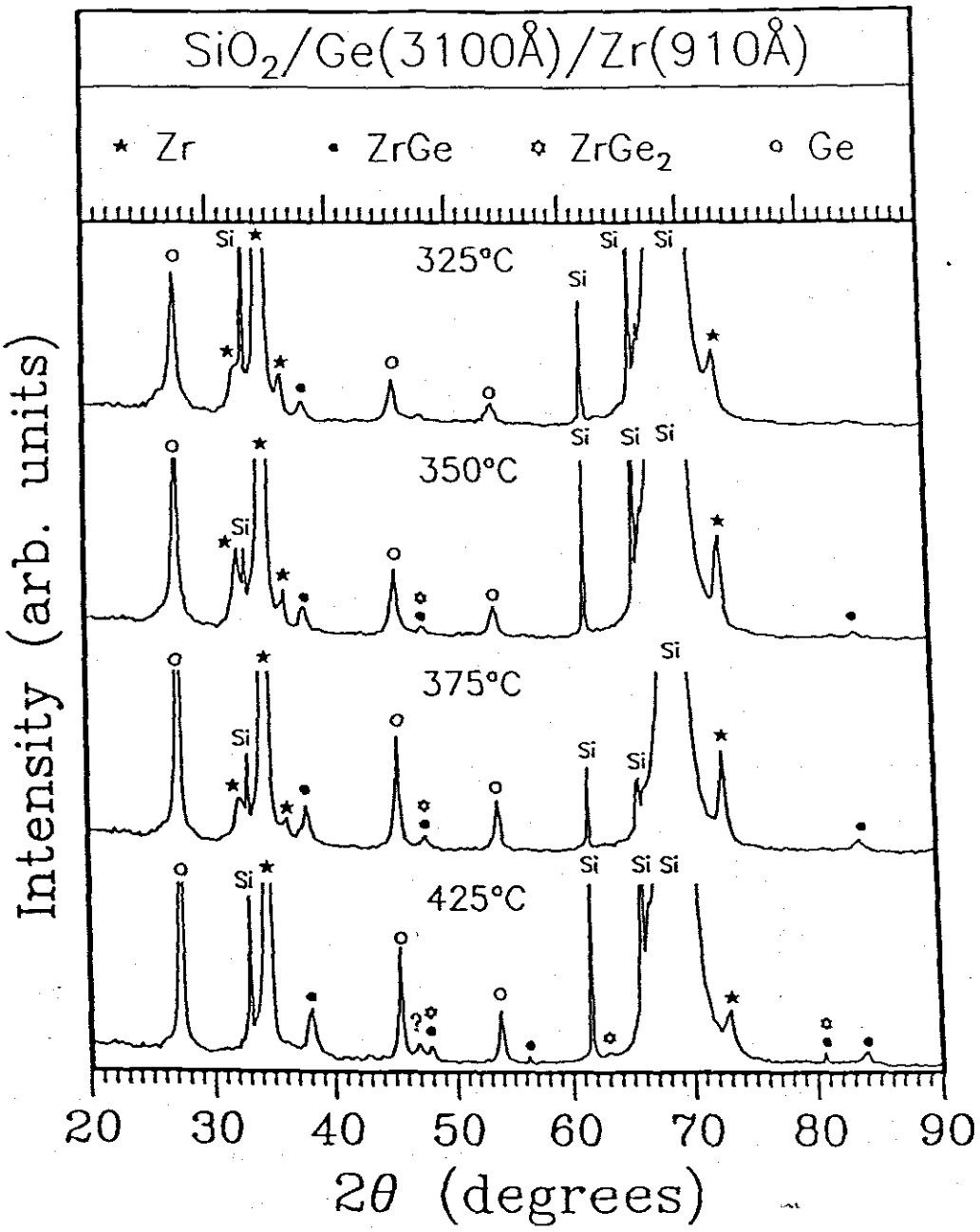

FIGURE 3.7: X-ray spectra of Si<>/SiO_2/Ge(3100Å)/Zr(910Å) samples annealed at various temperatures. The sample annealed at 325°C indicates the presence of ZrGe. At higher temperatures peaks belonging to $ZrGe_2$ can be seen.

TABLE 3.4: Crystallographic parameters for the Fe-Ge binary system. The table was compiled with data from reference [87].

Phase	Pearson symbol	Space group	Prototype	a b c (Å)
Fe	cI2	$Im\bar{3}m$	W	2.8665
Fe_3Ge	cP4	$Pm\bar{3}m$	$AuCu_3$	3.665
Fe_3Ge	hP8	$P6_3/mmc$	Ni_3Sn	5.169
				4.222
Fe_5Ge_3 [a]	hP22	$P6_3/mmc$	Fe_5Ge_3	7.976
				4.993
Fe_4Ge_3 [b]	hP14	$P6_3/mmc$	Fe_4Ge_3	3.998
				5.010
Fe_6Ge_5	mC44	C2/m	Fe_6Ge_5	9.9965 7.826 7.801
FeGe	mC16	C2/m	CuGe	11.838 3.937 4.933
FeGe	hP6	P6/mmm	CoSn	4.965
				4.054
FeGe	cP8	$P2_13$	FeSi	4.700
$FeGe_2$	tI12	I4/mcm	Al_2Cu	5.908
				4.957
Ge	cF8	$Fd\bar{3}m$	C(diamond)	5.658

[a] Referred to as $Fe_{13}Ge8$ by [87].
[b] Referred to as Fe_3Ge_2 by [87].

sample configurations were made to have as end phases Fe_5Ge_3, Fe_3Ge, Fe_6Ge_5 and Fe_4Ge_3 respectively. The reason for the above choice was to help with the identification of phases, since this system has not been documented before.

The SiO_2/Fe/Ge samples were annealed for 20 minutes in an oil free vacuum system, with vacuum better than 10^{-7} kPa.

Results from experiments with different thicknesses of Fe and Ge giving atomic ratios of Fe < Ge, Fe ≈ Ge, and Fe > Ge discussed next.

The Fe-Ge system has six equilibrium phases [87]. Data about the system was obtained from Massalski's book on Binary Alloy Phase Diagrams [16] and Pearson's Handbook of Crystallographic Data and Intermetallic Phases [87]. The Fe-Ge system has only one congruent phase viz. Fe_5Ge_3. Results were obtained for different thicknesses of Fe and Ge giving atomic ratios of Fe < Ge, Fe ≃ Ge, Fe > Ge and Fe >> Ge.

Fe < Ge

A thin layer of Fe (280Å) followed by a thicker Ge layer (2150Å) was evaporated onto oxidized Si. This corresponds to a composition $Fe_{0.20}Ge_{0.80}$. This sample configuration was chosen to have $FeGe_2$ (the most Ge rich phase) as the end phase. Results after RBS analyses are shown in **Fig. 3.8**. The heights of the possible Fe/Ge phases are shown on the Ge signal. Interaction between the layers already started to occur for a sample annealed at a temperature of 280°C (RBS spectrum not shown). It is not clear from these results which is the first phase that forms. However, a sample annealed at 400°C shows clearly the presence of $FeGe_2$ as the end phase and unreacted excess Ge. At 600°C considerable intermixing between the FeGe phase and remaining Ge is seen to take place.

XRD results (see **Fig. 3.9**) show no compound formation in the as deposited sample (virgin). For the sample annealed at 280°C the x-ray diffraction results indicate the presence of $FeGe_2$ and the monoclinic FeGe compound. For higher temperature anneals peaks from Ge appear together with $FeGe_2$ peaks. Ge is amorphous when deposited on a cold substrate, and these results show that it re-crystallizes at about

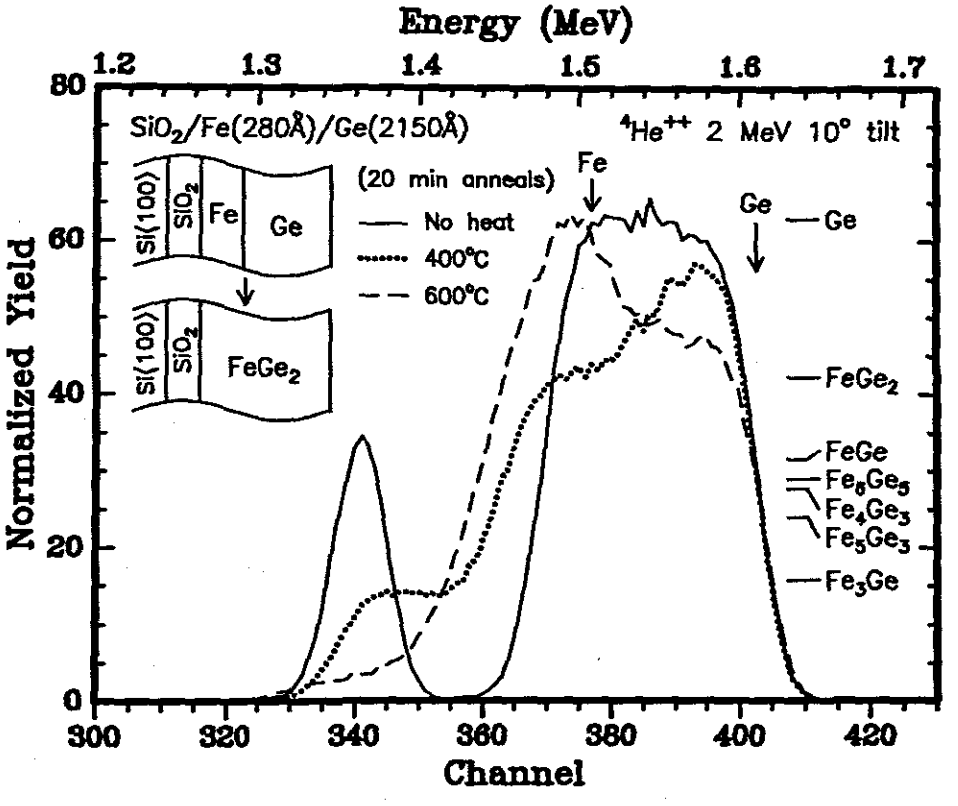

FIGURE 3.8: Backscattering spectra of Si<>/SiO_2/Fe(280Å)/Ge(2150Å) samples as-deposited and annealed for 20 minutes at various temperatures. The samples have composition $Fe_{0.20}Ge_{0.80}$ and were chosen to have excess Ge and $FeGe_2$ as the final phase after complete reaction. The expected germanium signal heights for the different germanide phases are indicated.

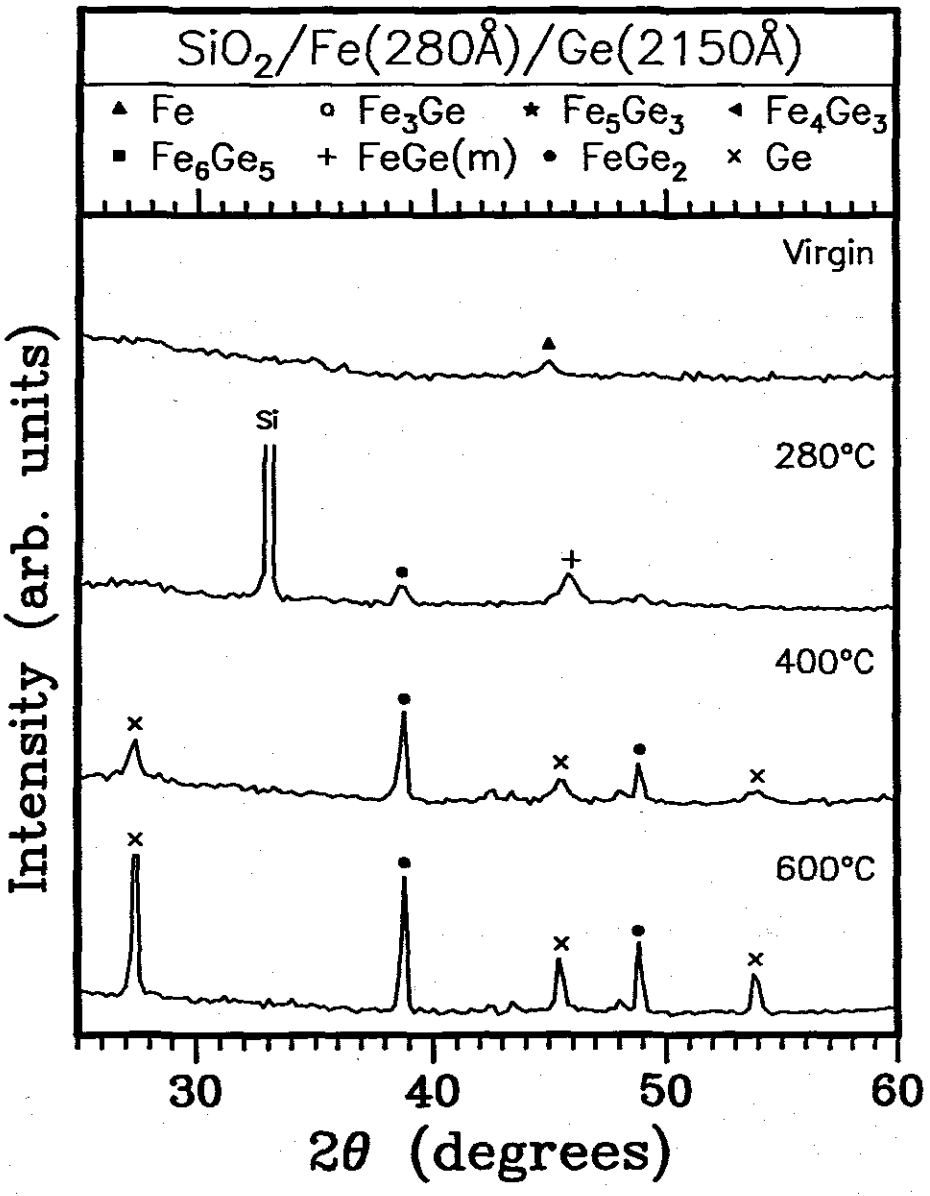

FIGURE 3.9: X-ray diffraction spectra of Si<>/SiO_2/Fe(280Å)/Ge(2150Å) samples annealed at temperatures of 280, 400 and 600°C. The sample annealed at 280°C indicates the presence of the monoclinic FeGe phase as well as $FeGe_2$. The latter phase grows with an increase in temperature. The sample annealed at 600°C shows only $FeGe_2$ and unreacted Ge.

400°C. The sample annealed at 600°C only shows $FeGe_2$ and unreacted Ge.

Fe ≃ Ge

For this experiment the aim was to have FeGe as the final phase. A thin layer of Fe (840Å) followed by a Ge layer (1750Å) was evaporated onto oxidized silicon . The overall composition of the samples was $Fe_{0.48}Ge_{0.52}$, which means that once FeGe has formed, there will be some free Ge left to form the next phase. The results after RBS analysis are shown in **Fig. 3.10**, with the corresponding heights of the six equilibrium phases for this system shown on the Ge signal. Little interaction between the layers was observed at 200°C (not shown). A considerable drop in the Ge signal is seen for the 300°C spectrum, but at 400°C (not shown), the height of the signal on the Ge peak corresponds to the formation of FeGe. For the 300°C and higher anneals it can also be seen that the Fe that was previously underneath the Ge has diffused towards the surface. It was found that for the 600°C spectrum, the signal height on the Ge signal tended towards the position where $FeGe_2$ is expected to form, indicating that apart from FeGe in the sample there is also some $FeGe_2$ present.

XRD results are given in **Fig. 3.11** for the 200°C, 300°C, 400°C and 600°C anneals. The 200°C anneal only shows the Fe peak. At 300°C the presence of the monoclinic form of FeGe can be seen, while at 400°C only peaks from hexagonal FeGe are seen. This agrees with the RBS results. It is interesting to note that at 600°C there are now also peaks from $FeGe_2$ together with the hexagonal form of FeGe. This is also in agreement with the RBS measurements.

Fe > Ge

A layer of Fe (800Å) was deposited on oxidized silicon followed by a layer of Ge (950Å). With this configuration the end phase is expected to be Fe_5Ge_3. The overall composition of the samples were $Fe_{0.62}Ge_{0.38}$ which is close to the composition of Fe_5Ge_3 ($Fe_{0.625}Ge_{0.375}$). RBS results from this experiment are shown in **Fig. 3.12**. Very little interaction between the layers could be detected with RBS for samples

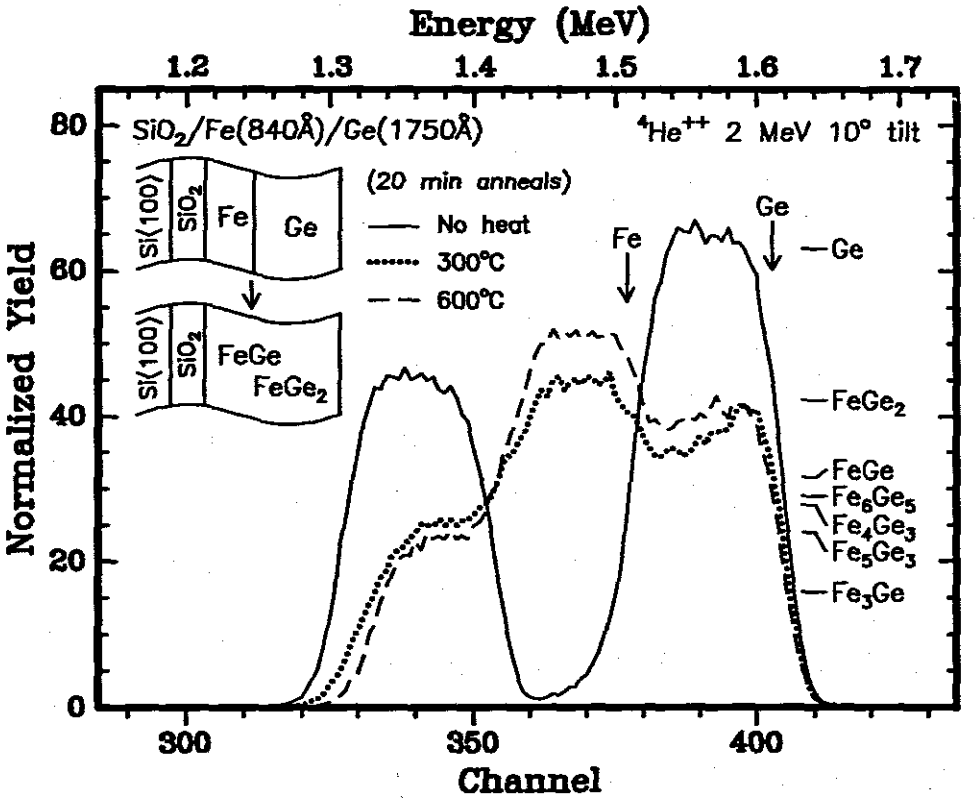

FIGURE 3.10: Backscattering spectra of Si<>/SiO_2/Fe(840Å)/Ge(1750Å) samples as-deposited and annealed for 20 minutes at various temperatures. These samples have composition $Fe_{0.48}Ge_{0.52}$. The 300°C spectrum indicates the presence of FeGe, with the Fe atoms having moved towards the sample surface. The 400°C spectrum (not shown) also indicated the presence of FeGe. At 600°C the spectrum height is at a position where $FeGe_2$ formation can be expected.

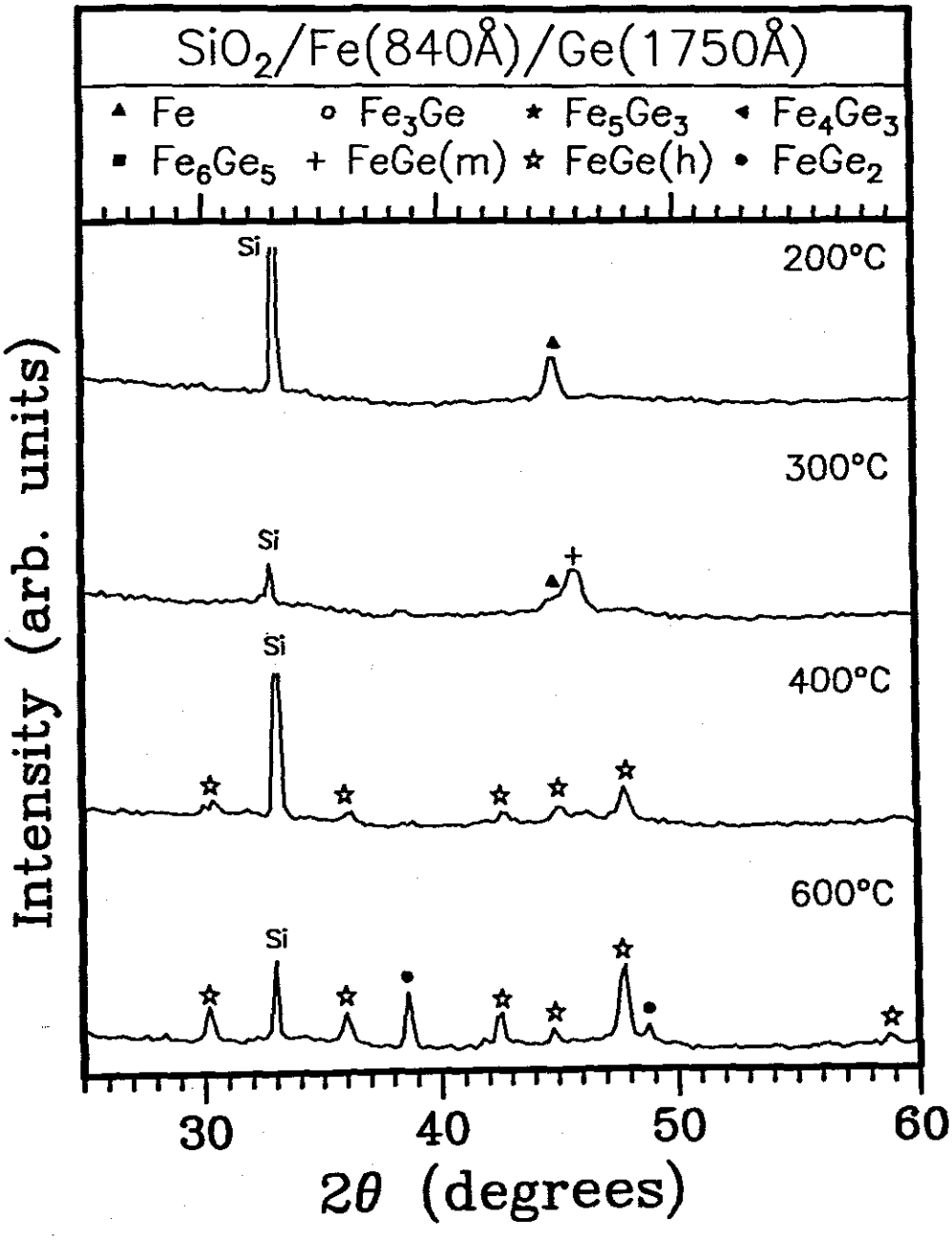

FIGURE 3.11: X-ray diffraction spectra of Si<>/SiO_2/Fe(840Å)/Ge(1750Å) samples annealed at temperatures of 200, 300, 500 and 600°C. The sample annealed at 300°C shows the presence of FeGe in the monoclinic and hexagonal forms. However, for higher temperatures we only see the hexagonal form of FeGe. The spectrum at 600°C shows both FeGe and $FeGe_2$.

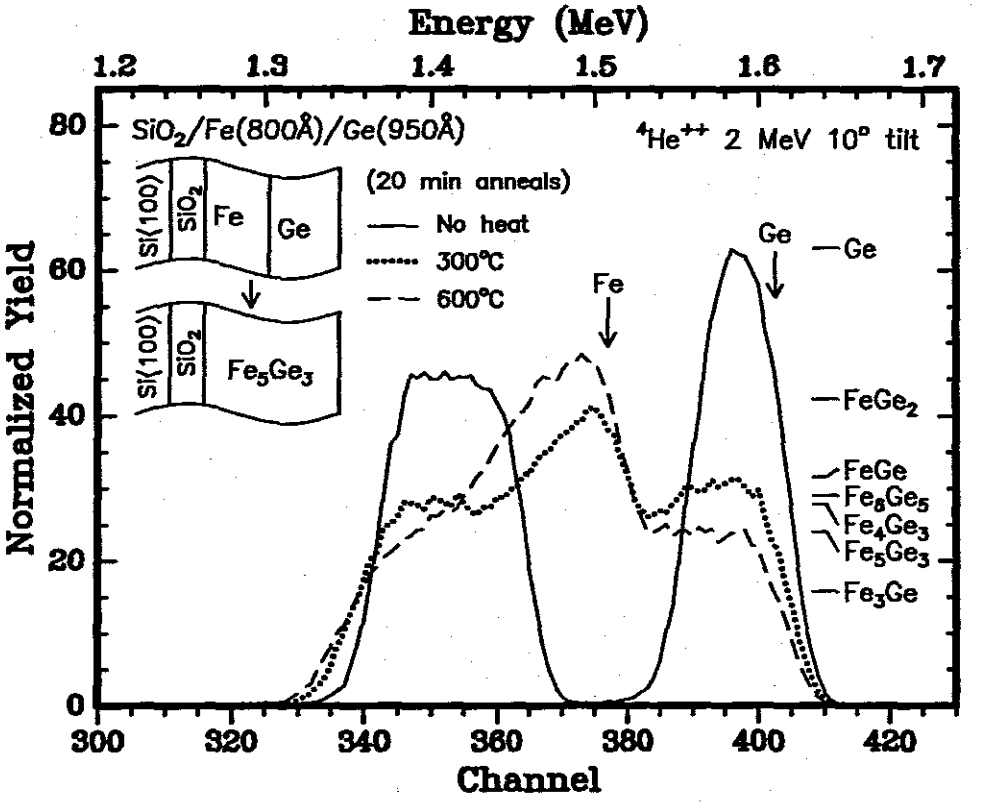

FIGURE 3.12: Backscattering spectra of Si<>/SiO_2/Fe(800Å)/Ge(950Å) samples as-deposited and annealed for 20 minutes at various temperatures. The overall composition of the samples is $Fe_{0.62}Ge_{0.38}$. No interaction for samples annealed at 100°C and 200°C was observed, but interaction was detected for an anneal at 300°C. The height of the signal on the Ge side, indicates formation of FeGe. With a further increase in temperature to 400°C (and higher temperatures) the height of the spectra drops to the composition where Fe_5Ge_3 is expected.

annealed at 100°C and 200°C although the x-ray diffraction shows the presence of FeGe (**Fig. 3.13**). For a sample annealed at 300°C, the height on the Ge signal corresponds to the formation of FeGe, which is the first phase to form. For these samples it can also be seen that the Fe atoms have moved toward the surface (see **Fig. 3.12**). At higher temperatures (>300°), the spectrum height on the Ge signal drops to the composition where Fe_5Ge_3 is expected. Since there is no appreciable change in the heights of these spectra on the Ge signal it can be concluded that Fe_5Ge_3 is the final phase to form. It is interesting to note that s that Fe_5Ge_3 forms very non-uniformly (see **Fig. 3.12**).

Results for the virgin, the 100°C, 300°C and 400°C samples after x-ray analysis are shown in **Fig. 3.13**. The virgin spectrum indicates the presence of Fe, however, the Ge peaks are not present since this layer is amorphous when evaporated. It is interesting to note that at 100°C the first phase to form is FeGe, which is present in a cubic, monoclinic and a hexagonal form. A unique peak belonging to Fe_5Ge_3 can also be seen, which grows stronger with increasing temperature. The 300°C spectrum shows the presence of the monoclinic and hexagonal phases of FeGe as well as Fe_5Ge_3. In many of our results we only observed the monoclinic FeGe phase at about this temperature ($\sim$ 300°C), having apparently missed the cubic and hexagonal forms. At 400°C, peaks belonging only to Fe_5Ge_3 can be seen. The absence of the Ge peaks at 400°C indicates that the Ge has all been reacted in the formation of Fe_5Ge_3. This is also the case for the 600° anneal (XRD spectrum not shown).

Fig. 3.14 shows the Fe-Ge phase diagram as well as phases that were observed experimentally for this system. For samples of overall composition $Fe_{0.20}Ge_{0.80}$ (Fe < Ge) phases observed first were FeGe(monoclinic) together with $FeGe_2$. At a higher temperature only $FeGe_2$ was observed. For the composition $Fe_{0.48}Ge_{0.52}$ (Fe $\approx$ Ge) the phase observed first was FeGe(monoclinic), followed by FeGe(hexagonal) at a higher temperature. At an even higher temperature some $FeGe_2$ was observed. For the case (Fe > Ge) of composition $Fe_{0.62}Ge_{0.38}$ the three FeGe phases were observed simultaneously at 100°C. These were FeGe(monoclinic), FeGe(cubic) and

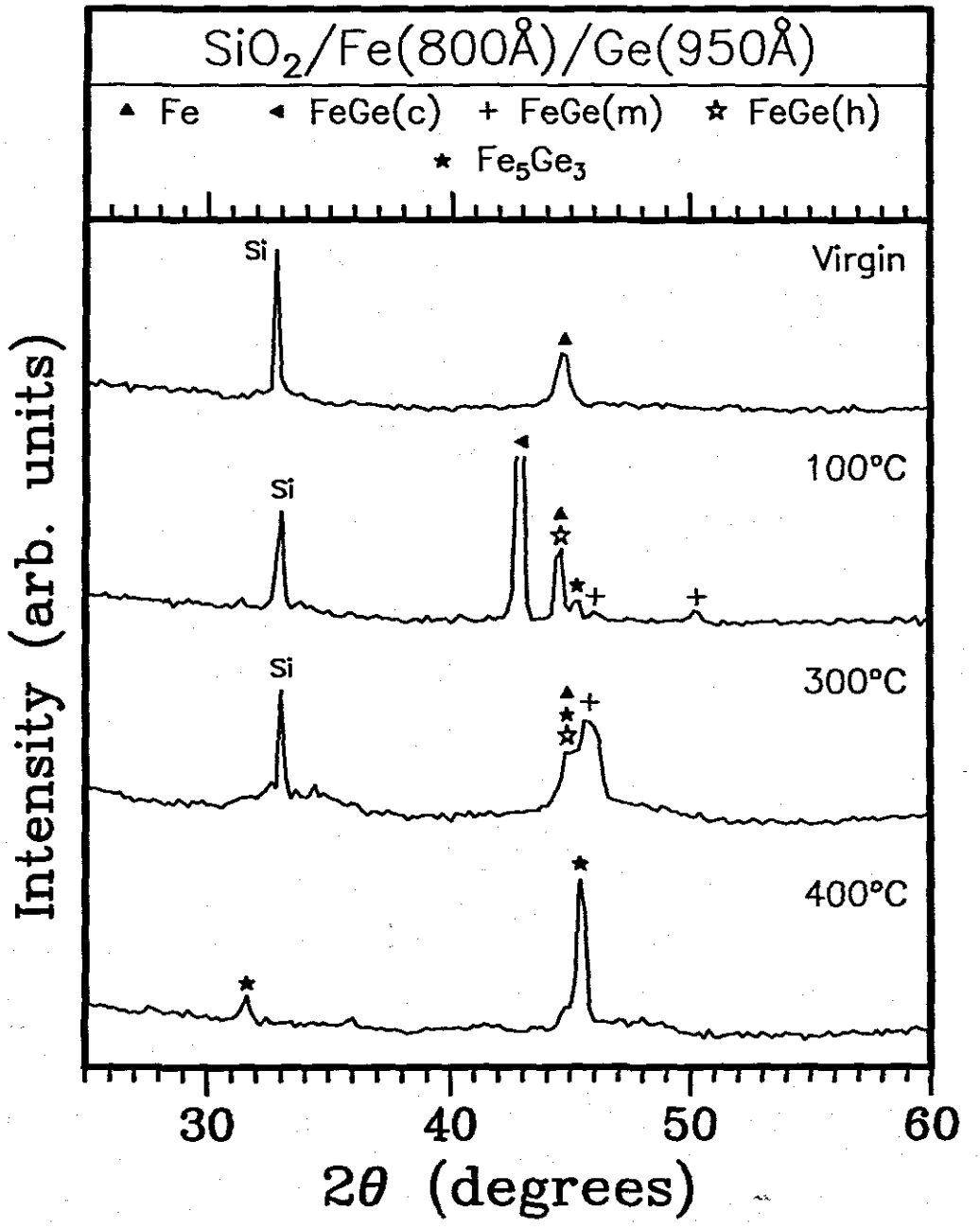

FIGURE 3.13: X-ray diffraction spectra of Si<>/SiO_2/Fe(800Å)/Ge(950Å) samples annealed at temperatures of 100, 300 and 400°C. The sample annealed at 100°C indicates the presence of a cubic, monoclinic and hexagonal form of FeGe, which is also the first phase to form. The 300°C spectrum only shows the monoclinic form of FeGe. At 400° only Fe_5Ge_3 is present in the sample.

	Anneal Temp.	Fe	Fe_5Ge_3	FeGe	$FeGe_2$	Ge
Fe<Ge ($Fe_{0.20}Ge_{0.80}$)	Virgin	X				X(a)
	280°C			X(m)	X	X(a)
	400°C				X	X
	600°C				X	X
Fe~Ge ($Fe_{0.48}Ge_{0.52}$)	Virgin	X				X(a)
	200°C	X				X(a)
	300°C	X		X(m)		
	400°C			X(h)		
	600°C			X(h)	X	
Fe>Ge ($Fe_{0.62}Ge_{0.38}$)	Virgin	X				X(a)
	100°C	X		X(c,m,h)		
	300°C		X	X(m,h)		
	400°C		X			
	600°C		X			

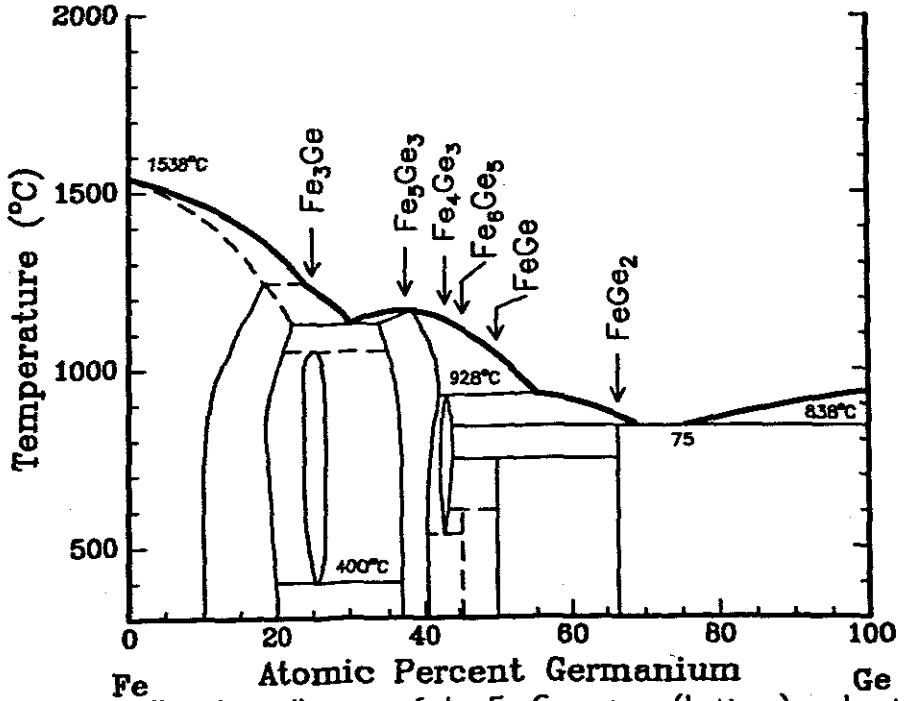

FIGURE 3.14: The phase diagram of the Fe-Ge system (bottom) and a table (top) showing experimentally observed phases in the Fe-Ge system. The observed first phase is FeGe. The range of temperatures (100°C—300°C) over which the first phase is observed may be due to Fe taking up oxygen either during deposition or annealing.

FeGe(hexagonal). At a higher temperature the phase Fe_5Ge_3 was observed. The lowest temperature at which FeGe(c) was observed is 100°C, whereas FeGe(m) was found at about 200°C. The hexagonal form of FeGe was found at about 300°C. It looks as if these phases occur in this order in thin films. According to Pearson's Handbook of Crystallographic Data and Intermetallic Phases [87], the cubic form of FeGe is a low temperature phase which exists below 620°C, the hexagonal form should exist between 630°C and 740°C and the monoclinic phase above 740°C. That FeGe(c) is a low temperature phase agrees with our results. The order in which FeGe(m) and FeGe(h) was observed experimentally does not agree with the information obtained from Pearson's Handbook. The handbook suggest the order FeGe(c), FeGe(h) followed by FeGe(m) as the temperature is raised. We found the order FeGe(c), FeGe(m) and then FeGe(h). This is not suprising because results in this handbook are for bulk samples whereas our results are for the the thin film case.

The two phases Fe_6Ge_5 and Fe_4Ge_3 were not observed experimentally. The reason may be that Fe_4Ge_3 is a high temperature phase and there are doubts as whether Fe_6Ge_5 really exists [16] (see also **Fig. 3.14**). The phase Fe_3Ge was not observed because no samples were Fe-rich enough to form this phase.

Cr-Ge system

In microelectronic fabrication chromium has many uses. It is used as a sacrificial barrier between aluminium and silicon. Thin films (e.g. Al) must be connected to the outside world by solder. Most of these solders are tin-lead alloys. The tin aluminium phase diagram has a eutectic at 232°C and 99,5 at.% tin. This temperature is far below the temperature at which tin-lead alloys become sufficiently fluid enough to effectively wet the aluminium. When soldering is done directly on aluminium an aluminium-tin eutectic melt tends to preferentially dissolve the grain boundaries in the aluminium films, thus creating open circuits. Thin chromium films are effective at separating these materials. Chromium is only slightly soluble in tin-lead solders. The chromium film will also stop any solid-state outdiffusion of aluminium which

could create a eutectic melt at a local hot spot on the metallisation surface. Thus chromium acts as both a sacrificial barrier and a diffusion barrier.

Noble metals like gold, and to a lesser extent copper, form weak bonds with most oxides and so adhesion of thin films of these metals to the surface of the microelectronic circuit can be poor. Intermediate glue layers of chromium(also titanium) can be used to improve adhesion of gold conduction tracks to oxides. Chromium -nickel alloys can be used to make low value resistors. These materials have a resistivity of about $108\mu\Omega$ and are very stable. Chromium also etches quite easily when one uses $Ce(NH_4)_2(NO_3)_6/HClO_4$.

The Cr-Ge system has five equilibrium phases [87]. Crystal parameters for this system are shown in **Table 3.5**. We will now discuss two cases namely Cr<Ge and Cr>Ge.

Cr < Ge

A thin layer of Cr (1200Å) followed by a thicker layer of Ge (4900Å) was deposited on clean oxidized Si. This sample configuration was chosen so as to end with the most Ge rich phase on the Cr-Ge phase diagram, $Cr_{11}Ge_{19}$. After complete formation of $Cr_{11}Ge_{19}$ there should be some unreacted Ge left over. **Fig. 3.15** shows RBS results for samples heated for 30 minutes at different temperatures. There is no observable interaction on the as deposited sample. The sample annealed at 360°C shows some interaction. The step height on the Ge signal indicates the formation of $Cr_{11}Ge_8$. This is the first phase to form. At 400°C the step height is still at a position corresponding to the formation of $Cr_{11}Ge_8$ (spectrum not shown). At this stage there is still unreacted Cr. The sample annealed at 500°C shows that the Cr has been used up, but there is still unreacted Ge. The step height on the Cr signal is almost midway between positions of CrGe and $Cr_{11}Ge_{19}$. It is not possible from this spectrum to say which of these two phases is present in the sample. XRD results of these samples are shown on **Fig. 3.16**. The as deposited sample showed no compound peaks(not shown). At 360°C Ge has re-crystallized. At 400°C peaks belonging to $Cr_{11}Ge_8$ are observed. This is the first phase to form. At 500°C it is observed that Cr has been totally consumed(there are no peaks corresponding

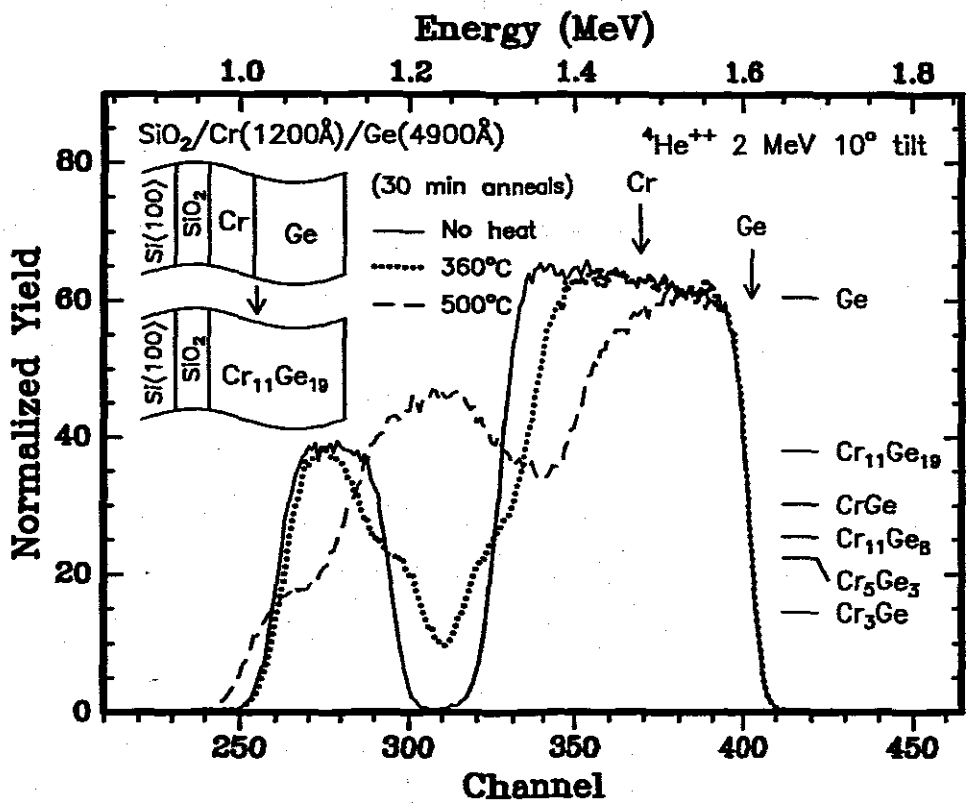

FIGURE 3.15: Backscattering spectra of Si<>/SiO_2/Cr(1200Å)/Ge(4900Å) samples as-deposited and annealed for 30 minutes at various temperatures. The overall atomic composition of the layers were $Cr_{0.31}Ge_{0.69}$, which is close to the compound composition of $Cr_{11}Ge_{19}$. The sample annealed at 360°C has a step height on the Ge signal corresponding to the formation of $Cr_{11}Ge_8$. At 500°C Cr has been completely consumed.

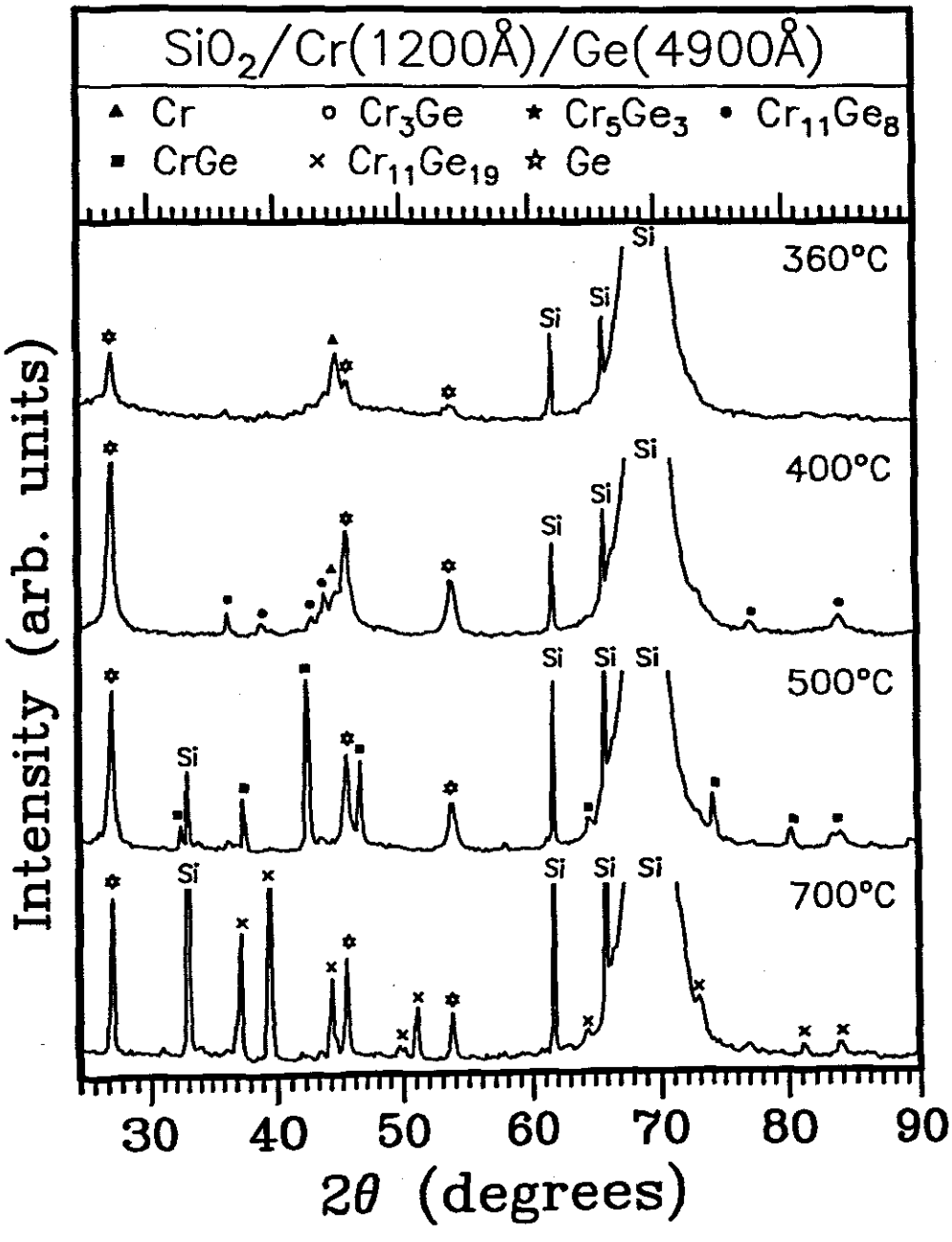

FIGURE 3.16: X-ray diffraction spectra of Si<>/SiO_2/Cr(1200Å)/Ge(4900Å) samples annealed at temperatures of 360, 400, 500 and 700°C. The sample annealed at 360°C shows no compound phase. The one at 400°C indicates the presence of $Cr_{11}Ge_8$. At 500°C one sees peaks belonging to CrGe and non of $Cr_{11}Ge_8$. Cr has been completely consumed. At 700°C there is $Cr_{11}Ge_{19}$ and unreacted Ge.

to Cr). This observation is consistent with the RBS results. At this stage the compound phase $Cr_{11}Ge_8$ has been completely transformed to CrGe. The x-ray spectrum of the sample annealed at 700°C shows peaks belonging to the most Ge-rich phase viz. $Cr_{11}Ge_{19}$ while peaks due to unreacted Ge can still be seen. This Ge must have moved into the $Cr_{11}Ge_{19}$ matrix since Cr lies on the sample surface at this stage(from RBS results which are not shown).

Cr > Ge

Samples made up of Si<>/SiO_2/Cr(2500Å)/Ge(1250Å) were each annealed in vacuum for 30 minutes at various temperatures. Their RBS spectra are shown in

TABLE 3.5: Parameters for the Cr-Ge binary system. The table was compiled with data from reference [87].

Phase	Pearson symbol	Space group	Prototype	$^{a}_{b}_{c}$ (Å)
Cr	cI2	$Im\bar{3}m$	W	2.884
Cr	cP8	$Pm\bar{3}n$	Cr_3Si	4.60
Cr	cP26	$Pm\bar{3}$	Cr	4.588
Cr_3Ge	cP8	$Pm\bar{3}n$	Cr_3Si	4.632
Cr_5Ge_3	tI32	I4/mcm	Si_3W_5	9.413
				4.780
$Cr_{11}Ge_8$	oP76	Pnma	$Cr_{11}Ge_8$	13.171
				4.939
				15.775
CrGe	cP8	$P2_13$	FeSi	4.800
$Cr_{11}Ge_{19}$	tP120	$P\bar{4}n2$	$Mn_{11}Si_{19}$	5.80
				52.34
Ge	cF8	$Fd\bar{3}m$	C(diamond)	5.658

Fig. 3.17. The virgin sample shows no interaction. The signal height for the sample annealed at 400°C shows formation of $Cr_{11}Ge_8$, which is the first phase to form. This sample still has unreacted Ge (and Cr). The sample annealed at 440°C shows that Ge has been completely consumed and that Cr has moved to the sample surface. The signal height for this spectrum is still at a position corresponding to the formation of $Cr_{11}Ge_8$. At 500°C the signal height is at a position corresponding to the formation of Cr_3Ge. There is simply no Ge left, but there is still unreacted Cr. According to the XRD results (see **Fig. 3.18**), no interaction has taken place on the virgin sample. The sample annealed at 400°C has peaks from to $Cr_{11}Ge_8$, which is the first phase to form. This confirms observations obtained using RBS. It can be seen that Ge has re-crystallized. At 440°C there is however no Ge peak, it must have been all used up (RBS results show this fact also and that Cr has moved to the sample surface). There is also a peak that might belong to Cr_5Ge_3 (it's not unique to this phase). At 540°C there are peaks belonging to Cr_3Ge. The peak at 27.4° is at a position where one expects a peak of re-crystallized Ge, but Ge has now been completely consumed, it can therefore only belong to Cr_3Ge. The peak that could possibly corresponding to Cr_5Ge_3 has also grown. RBS results confirm the presence of Cr_3Ge which is the most Cr-rich phase on the phase diagram.

Fig. 3.19 shows the phase diagram as well as phases that were observed in the Cr-Ge system. For the case Cr < Ge of composition $Cr_{0.32}Ge_{0.68}$ the first phase observed was $Cr_{11}Ge_8$. As the temperature was raised the phase CrGe was observed also. Finally at an even higher temperature, $Cr_{11}Ge_{19}$ was observed. For the case Cr > Ge of composition $Cr_{0.79}Ge_{0.21}$ the first phase observed was again $Cr_{11}Ge_8$. At a higher temperature (440°C) Cr_5Ge_3 was observed together with $Cr_{11}Ge_8$. At 540°C all three phases $Cr_{11}Ge_8$, Cr_5Ge_3 and Cr_3Ge were observed.

3.4 Comparison with EHF Predictions

The driving force for phase formation and transformation is the change in Gibbs free energy $\Delta G°$. Because the change in entropy is usually small during solid state reactions, $\Delta G°$ may be approximated by $\Delta H°$, where $H°$ is the heat of formation.

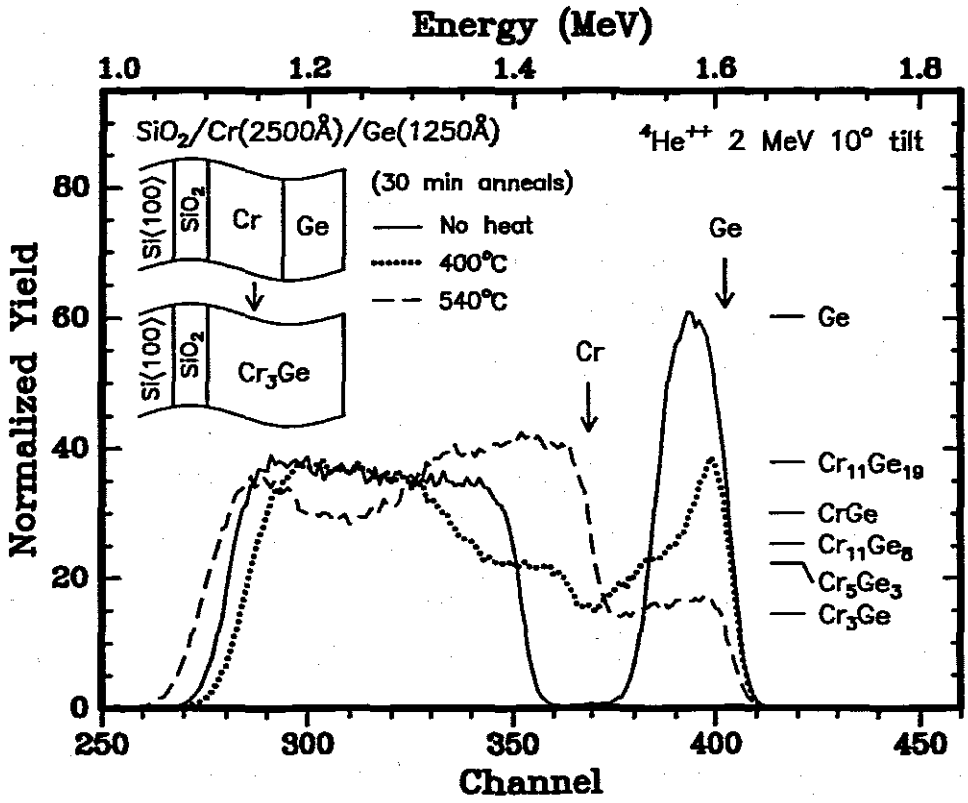

FIGURE 3.17: RBS spectra of Si<>/SiO_2/Cr(2500Å)/Ge(1250Å) samples showing a virgin sample with no interaction; a sample annealed at 400°C whose height ratio on the Ge signal indicates the formation of $Cr_{11}Ge_8$ as the first phase. The final phase is Cr_3Ge depicted by the spectra of the sample annealed at 540°C. Samples have composition $Cr_{0.79}Ge_{0.21}$.

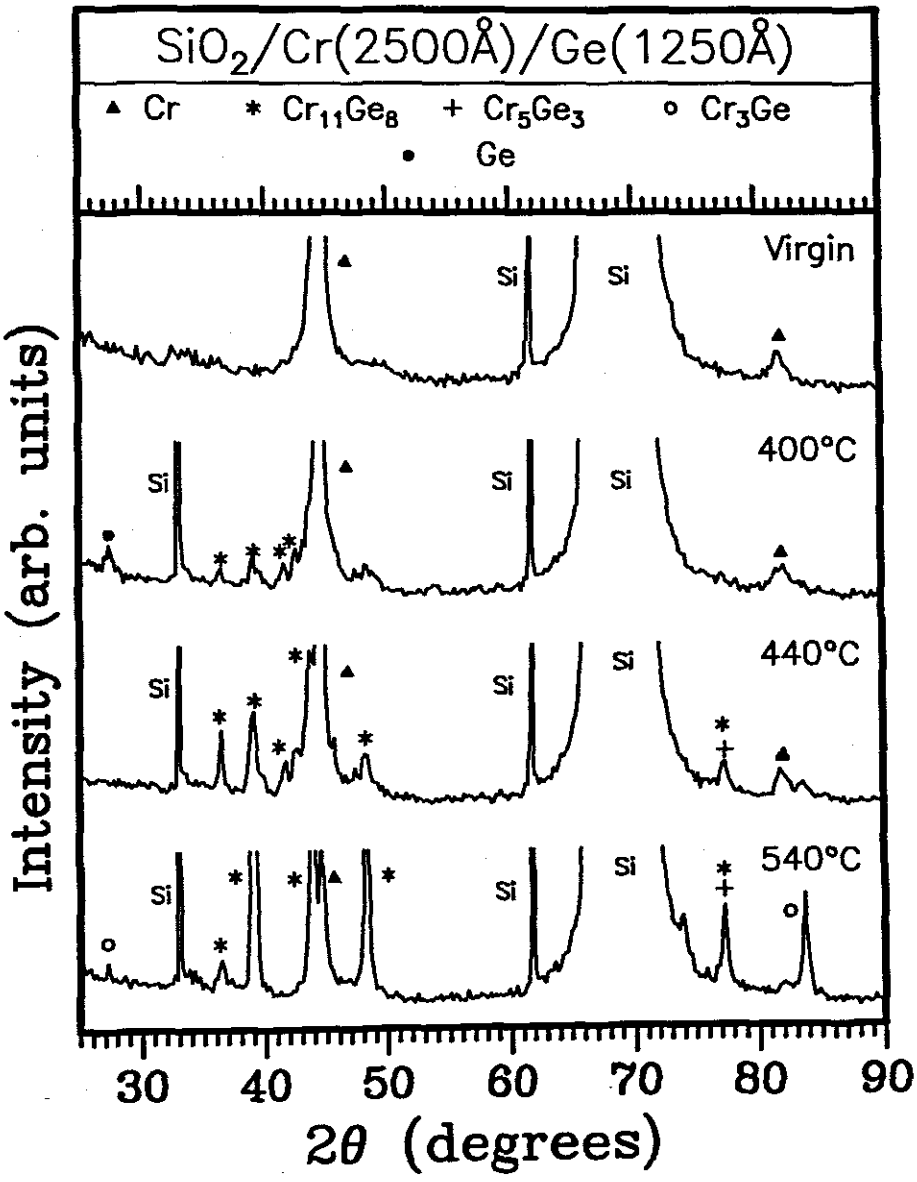

FIGURE 3.18: XRD diffraction spectra of Si<>/SiO_2/Cr(2500Å)/Ge(1250Å) samples showing a virgin sample with no interaction; a sample annealed at 400°C whose peaks indicate the formation of $Cr_{11}Ge_8$ as the first phase. The 440°C spectrum shows that Ge has been completely consumed. There might also be peaks corresponding to Cr_5Ge_3. The spectrum of the sample annealed at 540°C shows the presence of Cr_3Ge.

	Anneal Temp.	Cr	Cr_3Ge	Cr_5Ge_3	$Cr_{11}Ge_8$	CrGe	$Cr_{11}Ge_{19}$	Ge
Cr<Ge	Virgin	X						X(a)
	360°C	X						X
	400°C	X			X			X
($Cr_{0.31}Ge_{0.69}$)	500°C					X		X
	700°C						X	X
	Virgin	X						X(a)
Cr>Ge	400°C	X			X			X
($Cr_{0.79}Ge_{0.21}$)	440°C	X		X	X			
	540°C	X	X	X	X			

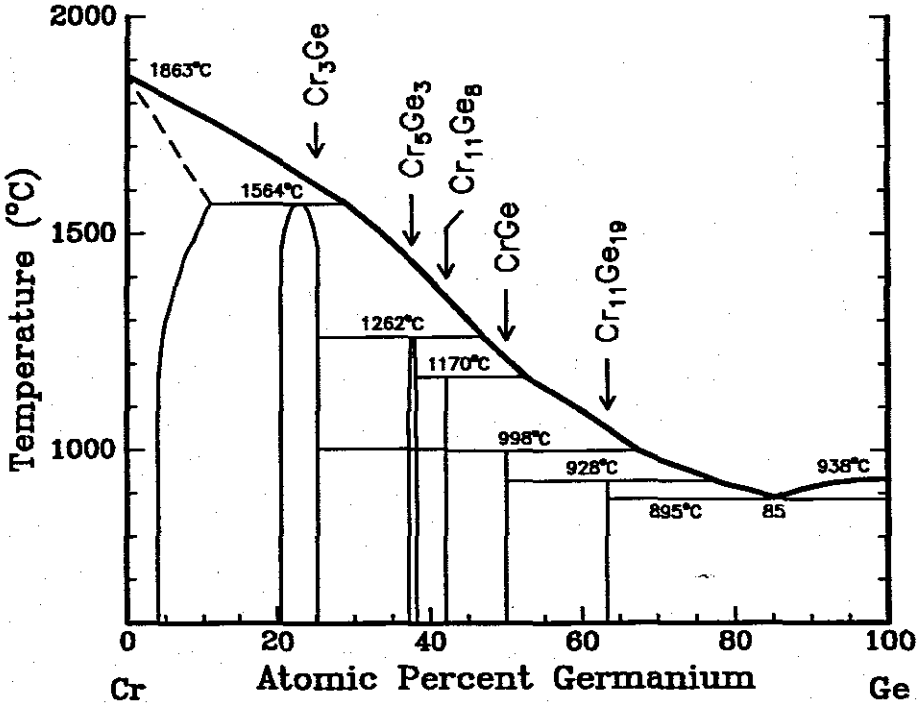

FIGURE 3.19: The phase diagram of the Cr-Ge system (bottom) and a table (top) showing experimentally observed phases in the Cr-Ge system.

TABLE 3.6: Effective heats of formation according to the EHF model. The predicted phase is Ti_5Ge_3. The experimentally observed phase is Ti_6Ge_5.

Phase	Congruency	Composition	$\Delta H°$ kJ/(mol.at)	$\Delta H'$ kJ/(mol.at)	Observed Phase	Predicted Phase	Ref
Liquidus Minimum	=	$Ti_{0.110}Ge_{0.890}$					
Ti_5Ge_3 (16)	C	$Ti_{0.625}Ge_{0.375}$	−59.4	−10.45	Ti_5Ge_3	Ti_5Ge_3	[78]
Ti_6Ge_5 (44)	NC	$Ti_{0.545}Ge_{0.455}$	−64.3	−12.98	Ti_6Ge_5		This work [84]
$TiGe_2$ (24)	NC	$Ti_{0.333}Ge_{0.667}$	−47.5	−15.69			
Liquidus Minimum	=	$Pd_{0.360}Ge_{0.640}$					
Pd_5Ge (24)	NC	$Pd_{0.833}Ge_{0.167}$	−23.8	−10.29			
Pd_3Ge (-)	NC	$Pd_{0.750}Ge_{0.250}$	−35.6	−17.09			
$Pd_{25}Ge_9$ (34)	NC	$Pd_{0.735}Ge_{0.265}$	−37.5	−18.37			
$Pd_{21}Ge_8$ (116)	NC	$Pd_{0.724}Ge_{0.276}$	−38.9	−19.34			
Pd_2Ge (9)	C	$Pd_{0.667}Ge_{0.333}$	−45.3	−24.45	Pd_2Ge		This work [80,78,83,89
PdGe (8)	C	$Pd_{0.500}Ge_{0.500}$	−51.4	−37.01		PdGe	
Liquidus Minimum	=	$Zr_{0.013}Ge_{0.987}$					
Zr_3Ge (32)	NC	$Zr_{0.750}Ge_{0.250}$	−57.4	−0.99			
Zr_5Ge_3 (16)	C	$Zr_{0.625}Ge_{0.375}$	−83.0	−1.73		Zr_5Ge_3	
Zr_5Ge_4 (36)	?	$Zr_{0.556}Ge_{0.444}$	−92.2	−2.16			
ZrGe (8)	NC	$Zr_{0.500}Ge_{0.500}$	−95.8	−2.49	ZrGe		This work
Zr_2Ge (12)	NC	$Zr_{0.333}Ge_{0.667}$	−79.8	−3.12			

The Effective Heat of Formation (E.H.F.) model takes into account both the concentrations of the elements at the interface and the heat of formation. An effective heat of formation $\Delta H'$ is defined which is linked to the concentration [11–15] by:

$$\Delta H' = \Delta H° \times \left(\frac{\textit{effective concentration limiting element}}{\textit{compound concentration limiting element}} \right) \qquad (3.1)$$

and $\Delta H°$ is in Joules per mole of atoms. The effective concentration is taken at the liquidus minimum of the binary system.

3.4.1 Ti-Ge, Pd-Ge and Zr-Ge systems

Table 3.6 summarises first phases observed experimentally and the predictions of the EHF model. The first experimentally observed phase was found to be Ti_6Ge_5. This phase is followed by $TiGe_2$ for samples with a thicker layer of Ge. Work by Thomas *et al* agrees with our results [84]. This group found Ti_6Ge_5 as a first phase followed by $TiGe_2$. Table 3.6 lists effective heats of formation calculated at the concentration of the liquidus minimum of the system, which is at 11 at. %

Ti. The congruent phase with the highest Effective Heat of Formation is Ti_5Ge_3. However as has been mentioned the experimentally found first phase is Ti_6Ge_5 which is non-congruent. The Pd-Ge system has only two congruent phases, namely Pd_2Ge and PdGe. The congruent phase with the largest (most negative) effective heat of formation is PdGe. This is therefore the phase predicted by the EHF model as a first phase. The experimentally found first phase however is PdGe. Both RBS and XRD results showed that the first phase to form in the Zr-Ge system is ZrGe. At higher temperatures both ZrGe and $ZrGe_2$ were observed to occur. An Effective Heat of Formation diagram as well as the phase diagram of the Zr-Ge system is shown in **Fig. 3.20.**

The first phase according to the EHF model should be Zr_5Ge_3 which is a congruent phase. Experimental results however show ZrGe to be the first phase. This is not surprising because ZrGe is slightly non-congruent (the temperature difference for this phase between the liquidus and the peritectic point is about 20°C).

3.4.2 Fe-Ge and Cr-Ge systems

If one makes use of the Miedema model to calculate the heat of formation of the phase $FeGe_2$ (see **Table 3.7**); it is found to be positive(it should be negative). Since this is an existing phase, one suspects that the transformation enthalpy term ΔH^{trans} = 25.00kJ/mole at., which converts a semiconducting element into a hypothetical metallic one in the Miedema model, is too large and it overcorrects in this case. We have therefore chosen a value of 15kJ/mole at. for ΔH^{trans}. The motivation for this also comes from the fact that the heat of reaction that must be obtained when FeGe reacts with Ge to form $FeGe_2$ must be negative. This is not the case if the value of ΔH^{trans} = 25.00kJ/mole at. is used to calculate $\Delta H°$. If however ΔH^{trans} = 15.00kJ/mole at. is used and it is remembered that values of the enthropy term, $T\Delta S$ may lower (make more negative) values of $\Delta G°$ by as much as 3kJ/mole.at.(see **Table 3 of [8]**), then it is found that, the heat of reaction of Ge interacting with FeGe to produce $FeGe_2$ just becomes negative.

$$FeGe + Ge \rightarrow FeGe_2 \tag{3.2}$$

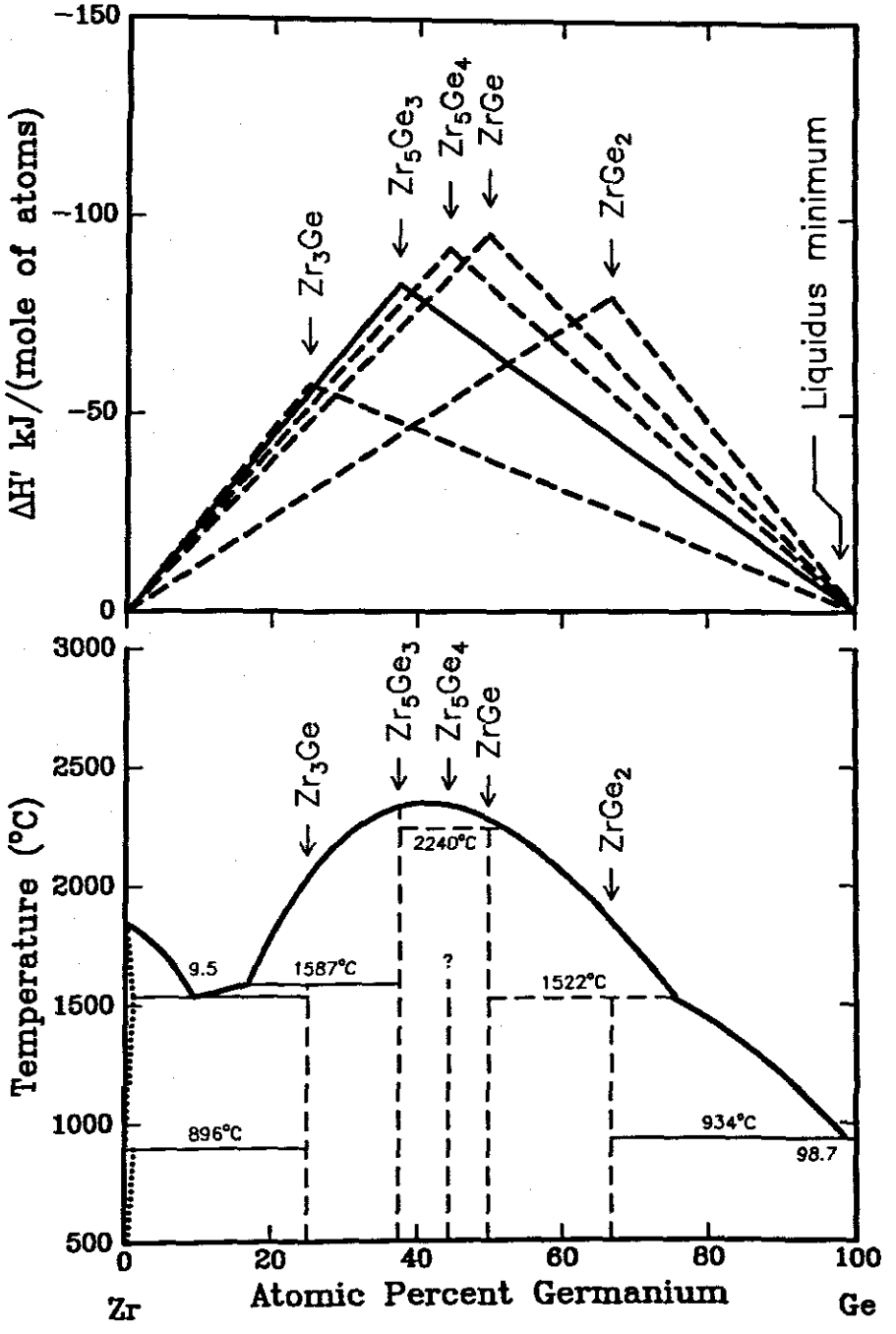

FIGURE 3.20: The phase diagram (bottom) of the Zr-Ge system and the EHF diagram (top)

TABLE 3.7: Heats of formation ($\Delta H°$) and effective heats of formation ($\Delta H'$) calculated with $\Delta H^{trans} = 25.0$ and 15.0kJ(mol.at.)$^{-1}$ for both Fe-Ge and Cr-Ge binary systems. The $\Delta H'$ values have been calculated at the concentration of the lowest temperature eutectic (liquidus) of the binary system. The number of atoms per unit cell are given in brackets behind each phase.

Phase	Congruency	Composition	$\Delta H°$ $\Delta H^{trans} = 25$ kJ(mol.at.)$^{-1}$	$\Delta H°$ $\Delta H^{trans} = 15$ kJ(mol.at.)$^{-1}$	$\Delta H'$ $\Delta H^{trans} = 15$ kJ(mol.at.)$^{-1}$	Observed Phases	ref
Liquidus Minimum	=	$Fe_{0.250}Ge_{0.750}$					
$Fe_3Ge(4)$	NC	$Fe_{0.750}Ge_{0.250}$	−9.1	−11.6	−3.9		
$Fe_5Ge_3(22)$	C	$Fe_{0.625}Ge_{0.375}$	−11.2	−15.0	−6.0		
$Fe_4Ge_3(14)$	NC	$Fe_{0.571}Ge_{0.429}$	−10.8	−15.1	−6.6		
$Fe_6Ge_5(44)$	NC	$Fe_{0.546}Ge_{0.454}$	−10.3	−14.9	−6.8		
FeGe(6,8,16)	NC	$Fe_{0.500}Ge_{0.500}$	−9.0	−14.0	−7.0	FeGe	This work
$FeGe_2(12)$	NC	$Fe_{0.333}Ge_{0.667}$	+0.1	−6.6	−5.0		
Liquidus Minimum	=	$Cr_{0.150}Ge_{0.850}$					
$Cr_3Ge(8)$	NC	$Cr_{0.750}Ge_{0.250}$	−12.1	−14.6	−2.9		
$Cr_5Ge_3(32)$	NC	$Cr_{0.625}Ge_{0.375}$	−15.3	−19.1	−4.6	Cr_5Ge_3	[90]
$Cr_{11}Ge_8(76)$	NC	$Cr_{0.579}Ge_{0.421}$	−15.2	−19.4	−5.0	$Cr_{11}Ge_8$	This work
CrGe(8)	NC	$Cr_{0.500}Ge_{0.500}$	−13.4	−18.4	−5.5		
$Cr_{11}Ge_{19}(120)$	NC	$Cr_{0.367}Ge_{0.633}$	−5.8	−12.2	−5.0		

$$2(-14.0) + (0.0) \rightarrow 3(-6.6 - 3.0) \tag{3.3}$$

which give a heat of reaction of about -1.5kJ/mole.at. Effective Heat of Formation values for the Fe-Ge system have been calculated for $\Delta H^{trans} = 25$ and 15kJ/mole at. and are given in **Fig. 3.21** and **Table 3.7**. When constructing effective heat of formation diagrams, the $\Delta H°$ value is used and plotted at the atomic concentration of a particular compound. Each triangle represents the energy released during the formation of a particular phase, as a function of concentration. $\Delta H'$ is then calculated at the liquidus minimum of the binary system. For the Fe-Ge system the calculated values appear in **Table 3.7**. The predicted phase for this system is FeGe as it has the most negative $\Delta H'$ value (−7.0kJ/mole.at.).

The Cr-Ge system has five equilibrium phases (see **Fig. 3.22**), all of which are non-congruent. It has a well-defined liquidus minimum at 85 at. % Ge. The Effective Heat of Formation diagram for the Cr-Ge system has been calculated for $\Delta H^{trans} = 25$ and 15kJ/mole at. and is given in **Fig. 3.22**.

It can be seen from the Effective Heat of Formation diagram and (see **Table**

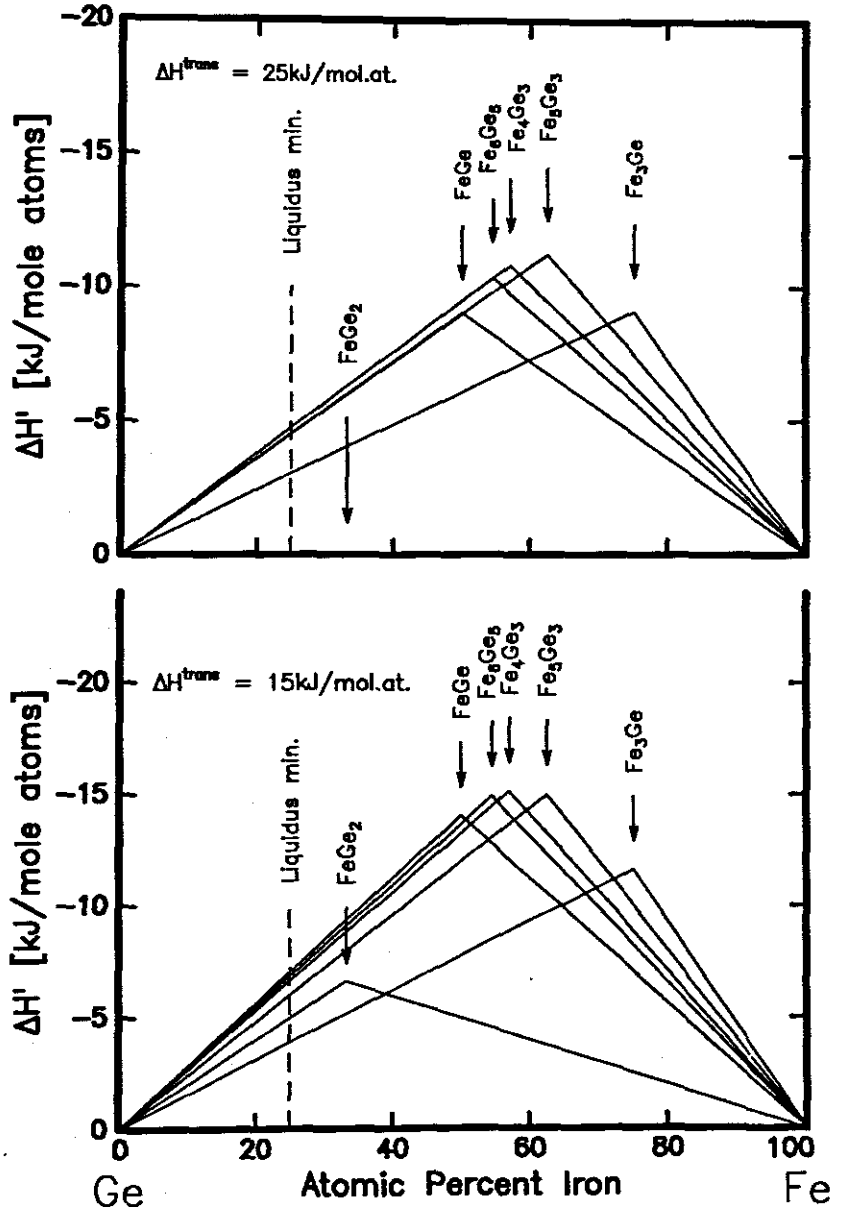

FIGURE 3.21: Effective Heat of Formation diagrams for the Fe-Ge system calculated for $\Delta H^{trans} = 25$kJ/mol.at. and 15kJ/mol.at.

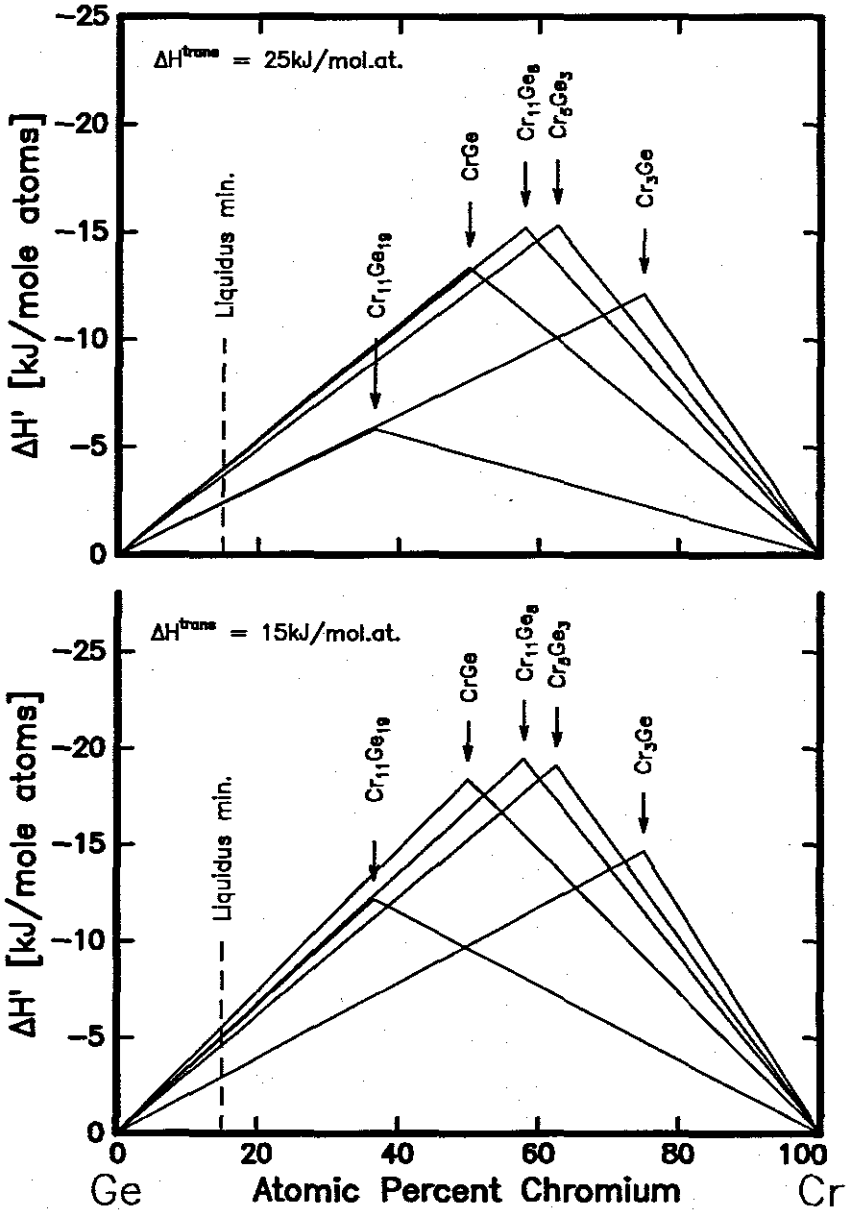

FIGURE 3.22: Effective Heat of Formation diagrams for the Cr-Ge system calculated for ΔH^{trans}=25kJ/mol.at. and 15kJ/mol.at.

3.7) that the phase CrGe has the most negative effective heat of formation. CrGe is therefore predicted by the EHF model to be the first phase.

3.4.3 First phase formation

Table 3.8 gives a comparison between the observed first phase and the phase as predicted by the EHF model. In cases where the binary system does not have congruent phases, for example in the Cu-Ge system, the non-congruent phase with the most negative Effective Heat of Formation forms first, which for this case is Cu_3Ge **[82]**. It is however interesting to note that for Co and Ti some researchers have reported first phase formation of CoGe **[81]** and Ti_6Ge_5 **[84]** which are non-congruent phases with $\Delta H'$ values more negative than the most negative congruent phase (see **Table 3.8**). For metal-metal systems the phase found to form first is the phase with the most negative $\Delta H'$, irrespective of whether it is congruent or non-congruent **[13–15]**. It can be seen (**Table 3.8**) that with the exception of Pd and Zr the agreement between predicted phase and the first phase found experimentally is excellent. The Pd-Ge phase diagram shows that the liquidus minimum and therefore the effective concentration is not well-defined due to the two eutectics at 36 and 81 at.% Pd which have similar temperatures (725°C and 760°C), the more Pd-rich eutectic (760°C) favouring Pd_2Ge **[80, 78, 83]** formation, which is also what was found experimentally by us. In the case of Zr (see **Fig. 4**), ZrGe is probably formed because it is only slightly non-congruent, with a small temperature difference ΔT ($\approx$ 20°C) between the peritectic point and the liquidus curve. Furthermore, it has a more negative $\Delta H'$ than the predicted Zr_5Ge_3 phase.

3.4.4 Phase sequence

To illustrate how the EHF model is used to predict phase formation sequence in germanides, we discuss the Pt/Ge thin film system as an example. In **Fig. 3.23** the Effective Heat of Formation (top) as well as the phase diagram for the Pt-Ge system (bottom) **[16]** is given. After the first phase Pt_2Ge has been completely formed, the evolution of the system further depends on the relative thicknesses of the unreacted

TABLE 3.8: Observed first phase formation and predicted first phase in metal-germanium systems using the Effective Heat of Formation model. In the case of the Fe-Ge and Cr-Ge systems, a value for ΔH^{trans} of 15kJ/mole.at. was used. In other cases the usual value 25kJ/mole.at. was used. The predicted phases are the congruent phases with the most negative $\Delta H'$ at the concentration of the liquidus minimum. The underlined phases are the phases found to form first in this work.

System	Liq. Min. (at.% Ge)	Predicted Phases	Observed Phases	Ref.	Congruency	ΔH° kJ(mol.at.)$^{-1}$	$\Delta H'$ kJ(mol.at.)$^{-1}$
Co	73	Co_5Ge_3	Co_5Ge_3 [a]	[80,81]	C	−19.1	−8.25
			CoGe	[81]	NC	−17.1	−9.23
Cr	85		Cr_5Ge_3	[90]	NC	−19.1	−4.6
			$\underline{Cr_{11}Ge_8}$	This work	NC	−19.4	−5.0
		$\underline{CrGe}$			NC	−18.4	−5.5
Cu	36.5	Cu_3Ge	Cu_3Ge	[82]	NC [b]	−4.20	−3.56
Fe	75	FeGe	$\underline{FeGe}$	This work	NC	−14.0	−7.0
Hf	97	Hf_5Ge_3	Hf_5Ge_3	[80]	C	−73.8	−3.54
Mn	52.5	Mn_5Ge_3	Mn_5Ge_3	[80]	C	−32.8	−24.93
Ni	67	Ni_5Ge_3	Ni_5Ge_3 [c]	[80,78,91]	C	−22.3	−11.77
Pd	64 [d]	PdGe	—		C	−51.4	−37.01
			$\underline{Pd_2Ge}$	This work [80,78,83]	C	−45.3	−24.45
Pt	78	Pt_2Ge	Pt_2Ge	[78,79]	C	−37.9	−34.14
Rh	77	RhGe	RhGe	[80]	C	−30.6	−14.08
Ti	89	Ti_5Ge_3	Ti_5Ge_3	[78]	C	−59.4	−10.45
			$\underline{Ti_6Ge_5}$	This work [84]	NC	−64.3	−12.98
Zr	98.7	Zr_5Ge_3	—		C	−83.0	−1.73
			$\underline{ZrGe}$ [e]	This work	NC	−95.8	−2.49

[a] Also referred to as Co_2Ge [80,81]. [b] No congruent phases. [c] This phase was previously referred to as Ni_2Ge [80,78,91]. [d] Liquidus Minimum not well defined as there are two lowest eutectics (30 at.% Pd and 81 at.% Pd) which have approximately the same temperatures (725°C and 760°C). [e] Only slightly non-congruent ($\Delta T = 20$°C).

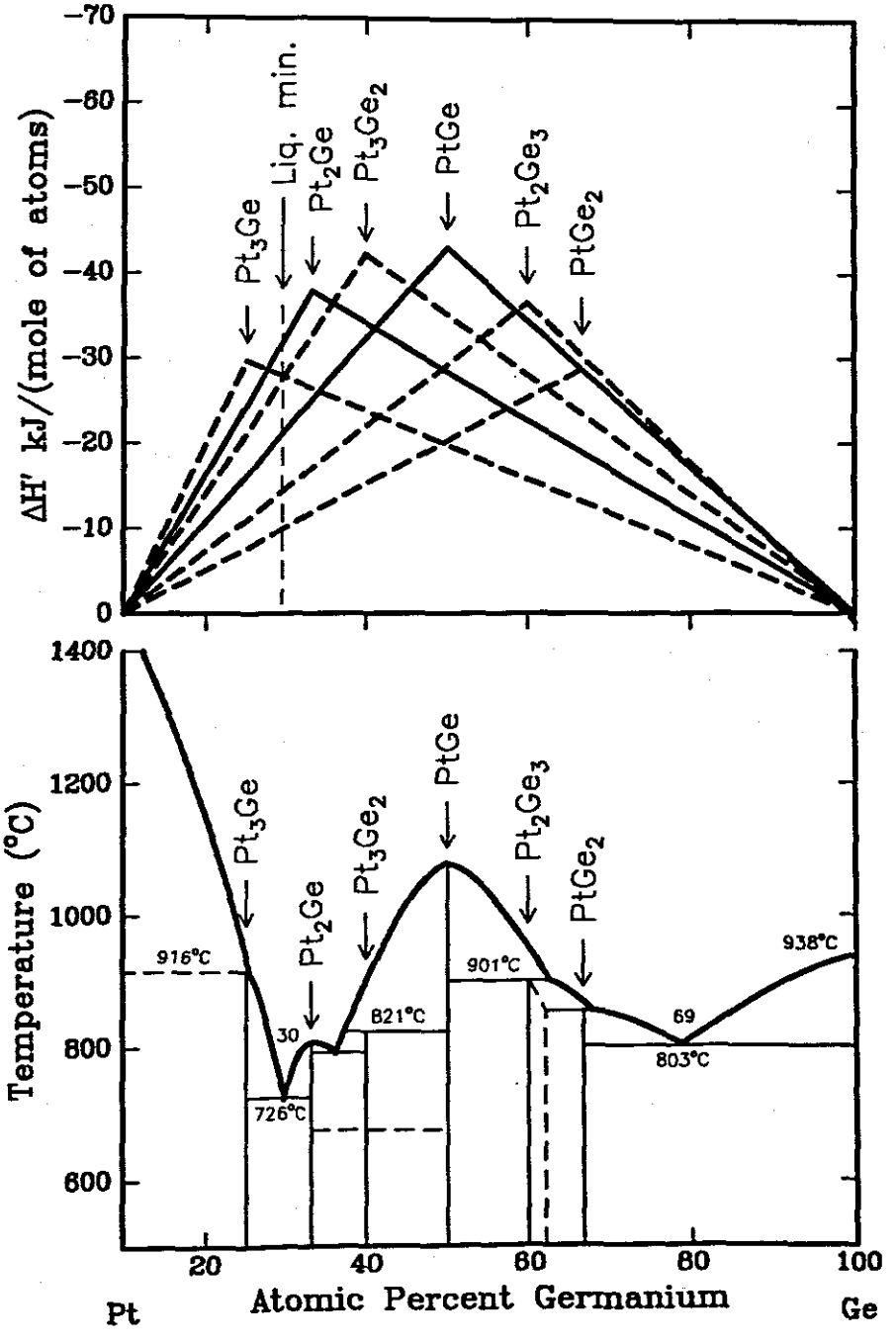

FIGURE 3.23: The phase diagram (bottom) of the Pt-Ge system and the EHf diagram (top)

elements in the sample. Consider the case where Pt $\ll$ Ge. After all the Pt has been used up to form the first phase Pt_2Ge, the effective concentration of the Ge is expected to increase and the relative concentration will move towards the right of the diagram, to a concentration region where formation of Pt_3Ge_2 will lead to the largest change in free energy, and would therefore be predicted to form. When all the Pt_2Ge has been transformed into Pt_3Ge_2, the effective concentration of the atoms at the interface will again move further to the Ge-rich side of the diagram to a concentration region where formation of PtGe can be expected, by interaction between Pt_3Ge_2 and Ge. This process will repeat itself until $PtGe_2$, which is the final phase, is formed.

Each of these phases in the order predicted should form, provided factors such as non-congruency, nucleation barriers, etc. do not inhibit their formation. It was found that in the case of silicides, phases with a large ΔT, tend to be skipped in the sequence [15]. The above argument also holds for the germanides in general. For example, if we look at the Co/Ge system, then the results by Wittmer *et al.* [78] are in agreement with the above phase sequence rule (see **Table 3.9**). However, the results by Hsieh *et al.* [81] indicates the formation of Co_5Ge_7 as the third phase, even though this phase has a $\Delta T \sim 130°C$, compared to $CoGe_2$ with $\Delta T \sim 40°C$. One would therefore have expected Co_5Ge_7 to be skipped and $CoGe_2$ to have formed instead. In the case of the Pt/Ge system, it would have been expected that the phase Pt_2Ge_3 should also have been skipped, since the next phase has a smaller ΔT.

The phase formation sequence found experimentally for the the case Ge>Fe was, FeGe followed by $FeGe_2$. For the case Ge<Fe it was FeGe followed by Fe_5Ge_3. Samples made were not Fe-rich enough to form Fe_3Ge. The first phase found for the Cr-Ge system was $Cr_{11}Ge_8$. For the case Cr<Ge, it was followed by CrGe and finally by $Cr_{11}Ge_{19}$. For the case Cr>Ge, $Cr_{11}Ge_8$ was found first followed by Cr_5Ge_3 and lastly by Cr_3Ge.

TABLE 3.9: Phase sequence in metal-germanium systems (Ge $\gg$ Metal) as predicted by the Effective Heat of Formation model. An experimentally observed phase sequence is also given. Good agreement is found between the two.

Equilibrium Phases		Observed Phases				ΔT
Co-Ge system		Hsieh *et al.* [81]		Wittmer *et al.* [80]		
1st	Co_5Ge_3 [a]	1st	Co_5Ge_3+CoGe	1st	Co_5Ge_3	0°C
2nd	CoGe (16)	2nd	CoGe	2nd	CoGe	80°C
3rd	Co_5Ge_7 (24)	3rd	Co_5Ge_7		—	130°C
4th	$CoGe_2$ (24)	4th	$CoGe_2$	3rd	$CoGe_2$	40°C
Ni-Ge system		Marshall *et al.* [78]		Hsieh *et al.* [91]		
1st	Ni_5Ge_3	1st	Ni_5Ge_3 [b]	1st	Ni_5Ge_3 [b]	0°C
2nd	NiGe (8)	2nd	NiGe	2nd	NiGe	10°C
Pd-Ge system [c]		Hsieh *et al.* [83]		This Work		
1st	Pd_2Ge (9)	1st	Pd_2Ge	1st	Pd_2Ge	0°C
2nd	PdGe (8)	2nd	PdGe	2nd	PdGe	0°C
Pt-Ge system		Hsieh *et al.* [79]		Marshall *et al.* [78]		
1st	Pt_2Ge (9)	1st	Pt_2Ge	1st	Pt_2Ge	0°C
2nd	Pt_3Ge_2 (20)	—		—		80°C
3rd	PtGe (8)	2nd	PtGe	2nd	PtGe	0°C
4rd	Pt_2Ge_3 (20)	3rd	Pt_2Ge_3	3rd	Pt_2Ge_3	50°C
5th	$PtGe_2$ (6)	4th	$PtGe_2$	4th	$PtGe_2$	10°C
Rh-Ge system		Marshall *et al.* [78]				
1st	RhGe (8)	1st	RhGe			0°C
2nd	$Rh_{17}Ge_{22}$	2nd	$Rh_{17}Ge_{22}$			180°C
Ti-Ge system		Marshall *et al.* [78]		This work		
1st	Ti_5Ge_3 (16)	1st	Ti_5Ge_3		—	0°C
2nd	Ti_6Ge_5 [d] (44)	2nd	Ti_6Ge_5	1st	Ti_6Ge_5	190°C
3rd	$TiGe_2$ (24)	3rd	$TiGe_2$	2nd	$TiGe_2$	360°C
Fe-Ge system				This work		
1st	FeGe (6,8,16)			1st	FeGe	300°C
2nd	$FeGe_2$ (12)			2nd	$FeGe_2$	25°C
Cr-Ge system				This work		
1st	$Cr_{11}Ge_8$ (76)			1st	$Cr_{11}Ge_8$	270°C
2nd	CrGe (8)			2nd	CrGe	230°C
3rd	$Cr_{11}Ge_{19}$ (120)			3rd	$Cr_{11}Ge_{19}$	140°C

[a] Also referred to as Co_2Ge [80,81]. [b] This phase was previously referred to as Ni_2Ge [80,78,91]. [c] *Liquidus minimum not* well defined as there are two lowest eutectics which have approximately the same temperatures. [d] This phase was originally identified as TiGe [16], but is given in newer phase diagrams as Ti_6Ge_5 [88].

3.5 Summary and Conclusion

Experiments were done on Ti-Ge, Pd-Ge, Zr-Ge, Fe-Ge and Cr-Ge thin film couples. Phase characterization was done by means of Rutherford Backscattering Spectrometry and by means of X-ray Diffraction Spectrometry. $Ti_6Ge_5$was found experimentally to be the first phase in the Ti-Ge system. In germanides non-congruent phases with more negative Effective Heats of Formation have been found as first phases at times e.g. CoGe in the Co-Ge system [83]. The predicted first phase according to the EHF model is the congruent phase, Ti_5Ge_3. The EHF model agrees in this case with what was found experimentally by Marshall *et. al.* [78], who found Ti_5Ge_3 as a first phase.

In the Pd-Ge system, Pd_2Ge was found as a first phase. The EHF model predicts PdGe as a first phase. If we look, however at the Pd-Ge phase diagram (see **Fig. 8 of [8]**) it is clear that the liquidus minimum and therefore the effective concentration is not well defined, due to the two eutectics at 36 and 81 at. % Pd which have similar temperatures, the more Pd-rich eutectic (760°C favouring Pd_2Ge formation.

In the Zr-Ge system, ZrGe was found as a first phase. The predicted first phase according to the EHF model is Zr_5Ge_3. Note that the experimentally found first phase has a more negative Effective Heat of Formation and is also slightly non-congruent, with a difference in temperature of only 20°C between the peritectoid and the liquidus. Non-congruent germanide phases with more negative Effective Heats of Formation tend to form first in some systems[8].

In this work the phase found to form first in the Fe-Ge system is FeGe. Of the three forms of FeGe, FeGe(cubic), FeGe(monoclinic) and FeGe(hexagonal), the cubic phase has been found to occur at the lowest temperature compared to the other two. It is most likely to be a true first phase. It is followed by FeGe(m) and FeGe(h) at higher temperatures. According to Pearson's Handbook, these phases should occur in the order FeGe(c), FeGe(h) and FeGe(m) as temperature is raised. That FeGe(c) should occur first agrees with this work, but the order of the two

other phases are observed in the reversed order. This is not too suprising because we are dealing with a thin film case here, whereas Pearson's Handbook refers to bulk cases. Heats of formation were calculated using the Miedema model [9], with a ΔH^{trans} of 15kJ/mole.at. The reason for choosing this value is that a ΔH^{trans} of 25kJ/mole.at. (which is usually used in this model) not only leads to a positive value of ΔH° but also gives a large positive value for the heat of reaction calculated for interaction between FeGe and Ge to produce $FeGe_2$. Using a ΔH^{trans} value of 15kJ/mole.at. the EHF model predicts the phase FeGe which we find experimentally to be the first phase. The EHF model predicts that there is thermodynamically not much to choose between FeGe ($\Delta H' = -7.0$) and Fe_6Ge_5 ($\Delta H' = -6.8$). The phase Fe_6Ge_5 was however not observed at all. This is not surprising because there are doubts as to whether this phase exists (see **Fig. 3.14[16]**). The phase formation sequence found for Fe<Ge, was FeGe as a first phase followed by $FeGe_2$. For the case Fe$\simeq$Ge, it was FeGe as a first phase followed by $FeGe_2$. For the case Fe>Ge, FeGe was found first followed by Fe_5Ge_3. Phases Fe_4Ge_3 and Fe_6Ge_5 which should have been observed for the case Fe>Ge were not observed probably because Fe_4Ge_3 is a high temperature phase and there are doubts about the existence of Fe_6Ge_5 according to the phase diagram. No samples were Fe-rich enough to produce the phase Fe_3Ge. According to the EHF model the sequence for the case Fe<Ge should be FeGe followed by $FeGe_2$. This is in agreement with the experimental results. For the case Fe>Ge the EHF model predicts the sequence (if one does not take into account Fe_4Ge_3 and Fe_6Ge_5 for reasons already given) FeGe, Fe_5Ge_3 followed by Fe_3Ge. This is in agreement with experimental results. Fe_3Ge was not observed because samples were not Fe-rich enough to produce this phase.

In the Cr-Ge system the first phase was found to be $Cr_{11}Ge_8$. This does not agree with the results of Lundberg *et. al.* [90] who found Cr_5Ge_3 as a first phase. They could however not index this phase unambiguosly. According to the predictions of the EHF model, the first phase should be CrGe. Such disagreements between experiments by different groups and between experiment and theory can be expected since Cr is a getterer of oxygen, something that may change atomic concentrations

at the growth interface, thus affecting the first phase that forms. It is however very interesting to note that there is according to the EHF model not much to choose thermodynamically between CrGe, $Cr_{11}Ge_8$ and $Cr_{11}Ge_{19}$ (see **Table 1**) especially if it is taken into consideration that thermodynamic quantities are usually not known with accuracies better than 10 %. The phase sequence observed experimentally for Cr-Ge for the case Cr<Ge was $Cr_{11}Ge_8$, CrGe followed by $Cr_{11}Ge_{19}$. For the case Cr>Ge, the sequence observed experimentally was $Cr_{11}Ge_8$, Cr_5Ge_3 followed by Cr_3Ge.

It should be remembered that elements such as Fe, Cr, Ti and Zr have a great affinity for oxygen. Impurities such as oxygen could therefore have a considerable influence on the effective concentration at the growth interface, which could lead to inconsistent results in phase formation.

CHAPTER 4

NUCLEATION AND PHASE SKIPPING IN GERMANIDES

4.1 Nucleation Theory

4.1.1 Metastable Phases

Amorphous thin films are metastable. Nucleation constitutes a barrier that prevents metastable phases from transforming into stable phases (e.g. the failure of diamond to transform to graphite at normal pressure and temperature). Processes that lead to metastable phases are accompanied by changes that happen fast. These may be changes in temperature and /or pressure. Metastable phases that form in thin film reactions, do so at constant temperature and pressure. These reactions are relatively slow. The big question then is, if temperature and pressure are kept constant, what is it that is varied to produce metastable phases in thin film reactions.

According to general theories of thermodnamics a change in Gibbs function may be written as

$$dG = -SdT + VdP + \sum_i \mu dN_i \tag{4.1}$$

where S is the entropy, T the temperature, V the volume, P the pressure, μ the chemical potential and N the number of particles per unit volume. If it is a binary

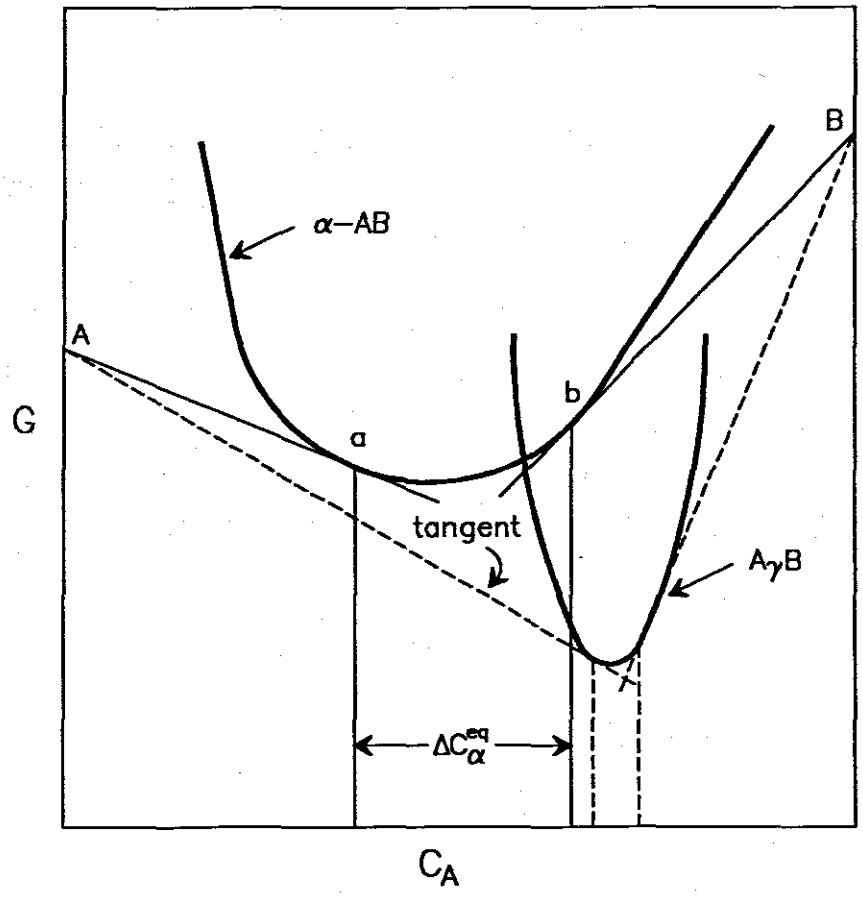

FIGURE 4.1: Variation of the Gibbs energy as a function of composition C in a binary system of A and B forming an amorphous alloy α-AB and an intermetalic compound $A_\gamma B$. [92]

system at constant pressure and temperature then

$$dG = (\mu_2 - \mu_1)dN \tag{4.2}$$

with $N_1 + N_2 =$ constant. N is a variable, and the reaction will happen in a direction towards equilibrium.

$$\frac{dG}{dN_1} = 0 \tag{4.3}$$

i.e. the reaction seeks a minimum in the free energy versus composition curve $G = G(c_1)$ where $c_1 = N_1/N_1 + N_2$ [92]. There can be several minima in the $G(c_1)$ curve. **Fig. 4.1** is a free energy versus composition diagram for a binary system of A and B. The free energy curves of an amorphous alloy α–AB and an intermetallic compound, $A_\gamma B$ are shown in this diagram. The composition limits of the product

phase is defined by tangents extending from a point of the free energy curve to the chemical potential of the element A or B. It is not possible to go from the elements to the amorphous alloy or the intermetallic compound by a continuous change in composition. Such a process requires free energy to decrease all the time, but part of the curve goes up in energy as composition changes. The same is true for the transition between the amorphous alloy and the compound. Formation of the alloy or compound can only occur by a jump from one composition to the other, i.e. by nucleation. The nucleation barrier may be different for different phases, therefore the stable phase or phases which have the largest free energy change is not necessarily the one with the lowest nucleation barrier. If the amorphous alloy can nucleate preferentially and can grow rapidly, then we have solid phase amorphization **[92]**

4.1.2 Solid phase amorphization

An amorphous solid is a one without long range order. In some cases (e.g. Si) the first neighbour covalent bond lengths may remain unchanged. The first neighbours around a certain atom form a tetrahedron, like in the crystal, but the angles between the tetrahedra are not fixed, and this lead to a loss of long range order **[92]**. In general amorphous thin films are made by ultrafast processes, in which there is rapid change in temperature, (e.g. quenching of a liquid alloy or vapour deposition of a thin film on a cold substrate, ion implantation, etc.) In these processes there is a rapid change in temperature, pressure or composition. These are accompanied by a high rate of energy change. Cases discussed here are the formation of alloys by a slow reaction of bilayer thin films. The rate of energy change is slow. The free energy change ΔG of the reactions that lead to the formation of amorphous layers from crystalline films must be negative. **Fig. 4.2** shows reaction paths and energy changes in a bilayer thin film of A and B, which reacts to form either metastable phase α−AB or an equilibrium intermetallic compound $A_\gamma B$. The broken line represents the reaction path leading to the metastable phase with a kinetic barrier of ΔH_1 (per atom) and an energy change of ΔG_1 (per atom). The solid line represents the reaction path leading to the stable (equilibrium) phase with a kinetic barrier of ΔH_o

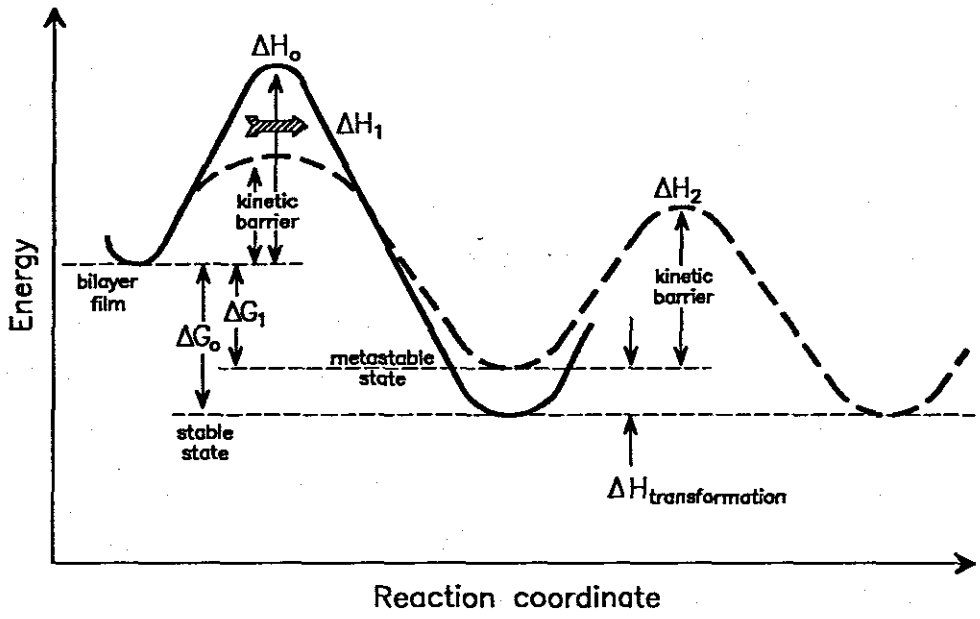

FIGURE 4.2: Reaction paths and energy changes in a bilayer thin film of A and B, which reacts to form either metastable phase α–AB or an equilibrium intermetallic compound $A_\gamma B$. The broken line represents the reaction path leading to the metastable phase with a kinetic barrier of ΔH_1 (per atom) and an energy change of ΔG_1 (per atom). The solid line represents the reaction path leading to the stable (equilibrium) phase with a kinetic barrier of ΔH_0 and an energy change of ΔG_0 (adapted from [92]).

and an energy change of ΔG_0. ΔH_0 is greater than ΔH_1 by assumption.

ΔH_0 and ΔH_1 are taken to be the activation energy barriers of nucleating the critical nuclei of the stable phase and of the amorphous phase, respectively. The ratio of their nucleation numbers according to K.N. Tu *et.al.* [92] are:

$$\frac{N_0}{N_1} = \exp[-\frac{(\Delta H_0 - \Delta H_1)}{kT} \tag{4.4}$$

where $\Delta H_0 = A_0(\gamma_0)^3/(\Delta G_0)^2$ $\Delta H_1 = A_1(\gamma_1)^3/(\Delta G_1)^2$, A_0 and A_1 are geometrical shape factors and γ_0 and γ_1 are the average surface energy per atom of the critical nuclei of the stable and amorphous phases, respectively. The ratio can be put in the form

$$\frac{N_0}{N_1} = \exp(-[\frac{A_0\gamma_0^3}{\delta G_0^2 kT}[1 - \frac{A_1}{A_0}(\frac{\gamma_1}{\gamma_0})^3(\frac{\Delta G_0}{\Delta G_1})^2]]) \tag{4.5}$$

ΔG_o and ΔG_1 are the driving forces of the reactions, thus the condition of the metastable phase formation is that the magnitude of ΔG_1 should be close to that of ΔG_o, so that kinetics rather than the driving force dominates the reaction. Since it has been assumed that $\Delta H_o > \Delta H_1$, then it follows that $\gamma_o > \gamma_1$, and thus $N_1 > N_o$ (if one neglects the ratio of the shape factors). The kinetic barrier ΔH_2 (see **Fig. 4.2**) prevents the transformation of the metastable phase into another phase.

The amorphous phase, according to this view **[92]**, will nucleate because its barrier is lower than that of the crystalline phase.

4.1.3 The critical nucleus

To form a critical nucleus of N atoms **[92]**, the energy change ΔH_N is

$$\Delta H_N = -N\Delta H_{AC} + bN^{\frac{2}{3}}\gamma_{AC} \tag{4.6}$$

where ΔH_{AC} and γ_{AC} are the heat (per atom) of amorphous-to-crystalline transformation and interfacial energy (per atom) between the crystalline and the amorphous phases, respectively. The geometric constant b depends on the shape of the nucleus (see **Fig. 4.3**).

$$\frac{\partial \Delta H_N}{\partial N} = 0 \tag{4.7}$$

thus

$$\Delta H_N = \frac{4b^3}{27}\frac{\gamma_{AC}^3}{\Delta H_{AC}^2} \tag{4.8}$$

The number of atoms in the critical nucleus is

$$N_{crit} = \frac{8b^3}{27}\left(\frac{\gamma_{AC}}{\Delta H_{AC}}\right)^3 = \frac{2\Delta H_N}{\Delta H_{AC}} \tag{4.9}$$

i.e. N_{crit} does not depend explicitly on b. From **eq.4.8** we get

$$b\gamma_{AC} = \left(\frac{27\Delta H_N \Delta H_{AC}^2}{4}\right)^{\frac{1}{3}} \tag{4.10}$$

N_{crit} and $b\gamma_{AC}$ can be determined if ΔH_N and ΔH_{AC} are known. In most cases N_{crit} is about equal to the number of atoms in a unit cell **[92]**.

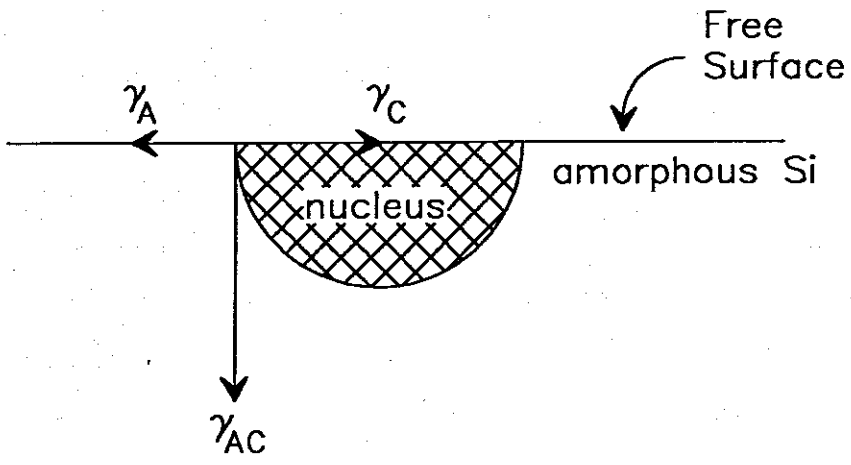

FIGURE 4.3: Heterogeneous nucleation of a nucleus on the free surface of an amorphous thin film [92].

4.2 Factors Affecting Nucleation

It has been observed that layer thicknesses of growing phases follow a linear dependance with time, if the interaction is reaction limited. If the interaction is diffusion-limited then layer thicknesses show a square root dependance with time. Several cases of silicide formation which are reaction-limited have been found to be reaction-controlled. Well known examples are NiSi→$NiSi_2$, RhSi→Rh_4Si_5 and MnSi→$Mn_{11}Si_{19}$. An excellent review of these transitions involving nucleation controlled silicide formation has been given by d'Heurle [93]:

1. Nucleation effects will be more prominant whenever the heat of reaction ΔH_R is small or nearly zero.

2. The small temperature range over which nucleation reactions occur requires a positive entropy so that the free energy change can become negative.

3. Compound phase formation in these reactions start at a specific nucleation site with rapid growth towards the surface, in the case of thin films, thereafter followed by lateral growth. The growth morphology of the sample surface makes

the sample look dull and wavy-like. This is characteristic of a discontinuous localized process.

4. A small heat of reaction and therefore nucleation controlled growth is likely to occur wherever a transition from one phase to the next results in a small change in composition e.g. RhSi→Rh_4Si_5.

Nucleation barriers may also prevent some phases from forming. Pretorius *et. al.* [94] has given these additional factors as those that might influence phase formation.

- Phases with large numbers of atoms per unit cell, might have difficulty in nucleating. In the Pt-Al system Pt_2Al_3 with $\Delta H' = -4.75$ is found to form first even though Pt_5Al_{21} has $\Delta H' = -5.94$kJ(mol.at.)$^{-1}$. Pt_5Al_{21} has 416 atoms per unit cell whereas Pt_2Al_3 has only 5 atoms per unit cell.
- Some crystal structures may be complex and might not nucleate as easily as others.
- Nucleation should be easier at higher temperatures due to greater mobility of the atoms.
- Non-congruent phases of the silicides and germanides do not nucleate easily. On the other hand metal-metal systems are found to nucleate readily.
- Directionality of bonds is thought to play a role in the phase formation of germanides and silicides.

All the factors mentioned above can contribute to a barrier for nucleation and the time available for nucleation thus becomes important. This is best illustrated in **Fig. 4.4.** If the system is in an initial state G_I it can lower its free energy to a value G_A by forming compound A or to a lower energy state by forming the compound B. However, if the nucleation barrier to form B is larger than that for forming A, formation of A after a time Δt_1 will lead to a larger free energy change than the formation of B. It is claer that for the equilibrium case, where the time available for nucleation Δt is infinity, formation of B and not A will lead to the biggest free energy change.

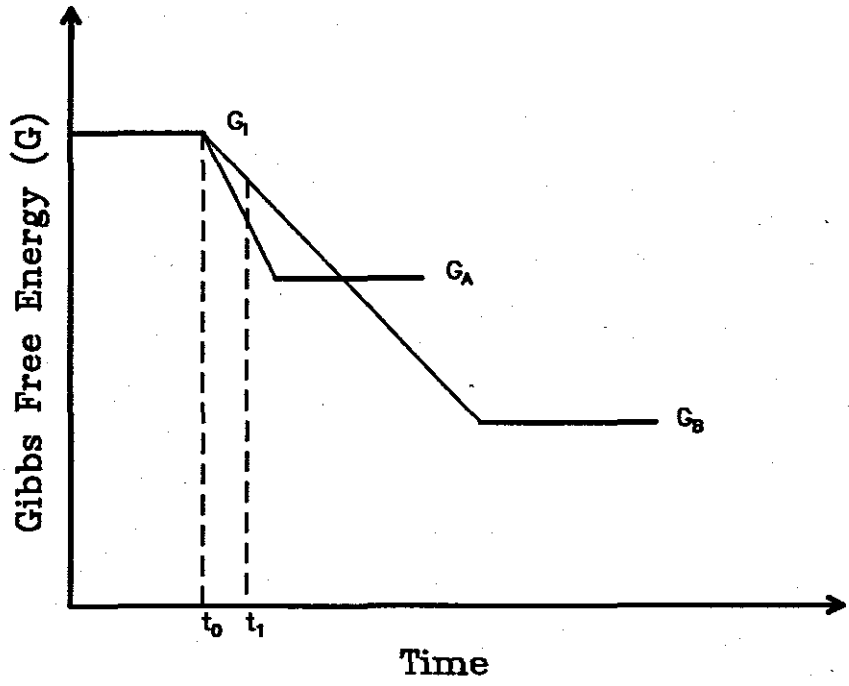

FIGURE 4.4: A system which has an initial energy G_I can lower its free energy to a value G_A by forming compound A or to a lower energy state G_B by forming compound B. If the nucleation barrier to form B is larger than to form A, then formation of A after a time t_1 will lead to a larger free energy change than formation of B.[8].

4.3 Nucleation of Congruent and Non-congruent Phases

4.3.1 Metal-metal systems

Congruency and directionality of bonds could somehow be interrelated. Congruency seems to play a role in phase formation where there are directional bonds. It is known that in metal-metal systems, congruency or non-congruency of phases does not seem to count when phase formation occurs. Non-congruent metal-metal phases seem to nucleate just as easily as congruent phases. The rule for predicting phase formation in metal-metal systems using the Effective Heat of Formation model[11] is:

The first phase to form during metal-metal interaction is the phase with the most negative effective heat of formation at the concentration of the liquidus mini-

mum of the binary system.

This rule works very well for metal-metal systems.

4.3.2 Metal-silicon systems

Silicon forms directional bonds with other atoms due to the sp^3 hybridisation of silicon. In metal-silicon systems congruency plays a decisive role in the formation of phases. The rule for predicting first phase formation in metal-silicon systems according to the EHF model [**11, 12, 8, 95, 96**] is:

The first compound to form during metal-silicon interaction is the congruent phase with the most negative effective heat of formation at the concentration of the liquidus minimum of the binary system.

This rule is followed very closely by metal-silicon systems.

4.3.3 Metal-germanium systems

Germanium is more metallic than silicon. The rule for first phase formation in metal-germanium systems according to the EHF model [**11, 12, 8, 95, 96**]is:

The first phase to form in metal-germanium systems is either the congruent phase or the non-congruent phase with the most negative effective heat of formation at the concentration of the liquidus minimum of the binary system.

Though congruent phases are more favoured in metal-germanium systems than non-congruent phases, there are cases where non-congruent phases have been found to form first. Well known examples include the Co-Ge system where CoGe has at times been found to form first. CoGe is non-congruent and has a more negative effective heat of formation than the congruent phase Co_5Ge_3 [**81**]. If one examines **Table 4.1**, one notices that for these three systems, Hf-Ge, Ni-Ge and Ti-Ge, there are non-congruent phases with more negative effective heats of formation than the congruent phases. The question to ask is: Is it possible to nucleate these non-congruent phases first? In this investigation this was attempted in the Ni-Ge and Ti-Ge systems by heating at low temperatures for long times.

TABLE 4.1: Effective heats of formation calculated for some germanide systems which have non-congruent phases with more negative Effective Heat of Formation values than the congruent phases in the same binary system.

System	Congruency	Composition	$\Delta H'$ $kJ(mol.at)^{-1}$	Predicted Phase	Observed Phase	Ref
Liquidus Minimum	=	$Hf_{0.030}Ge_{0.970}$				
Hf_3Ge (32)	NC	$Hf_{0.750}Ge_{0.250}$	−2.05			
Hf_2Ge (12)	NC	$Hf_{0.667}Ge_{0.333}$	−3.01			
Hf_5Ge_3 (16)	C	$Hf_{0.625}Ge_{0.375}$	−3.54	Hf_5Ge_3	Hf_5Ge_3	[80]
Hf_3Ge_2 (10)	NC	$Hf_{0.600}Ge_{0.400}$	−3.86			
HfGe (-)	NC	$Hf_{0.500}Ge_{0.500}$	−5.07			
$HfGe_2$ (12)	NC	$Hf_{0.333}Ge_{0.667}$	−6.21			
Liquidus Minimum	=	$Ni_{0.330}Ge_{0.670}$				
Ni_3Ge (4)	C	$Ni_{0.750}Ge_{0.250}$	−7.74			
Ni_2Ge (12)	NC	$Ni_{0.667}Ge_{0.333}$	−10.60			
Ni_5Ge_3 (4 or 32)	C	$Ni_{0.625}Ge_{0.375}$	−11.77	Ni_5Ge_3	Ni_5Ge_3	[78,80,91]
NiGe (8)	NC	$Ni_{0.500}Ge_{0.500}$	−13.40			
Liquidus Minimum	=	$Ti_{0.110}Ge_{0.890}$				
Ti_5Ge_3 (16)	C	$Ti_{0.625}Ge_{0.375}$	−10.45	Ti_5Ge_3	Ti_5Ge_3	[78]
Ti_6Ge_5 (44)	NC	$Ti_{0.545}Ge_{0.455}$	−12.98		Ti_6Ge_5	[84]
$TiGe_2$ (24)	NC	$Ti_{0.333}Ge_{0.667}$	−15.69			

4.4 Ni-Ge Binary System

Thin layers of Ni and Ge were deposited without breaking vacuum, on Si< 100 > covered with SiO_2. The thickness of the oxide was more than 4000Å. A sample configuration of SiO_2/Ni(1700Å)/Ge(1000Å) was prepared. The SiO_2/Ni/Ge samples were annealed for two days in vacuum. The vacuum was better than 10^{-7}kPa. Samples were analysed using Rutherford Backscattering Spectrometry (RBS). The RUMP (Rutherford Backscattering Utilities and Manipulation Program) was used to determine thicknesses and phases formed. Phase identification was also carried out with X-ray diffraction (XRD).

4.4.1 Results

The aim of this experiment was to see whether it is possible to nucleate the non-congruent phase NiGe as a first phase. Non-congruent phases are known to nucleate first in metal-germanide systems at times, especially when they have effective heats

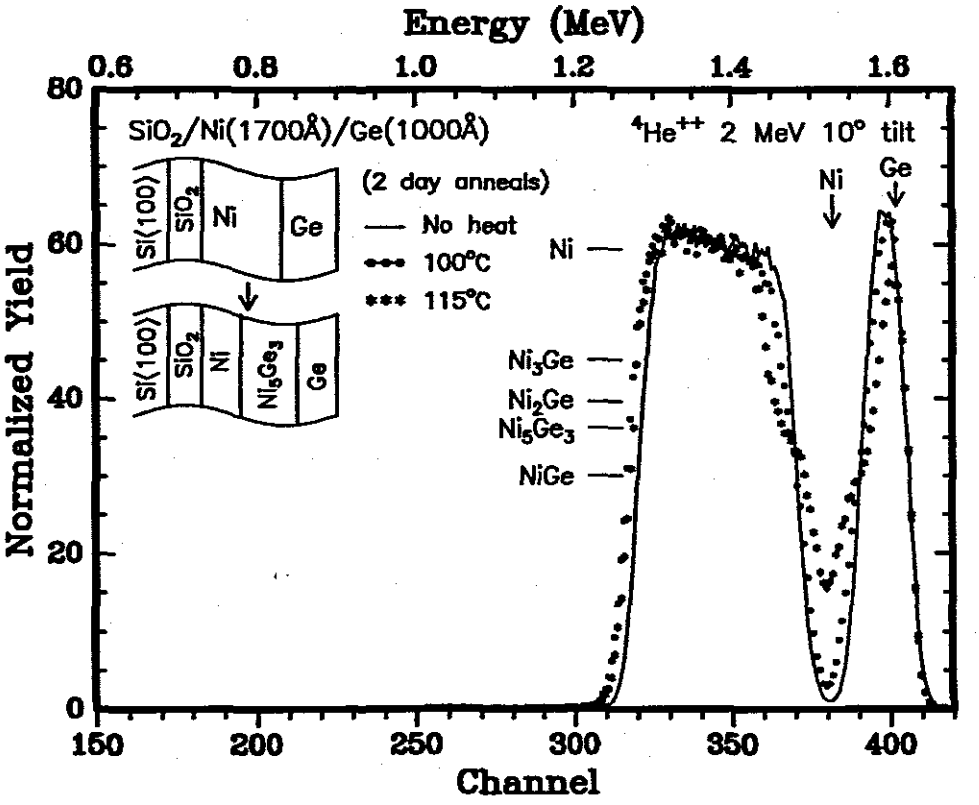

FIGURE 4.5: Backscattering spectra of Ni-Ge samples. They are made up of Si<>/SiO_2/Ni(1700Å)/Ge(1000Å). The step height on the Ni signal of the sample annealed at 115°C correspond to that of the phase Ni_5Ge_3. The 100°C as well as the spectrum of the as deposited sample show no interaction.

of formation which are much more negative than congruent phases in the same binary system [8]. In these experiments by annealing at a low temperature for a long time (2 days) the velocity of the growth interface is lowered, thus giving more chance to the non-congruent phase to nucleate.

Results obtained after RBS analysis are shown in Fig. 4.5 together with corresponding heights on the Ni signal. The as-deposited as well as the sample annealed at 100°C show no interaction. The signal height on the sample annealed at 115°C show the formation of Ni_5Ge_3. It is found that even if the temperature is lowered in this system, the first phase is still Ni_5Ge_3.

XRD results are shown in Fig. 4.6. The spectrum corresponding to the as deposited sample, show that Ni has crystallised. The sample annealed at 100°C for 2 days has no peaks corresponding to any compound phase of the Ni-Ge binary system. The

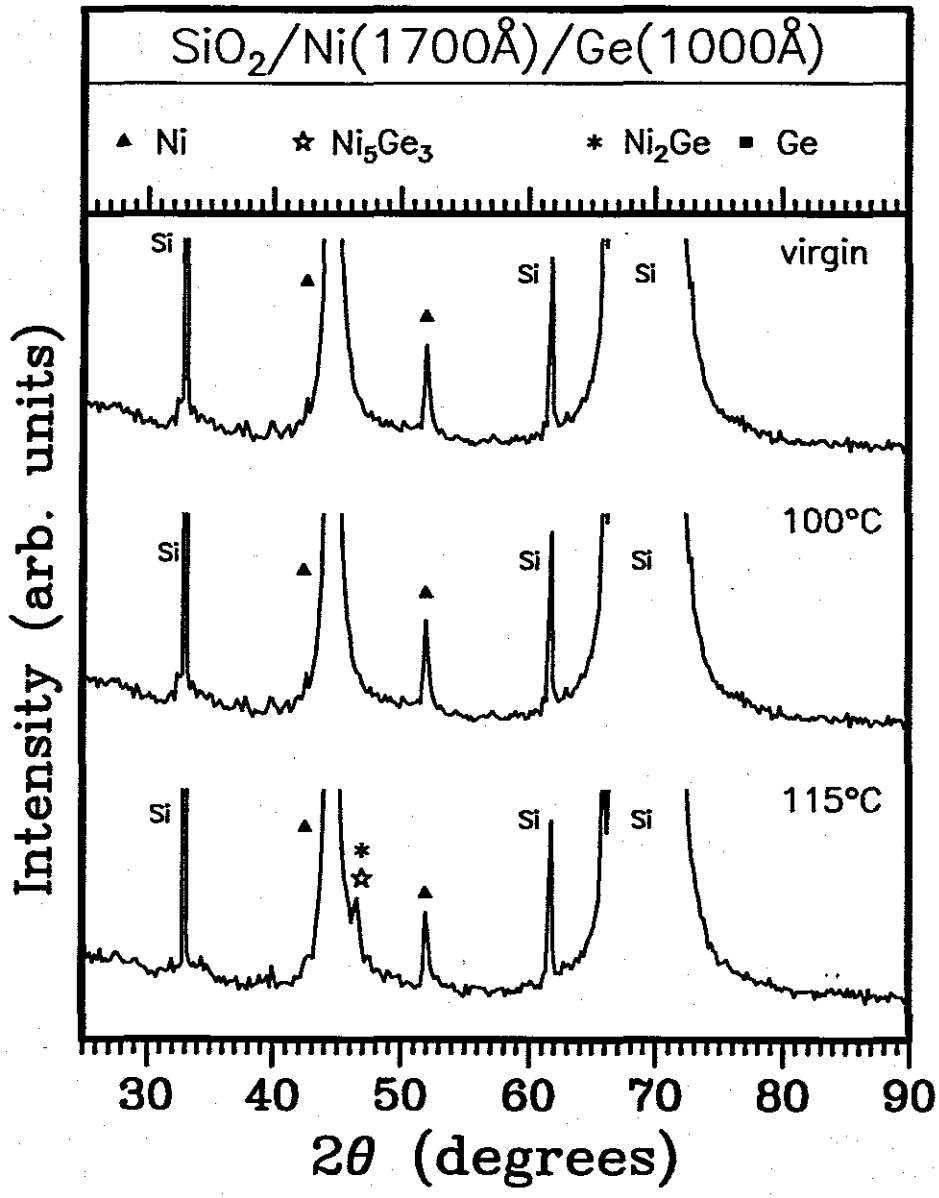

FIGURE 4.6: XRD spectra for a sample annealed at 115°C for 2 days, shows that either Ni_5Ge_3 or Ni_2Ge is the first phase to form. There are no peaks corresponding to the phase, NiGe.

spectrum of the sample annealed at 115°C for 2 days shows the presence of Ni_5Ge_3 (peaks of Ni_5Ge_3 overlap with those of Ni_2Ge). There are no peaks corresponding to NiGe.

4.5 Ti-Ge binary system

A layer of Ti of thickness 2500Åwas deposited onto oxidized Si wafers. Ge of thickness 2050Åwas deposited on top of the Ti layer. The overall atomic composition of the samples was, $Ti_{0.61}Ge_{0.39}$. The samples were annealed in vacuum better than 10^{-7}kPa at various temperatures for 1 day.

4.5.1 Results

Fig. 4.7 shows RBS results for these samples. There was no observable interaction on the as deposited sample. A sample annealed for 1 day at 400°C also showed little interaction. The step height on the sample annealed at 440°C indicates the formation of Ti_6Ge_5. This is the first phase to form according to these RBS results.

Fig. 4.8 shows XRD spectra of Ti-Ge samples. The vigin sample showed that Ti crystallises upon deposition. There are no other peaks on this virgin spectrum. The sample annealed at 400°C showed that Ge had crystalised. It also shows a peak belonging to Ti_6Ge_5. At 440°C peaks belonging to Ti_6Ge_5 can be clearly seen. At this stage there is still unreacted Ge and Ti. The XRD results agree with the RBS observations.

4.6 Discussion

Annealing samples at lower temperatures lowers the velocity of the growth interface, therefore giving all phases more time in which to nucleate, thus the phase with the most negative $\Delta H'$ would be expected to form. In the case of Ni-Ge it was expected that NiGe would nucleate first. NiGe is closest to the concentration corresponding to the liquidus minimum in the Ni-Ge phase diagram. It also has the largest effective

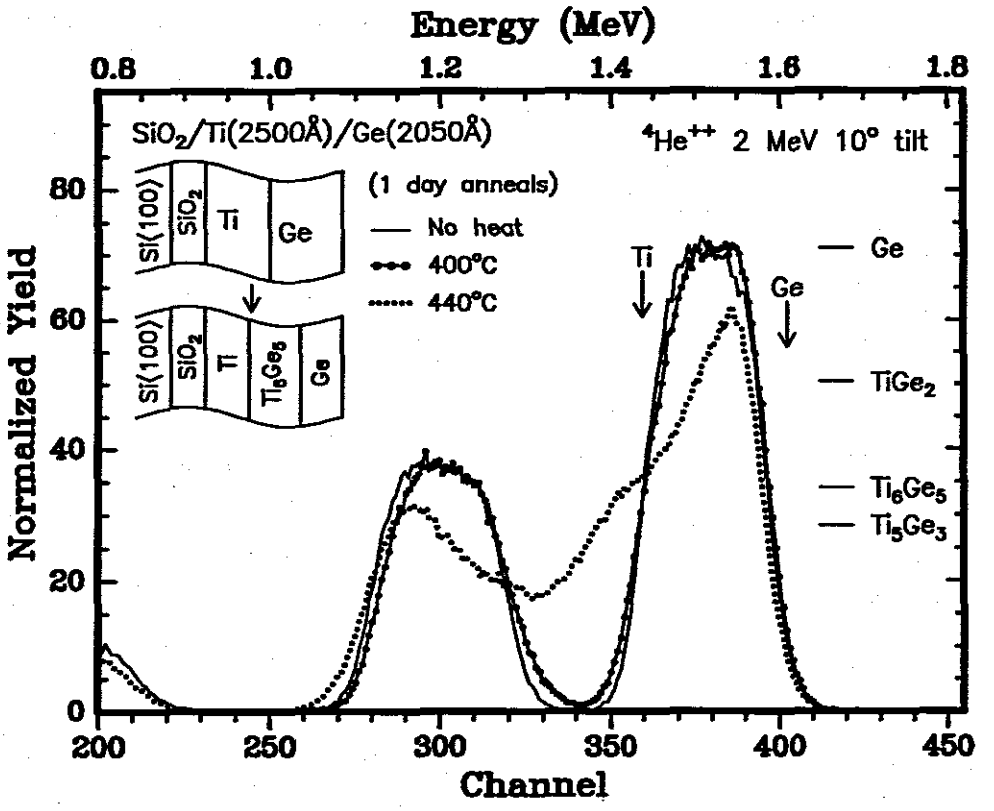

FIGURE 4.7: Backscattering diagram of Ti-Ge samples. They are made up of Si<>/SiO_2/Ti(2500Å)/Ge(2050Å). The step height on the Ti signal of the sample annealed at 440°C correspond to that of the phase Ti_6Ge_5. The 400°C shows little interaction. The spectrum of the as deposited sample show no interaction. Samples correspond to overall composition $Ti_{0.61}Ge_{0.39}$.

heat of formation. Annealing samples of Ni-Ge at about 115°C for two days only resulted in the formation of Ni_5Ge_3 as a first phase, which also is the first phase found at higher temperatures [78, 80, 91].

In the case of the Ti-Ge system, annealing for long periods of time at low temperature, even up to five days, resulted in no compound phases that could be detected within experimental limits. These attempts were aimed at obtaining the phase $TiGe_2$. Only annealing at temperatures above 400°C for 1 day resulted in any phases being formed. This temperature is very close to the normal temperature at which phases in this system occur during short period anneals. This may be due to a nucleation barrier that may have to be overcome before any nucleation takes place in this system. If this is the case then phases will form only above a certain

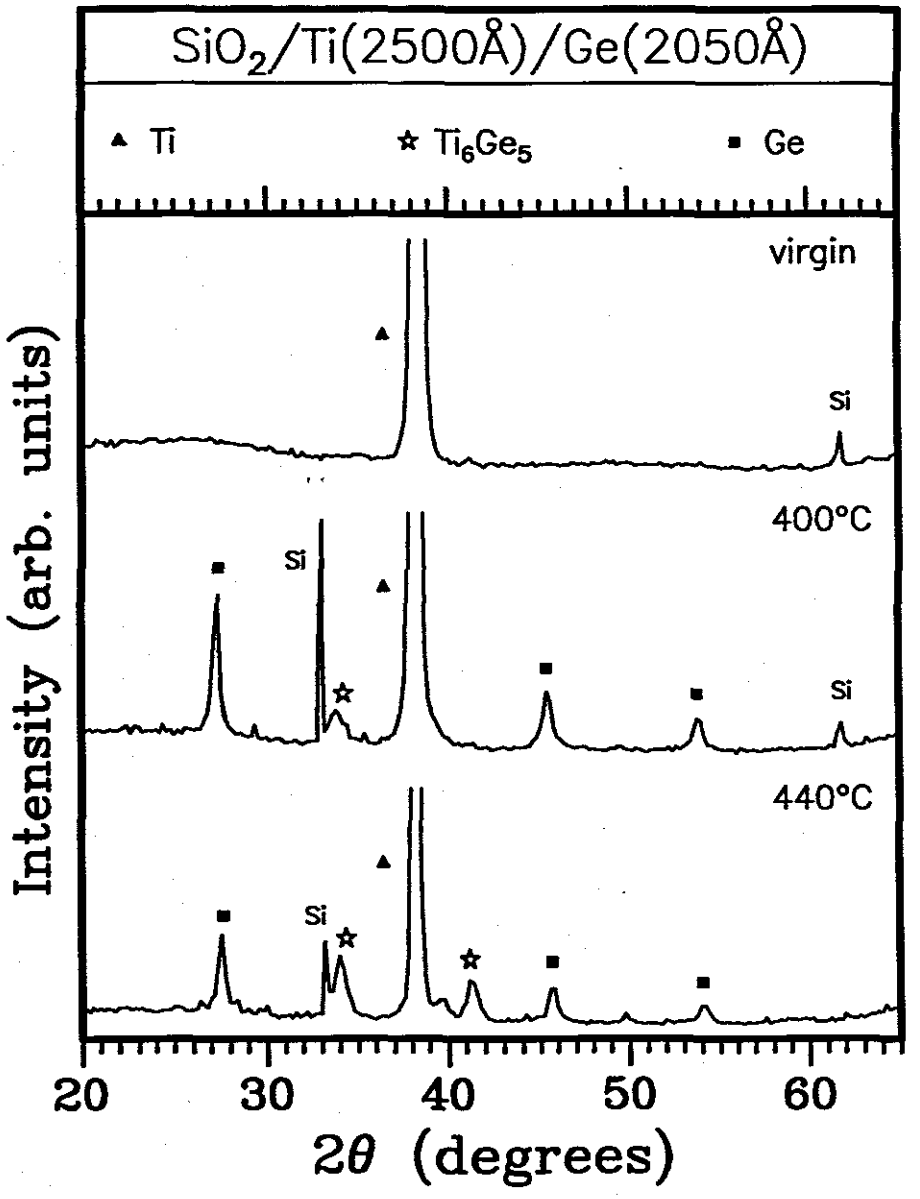

FIGURE 4.8: XRD spectra of Ti-Ge samples annealed for 1 day. The virgin sample shows only peaks of Ti. The sample annealed at 400°C shows that Ge has crystalised. There is also a peak belonging to Ti_6Ge_5. At 440°C peaks of Ti_6Ge_5 have grown larger. Both Ge and Ti are still present in the 440°C sample. No peaks corresponding to $TiGe_2$, which has the most negative $\Delta H'$ (-15.69kJ/mol.at.) are observed.

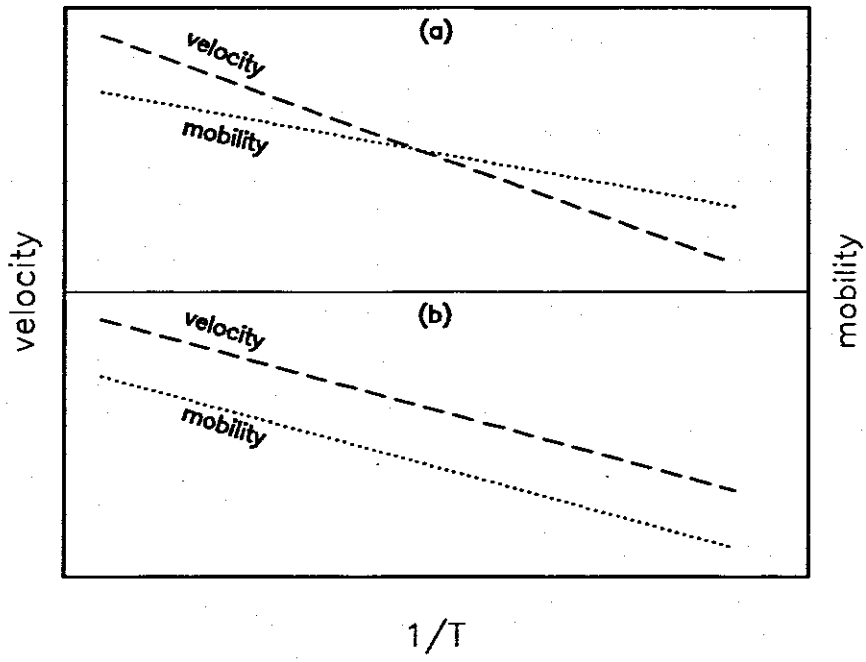

FIGURE 4.9: A diagram showing possible dependance of interfacial velocity and mobility on temperature during solid state phase formation. In (a) nucleation of a phase could be assisted at low temperature if the growth interface velocity decreases faster than the atomic mobility. The case illustrated in (b) however applies to the Ni-Ge and Ti-Ge systems as phases with the most negative $\Delta H'$ do not nucleate at very low temperatures.

temperature. Secondly phases may fail to nucleate because of contamination by oxygen. It is known that Ti is a getterer of oxygen. The presence of oxygen may delay nucleation of the phases at the growth interface by forming bonds with Ti atoms. It is important to note that reducing the anneal temperature will not only result in a lower velocity for the interface, but will also reduce mobility of the atoms. If the decrease in atomic mobility is less than the decrease in interfacial velocity then the phases we sought to nucleate (NiGe and $TiGe_2$) would have had a larger likelihood to form at lower temperatures (see **Fig. 4.9(a)**) The fact that these phases do not form first at lower temperatures suggest that atomic mobilities in the two systems (Ni-Ge and Ti-Ge) are reduced at a higher rate (or at least at the same rate) than is the reduction of interfacial velocities (see **Fig. 4.9(b)**).

CHAPTER 5

A STATISTICAL VIEW OF PHASE FORMATION

5.1 Theory

Consider thin films made up of two different elements A and B deposited on top of each other on top of a non-reactive substrate. At high enough temperatures atoms of A and B will be released into the reaction region, and will start to react. One needs to find out what factors lead to the formation of a compound phase A_sB_q . At the interface all percentage mixtures of A and B are possible from (A = 100 % atoms; B = 0 % atoms) to (A = 0 % atoms; B = 100 % atoms). There will thus be small regions with different compositions of A and B. Because of temperature atoms will be mixing and re-mixing between regions of different composition and within each region of the same composition. Diffusion is the process which gives rise to this re-mixing process. The activation energy E^A (E^B in the case of B) for diffusion of element A is expected to vary as concentration changes from A = 100 % atoms to A = 0 % atoms. E^B will vary likewise (see **Fig. 5.1**). The probability that an atom at temperature T will overcome the barrier E_A (and hence take part in re-mixing) is

$$p_1 = \exp(\frac{-E^A}{kT}) \tag{5.1}$$

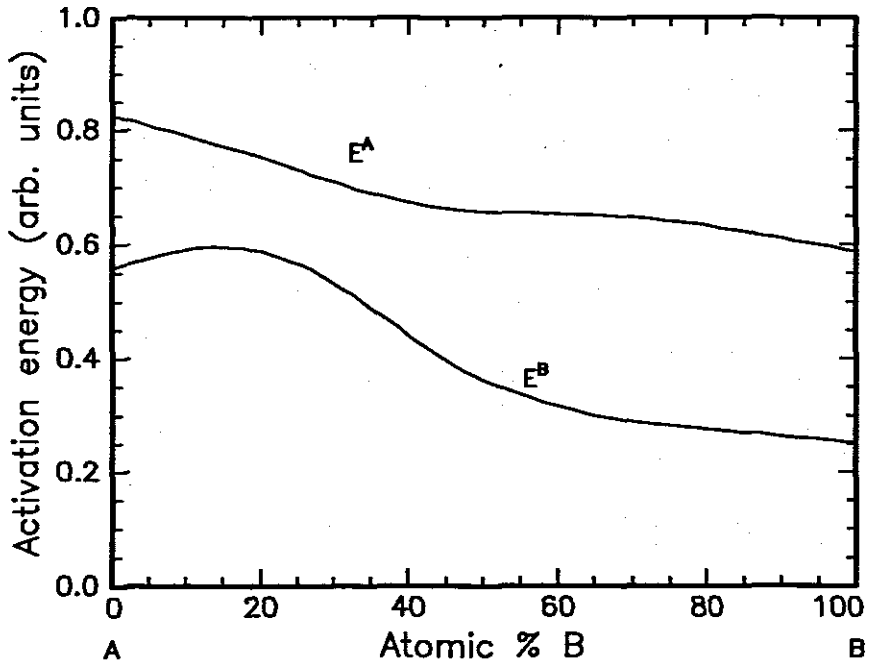

FIGURE 5.1: Hypothetical curves showing how activation energies of diffusion may vary with atomic % of one of the elements.

Values of p_1 corresponding to smaller values of E^A will be larger and will thus lead to greater re-mixing. The driving force for diffusional re-mixing is a change in Gibbs' free energy ΔG. Replacing E_A by ΔG we obtain

$$p_1 = exp(\frac{-\Delta G}{kT}) \tag{5.2}$$

where ΔG is a Gibbs function *barrier* presented to an atom which changes its Gibbs function value from G_1 to G_2(the overall change in Gibbs function is $G_2 - G_1 = \Delta G^*$ (see **Fig. 5.2**)). i.e. for an atom to move from one site to the next there should have been a thermal spike; (fluctuation) which might change other variables (locally) such as T as well as S (through dilation caused by an atom moving between others). T is the temperature and S is the entropy. We may therefore write 5.2 as

$$p_1 = exp\frac{-(\Delta E - T\Delta S + P\Delta V)}{kT} \tag{5.3}$$

The fluctuations are small, therefore one can perform a Taylor series expansion on ΔE and choose ΔT and ΔV as independent variables and arrive at;

$$p_1 = c_1 exp\frac{-C_v(\Delta T)^2}{2kT^2} \tag{5.4}$$

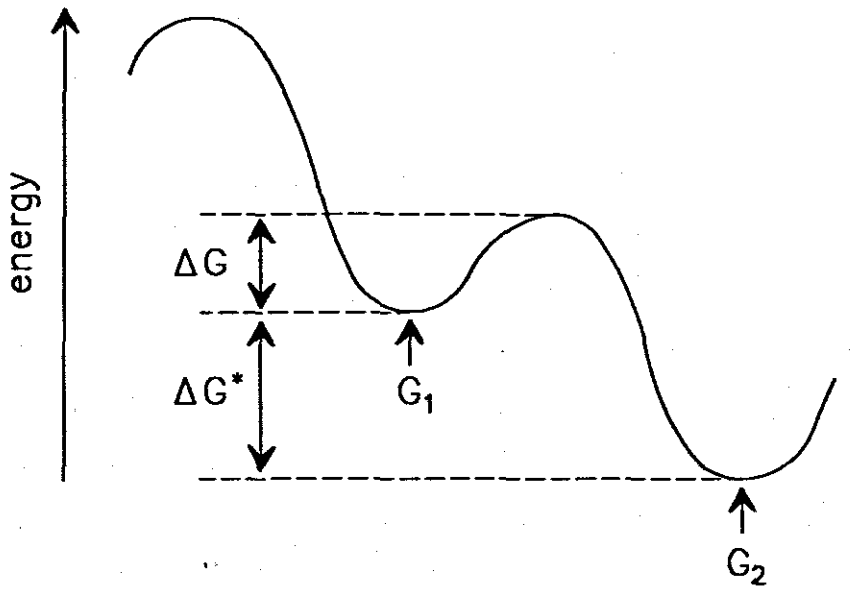

FIGURE 5.2: A curve of the Gibb's function, showing a barrier that must be overcome by an atom that changes it's Gibbs function value from G_1 to G_2. The Gibbs barrier height is ΔG and the overall change in the Gibbs function value is ΔG^*.

where c_1 is a normalization constant. For an experiment performed at constant T, one can average the amplitudes of vibration of the atoms to get an average amplitude. There are therefore atoms whose amplitude of vibration (considered at a given instant of time) is larger than the average (vibrant modes). These atoms may be considered to be at a higher temperature than the average temperature, while those with amplitudes of vibration is smaller than the average (more frozen modes) may be considered to be at a lower temperature. These local regions of higher and lower temperatures may be considered to add and give the average temperature T. In a solid at temperature T, there are thermal 'spikes' which when their magnitudes are greater than ΔT (for those modes of vibration which do not correspond to more frozen motion) , lead to a diffusion. The value of ΔT is expected to depend on composition(or concentration). This probability include both frozen modes, where the local temperature is lower than the average, T, and vibrant modes where it is greater than the average. These local temperature fluctuations are expected to be symmetrical about the average, T. The average of these fluctuations give the average temperature,T. The factor that correspond to a local raising temperature

fluctuation therefore should be

$$p_1 = c_1 exp \frac{-C_v(\Delta T)^2}{4kT^2} \tag{5.5}$$

There should exist therefore a curve on the phase diagram whose trend is expected to follows that of the liquid-solid transition curve.This is however not the liquid-solid transition curve. Call this curve a *minimum hurdle curve.* It gives a minimum temperature fluctuation that may lead to a diffusional intermixing. ΔT is a local temperature change from the average. This is supported by the findings of Brown and Ashby who found that activation energies of diffusion are proportional to the melting points of solids [**97**]. The probability curve $p_1(x)$ can therefore be based on the $\Delta T'$ values to obtain a new probability $p(x)$. The minimum of the liquid-solid transition curve should correspond to a maximum of both $p_1(x)$ and $p(x)$. Using this probability $p(x)$ one can easily obtain a concentration C_m corresponding to where intermixing is greatest (i.e the intermixing rate is higher). This is not the most probable concentration at the interface! Changing the anneal temperature should **not** change the position of the maximum of the probability $p_1(x)$ on the atomic % vs probability of diffusion diagram. In the absence of experimental values of E_A and E_B at all atomic % B, and as an approximation as to which concentration mixes at a faster rate one may use the minimum of the solid-liquid curve of the phase diagram of the binary system A and B to find C_m (see **Fig. 5.3**). Compound phases form depending partly on how often atoms of A and B meet in the correct ratio for a particular compound. This correct ratio happens in a given concentration (C_m initially). It is possible to calculate probability distribution functions $P^m_{A_sB_q}$, not only for C_m but at all atomic concentrations of A (and B). $P^m_{A_sB_q}(x)$ gives a comparison as to how often atoms meet (,in as yet unspecified time unit,) to form clusters that may lead to the formation of a particular compound phase. In forming clusters of three the following situation may arise:

AAA; BBB; AAB; ABB.

This can be written as A_3 ; B_3 ; A_2B; AB_2 . The last two clusters will lead to compound formation if A_2B and AB_2 are stable compounds. Let us calculate the

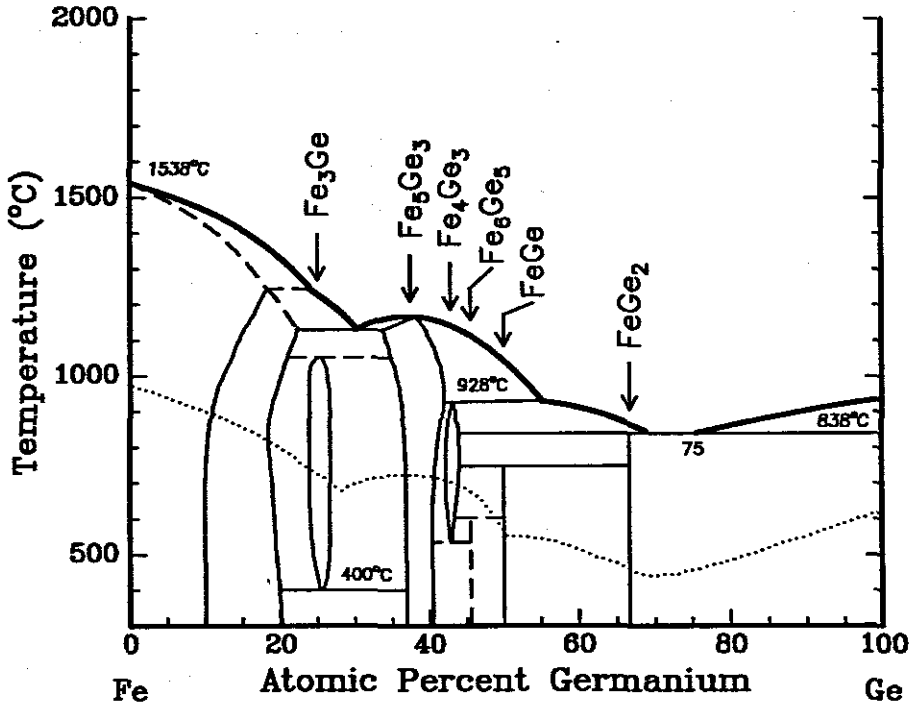

FIGURE 5.3: The dotted line shows how ΔT may vary with atomic % of one of the elements in a phase diagram. It is not an experimental curve, it is shown for illustrative purposes only. ΔT is the difference between the anneal temperature (say 450°C) and the dotted line. It is the minimum local temperature fluctuation that may lead to a diffusion at any atomic % B. $\Delta T'$ is the difference between the anneal temperature and the liquid-solid transition curve.

probability corresponding to the formation of AB_2 at a value of C_m of 25 at % B. Though one works with a large sample $\approx 10^{23}$ atoms, one may choose to do one's calculations based on a small manageable sample , say 100. Twenty five of these are atoms of B whereas 75 are atoms of A. What is the probability of picking two atoms of B and one atom of A from this sample? The probability of choosing the first atom of B is 25/100. Replace the atom of B because the actual sample is large ($\approx 10^{23}$). The probability of picking the second atom of B is 25/100, while that of picking A is 75/100. The probability of picking these three atoms from a concentration of 25% B is,

$$P^m_{A_1B_2}(C_m) = (\frac{25}{100})^2(\frac{75}{100})^1 \tag{5.6}$$

These probabilities can be worked out for any concentration x., We now work out these probability distributions for all concentrations x for compound phases shown

TABLE 5.1: Representative compound phases.

phase in standard form	phase in cluster of 9	meeting probability
A_3B	$A_{6.75}B_{2.25}$	$P^m_{A_3B}(x)$
A_5B_3	$A_{5.625}B_{3.375}$	$P^m_{A_5B_3}(x)$
A_5B_4	A_5B_4	$P^m_{A_5B_4}(x)$
AB	$A_{4.5}B_{4.5}$	$P^m_{AB}(x)$
AB_2	A_3B_6	$P^m_{AB_2}(x)$

in **Table 5.1.** A_3B can be thought of as having 4 atoms; three atoms of A and one atom of B. A_5B_4 has 9 atoms. Probabilities allow us to compare things. One requirement for using them is that the basis for comparison must be the same (there must be a fair comparison). We must therefore work with 9 atoms of A_3B_1. We therefore re-write A_3B_1 as $A_{6.75}B_{2.25}$ i.e. we have chosen to work with a basic cluster of 9(6.75+2.25=9) for all compounds . The probability density functions are given by:

$$P^m_{A_3B}(x) = c_1(100-x)^{6.75}x^{2.25} \tag{5.7}$$

$$P^m_{A_5B_3}(x) = c_2(100-x)^{5.625}x^{3.375} \tag{5.8}$$

$$P^m_{A_5B_4}(x) = c_3(100-x)^{5}x^{4} \tag{5.9}$$

$$P^m_{AB}(x) = c_4(100-x)^{4.5}x^{4.5} \tag{5.10}$$

$$P^m_{AB_3}(x) = c_5(100-x)^{2.25}x^{6.75} \tag{5.11}$$

where c_1 ... c_5 are normalization constants such that

$$\int_0^{100} P^m_{A_sB_q}(x)dx = 1 \tag{5.12}$$

and x is in atomic % of B. This type of normalization is called an *equal area normalization* because areas under all curves of $P^m_{A_sB_q}(x)$ will be equal (to unity). For meeting probabilities where equal area normalisation has been used we use the

symbol $P^m_{A_sB_q}$. We can introduce another form of normalization, called *vertical normalization* where all probabilities (now labelled $P^{mv}_{A_sB_q}$) must add up to unity at all x. It is assumed in the latter normalization that those clusters that cannot lead to stable compound phase formation (e.g. A_2B in a system where A_2B is not a stable compound according to the equilibrium phase diagram of system A-B) do not stay in that configuration for any appreciable length of time. It should be remembered also that atoms of A will be meeting in the interaction region and they may form solid A. This probability is given by:

$$P^m_A(x) = c_6(100 - x)^9 \tag{5.13}$$

The trivial case of B forming in the interaction region can also be included.

$$P^m_B(x) = c_7(x)^9 \tag{5.14}$$

Plots of meeting probability density vs concentration for all compound phases (including the two trivial cases of pure A and pure B forming clusters) are shown in **Fig. 5.4.** After coming together in the correct ratio atoms should bond. After bonding they should not migrate (i.e. move away from the cluster through diffusion). The probability that the i-th atom of element A belonging to a cluster migrates away from the cluster is:

$$exp(-\frac{E^A_i}{kT}) \tag{5.15}$$

The probability that it will not migrate is:

$$1 - exp(-\frac{E^A_i}{kT}) \tag{5.16}$$

If the compound phase that is being formed is A_sB_q then the average of E^A_i should be the activation energy for diffusion of atom A in composition A_sB_q (not yet a compound phase just an amorphous broth that will end up making the compound). The same can be said of atoms of B. Collecting these probabilities together one obtains a product:

$$P^{stab}_{A_sB_q} = \prod_{i=1}^{N}[1 - exp(-\frac{E_i}{kT})] \tag{5.17}$$

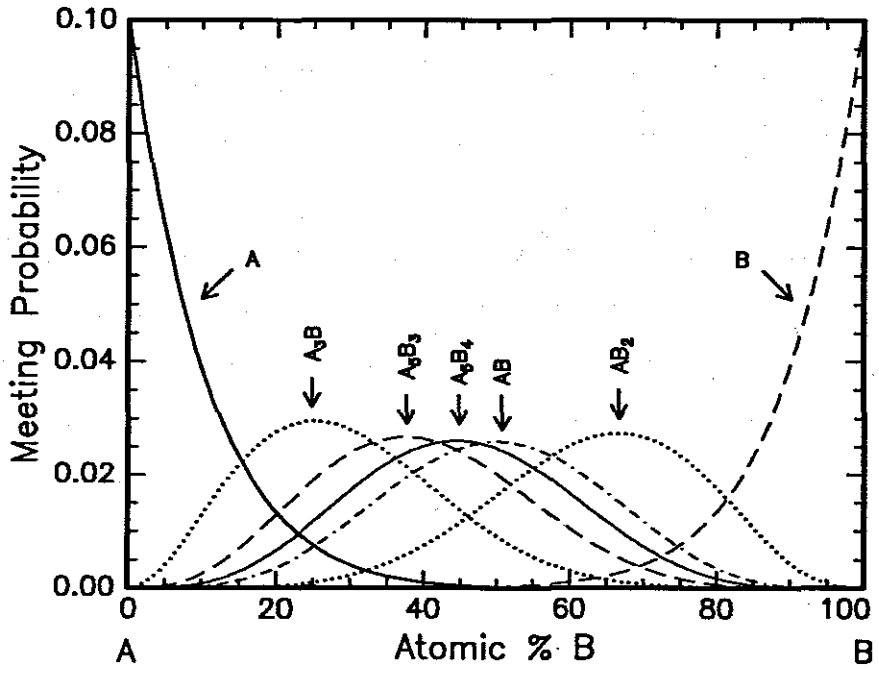

FIGURE 5.4: Probabilities $P^m_{A_sB_q}$ for atoms to meet in clusters of 9 to form phases in the A-B binary system. Trivial cases of atoms of A meeting to form clusters of A, and those of B making clusters of B are included. All curves are such that areas below them add up to unity (an equal area normalization).

Where N is the cluster number and E_i stands for either E_i^A or E_i^B. $P^{stab}_{A_sB_q}$ is the probability associated with the stability of a phase against breaking into its constituent atoms. Noticing that E_i^A is not known for particular lattice sites in a compound phase A_sB_q, but is simply known as an average, we split the product:

$$\prod_{i=1}^{s,q}[1-exp(-\frac{E_i^A}{kT})]^s[1-exp(-\frac{E_i^B}{kT})]^q \tag{5.18}$$

where s+q=N. Combining probabilities of meeting in the correct ratio $P^m_{A_sB_q}(x)$ and that of not moving away after forming bonds a probability of forming a compound phase is obtained.

$$P^{ms}_{phase}(x) = P_{sq}(x)\prod_{i=1}^{s,q}[1-exp(-\frac{E_i^A}{kT})]^s[1-exp(-\frac{E_i^B}{kT})]^q \tag{5.19}$$

where $P^{ms}_{phase}(x)$ is the probability to form a compound phase based on meeting probabilities and probability that the compound won't break into it's constituent parts. To predict the first phase these probabilities should be calculated where the

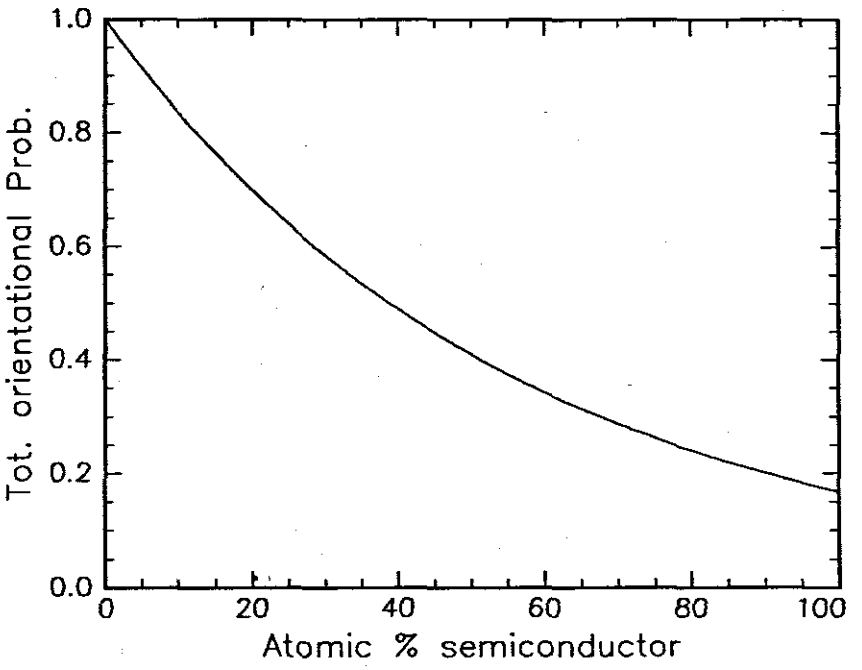

FIGURE 5.5: A graph of P^{tot}_{orient} versus concentration x, where it has been assumed that the orientational probability for a single semiconductor atom $P_{orient.}$ for proper bonding is 0.8 and that of a metal is unity. A basic cluster of eight was chosen to do this calculation.

intermixing rate is greatest (i.e. at the liquidus minimum of the binary system $x = c_m$). This should do for metal-metal systems.

For the case of metal-semiconductor systems a probability associated with the directionality of bonds should be included. Unlike metal atoms semiconductor atoms should be properly orientated in relation to those atoms they are bonding with before proper bonding occurs. Let the probability required for one semiconductor atom to have a proper orientation for bonding be $P_{orient.}$. In a cluster of N, if there are q atoms of the semiconductor the total orientational probability will be:

$$P^{tot.}_{orient.} = (P_{orient.})^q \tag{5.20}$$

The s atoms of metal A do not count. **Fig. 5.5** shows how orientational probability P^{tot}_{orient} varies with x (It has been assumed that $P_{orient} = 0.8$ for a semiconductor atom and it is unity for a metal atom. After making a proper orientation atoms

should bond to form a compound phase. Rotations on site may be executed by atoms without leaving their sites. If these rotations are executed by a semiconductor atom, bonds will be broken even though the atom has not left its position. Should this happen a cluster is lost. Energy is required by such an atom so that it may rotate. Let E_i^r be the rotational activation energy. Then the probability that the i-th atom will not rotate is:

$$1 - exp(-\frac{E_i^r}{kT}) \tag{5.21}$$

The probability that all q atoms in a cluster of N are not going to rotate is:

$$P_{rot}^{stab} = \prod_{i=1}^{q}[1 - exp(-\frac{E_i^r}{kT})] \tag{5.22}$$

where P_{rot}^{stab} is a probability associated with stability of a phase against rotations that tend to break its directional bonds. The probability of forming a metal-semiconductor phase will therefore be given by:

$$P_{phase}^{msr}(x) = P_{sq}(x)P_{orient.}^{tot.}(x)\prod_{i=1}^{N,q}[1 - exp(-\frac{E_i}{kT})][1 - exp(-\frac{E_i^r}{kT})] \tag{5.23}$$

5.2 First Phase Formation

5.2.1 Metal-metal systems

Metals find wide use in the microelectronics industry as interconnects between circuits; conduction paths for heat removal; passivation layers; diffusion barriers; adhesion promoters, etc. They also have a variety of other uses as coatings. Some of the metals like gold and silver are precious. There are other general uses in surgical instruments; cutlery; etc. They are also of tremendous importance to the metallurgical industry.

The simple statistical model developed will be used to predict the first phase that form during metal-metal interaction. As an example the case of the Ag-In binary system is considered. This system has three equilibrium phases,viz. $AgIn_2$, Ag_2In and Ag_3In. **Fig. 5.6** shows calculated meeting probabilities for this system. The equilibrium phase diagram for this system shows that the lowest temperature eutectic is at 97 atomic % In. At this concentration atoms are expected to be mixing

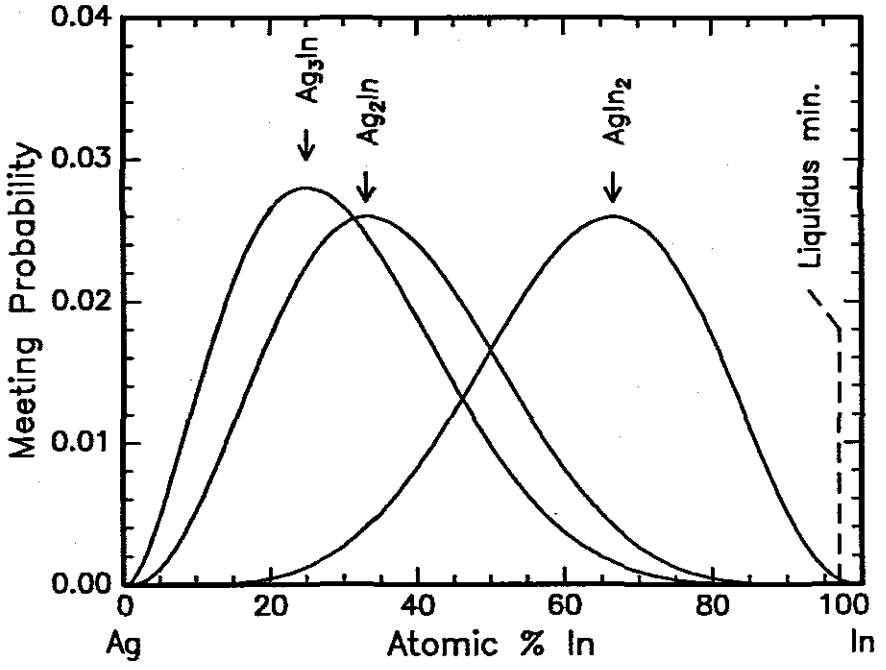

FIGURE 5.6: A graph of probability for atoms to meet in the correct ratio to form phases in the binary system Ag-In. In the absence of $P^{stab}_{A_pB_q}$ meeting probabilities are used to predict phase formation. The meeting probability for the phase $AgIn_2$ is much more than that of the other two phases at a concentration of 97 atomic % In. At this concentration the intermixing rate is higher than at any other concentration . A basic cluster of four was chosen to do the calculation. The phase $AgIn_2$ is therefore predicted as a first phase. It is also found experimentally to be the first phase.

at a higher rate compared to other concentrations. The meeting probability for the atoms to meet in the correct ratio to form a compound phase is greatest for the phase $AgIn_2$ at this concentration. This phase is therefore expected to form first. This is indeed the experimentally observed first phase [98]. We show here a model calculation as to how one can obtain these meeting probabilities. We now illustrate how a calculation can be done to find the meeting probabilities.

$$P^{m}_{AgIn_2}(x) = c_1(100 - x)^{2.67}x^{5.33} \tag{5.24}$$

is the probability for atoms in the Ag-In system to meet in the correct ratio so as to make a phase $AgIn_2$. c_1 is a normalisation constant found by integrating the

expression for the meeting probability and equating to one.

$$c_1 = 4.23 \times 10^{-16} \tag{5.25}$$

At $x = 20$ at.%

$$P^m_{AgIn_2} = 4.39 \times 10^{-4} \tag{5.26}$$

$$P^m_{Ag_2In}(x) = c_2(100 - x)^{5.33}x^{2.67} \tag{5.27}$$

one finds

$$c_2 = c_1 = 4.23 \times 10^{-16} \tag{5.28}$$

Therefore at 20 at.% In

$$P^m_{Ag_2In} = 1.75 \times 10^{-2} \tag{5.29}$$

Lastly

$$P^m_{Ag_3In} = c_3(100 - x)^6x^2 \tag{5.30}$$

with

$$c_3 = 2.52 \times 10^{-16} \tag{5.31}$$

thus at a value of x equal to 20 at.% In

$$P^m_{Ag_3In} = 2.64\text{x}10^{-2} \tag{5.32}$$

Table 5.2 shows calculated probabilities for atoms to meet in the correct ratio to form compound phases. This has been done at the liquidus minima of each binary system. If these values are used; even without taking into account probabilities associated with activation energies of migration, good agreement is found between predicted first phases and experimentally observed first phases. The case of the Ag-Ga system is trivial since it has only one known equilibrium phase viz. Ag_3Ga. For the system Cu-Ti there is more than one experimentally found first phase, CuTi and Cu_3Ti. Cu_3Ti is the phase predicted by this simple model to be a first phase.

There are fourteen binary systems for various metals which are predicted correctly by this model.

Table 5.3 shows those systems in which there isn't good agreement between predicted first phase and experimentally observed first phases. In both the Cr-Pt and

TABLE 5.2: Metal-metal systems where there is good agreement between theory and experiment. Meeting Probabilities are based on clusters of 8. These values have been calculated at the concentration of the lowest temperature eutectic (liquidus) of the binary system. For systems where the liquidus minimum coincides with the melting point of one of the elemental compounds , an arbitrary concentration value of 98 at.% of the element with the lowest melting point is taken. The number of atoms per unit cell is given in brackets behind each phase.

System	Congruency	Composition	Meeting Probability	Predicted Phase	Observed Phase	Ref
Liquidus Minimum	=	$Ag_{0.030}Ga_{0.970}$				
Ag_3Ga (2)	NC	$Ag_{0.750}Ga_{0.250}$	5.32×10^{-6}	Ag_3Ga	Ag_3Ga	[98]
Liquidus Minimum	=	$Ag_{0.030}In_{0.970}$				
$AgIn_2$ (12)	NC	$Ag_{0.333}In_{0.667}$	3.13×10^{-4}	$AgIn_2$	$AgIn_2$	[98]
Ag_2In (-)	NC	$Ag_{0.667}In_{0.333}$	3.06×10^{-8}			
Ag_3In_1 (-)	NC	$Ag_{0.750}In_{0.250}$	1.78×10^{-9}			
Liquidus Minimum	=	$Ag_{0.038}Sn_{0.962}$				
Ag_3Sn (8)	NC	$Ag_{0.750}Sb_{0.250}$	7.00×10^{-9}	Ag_3Sn	Ag_3Sn	[98,99]
Ag_7Sn (-)	NC	$Ag_{0.875}Sn_{0.143}$	1.17×10^{-10}			
Liquidus Minimum	=	$Cu_{0.011}In_{0.990}$				
$Cu_{11}In_9$ (20)	NC	$Cu_{0.550}In_{0.450}$	9.49×10^{-9}	$Cu_{11}In_9$	$Cu_{11}In_9$	[100]
$Cu_{16}In_9$ (6)	NC	$Cu_{0.640}In_{0.360}$	2.73×10^{-10}			
Cu_9In_4 (-)	NC	$Cu_{0.692}In_{0.308}$	3.08×10^{-11}			
Liquidus Minimum	=	$Cu_{0.145}Mg_{0.855}$				
$CuMg_2$ (48)	C	$Cu_{0.333}Mg_{0.667}$	1.07×10^{-2}	$CuMg_2$	$CuMg_2$	[100]
Cu_2Mg (24)	C	$Cu_{0.667}Mg_{0.333}$	9.67×10^{-4}			
Liquidus Minimum	=	$Cu_{0.980}Pd_{0.020}$				
Cu_3Pd (4)	NC	$Cu_{0.750}Pd_{0.250}$	9.00×10^{-3}	Cu_3Pd	Cu_3Pd	[98,100]
CuPd (-)	NC	$Cu_{0.500}Pd_{0.500}$	9.47×10^{-7}			
Liquidus Minimum	=	$Cu_{0.980}Pt_{0.020}$				
Cu_3Pt (4)	NC	$Cu_{0.750}Pt_{0.250}$	9.00×10^{-4}	Cu_3Pt	Cu_3Pt	[100]
CuPt (32)	NC	$Cu_{0.500}Pt_{0.500}$	9.47×10^{-7}			
$CuPt_3$ (4)	NC	$Cu_{0.250}Pt_{0.750}$	1.59×10^{-10}			
$CuPt_7$ (-)	NC	$Cu_{0.125}Pt_{0.875}$	9.37×10^{-13}			
Liquidus Minimum	=	$Cu_{0.623}Sb_{0.377}$				
Cu_2Sb (6)	NC	$Cu_{0.667}Sb_{0.333}$	2.51×10^{-2}	Cu_2Sb	Cu_2Sb	[100]
Cu_4Sb (-)	NC	$Cu_{0.800}Sb_{0.200}$	1.67×10^{-2}			
Liquidus Minimum	=	$Cu_{0.017}Sn_{0.983}$				
Cu_6Sn_5 (-)	NC	$Cu_{0.545}Sn_{0.455}$	6.60×10^{-8}	Cu_6Sn_5	Cu_6Sn_5	[98,101]
Cu_3Sn (-)	NC	$Cu_{0.750}Sn_{0.250}$	2.87×10^{-11}			
Liquidus Minimum	=	$Cu_{0.730}Ti_{0.270}$				
$CuTi_2$ (6)	NC	$Cu_{0.333}Ti_{0.667}$	1.74×10^{-3}			
CuTi (4)	C	$Cu_{0.500}Ti_{0.500}$	9.61×10^{-3}		CuTi	[100,102,103]
Cu_4Ti_3 (14)	NC	$Cu_{0.571}Ti_{0.429}$	1.58×10^{-2}			
Cu_3Ti_2 (10)	NC	$Cu_{0.600}Ti_{0.400}$	1.84×10^{-2}			
Cu_3Ti (8)	M	$Cu_{0.750}Ti_{0.250}$	2.77×10^{-2}	Cu_3Ti	Cu_3Ti	[104]
Cu_4Ti (10)	NC	$Cu_{0.800}Ti_{0.200}$	2.69×10^{-2}			

Cont...

System	Congruency	Composition	Meeting Probabilities	Predicted Phase	Observed Phase(s)	Ref
Liquidus Minimum	=	$Cu_{0.017}Zn_{0.983}$				
$CuZn_4$ (2)	NC	$Cu_{0.200}Zn_{0.800}$	$1.82x10^{-3}$	$CuZn_4$	$CuZn_4$	[98]
Cu_5Zn_8 (-)	C	$Cu_{0.385}Zn_{0.615}$	$1.19x10^{-5}$			
Liquidus Minimum	=	$Pb_{0.916}Pd_{0.084}$				
$PbPd_3$ (4)	C	$Pb_{0.250}Pd_{0.750}$	$8.18x10^{-7}$			
Pb_3Pd_5 (32)	NC	$Pb_{0.375}Pd_{0.625}$	$1.75x10^{-5}$			
Pb_9Pd_{13} (88)	NC	$Pb_{0.409}Pd_{0.591}$	$3.69x10^{-5}$			
PbPd (32)	NC	$Pb_{0.500}Pd_{0.500}$	$2.34x10^{-4}$			
Pb_2Pd (12)	C	$Pb_{0.667}Pd_{0.333}$	$3.69x10^{-3}$	Pb_2Pd	Pb_2Pd	[98]
Liquidus Minimum	=	$Pb_{0.947}Pt_{0.053}$				
Pb_4Pt (10)	NC	$Pb_{0.800}Pt_{0.200}$	$9.88x10^{-3}$	Pb_4Pt	Pb_4Pt	[99]
PbPt (4)	NC	$Pb_{0.500}Pt_{0.500}$	$3.26x10^{-5}$			
$PbPt_3$ (4)	NC	$Pb_{0.250}Pt_{0.750}$	$3.66x10^{-8}$			
Liquidus Minimum	=	$Pd_{0.020}Sn_{0.980}$				
$PdSn_4$ (20)	NC	$Pd_{0.200}Sn_{0.800}$	$2.79x10^{-3}$	$PdSn_4$	$PdSn_4$	[105]
$PdSn_3$ (32)	NC	$Pd_{0.250}Sn_{0.750}$	$9.00x10^{-4}$			
$PdSn_2$ (24)	NC	$Pd_{0.333}Sn_{0.667}$	$1.12x10^{-4}$			
PdSn (8)	NC	$Pd_{0.500}Sn_{0.500}$	$9.47x10^{-7}$			
Pd_3Sn_2 (6)	NC	$Pd_{0.600}Sn_{0.400}$	$3.68x10^{-8}$			
Pd_2Sn (12)	NC	$Pd_{0.667}Sn_{0.333}$	$3.62x10^{-9}$			
Pd_3Sn (4)	NC	$Pd_{0.750}Sn_{0.250}$	$1.59x10^{-10}$			

TABLE 5.3: Metal-metal systems where agreement between predicted phases and theory is not good when only meeting probabilities are used. Meeting probabilities are calculated for clusters of 8. These values have been calculated at the concentration of the liquidus minimum of the binary system. For systems where the liquidus minimum coincides with the melting point of one of the elemental compounds , an arbitrary concentration value of 98 at.% of the element with the lowest melting point is taken. The number of atoms per unit cell is given in brackets behind each phase.

System	Congruency	Composition	Meeting Probability	Predicted Phase	Observed Phase	Ref
Liquidus Minimum	=	$Cr_{0.870}Pt_{0.130}$				
Cr_3Pt (8)	C	$Cr_{0.750}Pt_{0.250}$	$1.72x10^{-2}$	Cr_3Pt		
CrPt (-)	NC	$Cr_{0.500}Pt_{0.500}$	$3.87x10^{-3}$		CrPt	[106]
$CrPt_3$ (4)	NC	$Cr_{0.250}Pt_{0.750}$	$3.88x10^{-4}$		$CrPt_3$	[106]
Liquidus Minimum	=	$Cu_{0.020}Ga_{0.980}$				
$CuGa_2$ (3)	NC	$Cu_{0.333}Ga_{0.667}$	$4.75x10^{-6}$	$CuGa_2$		
CuGa (-)	M	$Cu_{0.500}Ga_{0.500}$	$2.04x10^{-9}$		CuGa [b]	[98]
Cu_3Ga_2 (-)	NC	$Cu_{0.600}Ga_{0.400}$	$1.02x10^{-11}$			
Cu_9Ga_4 (52)	NC	$Cu_{0.692}Ga_{0.308}$	$4.94x10^{-14}$			

Cont...

System	Congruency	Composition	Meeting Probabilities	Predicted Phase	Observed Phase(s)	Ref
Liquidus Minimum	=	$Cu_{0.620}Zr_{0.380}$				
$CuZr_2$ (6)	NC	$Cu_{0.333}Zr_{0.667}$	8.52×10^{-3}			
CuZr (2)	C	$Cu_{0.500}Zr_{0.500}$	1.84×10^{-2}		CuZr	[100]
Cu_3Zr_2 (-)	NC	$Cu_{0.600}Zr_{0.400}$	2.22×10^{-2}	Cu_3Zr_2		
Cu_3Zr (-)	NC	$Cu_{0.750}Zr_{0.250}$	1.96×10^{-2}			
Cu_4Zr (-)	C	$Cu_{0.800}Zr_{0.200}$	1.67×10^{-2}			
Cu_5Zr (24)	NC	$Cu_{0.833}Zr_{0.167}$	1.45×10^{-2}			
Liquidus Minimum	=	$Pd_{0.340}Ti_{0.660}$				
$PdTi_4$ (8)	NC	$Pd_{0.200}Ti_{0.800}$	2.03×10^{-2}			
$PdTi_2$ (6)	NC	$Pd_{0.333}Ti_{0.667}$	2.59×10^{-2}	$PdTi_2$		
Pd_3Ti_4 (-)	NC	$Pd_{0.429}Ti_{0.571}$	2.18×10^{-2}			
PdTi (2,4)	C	$Pd_{0.500}Ti_{0.500}$	1.61×10^{-2}		PdTi	[107]
Pd_3Ti_2 (20)	NC	$Pd_{0.600}Ti_{0.400}$	8.29×10^{-3}			
Pd_5Ti_3 (8)	NC	$Pd_{0.625}Ti_{0.375}$	6.69×10^{-3}			
Pd_2Ti (-)	NC	$Pd_{0.660}Ti_{0.340}$	4.54×10^{-3}			
Pd_3Ti (16)	C	$Pd_{0.750}Ti_{0.250}$	1.74×10^{-3}			
Pd_4Ti (4)	NC	$Pd_{0.800}Ti_{0.200}$	8.73×10^{-4}			
Liquidus Minimum	=	$Pt_{0.330}Ti_{0.670}$ [a)]				
$PtTi_3$ (8)	C	$Pt_{0.250}Ti_{0.750}$	2.47×10^{-2}	$PtTi_3$		
PtTi (4)	C	$Pt_{0.500}Ti_{0.500}$	1.52×10^{-2}		PtTi	[107]
Pt_5Ti_3 (32)	C	$Pt_{0.625}Ti_{0.375}$	6.03×10^{-3}			
Pt_3Ti (16)	NC	$Pt_{0.750}Ti_{0.250}$	1.50×10^{-3}			
Pt_4Ti (-)	C	$Pt_{0.800}Ti_{0.200}$	7.39×10^{-4}			
Pt_8Ti (18)	NC	$Pt_{0.889}Ti_{0.111}$	1.64×10^{-4}			

a) There are two liquidus minima one at 16 at.% Pt and another one is at 33 at. % Pt (both have the same temperature [16]).

In Cu-Ga systems there is a big difference between meeting probabilities of the observed first phase(s) and the predicted first phases. It is difficult to explain this discrepancy. In the case of the Cu-Zr system, the probability between the experimentally observed first phase CuZr and the predicted first phase Cu_3Zr_2 is small. It may happen that the factor due to probability associated with the activation energy of migration in Cu_3Zr_2, lowers the probability of phase formation in this system. This will happen if the activation energy of migration in Cu_3Zr_2 is lower than that in CuZr. A probability of phase formation for a particular phase will be lowered much more than in other phases if in that phase any atom(s) has a smaller activation energy of migration. The same reasoning applies to the Pd-Ti system. In this case also, the meeting probability of formation between the predicted phase $PdTi_2$ and that of the experimentally observed phase PdTi may be different, with atoms of $PdTi_2$ (either Pd or Ti atoms or both) having a lower activation energy of migration. There are two liquidus minima for this system, one at 16 at.

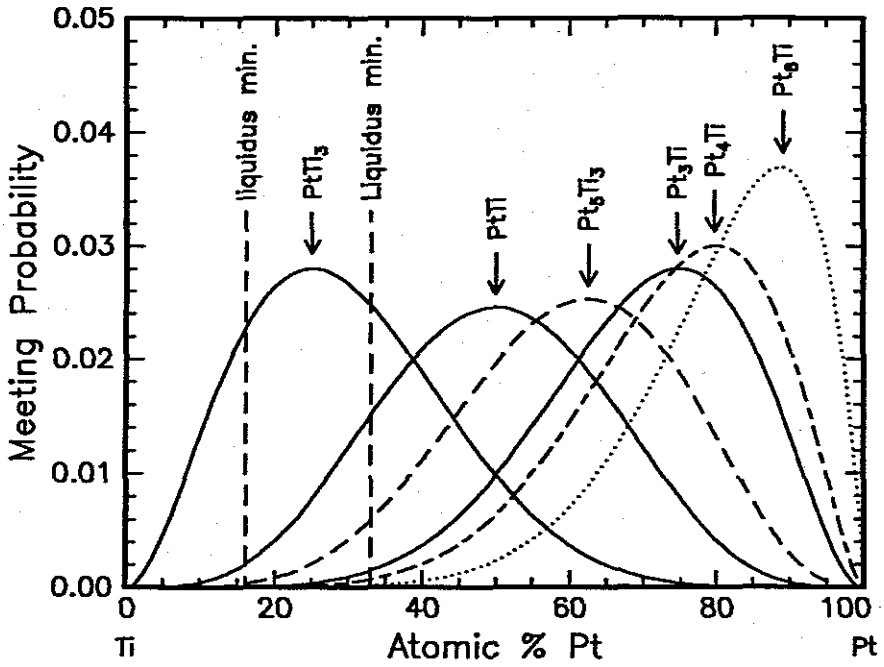

FIGURE 5.7: A graph showing probabilities of meeting for atoms to form different phases in the binary system Pt-Ti. The two liquidus minima of the system are shown. It can be clearly seen from the graph that at both minima probabilities of meeting to form the phase $PtTi_3$ are greater than those of other phases. This phase is therefore predicted to form first. This is however not the experimentally found first phase. The melting point of PtTi is higher than that of $PtTi_3$, therefore activation energies of diffusion should be higher in PtTi as compared to those in $PtTi_3$. This is expected to affect the probability of phase formation P^{ms}_{phase}.

% Pt and the other at 33 at. % Pt. They both have roughly the same temperature. Probabilities of meeting in the correct ratio to form a phases have been calculated at both liquidus minima for this system (see **Fig. 5.7**).

Comparing meeting probabilities calculated at these two concentrations one finds that those calculated at 33 at. % Pt have higher values than those calculated at 16 at. % Pt. If the rates of intermixing at these concentrations are the same, more compound phase clusters should be forming in a mixture with 33 at. % Pt. The predicted first phase should therefore be $PtTi_3$ based on the meeting probability calculated at 33 at. % Pt. That PtTi is the first experimentally observed phase may be due to a lower activation energy for migration for atoms of either Pt or Ti in the compound phase $PtTi_3$. Note there is very little difference between meeting probabilities of forming $PtTi_3$ and PtTi.

5.2.2 Al-metal systems

Predicted first phases are those with highest meeting probability at liquidus minima of binary systems. One notices from the table that in general there is good agreement predicted phases and experimentally observed first phases. In the binary system Au-Al, there are two experimentally observed first phases, namely Au_5Al_2 and Au_2Al. The phase predicted by this model is Au_4Al (if one uses probabilities of meeting only. It has never been found as a first phase. **Fig. 5.8** shows meeting probabilities in the Au-Al system. **Table 5.4** shows calculated meeting probabilities.

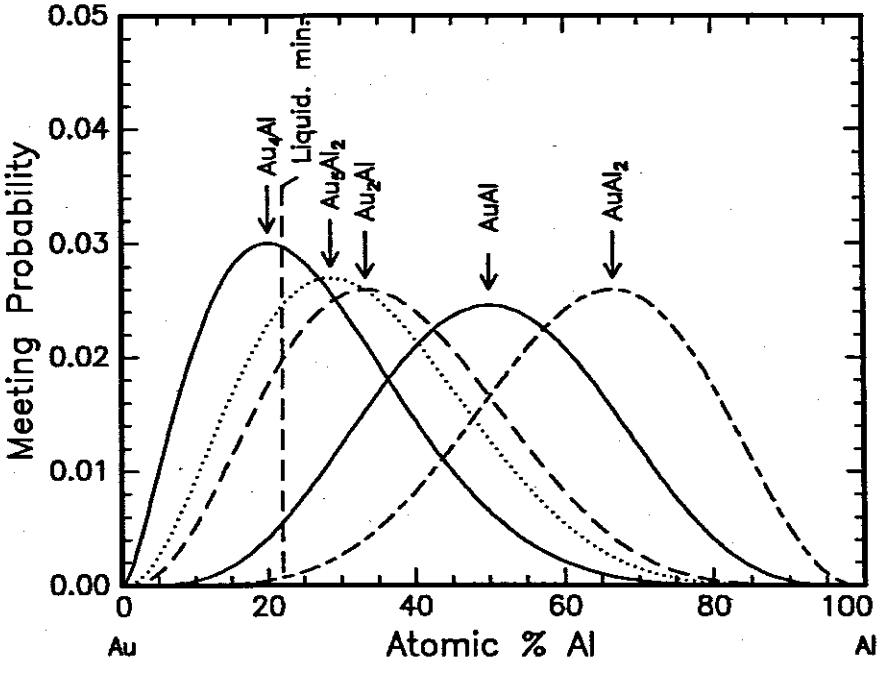

FIGURE 5.8: A graph of meeting probability for the binary system Au-Al. The liquidus minimum is at 22 atomic % Al. The predicted first phase Au_4Al is not an experimentally found first phase. Activation energies of diffusion of either Al or Au or both in Au_4Al are expected to be much lower than those in both Au_5Al_2 and Au_2Al.

TABLE 5.4: Metal-Aluminium systems. Meeting probabilities based on clusters of 8 have been calculated for metal-Al systems. These values have been calculated at the concentration of the lowest temperature eutectic (liquidus) of the binary system. For systems where the liquidus minimum coincides with the melting point of one of the elemental compounds, an arbitrary concentration value of 98 at.% of the element with the lowest melting point is taken. The number of atoms per unit cell is given in brackets behind each phase.

System	Congruency	Composition	Meeting Probability	Predicted Phase	Observed Phase	Ref
Liquidus Minimum	=	$Ag_{0.400}Al_{0.600}$				
Ag_3Al (20)	NC	$Ag_{0.750}Al_{0.250}$	7.78×10^{-3}			
Ag_2Al (2)	C	$Ag_{0.667}Al_{0.333}$	1.11×10^{-2}	Ag_2Al	Ag_2Al	[108]
Liquidus Minimum	=	$Au_{0.780}Al_{0.220}$				
Au_4Al (20)	NC	$Au_{0.800}Al_{0.200}$	2.97×10^{-2}	Au_4Al		
Au_5Al_2 (–)	NC	$Au_{0.714}Al_{0.286}$	2.46×10^{-2}		Au_5Al_2	[109–112]
Au_2Al (12)	C	$Au_{0.667}Al_{0.333}$	1.99×10^{-2}		Au_2Al	[110]
AuAl (8)	NC	$Au_{0.500}Al_{0.500}$	5.53×10^{-3}			
$AuAl_2$ (8)	C	$Au_{0.333}Al_{0.667}$	6.98×10^{-4}			
Liquidus Minimum	=	$Co_{0.020}Al_{0.980}$				
CoAl (2)	C	$Co_{0.500}Al_{0.500}$	9.47×10^{-7}			
Co_2Al_5 (28)	NC	$Co_{0.286}Al_{0.714}$	3.76×10^{-4}			
$CoAl_3$ (4)	NC	$Co_{0.250}Al_{0.750}$	9.00×10^{-4}			
Co_4Al_{13} (100)	NC	$Co_{0.235}Al_{0.765}$	1.28×10^{-3}			
Co_2Al_9 (22)	NC	$Co_{0.182}Al_{0.818}$	4.05×10^{-3}	Co_2Al_9	Co_2Al_9	[113–115]
Liquidus Minimum	=	$Cr_{0.020}Al_{0.980}$				
Cr_2Al (6)	NC	$Cr_{0.667}Al_{0.333}$	3.62×10^{-9}			
Cr_5Al_8 (26)	NC	$Cr_{0.385}Al_{0.615}$	2.80×10^{-5}			
Cr_4Al_9 (52)	NC	$Cr_{0.308}Al_{0.692}$	2.21×10^{-4}			
$CrAl_4$ (180)	NC	$Cr_{0.200}Al_{0.800}$	2.79×10^{-3}			
Cr_2Al_{11} (48)	NC	$Cr_{0.154}Al_{0.846}$	7.26×10^{-3}			
Cr_2Al_{13} (105)	NC	$Cr_{0.125}Al_{0.875}$	1.07×10^{-2}	Cr_2Al_{13}	Cr_2Al_{13}	[114–117]
Liquidus Minimum	=	$Cu_{0.170}Al_{0.830}$				
Cu_9Al_4 (52)	NC	$Cu_{0.690}Al_{0.310}$	1.31×10^{-4}			
Cu_3Al_2 (–)	NC	$Cu_{0.600}Al_{0.400}$	6.23×10^{-4}			
Cu_4Al_3 (21)	NC	$Cu_{0.570}Al_{0.430}$	9.61×10^{-4}			
CuAl (20)	NC	$Cu_{0.500}Al_{0.500}$	2.53×10^{-3}			
$CuAl_2$ (12)	C	$Cu_{0.333}Al_{0.667}$	1.39×10^{-2}	$CuAl_2$	$CuAl_2$	[4, 118–123]
Liquidus Minimum	=	$Fe_{0.009}Al_{0.991}$				
Fe_3Al (16)	NC	$Fe_{0.750}Al_{0.250}$	2.54×10^{-11}			
$FeAl_2$ (18)	NC	$Fe_{0.333}Al_{0.667}$	1.86×10^{-5}			
Fe_2Al_5 (–)	C	$Fe_{0.286}Al_{0.714}$	8.16×10^{-5}		Fe_2Al_5	[124]
$FeAl_3$ (102)	NC	$Fe_{0.250}Al_{0.750}$	2.39×10^{-4}			
$FeAl_6$ (28) [a)]	M	$Fe_{0.143}Al_{0.857}$	4.40×10^{-3}	$FeAl_6$	$FeAl_6$	[125]

Cont...

System	Congruency	Composition	Meeting Probability	Predicted Phase	Observed Phase(s)	Ref
Liquidus Minimum	=	$Gd_{0.050}Al_{0.950}$				
Gd_2Al (12 or 32)	NC	$Gd_{0.667}Al_{0.333}$	4.40×10^{-7}			
Gd_3Al_2 (20)	NC	$Gd_{0.600}Al_{0.400}$	2.70×10^{-6}			
GdAl (2 or 16)	NC	$Gd_{0.500}Al_{0.500}$	3.26×10^{-5}			
$GdAl_2$ (24)	C	$Gd_{0.333}Al_{0.667}$	1.10×10^{-3}			
$GdAl_3$ (8)	NC	$Gd_{0.250}Al_{0.750}$	4.66×10^{-3}			
$GdAl_4$ (20) [a]	M	$Gd_{0.200}Al_{0.800}$	9.88×10^{-3}	$GdAl_4$	$GdAl_4$	[126]
Liquidus Minimum	=	$Hf_{0.020}Al_{0.980}$				
Hf_2Al (12)	NC	$Hf_{0.667}Al_{0.333}$	3.62×10^{-9}			
Hf_3Al_2 (20)	C	$Hf_{0.600}Al_{0.400}$	3.68×10^{-8}			
Hf_4Al_3 (7)	NC	$Hf_{0.571}Al_{0.429}$	9.64×10^{-8}			
HfAl (8)	C	$Hf_{0.500}Al_{0.500}$	9.47×10^{-5}			
Hf_2Al_3 (40)	NC	$Hf_{0.400}Al_{0.600}$	1.85×10^{-5}			
$HfAl_2$ (12)	C	$Hf_{0.333}Al_{0.667}$	1.12×10^{-4}			
$HfAl_3$ (16)	C	$Hf_{0.250}Al_{0.750}$	9.00×10^{-4}	$HfAl_3$	$HfAl_3$	[114, 127, 128]
Liquidus Minimum	=	$Mo_{0.020}Al_{0.980}$				
Mo_3Al (8)	NC	$Mo_{0.750}Al_{0.250}$	1.59×10^{-10}			
Mo_3Al_8 (22)	C	$Mo_{0.272}Al_{0.728}$	5.27×10^{-4}			
$MoAl_4$ (30)	NC	$Mo_{0.200}Al_{0.800}$	2.79×10^{-3}			
Mo_4Al_{17} (–)	NC	$Mo_{0.190}Al_{0.810}$	3.46×10^{-3}			
Mo_5Al_{22} (–)	NC	$Mo_{0.185}Al_{0.815}$	3.85×10^{-3}			
$MoAl_5$ (12)	NC	$Mo_{0.167}Al_{0.833}$	5.67×10^{-3}			
$MoAl_6$ (–)	NC	$Mo_{0.143}Al_{0.857}$	9.05×10^{-3}			
$MoAl_{12}$ (26)	NC	$Mo_{0.077}Al_{0.923}$	2.84×10^{-2}	$MoAl_{12}$	$MoAl_{12}$	[115, 129]
Liquidus Minimum	=	$Nb_{0.020}Al_{0.980}$				
Nb_3Al (8)	NC	$Nb_{0.750}Al_{0.250}$	1.59×10^{-10}			
Nb_2Al (30)	NC	$Nb_{0.667}Al_{0.333}$	3.62×10^{-9}			
$NbAl_3$ (8)	C	$Nb_{0.250}Al_{0.750}$	9.00×10^{-4}	$NbAl_3$	$NbAl_3$	[130–135]
Liquidus Minimum	=	$Ni_{0.035}Al_{0.965}$				
Ni_3Al (4)	NC	$Ni_{0.750}Al_{0.250}$	4.44×10^{-9}			
NiAl (2)	C	$Ni_{0.500}Al_{0.500}$	8.35×10^{-6}			
Ni_2Al_3 (5)	NC	$Ni_{0.400}Al_{0.600}$	1.03×10^{-4}			
$NiAl_3$ (16)	NC	$Ni_{0.250}Al_{0.750}$	2.51×10^{-3}	$NiAl_3$	$NiAl_3$	[113, 136–138]
Liquidus Minimum	=	$Pd_{0.080}Al_{0.920}$				
Pd_2Al (12)	C	$Pd_{0.667}Al_{0.333}$	4.95×10^{-6}			
PdAl (26)	C	$Pd_{0.500}Al_{0.500}$	1.88×10^{-4}			
Pd_2Al_3 (5)	NC	$Pd_{0.400}Al_{0.600}$	1.15×10^{-3}		Pd_2Al_3	[138, 139]
$PdAl_3$ (–)	NC	$Pd_{0.250}Al_{0.750}$	9.84×10^{-3}		$PdAl_3$	[114]
$PdAl_4$ (90)	NC	$Pd_{0.200}Al_{0.800}$	1.70×10^{-2}	$PdAl_4$	$PdAl_4$	[113, 140]
Liquidus Minimum	=	$Pt_{0.020}Al_{0.980}$				
Pt_3Al (16)	NC	$Pt_{0.750}Al_{0.250}$	1.60×10^{-10}			
Pt_2Al (24)	NC	$Pt_{0.667}Al_{0.333}$	3.63×10^{-9}			
Pt_5Al_3 (16)	C	$Pt_{0.625}Al_{0.375}$	5.30×10^{-9}			
PtAl (8)	C	$Pt_{0.500}Al_{0.500}$	9.50×10^{-7}			
Pt_2Al_3 (5)	C	$Pt_{0.400}Al_{0.600}$	1.84×10^{-5}		Pt_2Al_3	[113, 140–144]
$PtAl_2$ (12)	NC	$Pt_{0.333}Al_{0.667}$	1.12×10^{-4}			
Pt_8Al_{21} (116)	NC	$Pt_{0.276}Al_{0.724}$	4.81×10^{-4}		Pt_8Al_{21}	
$PtAl_4$ (90) [a]	M	$Pt_{0.200}Al_{0.800}$	2.79×10^{-3}		$PtAl_4$	[114]
Pt_5Al_{21} (416)	NC	$Pt_{0.192}Al_{0.808}$	3.28×10^{-3}	Pt_5Al_{21}		
Liquidus Minimum	=	$Ta_{0.020}Al_{0.980}$				
Ta_2Al (30)	NC	$Ta_{0.667}Al_{0.333}$	3.62×10^{-9}			
$TaAl_3$ (8)	C	$Ta_{0.250}Al_{0.750}$	9.00×10^{-4}	$TaAl_3$	$TaAl_3$	[113–115, 145]

Cont...

System	Congruency	Composition	Meeting Probability	Predicted Phase	Observed Phase(s)	Ref
Liquidus Minimum	=	$Ti_{0.020}Al_{0.980}$				
Ti_3Al (8)	NC	$Ti_{0.750}Al_{0.250}$	1.59×10^{-10}			
Ti_2Al (–)	?	$Ti_{0.667}Al_{0.333}$	3.62×10^{-9}			
TiAl (4)	NC	$Ti_{0.500}Al_{0.500}$	9.47×10^{-7}			
$TiAl_3$ (8)	NC	$Ti_{0.250}Al_{0.750}$	9.00×10^{-4}	$TiAl_3$	$TiAl_3$	[113–115, 127, 146–148]
Liquidus Minimum	=	$V_{0.020}Al_{0.980}$				
V_5Al_8 (52)	NC	$V_{0.385}Al_{0.615}$	2.80×10^{-5}			
VAl_3 (8)	NC	$V_{0.250}Al_{0.750}$	9.02×10^{-4}		VAl_3	[126, 146, 149]
V_4Al_{23} (54)	NC	$V_{0.143}Al_{0.857}$	8.00×10^{-3}			
VAl_7 (104)	NC	$V_{0.125}Al_{0.875}$	1.26×10^{-2}			
VAl_{10} (176)	NC	$V_{0.091}Al_{0.909}$	2.26×10^{-2}	VAl_{10}	VAl_{10}	[126, 149]
Liquidus Minimum	=	$W_{0.020}Al_{0.980}$				
WAl_4 (30)	NC	$W_{0.200}Al_{0.800}$	2.79×10^{-3}			
WAl_5 (12)	NC	$W_{0.167}Al_{0.833}$	5.65×10^{-3}			
WAl_{12} (26)	NC	$W_{0.077}Al_{0.923}$	2.89×10^{-2}	WAl_{12}	WAl_{12}	[115, 150, 151]
Liquidus Minimum	=	$Zr_{0.020}Al_{0.980}$				
Zr_5Al_3 (16)	NC	$Zr_{0.625}Al_{0.375}$	1.56×10^{-8}			
Zr_3Al_2 (20)	NC	$Zr_{0.600}Al_{0.400}$	3.67×10^{-8}			
Zr_4Al_3 (7)	C	$Zr_{0.571}Al_{0.429}$	9.56×10^{-8}			
ZrAl (8)	NC	$Zr_{0.500}Al_{0.500}$	9.49×10^{-7}			
Zr_2Al_3 (40)	C	$Zr_{0.400}Al_{0.600}$	1.84×10^{-5}			
$ZrAl_2$ (12)	C	$Zr_{0.333}Al_{0.667}$	1.12×10^{-4}			
$ZrAl_3$ (16)	C	$Zr_{0.250}Al_{0.750}$	9.02×10^{-4}	$ZrAl_3$	$ZrAl_3$	[114, 128, 147]

[a] Metastable phase.

Because activation energies of migration are not available, it is not possible to compare probabilities of phase formation (P^{ms}_{phase}) in this system. It is suspected that the activation energy of migration of either Au or Al (or both) in the phase Au_4Al is much lower than that in the other two phases, Au_5Al_2 and Au_2Al. Activation energies are proportional to the melting point of a solid and the melting point of Au_4Al is lower than that of either Au_5Al_2 or Au_2Al. It is interesting to look at the general behaviour of the probability of phase formation, P^{ms}_{phase}. In this theory it is given by two factors, namely the probability associated with the stability of a phase, $P^{stab}_{A_sB_q}$, and the probability associated with the formation of clusters, $P^{m}_{A_sB_q}$.

One therefore concludes that *the probability for atoms to meet in the correct ratio to form a phase favours those phases which are close to the liquidus minimum of the binary system in composition. This comes from calculating meeting probabilities for concentrations corresponding to the liquidus minimum. The probability associated with the stability of a phase,* $P^{stab}_{A_sB_q}$ **in general** *will favour those phases that are removed from the liquidus minimum in composition (since these will in general*

have higher melting points and hence larger activation energies for diffusion). **A compromise between the two factors determines what the first phase will be.** In fact one should not be using the minimum of the solid-liquid transition curve of the phase diagram to find which composition mixes at the fastest rate but should be using a minimum of the average activation energies versus composition curve to find which composition mixes the fastest. Probabilities for atoms to meet in the correct ratio to form phases would then be calculated at the minimum of such a curve. These probabilities would therefore favour those phases that are nearest in composition to the minimum of such a curve. The probability associated with stability would (in general) favour those phases that are away from the minimum of the activation energy curve. A compromise between stability and the rate of forming correct clusters should then determine what the first phase should be. It can therefore be concluded that probabilities of meeting in the correct ratio , though they may give an indication as to which phase may form first, are but an approximation when used alone.

In the system Fe-Al, more than one phase is found experimentally to form first. These are the systems $FeAl_6$ and Fe_2Al_5. $FeAl_6$ is the predicted first phase. There is a huge difference between the meeting probability of forming $FeAl_6$ and that of forming Fe_2Al_5 as a first phase. If activation energies of migration are the only significant factors , besides meeting probabilities, that account for the appearance of Fe_2Al_5 as a first phase, then they must differ by a considerable amount. For the system Pd-Al there are three experimentally observed first phases. They are Pd_2Al_3, $PdAl_3$ and $PdAl_4$. The predicted first phase, based only on probability of atoms to meet in a correct ratio to form a phase, is $PdAl_4$. The meeting probability for the two phases $PdAl_4$ and $PdAl_3$ are close, it is therefore not surprising that these two are both found as first phases. It is hoped that activation energy of migration might account for the appearance of Pd_2Al_3 as an experimentally found first phase. The model predicts experimentally found first phases correctly in seventeen aluminium-metal systems. It fails to predict an experimentally observed first phase in the Pt-Al system. Values of activation energy for diffusion might solve this problem in this

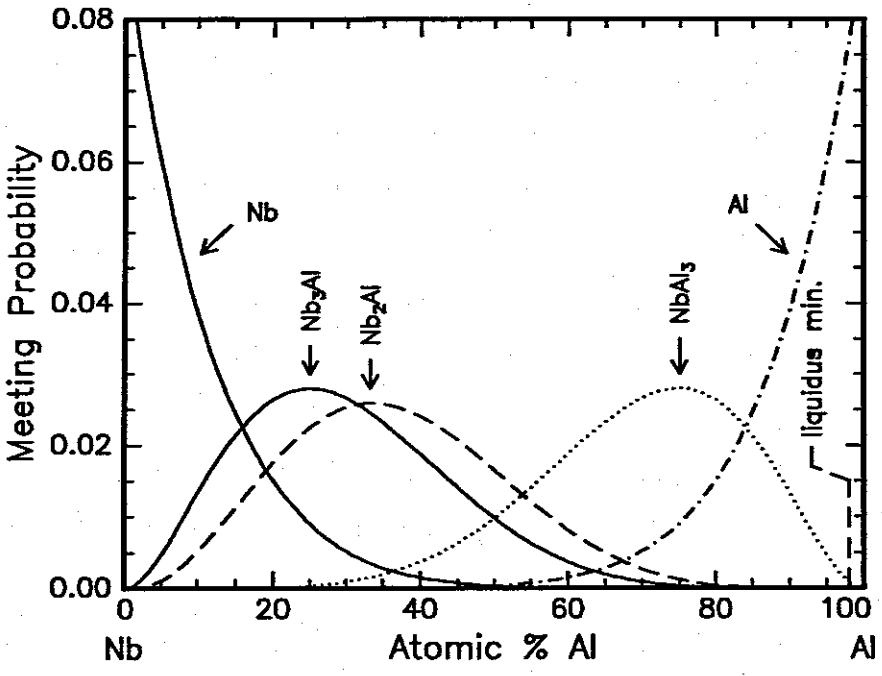

FIGURE 5.9: A graph of meeting probability for the binary system Nb-Al. The trivial case of clusters of atoms of pure Al meeting to form solid Al has been included. The liquidus minimum is on the Al side of the diagram at a concentration where the probability of Al atom meeting Al atom is much larger than that of Al atom meeting an Nb atom to form the first phase, $NbAl_3$. The clusters of $NbAl_3$ will therefore be in a predominantly aluminide environment.

system. **Fig. 5.9** shows the probability of meeting in the correct ratio to form phases in the system Nb-Al.

The trivial case of atoms of Nb coming together to form clusters of Nb has been calculated. The same calculation has been done also for atoms of Al. In most Al-metal systems the liquidus minimum is on the Al-rich side of the phase diagram. Comparing probability for atoms to meet in the correct ratio to form the phase $NbAl_3$ and that of forming clusters of pure Al, it is found that the meeting probability associated with pure Al is much larger. Clusters of $NbAl_3$ must therefore be meeting (initially) in a predominantly aluminium-rich environment. Contrast this with the case where meeting probabilities to form a phase are far removed from concentrations where one of the elements predominates. In this case after forming a few clusters of a phase, further clusters will be formed in a friendlier environment, because

neighbouring clusters are of their own kind. This is a homoepitaxy-like situation. Surface energies are reduced because clusters of the same kind are in contact.

5.2.3 Au-metal systems

Table 5.5 shows probabilities of atoms to meet in the correct ratio to form different phases for Au-Metal systems. Activation energies of migration could not be obtained for most systems and predictions are based only on meeting probabilities. There are eight systems in which there is agreement between predicted and observed phases. In the Au-Pb system there is more than one experimentally found first phase. These are the $AuPb_3$ and $AuPb_2$ compound phases. $AuPb_3$ is the predicted first phase. It is noticed that the probabilities for the two phases do not differ much. It is therefore understandable why at times $AuPb_2$ is found as a first phase. The same behaviour is observed in the Au-Sn system. But in this case the probabilities of meeting in the correct ratio between atoms of $AuSn_4$ and those of AuSn differ by a considerable amount. It is suspected therefore that the activation energy of migration in the phase $AuSn_4$ is less than that in $AuSn_2$, and that in $AuSn_2$ is in turn smaller than that in AuSn. This simple model predicts correctly, experimentally observed first phases in eight Au-metal systems.

It fails to predict first phases correctly in five Au-metal systems. In view of the fact that activation energies of migration are lacking in these systems, nothing much can be said about this failure.

TABLE 5.5: Au-metal systems Meeting probabilities for Au-metal atoms based on clusters of 8. These values have been calculated at the concentration of the lowest temperature eutectic (liquidus) of the binary system. For systems where the liquidus minimum coincides with the melting point of one of the elemental compounds , an arbitrary concentration value of 98 at.% of the element with the lowest melting point is taken. The number of atoms per unit cell is given in brackets behind each phase.

System	Congruency	Composition	Meeting Probability	Predicted Phase	Observed Phase	Ref
Liquidus Minimum	=	$Au_{0.070}Cd_{0.930}$				
$AuCd_5$ (-)	NC	$Au_{0.180}Cd_{0.820}$	$2.10x10^{-2}$	$AuCd_5$		
$AuCd_3$ (24)	C	$Au_{0.250}Cd_{0.750}$	$8.06x10^{-3}$		$AuCd_3$	[152]
Au_3Cd_5 (32)	NC	$Au_{0.375}Cd_{0.625}$	$1.22x10^{-3}$			
AuCd (2)	C	$Au_{0.500}Cd_{0.500}$	$1.15x10^{-4}$			
Au_2Cd (2)	NC	$Au_{0.667}Cd_{0.333}$	$2.15x10^{-6}$			
Au_3Cd (16)	NC	$Au_{0.750}Cd_{0.250}$	$2.64x10^{-7}$			
Liquidus Minimum	=	$Au_{0.565}Cu_{0.435}$				
$AuCu_3$ (4)	NC	$Au_{0.250}Cu_{0.750}$	$5.47x10^{-3}$		$AuCu_3$	[100]
AuCu (4)	NC	$Au_{0.500}Cu_{0.500}$	$2.30x10^{-2}$	AuCu		
Au_3Cu (4)	NC	$Au_{0.750}Cu_{0.250}$	$1.55x10^{-2}$			
Liquidus Minimum	=	$Au_{0.020}Ga_{0.980}$				
$AuGa_2$ (12)	C	$Au_{0.333}Ga_{0.667}$	$1.12x10^{-4}$	$AuGa_2$	$AuGa_2$	[152]
AuGa (8)	C	$Au_{0.500}Ga_{0.500}$	$9.49x10^{-7}$			
Au_2Ga (24)	C	$Au_{0.667}Ga_{0.333}$	$3.63x10^{-9}$			
Au_7Ga_2 (-)	NC	$Au_{0.778}Ga_{0.222}$	$5.44x10^{-11}$			
Liquidus Minimum	=	$Au_{0.020}In_{0.980}$				
$AuIn_2$ (12)	C	$Au_{0.333}In_{0.667}$	$1.12x10^{-4}$	$AuIn_2$	$AuIn_2$	[152–156]
AuIn (-)	C	$Au_{0.500}In_{0.500}$	$9.49x10^{-7}$			
Au_7In_3 (60)	NC	$Au_{0.700}In_{0.300}$	$1.06x10^{-9}$			
Au_3In (8)	NC	$Au_{0.750}In_{0.250}$	$1.60x10^{-10}$			
$Au_{10}In_3$ (26)	NC	$Au_{0.769}In_{0.231}$	$7.69x10^{-11}$			
$Au_{11}In_3$ (28)	NC	$Au_{0.786}In_{0.214}$	$3.83x10^{-11}$			
Au_4In (2)	NC	$Au_{0.800}In_{0.200}$	$2.20x10^{-11}$			
Au_7In (2)	NC	$Au_{0.875}In_{0.125}$	$9.36x10^{-13}$			
Liquidus Minimum	=	$Au_{0.980}Nb_{0.020}$				
$AuNb_3$ (8)	NC	$Au_{0.250}Nb_{0.750}$	$1.60x10^{-10}$			
Au_2Nb_3 (10)	NC	$Au_{0.400}Nb_{0.600}$	$3.67x10^{-8}$			
Au_2Nb (3)	NC	$Au_{0.667}Nb_{0.333}$	$1.12x10^{-4}$	Au_2Nb	Au_2Nb	[157]
Liquidus Minimum	=	$Au_{0.159}Pb_{0.841}$				
$AuPb_3$ (32)	NC	$Au_{0.250}Pb_{0.750}$	$2.28x10^{-2}$	$AuPb_3$	$AuPb_3$	[152]
$AuPb_2$ (12)	NC	$Au_{0.333}Pb_{0.667}$	$1.27x10^{-2}$		$AuPb_2$	[99, 158]
Au_2Pb (24)	NC	$Au_{0.667}Pb_{0.333}$	$1.56x10^{-4}$			
Liquidus Minimum	=	$Au_{0.640}Sb_{0.360}$				
$AuSb_2$ (12)	C	$Au_{0.333}Sb_{0.667}$	$5.67x10^{-3}$	$AuSb_2$	$AuSb_2$	[152]
Liquidus Minimum	=	$Au_{0.063}Sn_{0.937}$				
$AuSn_4$ (20)	NC	$Au_{0.200}Sn_{0.800}$	$1.59x10^{-2}$	$AuSn_4$	$AuSn_4$	[99, 152, 159–161]
$AuSn_2$ (24)	NC	$Au_{0.333}Sn_{0.667}$	$2.03x10^{-3}$		$AuSn_2$	[152, 160, 161]
AuSn (4)	C	$Au_{0.500}Sn_{0.500}$	$8.77x10^{-5}$		AuSn	[152, 162]
Au_5Sn (6)	NC	$Au_{0.833}Sn_{0.167}$	$1.33x10^{-8}$			
$Au_{10}Sn$ (16)	NC	$Au_{0.909}Sn_{0.091}$	$1.05x10^{-9}$			

Cont...

System	Congruency	Composition	Meeting Probability	Predicted Phase	Observed Phase(s)	Ref
Liquidus Minimum	=	$Au_{0.870}Ta_{0.130}$				
$AuTa_5$ (8)	NC	$Au_{0.167}Ta_{0.833}$	$1.23x10^{-6}$			
$AuTa_3$ (8)	NC	$Au_{0.250}Ta_{0.750}$	$9.48x10^{-6}$			
Au_2Ta_3 (-)	NC	$Au_{0.400}Ta_{0.600}$	$2.00x10^{-4}$			
AuTa (2) [a]	M	$Au_{0.500}Ta_{0.500}$	$1.05x10^{-3}$		AuTa	[145, 163, 164]
Au_2Ta (?) [b]	NC	$Au_{0.667}Ta_{0.333}$	$8.78x10^{-3}$	Au_2Ta		
Liquidus Minimum	=	$Au_{0.980}Ti_{0.020}$				
$AuTi_3$ (8)	C	$Au_{0.250}Ti_{0.750}$	$1.60x10^{-10}$			
AuTi (4)	C	$Au_{0.500}Ti_{0.500}$	$9.49x10^{-7}$			
Au_2Ti (6)	C	$Au_{0.667}Ti_{0.333}$	$1.12x10^{-4}$			
Au_4Ti (10)	NC	$Au_{0.800}Ti_{0.200}$	$2.79x10^{-3}$	Au_4Ti	Au_4Ti	[107, 157, 165]
Liquidus Minimum	=	$Au_{0.980}V_{0.020}$				
AuV_3 (4)	NC	$Au_{0.250}V_{0.750}$	$1.60x10^{-10}$			
Au_2V (12)	NC	$Au_{0.667}V_{0.333}$	$1.12x10^{-4}$		Au_2V	[157]
Au_4V (10)	NC	$Au_{0.800}V_{0.200}$	$2.79x10^{-3}$	Au_4V		
Liquidus Minimum	=	$Au_{0.020}Zn_{0.980}$				
$AuZn_8$ (2)	NC	$Au_{0.111}Zn_{0.889}$	$1.61x10^{-2}$	$AuZn_8$		
Au_2Zn_9 (-)	NC	$Au_{0.182}Zn_{0.818}$	$4.16x10^{-3}$			
$AuZn_3$ (32)	NC	$Au_{0.250}Zn_{0.750}$	$9.02x10^{-4}$		$AuZn_3$	[152]
Au_4Zn_9 (-)	C	$Au_{0.308}Zn_{0.692}$	$2.21x10^{-4}$			
Au_4Zn_5 (-)	NC	$Au_{0.444}Zn_{0.556}$	$5.02x10^{-6}$			
AuZn (2)	C	$Au_{0.500}Zn_{0.500}$	$9.49x10^{-7}$			
Au_5Zn_3 (16)	NC	$Au_{0.625}Zn_{0.375}$	$1.56x10^{-8}$			
Au_3Zn (32)	NC	$Au_{0.750}Zn_{0.250}$	$1.60x10^{-10}$			
Au_4Zn (-)	NC	$Au_{0.800}Zn_{0.200}$	$2.20x10^{-11}$			
Liquidus Minimum	=	$Au_{0.940}Zr_{0.060}$				
$AuZr_3$ (8)	C	$Au_{0.250}Zr_{0.750}$	$1.07x10^{-7}$			
$AuZr_2$ (6)	NC	$Au_{0.333}Zr_{0.667}$	$1.13x10^{-6}$			
Au_4Zr_5 (-)	C	$Au_{0.444}Zr_{0.556}$	$1.86x10^{-5}$			
$Au_{10}Zr_7$ (34)	NC	$Au_{0.588}Zr_{0.412}$	$4.08x10^{-4}$			
Au_2Zr (6)	C	$Au_{0.667}Zr_{0.333}$	$1.69x10^{-3}$			
Au_3Zr (8)	C	$Au_{0.750}Zr_{0.250}$	$6.32x10^{-3}$			
Au_4Zr (20)	NC	$Au_{0.800}Zr_{0.200}$	$1.24x10^{-2}$	Au_4Zr	Au_4Zr	[157]

[a] Metastable phase.
[b] There is uncertainty as to whether this phase exists [88].

5.2.4 Silicides

The full expression for phase prediction in silicides is:

$$P^{msr}_{phase}(x) = P^{m}_{A_sB_q}(x)P^{tot.}_{orient.}(x)\prod_{i,j=1}^{N,q}[1-exp(-\frac{E_i}{kT})][1-exp(-\frac{E^r_j}{kT})] \qquad (5.33)$$

where the value of x is the concentration corresponding to the liquidus minimum of the binary system under consideration. P^m_{sq} is the probability that atoms will come together in the correct ratio to form a phase A_sB_q. The factor,

$$\prod_{i=1}^{N}[1-exp(-\frac{E_i}{kT})] \qquad (5.34)$$

expresses the condition that atoms should not move away (migrate or diffuse) from each other after coming together. $P^{tot.}_{orient.}$ is the probability that the semiconductor atoms should have proper spatial orientation for bonding after coming together. The last probability expresses the condition that atoms of the semiconductor should not rotate after forming bonds. E_i is the activation energy for diffusion (migration) and E_i^r is the activation energy for rotation in the solid state. *If the activation energy for diffusion is proportional to the melting point of a solid shouldn't the activation energy for rotation be proportional to that temperature point at which phase cease to have a crystalline form - the peritectic point of the phase.* In general the temperature at which non-congruent phases cease to exist as phases (loose their crystalline structure) is lower than that of their congruent neighbours in the phase diagram. This suggest that the activation energy for rotations of non-congruent phases is much lower than that of congruent phases. A congruent phase should therefore be more stable against rotational thermal agitations which tend to break its bonds as compared to a non-congruent phase. *In the absence of values of $P^{tot.}_{orient}$; E_i and E_i^r, one should choose as a first phase, a congruent phase with the largest value of P^m_{sq} calculated at a concentration corresponding to the liquidus minimum of the binary system.* **Table 5.6** gives calculated values of the probability of meeting in the correct ratio to form silicide phases. Using probabilities of meeting in the correct ratio to form phases in the silicides, and taking into account the effect of atomic rotations which is due to the fact that the silicon bonds are directional in space, through congruency, good agreement is found between theoretical predictions and experimental observations. As can be seen from the accompanying table for silicides, correct predictions are made in twenty one silicide systems. There is failure to predict the first phase that forms in just four binary systems, viz. Gd-Si; Mn-Si; Ni-Si and Zr-Si.

TABLE 5.6: Metal-Si systems. Meeting probabilities for atoms of metal-silicon systems based on clusters of 8. These values have been calculated at the concentration of the lowest temperature eutectic (liquidus) of the binary system. For systems where the liquidus minimum coincides with the melting point of one of the elemental compounds , an arbitrary concentration value of 98 at.% of the element with the lowest melting point is taken. The number of atoms per unit cell is given in brackets behind each phase.

System	Congruency	Composition	Meeting Probability	Predicted Phase	Observed Phase	Ref
Liquidus Minimum	=	$Ca_{0.944}Si_{0.056}$				
Ca_2Si (12)	C	$Ca_{0.667}Si_{0.333}$	1.38×10^{-3}	Ca_2Si	Ca_2Si	[17]
CaSi (8)	C	$Ca_{0.500}Si_{0.500}$	4.69×10^{-5}			
$CaSi_2$ (3/6)	NC	$Ca_{0.333}Si_{0.667}$	7.23×10^{-7}			
Liquidus Minimum	=	$Co_{0.775}Si_{0.225}$				
Co_2Si (12)	C	$Co_{0.667}Si_{0.333}$	2.04×10^{-2}	Co_2Si	Co_2Si	[18–23]
CoSi (8)	C	$Co_{0.500}Si_{0.500}$	5.92×10^{-3}			
$CoSi_2$ (12)	C	$Co_{0.333}Si_{0.667}$	7.74×10^{-4}			
Liquidus Minimum	=	$Cr_{0.180}Si_{0.820}$				
Cr_3Si (8)	C	$Cr_{0.750}Si_{0.250}$	5.93×10^{-5}			
Cr_5Si_3 (32)	C	$Cr_{0.625}Si_{0.375}$	5.37×10^{-4}			
CrSi (8)	NC	$Cr_{0.500}Si_{0.500}$	3.04×10^{-3}			
$CrSi_2$ (9)	C	$Cr_{0.333}Si_{0.667}$	1.52×10^{-3}	$CrSi_2$	$CrSi_2$	[3, 18, 23–27]
Liquidus Minimum	=	$Cu_{0.700}Si_{0.300}$				
$Cu_{56}Si_{11}$ (–)	NC	$Cu_{0.836}Si_{0.164}$	2.14×10^{-2}			
Cu_4Si (–)	NC	$Cu_{0.800}Si_{0.200}$	2.43×10^{-2}			
$Cu_{19}Si_6$ (–)	C	$Cu_{0.760}Si_{0.240}$	2.64×10^{-2}	$Cu_{19}Si_6$	$Cu_{19}Si_6$	[18]
Liquidus Minimum	=	$Er_{0.150}Si_{0.850}$				
Er_5Si_3 (16)	C	$Er_{0.625}Si_{0.375}$	2.41×10^{-4}			
ErSi (8)	?	$Er_{0.500}Si_{0.500}$	1.70×10^{-3}			
Er_3Si_5 (–) [a]	?	$Er_{0.375}Si_{0.625}$	7.64×10^{-3}	Er_3Si_5	Er_3Si_5	[18, 28]
Liquidus Minimum	=	$Fe_{0.670}Si_{0.330}$				
Fe_3Si (16)	NC	$Fe_{0.750}Si_{0.250}$	2.47×10^{-2}			
FeSi (8)	C	$Fe_{0.500}Si_{0.500}$	1.52×10^{-2}	FeSi	FeSi	[18, 29]
$FeSi_2$ (3)	NC	$Fe_{0.333}Si_{0.667}$	4.03×10^{-3}			
Liquidus Minimum	=	$Gd_{0.847}Si_{0.153}$				
Gd_5Si_3 (16)	C	$Gd_{0.625}Si_{0.375}$	7.67×10^{-3}	Gd_5Si_3		
Gd_5Si_4 (36)	?	$Gd_{0.556}Si_{0.444}$	3.80×10^{-3}			
GdSi (8)	?	$Gd_{0.500}Si_{0.500}$	1.89×10^{-3}			
Gd_2Si_3 (–)	?	$Gd_{0.400}Si_{0.600}$	4.23×10^{-4}			
$GdSi_2$ (12)	C	$Gd_{0.333}Si_{0.667}$	1.14×10^{-4}		$GdSi_2$	[30, 31]
Liquidus Minimum	=	$Hf_{0.080}Si_{0.920}$				
Hf_3Si (–)	NC	$Hf_{0.750}Si_{0.250}$	5.76×10^{-7}			
Hf_2Si (12)	NC	$Hf_{0.667}Si_{0.333}$	4.96×10^{-6}			
Hf_5Si_3 (16)	NC	$Hf_{0.625}Si_{0.375}$	1.32×10^{-5}			
Hf_3Si_2 (10)	NC	$Hf_{0.600}Si_{0.400}$	2.32×10^{-5}			
Hf_5Si_4 (36)	NC	$Hf_{0.556}Si_{0.444}$	6.17×10^{-5}			
HfSi (8)	C	$Hf_{0.500}Si_{0.500}$	1.89×10^{-4}	HfSi	HfSi	[18, 32, 33]
$HfSi_2$ (12)	NC	$Hf_{0.333}Si_{0.667}$	2.24×10^{-3}			

Cont...

System	Congruency	Composition	Meeting Probabilities	Predicted Phase	Observed Phase(s)	Ref
Liquidus Minimum	=	$Mg_{0.988}Si_{0.012}$				
Mg_2Si (12)	C	$Mg_{0.667}Si_{0.333}$	1.86×10^{-5}	Mg_2Si	Mg_2Si	[34]
Liquidus Minimum	=	$Mn_{0.790}Si_{0.210}$				
Mn_6Si (13)	NC	$Mn_{0.857}Si_{0.143}$	3.00×10^{-2}			
Mn_9Si_2 (110)	NC	$Mn_{0.818}Si_{0.182}$	3.04×10^{-2}			
Mn_3Si (16)	NC	$Mn_{0.750}Si_{0.250}$	2.71×10^{-2}		Mn_3Si	[35]
Mn_5Si_2 (56)	NC	$Mn_{0.714}Si_{0.286}$	2.38×10^{-2}			
Mn_5Si_3 (16)	C	$Mn_{0.625}Si_{0.375}$	1.45×10^{-2}	Mn_5Si_3		
MnSi (8)	C	$Mn_{0.500}Si_{0.500}$	4.85×10^{-3}		MnSi	[18,36]
$Mn_{11}Si_{19}$ (120)	C	$Mn_{0.367}Si_{0.633}$	9.14×10^{-4}			
Liquidus Minimum	=	$Mo_{0.017}Si_{0.983}$				
Mo_3Si (8)	NC	$Mo_{0.750}Si_{0.250}$	2.87×10^{-11}			
Mo_5Si_3 (16/32)	C	$Mo_{0.625}Si_{0.375}$	3.75×10^{-9}			
$MoSi_2$ (6)	C	$Mo_{0.333}Si_{0.667}$	5.35×10^{-5}	$MoSi_2$	$MoSi_2$	[18,37–40]
Liquidus Minimum	=	$Nb_{0.050}Si_{0.950}$				
Nb_5Si_3 (32)	C	$Nb_{0.625}Si_{0.375}$	1.39×10^{-6}			
$NbSi_2$ (9)	C	$Nb_{0.333}Si_{0.667}$	1.10×10^{-3}	$NbSi_2$	$NbSi_2$	[18,39]
Liquidus Minimum	=	$Ni_{0.535}Si_{0.465}$				
Ni_3Si (4)	NC	$Ni_{0.750}Si_{0.250}$	1.26×10^{-2}			
Ni_5Si_2 (43)	C	$Ni_{0.714}Si_{0.286}$	1.56×10^{-2}			
Ni_2Si (6/12)	C	$Ni_{0.667}Si_{0.333}$	1.94×10^{-2}		Ni_2Si	[18,41–49]
Ni_3Si_2 (80)	NC	$Ni_{0.600}Si_{0.400}$	2.33×10^{-2}			
NiSi (8)	C	$Ni_{0.500}Si_{0.500}$	2.42×10^{-2}	NiSi	NiSi	
$NiSi_2$ (12)	NC	$Ni_{0.333}Si_{0.667}$	1.37×10^{-2}			
Liquidus Minimum	=	$Os_{0.120}Si_{0.880}$				
OsSi (2/8)	NC	$Os_{0.500}Si_{0.500}$	7.98×10^{-4}			
Os_2Si_3 (40)	C	$Os_{0.400}Si_{0.600}$	3.39×10^{-3}	Os_2Si_3	Os_2Si_3	[18,50]
$OsSi_2$ (12/48)	NC	$Os_{0.333}Si_{0.667}$	7.54×10^{-3}			
Liquidus Minimum	=	$Pd_{0.845}Si_{0.155}$				
Pd_5Si (24)	NC	$Pd_{0.833}Si_{0.167}$	3.18×10^{-2}			
Pd_9Si_2 (44)	NC	$Pd_{0.818}Si_{0.182}$	3.05×10^{-2}			
Pd_3Si (16)	NC	$Pd_{0.750}Si_{0.250}$	2.22×10^{-2}			
Pd_2Si (9)	C	$Pd_{0.667}Si_{0.333}$	1.20×10^{-2}	Pd_2Si	Pd_2Si	[18,39,34,51,52]
PdSi (8) [b]	C	$Pd_{0.500}Si_{0.500}$	1.89×10^{-3}			
Liquidus Minimum	=	$Pt_{0.770}Si_{0.230}$				
Pt_3Si (16)	NC	$Pt_{0.750}Si_{0.250}$	2.78×10^{-2}			
Pt_7Si_3 (–) [c]	NC	$Pt_{0.700}Si_{0.300}$	2.41×10^{-2}			
Pt_2Si (6)	C	$Pt_{0.667}Si_{0.333}$	2.09×10^{-2}	Pt_2Si	Pt_2Si	[51,53–55]
Pt_6Si_5 (22)	NC	$Pt_{0.545}Si_{0.455}$	9.42×10^{-3}			
PtSi (8)	C	$Pt_{0.500}Si_{0.500}$	6.29×10^{-3}			
Liquidus Minimum	=	$Rh_{0.315}Si_{0.685}$				
Rh_2Si (12)	C	$Rh_{0.667}Si_{0.333}$	3.34×10^{-3}			
Rh_5Si_3 (16)	NC	$Rh_{0.625}Si_{0.375}$	5.12×10^{-3}			
Rh_3Si_2 (6)	NC	$Rh_{0.600}Si_{0.400}$	6.47×10^{-3}			
RhSi (8)	C	$Rh_{0.500}Si_{0.500}$	1.38×10^{-2}	RhSi	RhSi	[18,56]
Rh_4Si_5 (18)	NC	$Rh_{0.444}Si_{0.556}$	1.86×10^{-2}			
Rh_3Si_4 (28)	NC	$Rh_{0.429}Si_{0.571}$	1.98×10^{-2}			
Liquidus Minimum	=	$Ru_{0.170}Si_{0.830}$				
Ru_4Si_3 (28)	?	$Ru_{0.571}Si_{0.429}$	8.90×10^{-4}			
RuSi (8)	C	$Ru_{0.500}Si_{0.500}$	2.54×10^{-3}			
Ru_2Si_3 (40)	C	$Ru_{0.400}Si_{0.600}$	7.78×10^{-3}	Ru_2Si_3	Ru_2Si_3	[18,50]

Cont...

System	Congruency	Composition	Meeting Probability	Predicted Phase	Observed Phase(s)	Ref
Liquidus Minimum	=	$Ta_{0.010}Si_{0.990}$				
$Ta_{4.5}Si$ (–)	C	$Ta_{0.818}Si_{0.182}$	$1.11x10^{-13}$			
Ta_2Si (12)	C	$Ta_{0.667}Si_{0.333}$	$9.27x10^{-11}$			
Ta_5Si_3 (32)	C	$Ta_{0.625}Si_{0.375}$	$5.02x10^{-10}$			
$TaSi_2$ (9)	C	$Ta_{0.333}Si_{0.667}$	$1.86x10^{-5}$	$TaSi_2$	$TaSi_2$	[18,39]
Liquidus Minimum [d]	=	$Ti_{0.160}Si_{0.840}$				
Ti_3Si (32)	NC	$Ti_{0.750}Si_{0.250}$	$3.07x10^{-5}$			
Ti_5Si_3 (16)	C	$Ti_{0.625}Si_{0.375}$	$3.21x10^{-4}$		Ti_5Si_3	[32,58,66–69]
Ti_5Si_4 (36)	NC	$Ti_{0.556}Si_{0.444}$	$9.68x10^{-4}$			
TiSi (8)	NC	$Ti_{0.500}Si_{0.500}$	$2.09x10^{-3}$		TiSi	[18,32,58,69,63–65,70–
$TiSi_2$ (24)	C	$Ti_{0.333}Si_{0.667}$	$1.27x10^{-2}$	$TiSi_2$	$TiSi_2$	[18,34,58,66,67,63–65,57,
Liquidus Minimum	=	$V_{0.030}Si_{0.970}$				
V_3Si (8)	C	$V_{0.750}Si_{0.250}$	$1.78x10^{-9}$			
V_5Si_3 (32)	C	$V_{0.625}Si_{0.375}$	$1.15x10^{-7}$			
VSi_2 (9)	C	$V_{0.333}Si_{0.667}$	$3.14x10^{-4}$	VSi_2	VSi_2	[18,39,34,74]
Liquidus Minimum	=	$W_{0.010}Si_{0.990}$				
W_5Si_3 (16/32)	C	$W_{0.625}Si_{0.375}$	$5.02x10^{-10}$			
WSi_2 (6)	C	$W_{0.333}Si_{0.667}$	$1.86x10^{-5}$	WSi_2	WSi_2	[18,39,40,28,75]
Liquidus Minimum	=	$Y_{0.180}Si_{0.820}$				
Y_5Si_3 (16)	C	$Y_{0.625}Si_{0.375}$	$5.73x10^{-4}$			
Y_5Si_4 (36)	C	$Y_{0.556}Si_{0.444}$	$1.50x10^{-3}$			
YSi (8)	C	$Y_{0.500}Si_{0.500}$	$3.04x10^{-3}$			
Y_3Si_5 (3)	C	$Y_{0.375}Si_{0.625}$	$1.10x10^{-2}$	Y_3Si_5	Y_3Si_5	[18,28]
Liquidus Minimum	=	$Zr_{0.100}Si_{0.900}$				
Zr_2Si (12)	NC	$Zr_{0.667}Si_{0.333}$	$1.54x10^{-5}$			
Zr_5Si_3 (16)	NC	$Zr_{0.625}Si_{0.375}$	$2.30x10^{-5}$			
Zr_3Si_2 (10)	NC	$Zr_{0.600}Si_{0.400}$	$6.32x10^{-5}$			
Zr_5Si_4 (36)	C	$Zr_{0.556}Si_{0.444}$	$1.54x10^{-4}$	Zr_5Si_4		
ZrSi (8)	NC	$Zr_{0.500}Si_{0.500}$	$4.21x10^{-4}$			
$ZrSi_2$ (12)	NC	$Zr_{0.333}Si_{0.667}$	$4.18x10^{-3}$		$ZrSi_2$	[18,23]

[a] This phase is sometimes referred to as $ErSi_{1.7}$[166].
[b] A recent publication [167] shows that this phase is probably only stable above 824°C.
[c] Also referred to as Pt_5Si_2 or $Pt_{12}Si_5$ [16].
[d] Ti has another lowest eutectic point at the same temperature (1330°C) for a composition of 14 at % Si [16].

In the Gd-Si system, Gd_5Si_3 is predicted, but $GdSi_2$ is found to form as a first phase experimentally. There is a large difference between the probabilities of meeting in the correct ratio to form phases for atoms of the phases Gd_5Si_3 and those of $GdSi_2$. An explanation that may be given is that the activation energy of diffusion in Gd_5Si_3 of either Gd or Si is very low or that the activation energy of rotation of Si in Gd_5Si_3 is low. The same argument can be used in the case of the Mn-Si system. It is interesting to note in this system that the non-congruent phase Mn_3Si is also found as a first phase. It is not the congruency or non-congruency of a phase that determines whether the phase will form first or not, but the underlying physical property of ease of rotation of an atom with directional bonds. $P^m_{A_sB_q}$ for this phase

(Mn_3Si) is a little larger than that of the phase MnSi. If the effect of the probability associated with the activation energy of rotation is to reduce the overall probability P^{msr}_{phase}, then the two overall probabilities for both systems may end up being nearly equal. In the case of the Ni-Si system, values of P^{m}_{sq} for both phases, Ni_2Si and NiSi are nearly equal. Both phases are congruent. It is therefore not surprising that both are found experimentally as first phases. The case of Zr-Si is straightforward to explain because the experimentally found first phase $ZrSi_2$ is non-congruent and has a large $P^{m}_{A_sB_q}$. If the effect of rotations is to reduce the overall probability of phase formation P^{msr}_{phase}, and this reduction is not that large in this case, then $ZrSi_2$ should form first.

5.2.5 Germanides

Probabilities for atoms to meet in the correct ratio to form phases have been calculated for germanide systems. these are shown in **Table 5.7**. Predicted first phases are those which are congruent and have largest meeting probabilities. As can be seen from the table there is good agreement between predicted first phases and experimentally observed first phases. Out of ten systems, first phases are predicted correctly in eight systems. In the case of the Co-Ge system the non-congruent phase CoGe is found to form first at times. Its meeting probability is slightly larger than that of the congruent first phase, Co_5Ge_3. Such behaviour may happen if the activation energies of rotation of Ge atoms in the phase CoGe are not that small. Pt-Ge is another system where more than one first phase is found. One of the phases found experimentally to form first is the non-congruent phase, Pt_3Ge_2. Note how close the probabilities of meeting in the three experimentally found first phases are. The Ti-Ge system is another system where one of the experimentally found first phases is non-congruent. Note that in the three cases where a non-congruent phase is found to form first, its meeting probability is larger than that of the experimentally found congruent phase.

TABLE 5.7: Metal-Ge systems. Meeting Probabilities for atoms of metal-Ge systems based on clusters of 8. These values have been calculated at the concentration of the lowest temperature eutectic (liquidus) of the binary system. A basic cluster of eight was chosen for all systems. For systems where the liquidus minimum coincides with the melting point of one of the elemental compounds , an arbitrary concentration value of 98 at.% of the element with the lowest melting point is taken. The number of atoms per unit cell is given in brackets behind each phase.

System	Congruency	Composition	Meeting Probability	Predicted Phase	Observed Phase	Ref
Liquidus Minimum	=	$Co_{0.270}Ge_{0.730}$				
Co_5Ge_2 (6)	NC	$Co_{0.714}Ge_{0.286}$	$9.17x10^{-4}$			
Co_5Ge_3 (12) [a]	C	$Co_{0.625}Ge_{0.375}$	$2.87x10^{-3}$	Co_5Ge_3	Co_5Ge_3	[80,81]
CoGe (8 or 16)	NC	$Co_{0.500}Ge_{0.500}$	$9.64x10^{-3}$		CoGe	[81]
Co_5Ge_7 (24)	NC	$Co_{0.417}Ge_{0.583}$	$1.69x10^{-2}$			
$CoGe_2$ (24)	NC	$Co_{0.333}Ge_{0.667}$	$2.41x10^{-2}$			
Liquidus Minimum	=	$Cu_{0.635}Ge_{0.365}$				
Cu_5Ge (2)	NC	$Cu_{0.833}Ge_{0.167}$	$1.46x10^{-2}$			
Cu_3Ge (8)	NC	$Cu_{0.750}Ge_{0.250}$	$2.19x10^{-2}$	Cu_3Ge	Cu_3Ge	[82]
Liquidus Minimum	=	$Hf_{0.030}Ge_{0.970}$				
Hf_3Ge (32)	NC	$Hf_{0.750}Ge_{0.250}$	$1.78x10^{-9}$			
Hf_2Ge (12)	NC	$Hf_{0.667}Ge_{0.333}$	$3.07x10^{-8}$			
Hf_5Ge_3 (16)	C	$Hf_{0.625}Ge_{0.375}$	$1.15x10^{-7}$	Hf_5Ge_3	Hf_5Ge_3	[80]
Hf_3Ge_2 (10)	NC	$Hf_{0.600}Ge_{0.400}$	$2.49x10^{-7}$			
HfGe (-)	NC	$Hf_{0.500}Ge_{0.500}$	$4.61x10^{-6}$			
$HfGe_2$ (12)	NC	$Hf_{0.333}Ge_{0.667}$	$3.14x10^{-4}$			
Liquidus Minimum	=	$Mn_{0.475}Ge_{0.525}$				
$Mn_{3.25}Ge$ (2)	NC	$Mn_{0.765}Ge_{0.235}$	$1.17x10^{-3}$			
Mn_5Ge_2 (28)	NC	$Mn_{0.714}Ge_{0.286}$	$1.08x10^{-2}$			
Mn_5Ge_3 (16)	C	$Mn_{0.625}Ge_{0.375}$	$1.79x10^{-2}$	Mn_5Ge_3	Mn_5Ge_3	[80]
$Mn_{11}Ge_8$ (76)	NC	$Mn_{0.579}Ge_{0.421}$	$2.11x10^{-2}$			
Liquidus Minimum	=	$Ni_{0.330}Ge_{0.670}$				
Ni_3Ge (4)	C	$Ni_{0.750}Ge_{0.250}$	$1.50x10^{-3}$			
Ni_2Ge (12)	NC	$Ni_{0.667}Ge_{0.333}$	$4.03x10^{-3}$			
Ni_5Ge_3 (4 or 32) [b]	C	$Ni_{0.625}Ge_{0.375}$	$6.04x10^{-3}$	Ni_5Ge_3	Ni_5Ge_3	[78,80,91]
NiGe (8)	NC	$Ni_{0.500}Ge_{0.500}$	$1.52x10^{-2}$			
Liquidus Minimum	=	$Pd_{0.360}Ge_{0.640}$				
Pd_5Ge (24)	NC	$Pd_{0.833}Ge_{0.167}$	$7.30x10^{-4}$			
Pd_3Ge (-)	NC	$Pd_{0.750}Ge_{0.250}$	$2.31x10^{-3}$			
$Pd_{25}Ge_9$ (34)	NC	$Pd_{0.735}Ge_{0.265}$	$2.75x10^{-3}$			
$Pd_{21}Ge_8$ (116)	NC	$Pd_{0.724}Ge_{0.276}$	$3.13x10^{-3}$			
Pd_2Ge (9)	C	$Pd_{0.667}Ge_{0.333}$	$5.67x10^{-3}$		Pd_2Ge	[78,80,83,89]
PdGe (8)	C	$Pd_{0.500}Ge_{0.500}$	$1.79x10^{-2}$	PdGe		
Liquidus Minimum	=	$Pt_{0.700}Ge_{0300}$				
Pt_3Ge (16)	NC	$Pt_{0.750}Ge_{0.250}$	$2.66x10^{-2}$			
Pt_2Ge (9)	C	$Pt_{0.667}Ge_{0.333}$	$2.55x10^{-2}$	Pt_2Ge	Pt_2Ge	[78,79]
Pt_3Ge_2 (20)	NC	$Pt_{0.600}Ge_{0.400}$	$2.10x10^{-2}$		Pt_3Ge_2	[85]
PtGe (8)	C	$Pt_{0.500}Ge_{0.500}$	$1.24x10^{-2}$		PtGe	[85]
Pt_2Ge_3 (20)	NC	$Pt_{0.400}Ge_{0.600}$	$5.49x10^{-3}$			
$PtGe_2$ (6)	NC	$Pt_{0.333}Ge_{0.667}$	$2.73x10^{-3}$			

Cont...

System	Congruency	Composition	Meeting Probability	Predicted Phase	Observed Phase(s)	Ref
Liquidus Minimum	=	$Rh_{0.230}Ge_{0.770}$				
Rh_2Ge (12)	?	$Rh_{0.667}Ge_{0.333}$	$8.55\text{x}10^{-4}$			
Rh_5Ge_3 (16)	NC	$Rh_{0.625}Ge_{0.375}$	$1.51\text{x}10^{-3}$			
RhGe (8)	C	$Rh_{0.500}Ge_{0.500}$	$6.29\text{x}10^{-3}$	RhGe	RhGe	[80]
$Rh_{17}Ge_{22}$ (156)	NC	$Rh_{0.436}Ge_{0.564}$	$1.10\text{x}10^{-2}$			
Liquidus Minimum	=	$Ti_{0.110}Ge_{0.890}$				
Ti_5Ge_3 (16)	C	$Ti_{0.625}Ge_{0.375}$	$5.86\text{x}10^{-5}$	Ti_5Ge_3	Ti_5Ge_3	[78]
Ti_6Ge_5 (44)	NC	$Ti_{0.545}Ge_{0.455}$	$2.70\text{x}10^{-4}$		Ti_6Ge_5	[84]
$TiGe_2$ (24)	NC	$Ti_{0.333}Ge_{0.667}$	$6.35\text{x}10^{-3}$			
Liquidus Minimum	=	$Zr_{0.013}Ge_{0.987}$				
Zr_3Ge (32)	NC	$Zr_{0.750}Ge_{0.250}$	$2.87\text{x}10^{-11}$			
Zr_5Ge_3 (16)	C	$Zr_{0.625}Ge_{0.375}$	$3.75\text{x}10^{-9}$	Zr_5Ge_3		
Zr_5Ge_4 (36)	?	$Zr_{0.556}Ge_{0.444}$	$4.66\text{x}10^{-8}$			
ZrGe (8)	NC [c]	$Zr_{0.500}Ge_{0.500}$	$3.07\text{x}10^{-7}$		ZrGe	[168]
$ZrGe_2$ (12)	NC	$Zr_{0.333}Ge_{0.667}$	$5.35\text{x}10^{-5}$			

[a] Also referred to as Co_2Ge [81].
[b] This phase was previously referred to as Ni_2Ge [80,78] due to insufficient data on the phase diagram [169].
[c] Only slightly non-congruent ($\Delta T = 20°C$).

The extent to which the Ge atoms in the non-congruent phases rotate (which is determined by the activation energy of rotation) must be reducing the probability of forming these phases to a value which is close to that of forming the congruent phases. There is failure to predict experimentally found first phases correctly in two systems, Pd-Ge and Zr-Ge. In the Pd-Ge system Pd_2Ge is found experimentally as a first phase but PdGe is the predicted first phase. Both phases are congruent. In the Zr-Ge system, Zr_5Ge_3 is predicted to form first, but ZrGe is the experimentally found first phase. Note the large difference in the probabilities of meeting in the phase Zr_5Ge_3 and ZrGe.

5.3 Solid State Kinetics

There are interesting questions that need to be answered. How much first phase forms before there is a changeover to the next phase? What is the physics governing this formation in the solid state?

Consider the reaction region. Atoms which are not bonded to any cluster belong to the broth x_b and are milling around in the reaction region.For each compound phase there is a rate a at which it is forming and another rate b at which it is dissolving into it's constituent parts. The rate at which a compound phase forms

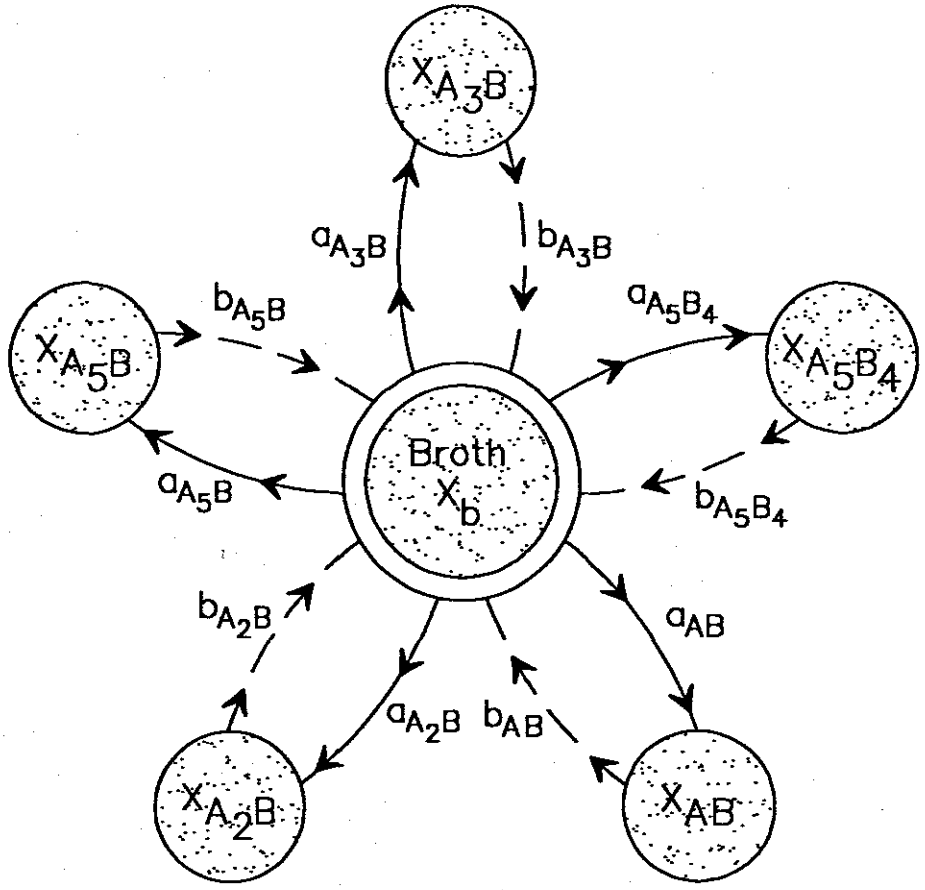

FIGURE 5.10: Diagram showing rates of forming different phases.

will be proportional to the amount of the broth x_b. The rate at which it breaks into its constituent parts is proportional to the amount that has formed e.g.x_{A_3B}. We therefore obtain the rate equations (see **Fig. 5.10**):

$$\frac{dx_{A_3B}}{dt} = a_{A_3B}x_b - b_{A_3B}x_{A_3B} \tag{5.35}$$

$$\frac{dx_{A_5B}}{dt} = a_{A_5B}x_b - b_{A_5B}x_{A_5B} \tag{5.36}$$

$$\frac{dx_{A_5B_4}}{dt} = a_{A_5B_4}x_b - b_{A_5B_4}x_{A_5B_4} \tag{5.37}$$

$$\frac{dx_{AB}}{dt} = a_{AB}x_b - b_{AB}x_{AB} \tag{5.38}$$

$$\frac{dx_{AB_2}}{dt} = a_{AB_2}x_b - b_{AB_2}x_{AB_2} \tag{5.39}$$

and the rate of change of the broth is :

$$\frac{dx_b}{dt} = -[\frac{dx_{A_3B}}{dt} + \frac{dx_{A_5B_3}}{dt} + \frac{dx_{AB}}{dt} + \frac{dx_{AB_2}}{dt}] \tag{5.40}$$

where a_{A_3B} ... a_{AB_2} ; b_{A_3B} ... b_{AB_2} are rate constants(variables in a non-equilibrium environment). They will of course depend on temperature.

To solve this system of equations try a solution of the form:

$$x_{A_3B} = c_1 \exp(\lambda t) \tag{5.41}$$

$$x_{A_5B} = c_2 \exp(\lambda t) \tag{5.42}$$

and substitute into the rate equations. What is the form of the rate constants (variables) a and b ? The value of a is obtained from the probability of phase formation P^{msr}_{phase}. It is;

$$a_{A_sB_q} = \nu_o k_{A_sB_q} P^{mv}_{A_sB_q}(x) P^{tot.}_{orient.} \prod_{i,j=1}^{N,q} [1 - exp(-\frac{E_i}{kT})][1 - exp(-\frac{E^r_j}{kT})] \tag{5.43}$$

$$b_{A_sB_q} = \nu_o l_{A_sB_q} \prod_{i,j=1}^{N,q} [exp(-\frac{E_i}{kT})][exp(-\frac{E^r_j}{kT})] \tag{5.44}$$

ν_o is the vibrational frequency of the solid and $k_{A_sB_q}$ and $l_{A_sB_q}$ are fitting constants.

$\mathrm{P}^{mv}_{A_sB_q}(x)$ is a probability for atoms to meet in the correct ratio to form a phase $\mathrm{A_sB_q}$ at a prevailing concentration x of the growth interface, $1 - \frac{\exp(-E_i)}{kT}$ has something to do with stability against breaking into constituent parts, $\mathrm{P}^{tot.}_{orient}$ has something to do with directionality of bonding for semiconductor atoms , $1 - \frac{\exp(-E^r_j)}{kT}$ expresses stability against rotational effects that may break bonds in semiconductor-metal phases. ν_o is the vibrational frequency of the solid. The units of a are in per second, as can be expected. It is noticed from the expression for a that its dependance on concentration comes only through the probability of atoms to meet in the correct ratio to form a phase. This is the only part that determines the non-equilibrium nature of the rate equations. In an equilibrium environment a does not vary with time. In thin films its variation with time comes from the rate at which atomic concentrations are changing at the interface. This rate of change is expressed mathematically by the diffusion equation.

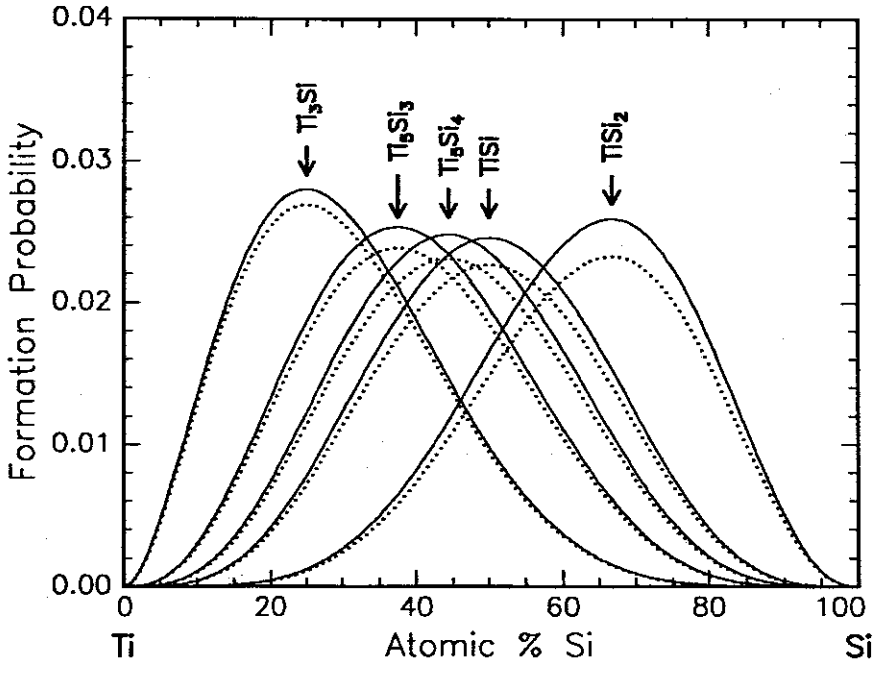

FIGURE 5.11: A graph showing the effect of the orientational probability for the binary system Ti-Si. $P_{orient.}$, tend to depress the probability of formation depending on atomic % composition of the semiconductor on a phase. Dotted lines include the effect of $P_{orient.}$, and the solid lines do not take it into account. Pure metals are not affected whereas a pure semiconductor crystal like Si is affected the most. A basic cluster of eight was chosen and P_{orient} was put equal to 0.98 for this calculation .

The probability $P_{orient.}$ expresses the fact that all semiconductor atoms must be properly orientated in the cluster of a particular phase so that , that phase is formed. The effect of $P_{orient.}$ is to favour the more metal-rich phases when first phase formation occurs. This effect is clearly demonstrated in **Fig. 5.11**. The dotted lines are for the probability P^{mvr}_{phase} with the effect of $P_{orient.}$, and the solid lines are without the effect of $P_{orient.}$ (Both cases do not include (stability) probabilities associated with activation energies).

Meeting probabilities $P^{mv}_{A_sB_q}$ are vertically normalized. This means that at any concentration x if they are added for different phases within one system the sum obtained will be unity. In this case it is important to include the two trivial cases of atoms of A meeting to form solid A, and atoms of B meeting to form solid B. As an example the Nb-Al system is looked at. **Fig. 5.12** shows the meeting probabilities

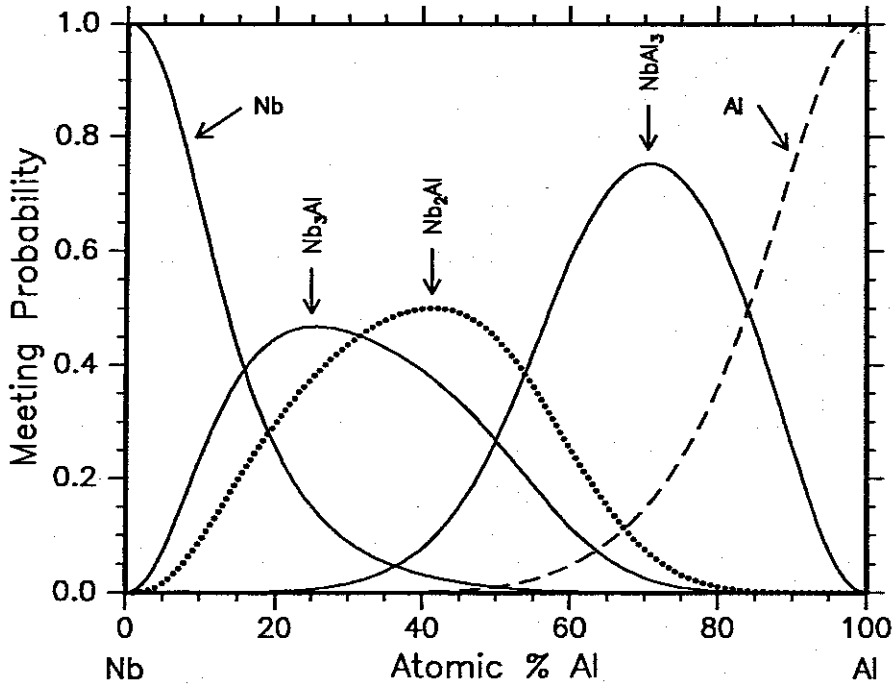

FIGURE 5.12: A graph of meeting probability for the binary system Nb-Al. Meeting probabilities are normalized such that at any atomic % composition they add up to unity. A basic cluster of eight was chosen for this calculation.

normalized vertically for this system.

5.4 Relationship Between Statistical and EHF Model

In equations 5.1 and 5.2 the activation energy E is replaced by ΔG. For interactions happening in the solid state the following approximation may be made:

$$\Delta G \approx \Delta H \tag{5.45}$$

since TΔS is small. ΔG is a change in Gibbs free energy, T is the temperature and H is the enthalpy. We may therefore infer that activation energies are proportional to the heats of formation of the phases i.e.

$$E \propto \Delta H \tag{5.46}$$

It is informative to look more closely to the behaviour of the activation energy while the phase is forming. Before the phase begins to form there should be a mixture of

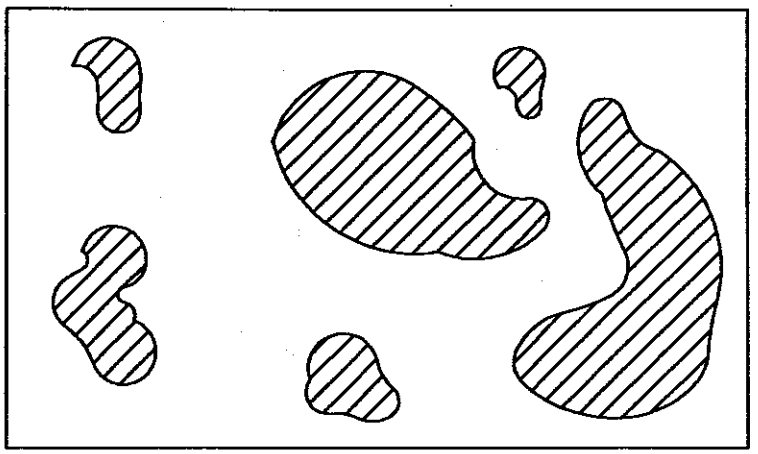

FIGURE 5.13: Sketch showing shaded regions of growing clusters that make up a crystalline phase A_sB_q. When there is no crystalline phase present the activation energy (a small positive value) of diffusion is that of an amorphous phase of composition A_sB_q. The heat of formation is that of an amorphous phase A_sB_q (a small negative value). As clusters of the crystalline phase grow magnitudes of both heat of formation and activation energy tend to that of a crystalline phase A_sB_q.

atoms which are not bonded to each other. The state in the reaction interface, can be thought of as amorphous. The activation energy is the average of the barrier heights presented to each atom that attempts to leave its position (atoms are hopping from point to point in the interaction region, a process which is clearly diffusional). As the phase forms more and more atoms will be anchored in position, and it will be more difficult for them to migrate (i.e. they have gone into a state of lower energy which is more stable). Since activation energies are an average over all diffusional barriers under consideration, then its value will rise, depending on how much phase has formed. The activation energy will therefore evolve from that of an amorphous phase A_sB_q towards that of a crystalline phase A_sB_q (a larger more positive value). If the activation energies in the amorphous phase are large i.e. the atoms do not hop from position to position that often, trying to position themselves in proper lattice positions, then the crystalline phase will not form. **Fig. 5.13** shows clusters of a crystalline phase growing in a sea of an amorphous composition A_sB_q. Heats of formation have a similar behaviour. The heat of formation of a mixture that will finally make up the first phase, is after the atoms have been released into

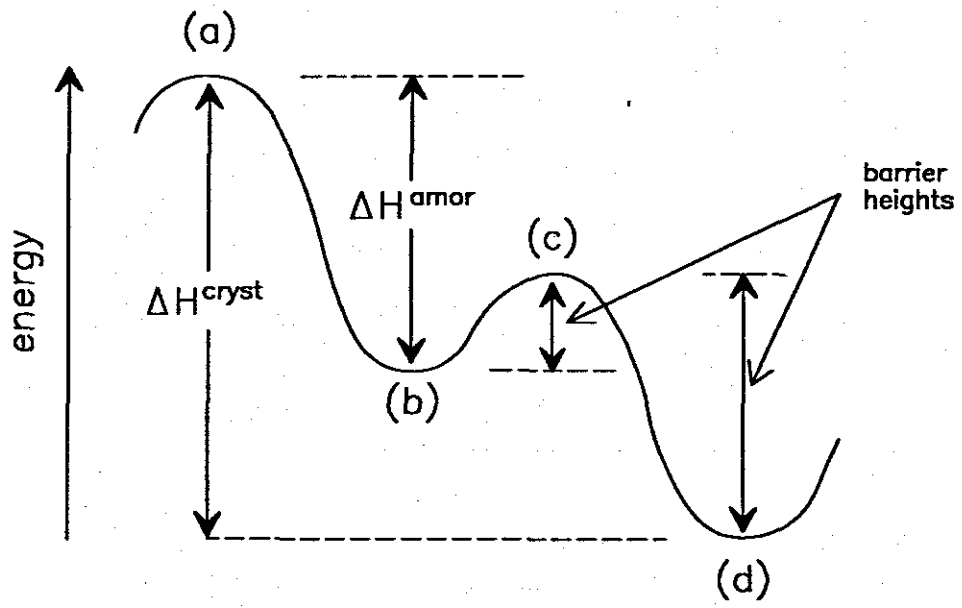

FIGURE 5.14: Solid state interaction in the reaction region. Various states discussed in the text are shown.

the interaction region, that of an amorphous phase. Treat heats of formation as averages of heats released as phases form. Then, as more atoms cluster together to form a phase (e.g. a first phase,) heats of formation will be evolving from that of an amorphous phase (a smaller negative value) approaching those of crystalline phases (larger more negative values) as more of the phase forms. It can be seen that in these activation energies can be used interchangeable with heats of formation as described in the EHF model. **Fig. 5.14.** shows changes in heats of formation for various states during phase formation. The standard reference point for heats of formation here has been taken to be the gaseous state. The difference in energy between state (a) and state (d) gives the usual heat of crystallization. The difference between state (a) and (b) is the heat of amorphization. The difference between states (b) and (c) is the barrier height against diffusion in the amorphous state. The difference between states (c) and (d) is the barrier height against diffusion in the crystalline state. The following points are worth mentioning:

1. After being released into the interaction region atoms (those mixing at the fastest rate), find themselves in state (*b*). If the barrier height (difference

between (b) and (c) is large) then the first phase should be amorphous. (Pretorius *et al* in his article [15] has, when explaining the formation of amorphous phases, mentioned this barrier to be that due to nucleation). The amorphous phase is stable and will be the first phase (the statistical model is in this case in complete agreement with the EHF model).

2. If the barrier height between (b) and (c) is not that large, then atoms will continue intermixing, and correct configurations will lead them into state (d). This should be the first phase, if the barrier height between (d) and (c) is large enough (i.e. intermixing rate is reduced – phase is stable).

3. If the barrier height (difference between (c) and (d)) is not that large than the clusters will not stay in state (d), their atoms will continue intermixing. The phase whose clusters are meeting correctly in the next fastest rate, if they are stable enough, will in this case form the first phase.

In all these cases it can be seen that it is changes in energy (or heats of formation that play a role in phase formation). If the barrier height between (d) and (c) is not that large then it can be written,

$$E \simeq \Delta H^{amor} - \Delta H^{cryst} \tag{5.47}$$

which means

$$E \propto \Delta H^{cryst} \tag{5.48}$$

or

$$E = \beta \Delta H \tag{5.49}$$

it is seen that β must be a small negative fraction.

A question is often asked why doesn't a phase with the largest heat of formation form first. The answer to this question is simple. Introduce an **equal a priori** probability postulate : *Let there be an equal a priori probability for atoms to meet in the same rate to form clusters that end up making different phases* . If such a postulate is satisfied then that phase with the largest heat of formation will form first (see **Fig. 5.15**). In this case equal attempts are made by atoms to form all

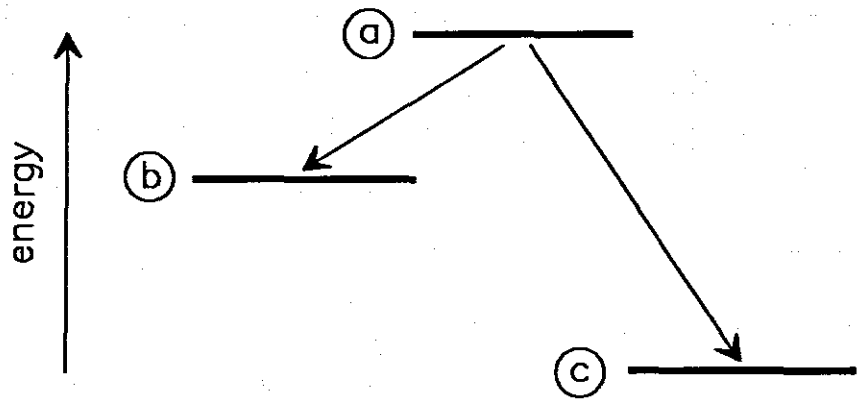

FIGURE 5.15: *Sketch showing different energy levels in a system. The transition* probabilities from (a) to (b) may be different from those from (a) to (c). If this is the situation than the *equal a priori* probability postulate does not apply, and state (b) may fill faster than state (c).

compound phases. **Fig. 5.15** shows this behaviour diagrammatically.

1. If the transition probabilities to go from state (a) to state (b) is the same as that to go from state (a) to state (c) then state (c) will fill up much more quicker then state (b). It is much more difficult for atoms to leave state (c) as compared to (b). An *equal a priori* postulate for the two transitions is satisfied.

2. If the transition probability to go from state (a) to state (b) is much larger than that to go from state (a) to state (c), then state (b) may fill faster than state (c). [In this case an *equal a priori* probability for transitions into these states is not satisfied.]

During phase formation in thin films this *equal a priori* postulate is not satisfied. This is in the form of unequal rates in which atoms meet in correct ratios to form different phases. This is the reason why that phase with the largest heat of formation is not necessarily the first phase. Pretorius *et al* in their papers **[11–15]** used this fact in their formulation of the EHF model. This is done by introducing that faster mixing concentration at the liquidus minimum of the binary system. The heat that is evolved is not just the largest heat of formation, but the largest effective heat of formation at the liquidus minimum.

5.5 Summary and Conclusion

The first phase forms first at the reaction interface partly because atoms that end up forming this phase mix at a faster rate than atoms belonging to other concentrations. This means that the attempt rate by atoms as they meet in correct ratios to form each phase is larger for that phase closest in composition to the liquidus minimum. This concentration is **not** necessarily the most probable at the growth interface. The probability of atoms to meet in the correct ratio to form a phase is a determining factor in solid state phase formation. Activation energies of diffusion determine how stable the phase that has formed will be. Since they are proportional to the melting point of a solid, stability probabilities will favour those phases with higher melting points. A compromise between meeting probability and stability probability should determine what the first phase will be. For semiconductor-metal interactions atomic rotations of the semiconductor atoms play a role in phase formation. It is assumed in this model that activation energies of rotation are proportional to temperatures at which phases cease being crystalline as temperature is raised. Non-congruent phases generally loose their crystalline structure at temperatures which are much lower than their congruent neighbours on the phase diagram. Because of this congruent phases of semiconductor-metal systems are more favoured than non-congruent phases when phase formation occurs. The solid state rate differential equations determine which phase and how much of it forms in a given period of time. The rate constants found in these equations become variables in the non-equilibrium case for example the thin film case. The only thing that makes them variables is the change of concentration at the growth interface. The rate of change of this concentration at the growth interface is determined by the diffusion differential equation.

CHAPTER 6

CRITICAL EVALUATION OF MODELS

6.1 Introduction

The formation of compound phases in the solid state has been the subject of careful analysis and study for more than 20 years. This interest is due to a widespread use of thin films in modern electronic and optical devices. A number of phenomena have been observed to occur, i.e. the absence of some of the phases during growth, reactions that occur at very low temperature (less than half the lowest eutectic temperature), competitive growth, sequential phase formation, island formation in some cases during growth, the formation of metastable phases, etc. A number of models and theories have been proposed to explain the observed phenomena. Some of them deal only with kinetics while others concentrate on thermodynamics. Some of the models are so restrictive with regard as to under which conditions to use them, that they are almost impossible to use. No single model has been able to explain all the phenomena observed in thin film couples.

Renewed interest in thin films stems from their technological applications as, for example, anti-reflection or corrosive-resistant coatings, protective coatings for friction and wear, layers for either magnetic or optical storage and of course their varied use in the micro-electronics industry. One of the ways that these layered

structures are formed is through the process of thin film solid-state reactions. Thin film reactions of interest are those that occur below one half or two thirds of the melting point (°C) of the solid. In these non-equilibrium reactions one phase usually forms at a time, in contrast to some early expectations [10] that all compounds in the phase diagram should be formed at the interface. This is also the case for the bulk diffusion couples, greater than about 10μm, where the equilibrium compound phases are usually found to grow simultaneously. It is thus important to know which phase forms first in thin film reactions. Due to the non-equilibrium nature of the reaction, standard equilibrium rules fail to predict the identity of the first phase formed. Yet first attempts [2–4] at formulating rules to predict first phase formation and phase formation sequence did acknowledge the importance of metal-silicon equilibrium phase diagrams. Since then interest in predicting first phase compound formation has increased [5, 6, 8, 11, 12, 18, 93, 95, 96, 170, 171, 168]. Apart from the obvious academic interest, knowledge of phase formation sequence should enable the materials scientist to control experimental parameters in such a way as to form specific phases with desirable properties.

In this chapter some of the better known models will be described critically and compared to each other.

6.2 Walser-Bené model

6.2.1 Introduction

One of the earliest models for predicting first phase formation at interfaces is the Walser-Bené model [2]. The original paper by Walser and Bene [2] dealt with first phase formation in silicon-transition metal planar interfaces. It had by this time been realised already that not all compound phases as given by the equilibrium phase diagram form readily in thin film binary couples. Solid phase growth of interest is that occurring below half the lowest eutectic temperature of the binary system.

6.2.2 The model

This model tackled the problem of first phase formation in thin film metal-silicon binary couples. The authors argue that the initial condition of the interface consists essentially of a "metallic glass", of a concentration near the lowest-temperature eutectic in the binary system and that this is also the concentration where metallic glasses are found to be most stable in a super cooled state. The first predictions were mainly concerned with predicting first phase nucleation in silicon-metal planar interfaces and this was most probably due to their technological importance. In these systems it was well known that non-congruently melting phases were skipped during phase formation. Walser and Bené [2] attributed this to the higher energy barrier associated with the large rearrangement in short-range order (SRO) required to go from liquid like SRO to crystalline SRO for non-congruent states, contrasted to the much smaller change in SRO associated with congruently melting states. They therefore expected that the phase nucleated would be the congruent phase closest in concentration to the initial eutectic composition. In the case that two congruently melting phases existed on both sides of the eutectic, the most stable compound, as indicated by the higher melting temperature, was expected to form.

Using this model of the reaction process at the reaction interface the following rule was formulated for predicting phase formation at silicon/metal planar interfaces [2]:

> *"The first compound nucleated in planar binary reaction couples is the most stable congruently melting compound adjacent to the lowest-temperature eutectic on the bulk equilibrium phase diagram."*

This rule also applies to metal/germanium systems and was generalized as a metal-covalent rule for phase selection [4]. The rule was later extended to metal-metal systems by relaxing the requirement that the first phase that forms needs to be congruently melting [4]:

> *"The first phase nucleated in metal-metal thin-film reactions is the phase immediately adjacent to the low-temperature eutectic in the binary phase*

diagram."

The main difference in the two rules being that the metal-covalent rule predicts "phase skipping" away from the low-temperature eutectic if the adjacent phases are non-congruently melting [4]. It is also important to note another subtle difference in the way the metal-metal rule was formulated. It makes no reference to the stability of the compound in the case that the eutectic lies between two phases, instead it is the phase immediately adjacent to the lowest-temperature eutectic that is predicted.

6.3 Kinetic Model of Gosele and Tu

6.3.1 Introduction

In this model [5] it is assumed that interface reaction barriers in binary A/B diffusion couples lead to the absence of phases predicted by the equilibrium phase diagram, if the diffusion zones are sufficiently thin. As the thickness of the diffusion zone increase ,the model claims, the influence of interfacial reaction barriers decrease and the simultaneous existence of diffusion-controlled growth of all equilibrium phases will begin.

6.3.2 Influence of interfacial reaction barriers on the growth kinetics of a single compound layer

The model asserts that the growth of a single compound layer is determined by [5]:

1. diffusion of matter across the compound layer where diffusion flux slows down with increasing layer thickness,

2. and, the rearrangement of the atoms at the interface required for the growth of the compound layer which may involve a reaction barrier.

Two types of kinetics are defined:

- **Diffusion controlled kinetics**, where the diffusion process is rate limiting and controls the growth. Layer thickness in this case increases proportional to the square root of time t.

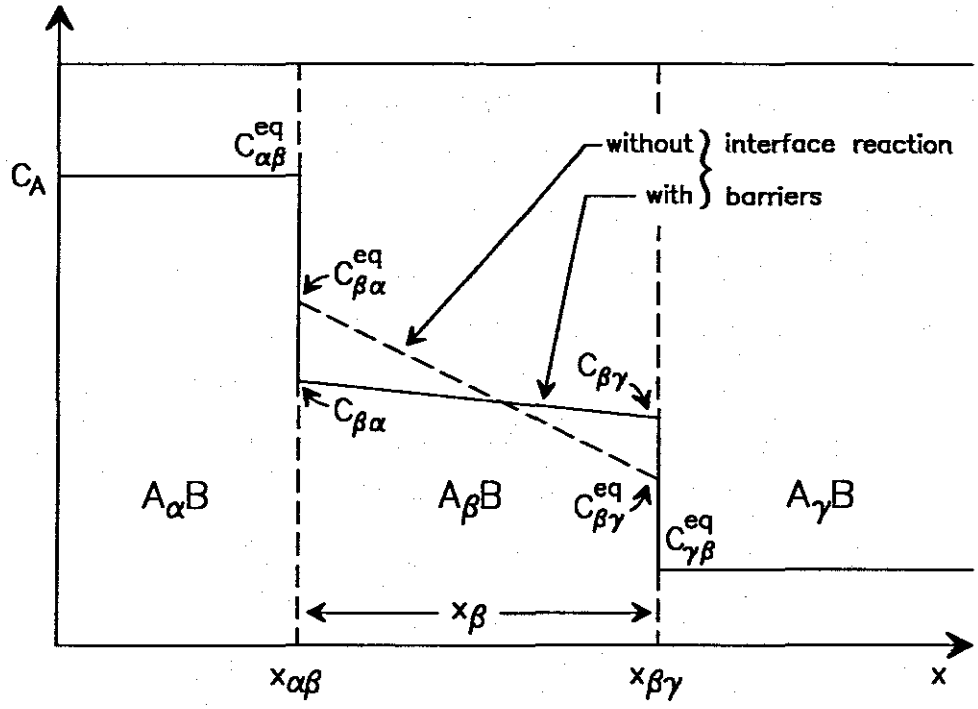

FIGURE 6.1: Sketch showing changes in concentration profiles when there is an interfacial reaction barrier (solid line) and when there is no interfacial reaction barrier (dashed line) (adapted from [5]).

- **Interface controlled** (or boundary or reaction controlled), where interfacial reaction barriers control the kinetics. In this case layer thickness increase linearly with time.

Fig. 6.1 shows a compound layer $A_\beta B$ of thickness x_β growing between two saturated phases $A_\alpha B$ and $A_\gamma B$ (where $\alpha > \beta > \gamma$ characterize the composition of the compound). If α and γ are ∞ and 0, respectively, then $A_\alpha B$ and $A_\gamma B$ will represent pure phases A and B. In the absence of interfacial reaction barriers, the concentration profile of A as shown by the dashed line, with the concentration of A at the two interfaces equal to the equilibrium values $C^{eq}_{\beta\alpha}$ and $C^{eq}_{\beta\gamma}$. If there are interfacial reaction barriers, then $C_{\beta\alpha} < C^{eq}_{\beta\alpha}$ and $C_{\beta\gamma} > C^{eq}_{\beta\gamma}$. It is asumed that the $A_\beta B$ layer may be characterised by a constant chemical interdiffusion constant $\tilde{D}_\beta$. The change in position of the two interfaces with time is;

$$(C^{eq}_{\alpha\beta} - C_{\beta\alpha})\frac{dx_{\alpha\beta}}{dt} = \tilde{D}_\beta(\frac{dC^A_\beta}{dx})_{\beta\alpha} \qquad (6.1)$$

for the $\alpha\beta$ interface and

$$(C_{\beta\gamma} - C^{eq}_{\gamma\beta})\frac{dx_{\beta\gamma}}{dt} = -\tilde{D}_\beta(\frac{dC^A_\beta}{dx})_{\beta\gamma} \tag{6.2}$$

for the $\beta\gamma$ interface. C^A_β is the concentration of A in the $A_\beta B$ layer. If compound formation is only at the interfaces and steady state conditions apply for the diffusion fluxes,

$$j^A_\beta = -\tilde{D}_\beta(\frac{dC^A_\beta}{dx})_{\beta\alpha} = -\tilde{D}_\beta(\frac{dC^A_\beta}{dx})_{\beta\gamma} \tag{6.3}$$

or

$$j^A_\beta = -\tilde{D}_\beta\frac{(C_{\beta\alpha} - C_{\beta\gamma})}{x_\beta} \tag{6.4}$$

where j^A_β is the diffusion flux of A atoms in the $A_\beta B$ phase. The following expression may also be written when the flux is considered from the reaction-limited viewpoint:

$$j^A_\beta = \kappa_{\beta\alpha}(C^{eq}_{\beta\alpha} - C_{\beta\alpha}) \tag{6.5}$$

or

$$j^A_\beta = \kappa_{\beta\gamma}(C_{\beta\gamma} - C^{eq}_{\beta\gamma}) \tag{6.6}$$

where $\kappa_{\beta\alpha}$ and $\kappa_{\beta\gamma}$ are reaction constants at the two interfaces. The concentration difference $C_{\beta\alpha}$–$C_{\beta\gamma}$ may be expressed in terms of the time independent equilibrium value:

$$\Delta C^{eq}_\beta = C^{eq}_{\beta\alpha} - C^{eq}_{\beta\gamma} \tag{6.7}$$

by combining **eq. 6.4, eq. 6.5** and **eq. 6.6**.

$$j^A_\beta = \frac{\Delta C^{eq}_\beta \kappa^{eff}_\beta}{1 + \frac{x_\beta \kappa^{eff}_\beta}{\tilde{D}_\beta}} \tag{6.8}$$

for the layer $A_\beta B$, where the interfacial reaction barrier κ^{eff}_β is

$$\frac{1}{\kappa^{eff}_\beta} = \frac{1}{\kappa_{\beta\alpha}} + \frac{1}{\kappa_{\beta\alpha}} \tag{6.9}$$

The change in layer thickness $x_\beta = x_{\beta\gamma} - x_{\alpha\beta}$ with time is given by

$$\frac{dx_\beta}{dt} = \left\{\frac{1}{C^{eq}_{\alpha\beta} - C_{\beta\alpha}} + \frac{1}{C_{\alpha\gamma} - C^{eq}_{\gamma\beta}}\right\} j^A_\beta \tag{6.10}$$

In this model [5], **eq. 6.10** is simplified by assuming a narrow range of homogeneity for the compound $A_\beta B$, so that in the composition factor in curly brackets, $C_{\beta\alpha}$ and $C_{\beta\gamma}$ may be approximated by the same value,

$$\frac{\beta}{[\Omega_o(1+\beta)]} \tag{6.11}$$

where Ω_o is the volume per A or B atom (assumed constant throughout the sample). β is the number of A atoms per B atom in the $A_\beta B$ compound. Substituting **eq. 6.8** into **eq. 6.10**

$$\frac{dx_\beta}{dt} = \frac{G_\beta \Delta C_\beta^{eq} \kappa_\beta^{eff}}{1 + \frac{x_\beta \kappa^{eff}}{\tilde{D}_\beta}} \tag{6.12}$$

G_β is a constant determined by the composition of the three phases, $A_\alpha B$, $A_\beta B$ and $A_\gamma B$

$$G_\beta = \Omega_o(1+\beta)^2\left(\frac{1}{\alpha-\beta} + \frac{1}{\beta-\gamma}\right) \tag{6.13}$$

α and γ represent the number of A atoms per B atom in the $A_\alpha B$ or $A_\gamma B$ compound, respectively. There is a changeover thickness x_β^* for the change from reaction controlled to diffusion controlled, defined by

$$x_\beta^* = \frac{\tilde{D}_\beta}{\kappa_\beta^{eff}} \tag{6.14}$$

From **eq. 6.12**

$$\frac{dx_\beta}{dt} \sim G_\beta \Delta C_\beta^{eq} \kappa_\beta^{eff} \text{ for } x_\beta \ll x_\beta^*, \text{and} \tag{6.15}$$

$$\frac{dx_\beta}{dt} \sim \frac{G_\beta \Delta C_\beta^{eq} \tilde{D}_\beta}{x_\beta} \text{ for } x_\beta \gg x_\beta^* \tag{6.16}$$

integrated

$$x_\beta \propto t \text{ for } x_\beta \ll x_\beta^* \tag{6.17}$$

(for the reaction controlled case)

$$x_\beta \propto t^{\frac{1}{2}} \text{ for } x_\beta \gg x_\beta^* \tag{6.18}$$

(for the diffusion controlled case).

6.3.3 Diffusion-controlled growth in the absence of reaction barriers

According to Gosele and Tu most models [5] assume that material transport across the compound layers with thicknesses x_α, x_β, x_γ, etc by diffusion is rate limiting, which is justified if $x_\alpha \gg x_\alpha^*$, $x_\beta \gg x_\beta^*$, $x_\gamma \gg x_\gamma^*$, etc. What these models [5] mean is that:

1. All phases predicted by the equilibrium phase diagram should be present in an A/B diffusion couple.

2. All the layer thicknesses x_α, x_β, x_γ, etc should grow proportional to $t^{\frac{1}{2}}$, which means x_α/x_β or x_β/x_γ should remain constant in time at constant temperature.

6.3.4 Two intermediate compound layers

Basic assumptions and equations

To explain the influence of interfacial reaction barriers in a multiphase system the Gosele and Tu model [5] considers a system of two intermediate compound layers of composition $A_\beta B$ and $A_\gamma B$ between saturated phases $A_\alpha B$ and $A_\delta B$, where $\alpha > \beta > \gamma > \delta$. It is also assumed that the two compound layers $A_\beta B$ and $A_\gamma B$ are already present with given thicknesses x_β and x_γ, respectively. According to the model one of the layers may shrink away completely depending on various kinetic conditions. This phase will not form in a diffusion experiment for the given kinetic conditions, which are characterised by a set of kinetic parameters (thickness of the compound layer, diffusivities, interfacial reaction barriers). This is called a *kinetic growth* or *growth instability.* The model differentiates between kinetic instability induced by interfacial reaction barriers from that of phase repression by a *nucleation barrier.* A kinetically unstable phase shrinks away (or does not form) even if it can nucleate.

The model characterizes the system by chemical interdiffusion coefficients $\tilde{D}_\beta$ and $\tilde{D}_\gamma$ in the $A_\beta B$ and $A_\gamma B$ layer, respectively. $\tilde{D}_\beta$ may be approximated in simple

cases in terms of component diffusion coefficients D_β^A and D_β^B by

$$\tilde{D}_\beta = \frac{D_\beta^A}{\beta+1} + \frac{\beta D_\beta^B}{\beta+1} \tag{6.19}$$

The volume Ω_o per atom is assumed to be constant in all phases. κ_γ^{eff} is an effective interfacial reaction barrier for the $A_\gamma B$ layer composed of two interfacial reaction barriers $\kappa_{\gamma\beta}$ and $\kappa_{\gamma\delta}$. The change of x_β and x_γ with time is

$$\frac{dx_\beta}{dt} = G_\beta j_\beta^A - G_{\beta\gamma} j_\gamma^A \tag{6.20}$$

$$\frac{dx_\gamma}{dt} = G_\gamma j_\gamma^A - G_{\gamma\beta} j_\beta^A \tag{6.21}$$

with the positive diffusion fluxes of A atoms in the $A_\beta B$ and the $A_\gamma B$ layer given by

$$j_\beta^A = \frac{\Delta C_\beta^{eq} \kappa_\beta^{eff}}{1 + \frac{x_\beta \kappa_\beta^{eff}}{\tilde{D}_\beta}} \tag{6.22}$$

$$j_\gamma^A = \frac{\Delta C_\gamma^{eq} \kappa_\gamma^{eff}}{1 + \frac{x_\gamma \kappa_\gamma^{eff}}{\tilde{D}_\gamma}} \tag{6.23}$$

The quantities G_β, $G_{\beta\gamma}$, G_γ and $G_{\gamma\beta}$ are given by

$$G_\beta = \Omega_o (1+\beta)^2 \left(\frac{1}{\alpha-\beta} + \frac{1}{\beta-\gamma}\right) \tag{6.24}$$

$$G_\gamma = \Omega_o (1+\gamma)^2 \left(\frac{1}{\beta-\gamma} + \frac{1}{\gamma-\delta}\right) \tag{6.25}$$

$$G_{\beta\gamma} = G_{\gamma\beta} = \Omega_o (1+\beta) \frac{(1+\gamma)}{(\beta-\gamma)} \tag{6.26}$$

This model considers fluxes j_β^A and j_γ^A to be independent of each other. They may be described at the interface between $A_\beta B$ and $A_\gamma B$ by

$$j_\beta^A = \kappa_{\beta\gamma} (C_{\beta\gamma} - C_{\beta\gamma}^{eq}) \tag{6.27}$$

$$j_\gamma^A = \kappa_{\gamma\beta} (C_{\gamma\beta}^{eq} - C_{\gamma\beta}) \tag{6.28}$$

$\kappa_{\beta\gamma}$ characterizes the reaction barrier against the growth of the $A_\beta B$ layer at the expense of the $A_\gamma B$ layer. $\kappa_{\gamma\beta}$ characterizes the reaction barrier against the growth

of the $A_\gamma B$ layer at the expense of the $A_\beta B$ layer. A special situation that may happen at the interface which may not be consistent with the boundary conditions **6.27** and **6.28** is recognized in the model e.g. if compound formation at the interface were not possible at all, but diffusion across the interface were easily accomplished, an additional parameter would be required to describe the direct transfer of atoms across the interface. There is therefore an awareness about the limitations in the said boundary conditions. For a fast reaction at the interface κ_β^{eff} and $\kappa_\gamma^{eff} \rightarrow \infty$ and the equations **6.20**— **6.23** can be simplified to those for diffusion-controlled multilayer growth kinetics [5].

Criteria for growth/shrinkage behaviour

The model [5] gives a condition for growth of the $A_\beta B$,$dx_\beta/dt > 0$, as a ratio r of the diffusion fluxes j_β^A and j_γ^A,

$$r = \frac{j_\beta^A}{j_\gamma^A} \tag{6.29}$$

as

$$r > \frac{G_{\beta\gamma}}{G_\beta} = r_1 \tag{6.30}$$

For the $A_\gamma B$ layer

$$r < \frac{G_\gamma}{G_{\gamma\beta}} = r_2 \tag{6.31}$$

with

$$r_1 = \frac{(1+\gamma)(\delta-\beta)}{(1+\beta)(\delta-\gamma)} \tag{6.32}$$

and

$$r_2 = \frac{(1+\gamma)(\beta-\delta)}{(1+\beta)(\gamma-\delta)} \tag{6.33}$$

where $r_2 > r_1$ because $(\alpha-\beta) < (\alpha-\gamma)$ and $(\beta-\delta) > (\gamma-\delta)$. Since the ratios r_1 and r_2 depend on compositions of the compounds only, they do not change with time. According to the model both compound layers can grow simultaneously depending on a combination of the parameters $x_\beta, x_\gamma, D_\beta, D_\gamma, \kappa_\beta^{eff}$ and κ_γ^{eff} and because $r_2 > r_1$. If the flux ratio is not between r_1 and r_2, one of the layers should, according to this model, shrink, whereas the other one should grow.

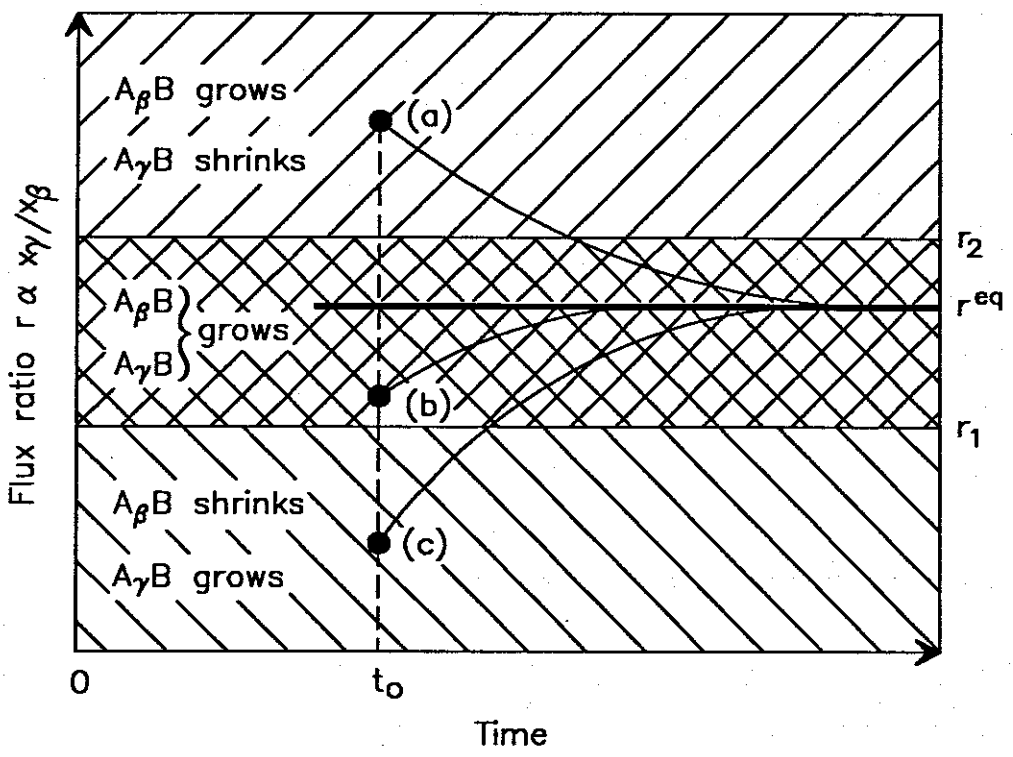

FIGURE 6.2: Sketch showing growth and shrinkage behaviour of compound phases in various regimes according to the Gosele and Tu model (adapted from [5]).

Diffusion-controlled transport across both layers

The model [5] assumes that x_β and x_γ of the two compound layers are already such that transport across each compound layer is diffusion-controlled i.e. $x_\beta >> x_\beta^*$ and $x_\gamma >> x_\gamma^*$. where $x_\gamma^* = \tilde{D}_\gamma/\kappa_\gamma^{eff}$. For this case the flux ratio is simplified to

$$r = \frac{(\Delta C_\beta^{eq} \tilde{D}_\beta)}{(\Delta C_\gamma^{eq} \tilde{D}_\gamma)} \frac{x_\gamma}{x_\beta} \tag{6.34}$$

It is assumed [5] that interdiffusion experiments start with a thickness ratio x_γ/x_β so that either $r > r_2$ (case a), or $r_1 < r < r_2$ (case b), or $r < r_1$ (case c) as shown in **Fig. 6.2** For the case $r > r_2$ the $A_\beta B$ layer grows and the $A_\gamma B$ layer shrinks. This should because of $r < x_\gamma/x_\beta$, lead to a decreasing value of r until it is so small ($r < r_2$) that the AγB layer starts to grow simultaneously with the $A_\beta B$ layer. Finally a time independent flux ratio r^{eq} is reached where both layers grow proportional to $\sqrt{t}$. according to the model [5] r^{eq} is reached independent of the actual starting ratios r andx_γ/x_β and is the same for all cases (a–c).

Interface-controlled transport across both layers

The model assumes in this case that x_β and x_γ are so small that ($x_\beta \ll x_\beta^*$, $x_\gamma \ll x_\gamma^*$) transport across each layer is controlled by interface reaction barriers.

$$r = \frac{\Delta C_\beta^{eq} \kappa_\beta^{eff}}{\Delta C_\gamma^{eq} \kappa_\gamma^{eff}} \tag{6.35}$$

where r is not expected to depend on time or x_β or x_γ if $x_\beta \ll x_\beta^*$ and $x_\gamma \ll x_\gamma^*$. If κ_β^{eff} and κ_γ^{eff} are such that r lies between r_1 and r_2 both layers will grow simultaneously. If r is somewhere outside this range one of the phases will shrink away completely, which means that a phase like $A_\beta B$ may not start to grow at all in a usual diffusion experiment as long as $x_\gamma < x_\gamma^*$ holds. When x_γ is sufficiently large ($x_\gamma > x_\gamma^*$) the system will change form interface controlled to a mixed interface and diffusion controlled situation.

Different transport-controll mechanisms across both layers

The model [5] also describes a case where the transport across one layer, say the $A_\gamma B$ layer, is diffusion controlled ($x_\gamma \gg x_\gamma^*$) whereas the transport across $A_\beta B$ is interface controlled ($x_\beta \ll x_\beta^*$). The flux ratio becomes

$$r = \left(\frac{\Delta C_\beta^{eq} \kappa_\beta^{eff}}{\Delta C_\gamma^{eq} D_\gamma}\right) x_\gamma \tag{6.36}$$

For the two cases either $r > r_2$ or $r_1 < r < r_2$ the two layers can coexist all the time. For $r > r_2$ the the $A_\gamma B$ layer shrinks until it reaches a constant thickness and the $A_\beta B$ layer grows all the time. For $r_1 < r < r_2$ the $A_\gamma B$ layer grows until it reaches the same constant thickness as for the case $r > r_2$ and the $A_\beta B$ layer grows all the time. For a case where r is smaller than r_1, the $A_\gamma B$ layer grows and the $A_\beta B$ layer shrinks as long as x_γ is so small that $r < r_1$ holds. The flux ratio r is independent of the thickness x_β (if $x_\beta \ll x_\beta^*$). As a result, for kinetic reasons in a usual interdiffusion experiment the $A_\beta B$ layer cannot coexist with the $A_\gamma B$ layer as long as x_γ is below a critical thickness x_γ^{crit} given by

$$x_\gamma^{crit} = \frac{r_1 \Delta C_\gamma^{eq} D_\gamma}{\Delta C_\beta^{eq} \kappa_\beta^{eff}} \tag{6.37}$$

The $A_\beta B$ layer can grow simultaneously with the $A_\gamma B$ layer if $x_\gamma > x_\gamma^{crit}$. As the $A_\beta B$ layer grows, a situation will be reached where $x_\beta \ll x_\beta^*$ is no longer satisfied. The transport across both layers will be diffusion controlled and both layers will grow proportional to $\sqrt{t}$ with a constant thickness ratio x_γ/x_β.

6.3.5 Application of the model in thin film silicide formation

Restrictions on the model

There are situations where the Gosele and Tu model has limited applicability [5].

1. In cases where the diffusion of A and B in a compound phase are independent of each other, the diffusion process cannot be described only by a single chemical interdiffusion coefficient $\tilde{D}$, more parameters must be introduced. The basic conclusions of the model remain unchanged.

2. If there are more than two competing compound phases, (i.e. not only $A_\beta B$ and $A_\gamma B$) in the phase diagram, then all these are competing with each other and must be taken into account.

3. Energy contributions and changes associated with the creation of new interfaces must be taken into account in the model, but have been neglected.

4. The concept of an interface-induced kinetic instability of compound phases in thin film diffusion couples remain applicable (though only in its qualitative aspects) even if the effective diffusivity is dependant on time and layer thickness.

5. The model does not take into account the possibility of metastable thin film phases. They can be stabilized by mismatch stresses or by excessive lattice disorder.

6. Influence of impurities is neglected by the model.

General behaviour

In the following discussion the Gosele and Tu model [5] uses A for silicon and B for metal in silicon-metal diffusion couples. The model states that if nucleation problems are neglected, then an A/B diffusion couple will have the following behaviour: The compound phase with the lowest effective interface reaction barrier, say $A_\gamma B$, should according to this model, form first and initially grow linearly with time and thereafter with a parabolic growth law. According to the model the thickness x_γ of the first compound phase will grow up to a critical thickness x_γ^{crit}, which is supposed to depend on the microstructure of the compound layer and in general also on temperature, thereafter the second compound phase ($A_\beta B$) will form and grow. Its growth will be at first linear with time and later it will be diffusion controlled i.e. proportional to the square root of time and with a time independent ratio x_γ/x_β. The model does not exclude cases where interfacial reaction barriers are such that both phases $A_\gamma B$ and $A_\beta B$ grow simultaneously from the beginning.

It is noted in the model that in sufficiently pure thin-film silicon-metal diffusion couples, which may form a number of silicides according to the phase diagram, usually only one compound phase is observed as long as unreacted metal and silicon are still available. It is found that in the few Angstrom range (a couple of hundred to some thousand Angstrom), the first silicide phase grows diffusion controlled proportional to $\sqrt{t}$ in diffusion couples of silicon with near-noble metals and interface controlled proportional to t in silicon-refractory metal systems. It is claimed in the model that if the first phase growth is interface controlled, then the predictions of the model will be in agreement with experimental observations, that a second silicide phase cannot grow or simultaneously exist at all together with the first silicide phase (except in the case where r lies between r_1 and r_2). Where only one silicide layer is present and the layer growth is diffusion controlled, then the model suggest that x must be below its critical value x^{crit}, otherwise a second silicide phase would have started to grow.

According to the model the first silicide phase forming and growing is that with the lowest effective interface reaction barrier.

6.3.6 Critical evaluation of the Gosele and Tu model

The model of Gosele and Tu [5] seems to be well derived theoretically. It describes conditions under which thicknesses grow linearly with time and conditions under which layer thicknesses are proportional to the square root of time. In a novel way interfacial reaction barriers in a thin binary A/B diffusion couple are introduced and used to explain why if the diffusion zones are thin only one phase grows, even though the equilibrium phase diagram predicts many equilibrium phases. The contrast between the *bulk* case, where all phases grow simultaneously, and the *thin* film case where under certain conditions only one phase grows at a time is well explained.

Most binary systems have about five different compound phases given by the bulk equilibrium phase diagram and in some cases there can be as many as nine different compound phases belonging to one system. If the equations for analyzing a system with *only two* compound phases are as many and the analysis as complicated as given in the model it may be appreciated how much difficulty will be encountered if a binary system with nine intermediate phases between the pure A and B phases is to be analyzed. In a system with nine compound phases there can be as many as ten interfaces, each one of them described by its own interfacial barrier symbols. The difficulty in handling and analyzing such equations would be enormous.

The model defines a critical thickness, x^{crit}, for which if there is only one layer growing at a time and layer growth is diffusion controlled, there cannot be another layer as long as the thickness of the growing layer is below this critical thickness x^{crit}. It is said that this critical thickness depends on the microstructure of the compound layer and in general also on temperature. It might not be necessary at all to define a critical thickness! This is due to the fact that phases that grow are determined to a large extent by concentration at the growth interface (i.e. atomic % of one of the elements). Information at the growth interface should at all times, except during the initial period, be determined by the diffusion equation with appropriate boundary conditions.

The model seems to neglect some of the most important parameters that play a role in thin film phase formation. Some of these have been shown in many

experiments to be atomic concentration corresponding to the liquidus minimum, and in the case of silicides and to a lesser extent, germanides, congruency. Any model dealing with phase formation should take these parameters into account. This should however not be viewed as impacting bad on this model. The model is a good attempt at explaining diffusion in the presence of the accompanying phenomenon of phase formation in thin films.

6.4 Kinetic Plot Model of Zhang and Ivey

6.4.1 Introduction

This model [172] describes solid state reactions in thin film metal-silicon diffusion couples. Only cases where one species diffuses significantly faster than the other species are considered. According to the model silicide formation occurs as a result of the non-moving reactant being released from its lattice and interacting with the moving reactant. Relative Maximum Release rates (RMR rates) and Semiquantitative Reaction Process plots (SRP plots) are introduced in this model. In the case of non-moving reactant atoms, the expression for the maximum release rate is exponentially dependent on the free energy change caused by releasing one non-moving reactant atom or formula unit.

6.4.2 The model

In this model [172] only type (ii) reactions are considered i.e. those in which one of the two reactants diffuses much faster in the growing silicide than the other reactant. The predominant diffuser is called the moving reactant (M) and the other reactant is the non-moving reactant (N). Reactions considered in the model are those that occur below half of the lowest eutectic temperature in the binary phase diagram for a given diffusion couple.

The basic assumptions of this model [172] are:

1. In a silicide reaction the reactive interface between the growing phase (product) and the contracting phase (made up of N atoms or molecules) is the reaction

region.

2. The reaction process has three steps:

   (a) M atoms diffuse through the growing phase into the reaction region.

   (b) M atoms in the reaction region interact with the N atoms that are exposed to this region, which causes the N atoms to be released from their lattice into the reaction region, forming product 'molecules' with the M atoms.

   (c) The 'molecules' rearrange themselves on the lattice of the growing phase.

Physical quantities used to describe these three steps are the diffusion flux (ΔJ) of M to the reaction region, the release rate (r) of N and the formation rate (F) of the growing phase. The difference between the diffusion fluxes into and out of the reaction region is $\Delta J = J_{in}-J_{out}$. If $J_{out} \ll J_{in}$, then $\Delta J \approx J_{in}$ and J is used for either ΔJ or J_{in}. The model uses a diagram such as that shown in **Fig. 6.3** to find a highest release rate at any composition. It is a schematic reaction process plot for reactions between a moving reactant and a non-moving reactant. Each curve represent r vs. J for a given silicide whose composition is indicated by the slope of the inclined segment of the curve. The highest curve at any flux represents the highest release rate (it is called the reaction process plot). For J_0 in this diagram the highest release rate is r_2.

According to the model the silicide that will form is determined by the second step, and its form by the third, and this, it is claimed, explains why metastable phases or amorphous phases form. It predicts that any silicide in the equilibrium phase diagram of a metal-Si diffusion couple can form (if the release rate for this reaction is on the stepped curve of the reaction process plot, and the initial diffusion flux between J_{LC} (lower critical flux) and J_{UC} (upper critical flux) for this silicide). The diffusion flux will continuously decrease as the first phase grows. If the diffusion flux reaches a critical value, J_{UC}, a new reaction with its release rate related to this J_{UC} is initiated and a new phase will begin to grow.

The model requires that reaction process plots be determined before it can be used for phase prediction.

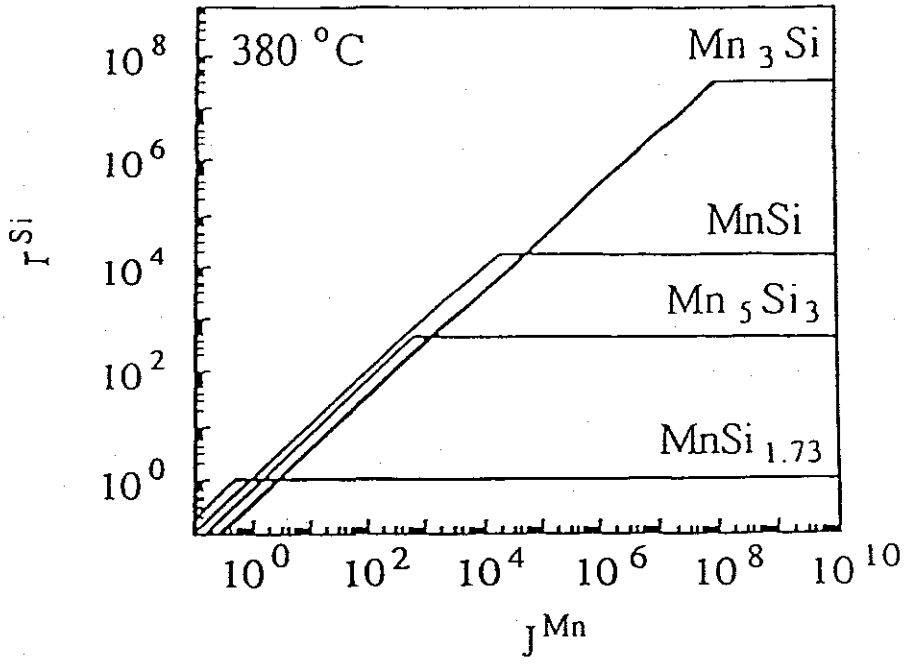

FIGURE 6.3: Semiquantitative Reaction Process (SRP) plot for the Mn-Si system (adapted from [172]).

Maximum Release Rate of Non-moving reactant.

An N atom crystal lattice is considered, with atoms on the surface having vibrational frequency ν_0. The release rate of atoms on the surface is,

$$r_\nu = n^* \nu_0 \exp(-\frac{E}{kT}) \tag{6.38}$$

where n* is the number density of non-moving reactant atoms per unit area of surface layer (E is the binding energy per N atom or molecule). It may vary with crystallographic orientation of the surface because the binding states for different crystalline planes may not be the same. The N atoms in the surface layer and the M atoms in the reaction region come into contact, and a chemical reaction takes place. The driving force ΔG_i for the reaction makes it easier for the N atoms to escape from the surface, therefore

$$r_{imax} = n^* \nu \exp(-\frac{E}{kT}) \exp(-\frac{\Delta G}{kT}) \tag{6.39}$$

or

$$r_{imax} = n^* \nu \exp(-\frac{E + \Delta G}{kT}) \tag{6.40}$$

where ν is the vibrational frequency of N atoms at the surface exposed to a reaction region; ΔG_i is the driving force for the reaction i.e. the free energy change of the reaction, per N atom, for i th silicide to form . In a given reaction region of a metal-Si diffusion couple n^*, ν and E are the same for all possible reactions so that r_{imax} is exponentially dependant on the driving force for the reaction, ΔG_i. A reaction with a larger negative ΔG_i is therefore expected to have a higher maximum release rate [172].

The free energy change ΔG, for a chemical reaction is written as

$$\Delta G = \Delta G^\circ + kT \ln Q \tag{6.41}$$

where ΔG° is the standard free energy change for the reaction and Q is the activity quotient for the products and reactants.

$$\Delta G^\circ \simeq \Delta H^\circ_{298} \tag{6.42}$$

in the solid state.

$$\Delta G = kT \ln(\frac{Q}{K}) \tag{6.43}$$

where

$$K = \exp(-\frac{\Delta G^\circ}{kT}) \tag{6.44}$$

is the equilibrium constant. If $Q < K$ and $\Delta G < 0$, the reaction is thermodynamically allowed. An approximation is made that 'only a single atomic layer N and M atoms which are nearest neighbors to the N atoms in this layer can react at once. The N atoms next to the top layer cannot be released until the N atoms in the top layer are removed. The model assumes that the reaction occurs in two-dimensional space, defined by the surface atomic layer of N atoms. The non-moving reactant atoms in this space are considered by this model to be fixed on a two dimensional net and the moving reactant atoms are mobile. The M atoms are brought by diffusion, into intimate contact with N atoms in the net, and reaction between atoms take place.

When these silicide molecules are formed, bonds between the N atoms in the net and those in the next layer are broken, i.e. silicide molecules are removed from the surface of the N lattice. A new two dimensional net of N will then be exposed for the next reaction to take place. It is argued that some of the product molecules will stay on the two dimensional net longer than other molecules. This is ascribed by the model to different energy barriers that may be presented to N atoms. Defects such as steps, kinks, vacancies, and dislocation intersections with the surface, are said to produce this effect.

The net number of N atoms which can be released is

$$N_N = n^* - n_d \tag{6.45}$$

where n^* is the number density of N atoms in a perfect surface layer and n_d is the number density of atomic defect positions in the surface layer. n_d is equal to the number density of product molecules which cannot be removed promptly due to the presence of defects. N_N is the number density of N atoms that can be released promptly during the release process. The number of M atoms which can react with the N_N atoms to form the i th silicide is

$$N_M = (\frac{m_i}{n_i})(n^* - n_d) \tag{6.46}$$

where m_i and n_i are the number of M and N atoms per i th silicide formula unit respectively. It is noticed that $n_d \ll n^*$, $N_N \simeq n^*$ and

$$N_M \simeq (\frac{m_i}{n_i}) \tag{6.47}$$

The mole fractions of N and M reactants, X_i^N and X_i^M, and product X_i^i (remaining on the two-dimensional net), is given by

$$X_i^N = \frac{n^*}{[n^* + (\frac{m_i}{n_i})n^* + n_d]} \tag{6.48}$$

or

$$X_i^N = \frac{n^*}{[n^* + (\frac{m_i}{n_i})n^*]} \tag{6.49}$$

because $n_d \ll n^*$

$$X_i^M = \frac{\frac{m_i}{n_i} n^*}{[n^* + (\frac{m_i}{n_i}) n^*]} \tag{6.50}$$

$$X_i^i = \frac{n_d}{[n^* + (\frac{m_i}{n_i}) n^*]} \tag{6.51}$$

The Q for the reaction is

$$Q = \frac{X_i^i}{(X_i^N)^{n_i} (X_i^M)^{m_i}} \tag{6.52}$$

Or

$$Q = [\frac{n^d}{n^*[1 + (\frac{m_i}{n_i})]}][(\frac{1}{1 + \frac{m_i}{n_i}})^{n_i} (\frac{1}{1 + (\frac{n_i}{m_i})})^{m_i}]^{-1} \tag{6.53}$$

where n^d/n^* is the concentration of the defects in the surface. ΔG_i is thus given by

$$\Delta G_i = \frac{\Delta G_i^\circ + kT \ln[\frac{X_i^i}{[(X_i^N)^{n_i} (X_i^M)^{m_i}]}]}{n_i} \tag{6.54}$$

The model uses this equation for comparing driving forces for different silicides to form. This comparison is based on the free energy change per non-moving reactant atom (or per mole) which is released. It can be seen from the equation that a silicide molecule with more than one non-moving reactant atom has a lower likelihood of forming because its formation requires more non-moving reactant atoms to be released at the same time. The ratio n_d/n^* is estimated to be about 10^{-6}.

When values of E and n_d are not available the model calculates relative maximum release rates (RMR rates). This is done by first finding ΔH_{i298}° for all silicides in a binary metal-Si diffusion system. An arbitrary value of 1 at/cm^2 s is assigned to the maximum release rate (r_{1max}) which has the smallest negative value of ΔH_{i298}° (or ΔG_1). N^*, ν and E are the same for reactions in the same reaction region of a diffusion couple. Thus,

$$\frac{r_{i\ \max}}{r_{1\ \max}} = \exp[-\frac{\Delta G_i - \Delta G_1}{kT}] \tag{6.55}$$

Using this expression RMR rates are calculated and used to construct a semiquantitative plot (SRP plot) (see **Fig. 6.3**). The paper describing the model lists only 15 silicides, for which predictions are made [**172**].

The reasons for such a limited number of systems and limited use of the model are:

1. A difficulty in finding standard heats of formation and major diffusers in other systems.

2. Reactions must remain type two reactions at all temperatures where the model is used. There are also different RMR rates at different temperatures.

6.4.3 Criticism of the Zhang and Ivey Model

A few points need to be noted about the Zhang and Ivey model:

1. It is not explained why the model cannot be used on metal-metal systems. There is no restriction based on physics principles in the model that should prevent it from being used on metal-metal systems.

2. The major diffuser must be known for all the phases of a system under consideration before the model can be used.

3. It is not explained in the model how to treat a case where a predominant diffuser in one phase is not a predominant diffuser in other phases.

4. Diffusion flux is a function of temperature. According to this model the first phase is determined by the flux of M atoms that reach the non-moving reactant. If the temperature is changed (say reduced) the flux will change and this by implication from this model should change the phase that is forming. There is no evidence from the literature that annealing diffusion couples at different temperatures (below one-half of the lowest eutectic temperature) result in different first phases.

5. Defect concentrations are taken into account when the model is developed. Only atoms on the surface are considered and defect positions are treated as though the moving reactant atoms will avoid these positions. The opposite actually is true, M atoms will move readily into such positions. The presence of defects will increase the rate of reaction because:

   - defects increase the effective surface area on which reaction will take place.

- N atoms neighbouring defect positions are not held that tightly by the host crystal as other atoms far removed from defect positions.

6. It is well known that non-congruent phases in the silicides do not nucleate easily and are skipped. This fact is not taken into account in the model.

In spite of these criticisms, the Zhang and Ivey model is a good attempt at explaining phase formation in thin films.

6.5 Effective Heat of Formation model

The EHF model, as proposed by Pretorius [11,12,168,8,95,96] has been successfully applied to silicon-metal, metal-metal as well as germanium-metal systems. In this model a modified heat of formation (the effective heat of formation) is calculated as a function of the standard heat of formation and the effective concentration of the elements at the reaction interface. In this way the EHF model links standard thermodynamic concepts (heats of formation) with kinetics (effective concentration) and evaluates phase formation from a thermodynamic-kinetic viewpoint. The background to this approach will first be discussed.

The driving force for a process to take place is the change in Gibbs free energy:

$$\Delta G^{\circ} = \Delta H^{\circ} - T\Delta S^{\circ} \tag{6.56}$$

where ΔH° is the change in enthalpy, ΔS° is the change in entropy while T is the temperature. Since the value of the product of T and ΔS° is small during solid state formation of compound phases, ΔG° may be approximated by ΔH°. It must be emphasized that phase formation at an interface during solid-state reaction is a dynamic non-equilibrium process and that equilibrium rules can not directly be applied. The basic idea of the EHF model is that it is concentration dependent and that elements will mix at the growth interface at an effective concentration (as yet undetermined), which could differ significantly from the physical concentration at the growth interface. The effective heat of formation, $\Delta H'$, for a specific phase is then calculated as the maximum heat released per mole of available atoms during

formation of that specific compound at a given effective concentration at the growth interface. To be more precise, if a compound $A_{1-x}B_x$ is to be formed for an effective concentration x' of element B at the growth interface, then element B will be the limiting element if $x' < x$. If $\Delta H°$ is the heat of formation of the compound phase $A_{1-x}B_x$ with x the compound concentration of the limiting element B, then the heat released per mole of available atoms is dictated by the effective concentration of the limiting element and the concentration of the limiting element in the compound to be formed. An effective heat of formation $\Delta H'$ can therefore be defined as:

$$\Delta H' = \Delta H° \times \left(\frac{\textit{effective concentration limiting element}}{\textit{compound concentration limiting element}} \right) = \Delta H° \times \left(\frac{x'}{x} \right) \quad (6.57)$$

where $\Delta H'$ and $\Delta H°$ are expressed in kJ per mole of atoms. With eq. (6.57) the effective heat of formation of any compound can be calculated as a function of the concentration of the limiting element. The effective concentration expresses the availability of the limiting element at the growth interface. The excess atoms should be regarded as being available for formation of the next increment of the compound at the moving interface.

To predict phase formation using the EHF concept one has to know the effective concentrations of the reacting species at the growth interface. The effective concentration can not be calculated directly. It is known, however, that for a large variety of systems with a given structure and bond type, the activation energy for solid-state interdiffusion is directly proportional to the melting point of the solid [97]. The activation energy determines the mobility, the smaller the activation energy the greater the mobility. The greatest mobility of the atoms and the most effective mixing at the reaction interface is expected to be at the composition of the liquidus minimum (in many cases the lowest temperature eutectic). The effective concentration is thus chosen to be at the liquidus minimum of the binary system. The EHF rule for predicting phase formation in metal-metal systems therefore states [95]:

> *"The first compound phase to form during metal-metal interaction is the phase with the most negative effective heat of formation at the concentration of the liquidus minimum of the binary system."*

For silicides non-congruently melting phases do not nucleate readily and since nucleation barriers can not be taken into account when calculating EHF values, they must be considered when proposing rules for phase prediction. This is done in a similar way as proposed for the W-B model, which applies the restriction of congruency. The corresponding EHF rule for silicide compound formation is [168]:

> *"The first compound to form during metal-silicon interaction is the congruent phase with the most negative effective heat of formation at the concentration of the liquidus minimum of the binary system."*

In this regard it is worth noting that the germanides occupy a position somewhat between that of the silicides, in which only congruent phases are formed, and metal-metal systems where the phase with the most negative $\Delta H'$ forms regardless of congruency [168, 8]. This is not too surprising from a chemical point of view since Ge is more metallic in nature than Si and therefore lies somewhere between silicon and the metals. It has been found that non-congruent germanide phases with a more negative $\Delta H'$ sometimes tend to form first [81, 84, 85].

Recently a general EHF rule for phase formation has been formulated [8], which states:

> *"Phases will react with each other to form a phase with a composition lying between that of the interacting phases, whose effective heat of formation, calculated at the concentration closest to that of the liquidus minimum within this composition range, is the most negative."*

This general rule not only applies to first phase formation, but also applies to phase formation sequence and phase decomposition. In conjunction with this rule aspects regarding the ease of nucleation (eg. congruency) should be taken into account as was the case for specific rules on silicide first phase formation.

6.6 Statistical Model

In this model (which has been developed as part of this thesis and is more fully described in chapter 4)elementary probability theory is used to predict compound

phases, A_sB_q (where s+q=N is the cluster number) that form in couples made up of solid films of element A and B. It is assumed that all atomic % mixtures are available at the reaction interface. Activation energies of diffusion are expected to vary with concentration. They are known to be proportional to the melting points of solids. Greatest rates of intermixing should therefore be at the liquidus minimum as given by the bulk phase diagram.

Probabilities of forming clusters which are in correct ratios to form phases can be calculated

$$P^m_{A_sB_q}(x) = c(100 - x)^s x^q \tag{6.58}$$

where c is a normalisation constant and x is concentration in atom % B. They can be normalised

$$\int_0^{100} P^m_{A_sB_q}(x)dx = 1 \tag{6.59}$$

Fig. 5.9 shows the relative probability of meeting in the correct ratio to form phases in the system Nb-Al. These probabilities can be calculated for any system. Clusters that form may break up into constituent parts. The probability that they do not break is

$$\prod_{i=1}^{N}[1 - exp(-\frac{E_i}{kT})] \tag{6.60}$$

Where k is the Boltzmann constant, T the temperature and E_i the activation energy for diffusion of the i-th atom in the cluster. The probability of forming a phase for metal-metal systems is

$$P^{ms}_{phase}(x) = P^m_{A_sB_q}(x)\prod_{i=1}^{N}[1 - exp(-\frac{E_i}{kT})] \tag{6.61}$$

In cases where there are atoms which form directional bonds (Si and Ge), the probability that electronic configurations have proper orientation in space must be taken into account. Let this probability be P_{orient} for a single atom of either Si or Ge. For all atoms in a cluster of N the total probability is

$$P^{tot}_{orient} = (P_{orient})^q \tag{6.62}$$

P_{orient}=1 for metal atoms and is expected to be smaller than unity for a semiconductor atom. Let the activation energy of rotation of the j-th atom of element B

(either Ge or Si) in a cluster be E_j^r. The probability that atoms won't break free from their bonds through rotations is

$$\prod_{j=1}^{q}[1 - exp(-\frac{E_j^r}{kT})] \tag{6.63}$$

The probability of forming a compound phase A_sB_q, is:

$$P_{phase}^{msr}(x) = P_{A_sB_q}^{m}(x)P_{orient.}^{tot.}\prod_{i,j=1}^{N,q}[1 - exp(-\frac{E_i}{kT})][1 - exp(-\frac{E_j^r}{kT})] \tag{6.64}$$

Deriving rate equations for solid state kinetics is straightforward. If x_b is the amount of the mixture at the growth interface, and $x_{A_sB_q}$ is the amount of the compound that has formed, then the rate at which a phase is forming is

$$\frac{dx_{A_sB_q}}{dt} = a_{A_sB_q}x_b - b_{A_sB_q}x_{A_sB_q} \tag{6.65}$$

Similar equations may be written for other phases, and are then solved simultaneously. The value of the rate constants $a_{A_sB_q}$ and $b_{A_sB_q}$ appearing in the rate equations is

$$a_{A_sB_q} = \nu_o k_{A_sB_q}P_{A_sB_q}^{v}(x)P_{orient.}^{tot.}\prod_{i,j=1}^{N,q}[1 - exp(-\frac{E_i}{kT})][1 - exp(-\frac{E_j^r}{kT})] \tag{6.66}$$

$$b_{A_sB_q} = \nu_o l_{A_sB_q}\prod_{i,j=1}^{N,q}[exp(-\frac{E_i}{kT})][exp(-\frac{E_j^r}{kT})] \tag{6.67}$$

ν_o is the vibrational frequency of the solid and $k_{A_sB_q}$ and $l_{A_sB_q}$ are fitting constants. It is seen from these rate equations that they will describe a non-equilibrium situation only if the concentration x is changing with time. This change in concentration is governed by the diffusion equation.

6.7 Comparison of Models

6.7.1 Comparison of the Gosele and Tu model to the EHF model

The Gosele and Tu model explains the absence of some compound phases in thin film couples, which are predicted by the bulk equilibrium phase diagram, as due to

a kinetic instability. This kinetic instability is said to be the result of interfacial reaction barriers. The EHF model uses the concentration of atoms at the liquidus minimum (because this is where the mobility of the atoms is greatest,) and heats of formation. These two factors are combined to calculate effective heats of formation $\Delta H'$. According to the EHF model phases will form depending on how much effective heats of formation they can evolve. Therefore according to this model a compound most likely to form is the one with the most negative effective heat of formation at a given concentration. This way there is no need to introduce any interfacial reaction barriers. The EHF model is also not limited to silicides only, it can explain phase formation in silicides, in addition to metal-metal systems and germanium-metal systems.

The Gosele and Tu model is basically a kinetic model. It cannot however predict which phases should form in a thin binary reaction couple (e.g. predict what the first phase is). Kinetic models are expected to be predictive. They should be able to tell amounts that form in a given period of time i.e. they should tell which phase is forming and at what rate. The Gosele and Tu model can however explain linear growth with time of compound phases (i.e. where the growth behaviour of a phase varies linearly with time). It can also explain parabolic behaviour (where the thickness of a grown phase is proportional to the square root of time). On the other hand the EHF model, since it is not a kinetic model, (though it uses kinetic behaviour of the system through the use of atomic concentrations), cannot explain linear and parabolic growth behaviour of layer thicknesses of various compound phases.

Both models can explain compound phase formation sequence. The EHF model can explain which phase will form second, and what the phase sequence will be. This it does by noting which supply (A or B) is larger. The EHF model [8] states that: *"After first phase formation, in Si-metal and Ge-metal systems the effective concentration moves in the direction of the remaining element and the next phase to form at the growth interface is the next phase richer in the unreacted element, which has the most negative effective heat of formation "*. The EHF model is very

successful in predicting phase formation sequence (this is borne out by experimental observations). Whereas the Gosele and Tu kinetic model just gives a descriptive explanation in which sequence phases should form (it cannot give specific compound phases because the starting point which is the first phase cannot be predicted), the EHF model can name specific phases as first, second, third, etc as compound phases that will form.

The EHF model is very easy to use, and uses just one simple equation to find effective heats of formation. The Gosele and Tu model is truly cumbersome, (has many equations) especially in systems with many phases. To analyze and extract information from this model is difficult.

Careful observation in many experiments by different groups has shown conclusively that congruency of phases in silicon-metal and germanium-metal systems play a significant role in phase formation. The concentration of atoms in that composition corresponding to the liquidus minimum is also important. These two factors are both taken into account in the formulation of the EHF model. The Gosele and Tu model has no mention whatsoever of these two factors. Any model that does not include congruency and concentration of atoms at the liquidus minimum of a binary system is bound to fail. **Table 6.1** shows predictions of the first phase based on both these two models.

TABLE 6.1: COMPARISON OF EHF AND ZHANG AND IVEY MODELS. Predicted first phases in silicides according to the EHF and Zhang and Ivey models. The effective heats of formation of phases found to form first, experimentally, are underlined.

System	Congruency	Composition	$\Delta H'$ kJ(mol.at.)$^{-1}$	EHF Model	Zhang Ivey	Observed Phases	Ref
Liquidus Minimum	=	$Co_{0.775}Si_{0.225}$					
Co_2Si (12)	C	$Co_{0.667}Si_{0.333}$	<u>−26.01</u>	Co_2Si	Co_2Si	Co_2Si	[18–23]
CoSi (8)	C	$Co_{0.500}Si_{0.500}$	−22.59				
$CoSi_2$ (12)	C	$Co_{0.333}Si_{0.667}$	−11.57				
Liquidus Minimum	=	$Cr_{0.180}Si_{0.820}$					
Cr_3Si (8)	C	$Cr_{0.750}Si_{0.250}$	−8.26				
Cr_5Si_3 (32)	C	$Cr_{0.625}Si_{0.375}$	−10.08				
CrSi (8)	NC	$Cr_{0.500}Si_{0.500}$	−10.87				
$CrSi_2$ (9)	C	$Cr_{0.333}Si_{0.667}$	<u>−13.95</u>	$CrSi_2$	$CrSi_2$	$CrSi_2$	[3,18,23–27]
Liquidus Minimum	=	$Fe_{0.670}Si_{0.330}$					
Fe_3Si (16)	NC	$Fe_{0.750}Si_{0.250}$	−23.05				
FeSi (8)	C	$Fe_{0.500}Si_{0.500}$	<u>−25.94</u>	FeSi		FeSi	[18,29]
$FeSi_2$ (3)	NC	$Fe_{0.333}Si_{0.667}$	−15.15		$FeSi_2$		
Liquidus Minimum	=	$Hf_{0.080}Si_{0.920}$					
Hf_3Si (–)	NC	$Hf_{0.750}Si_{0.250}$	−5.65				
Hf_2Si (12)	NC	$Hf_{0.667}Si_{0.333}$	−8.38				
Hf_5Si_3 (16)	NC	$Hf_{0.625}Si_{0.375}$	−9.88				
Hf_3Si_2 (10)	NC	$Hf_{0.600}Si_{0.400}$	−10.80				
Hf_5Si_4 (36)	NC	$Hf_{0.556}Si_{0.444}$	−12.43				
HfSi (8)	C	$Hf_{0.500}Si_{0.500}$	<u>−14.42</u>	HfSi		HfSi	[18,32,33]
$HfSi_2$ (12)	NC	$Hf_{0.333}Si_{0.667}$	−18.02		$HfSi_2$		
Liquidus Minimum	=	$Mn_{0.790}Si_{0.210}$					
Mn_6Si (13)	NC	$Mn_{0.857}Si_{0.143}$	−16.50				
Mn_9Si_2 (110)	NC	$Mn_{0.818}Si_{0.182}$	−22.11				
Mn_3Si (16)	NC	$Mn_{0.750}Si_{0.250}$	<u>−26.12</u>		Mn_3Si	Mn_3Si	[35]
Mn_5Si_2 (56)	NC	$Mn_{0.714}Si_{0.286}$	−25.65				
Mn_5Si_3 (16)	C	$Mn_{0.625}Si_{0.375}$	−23.30	Mn_5Si_3			
MnSi (8)	C	$Mn_{0.500}Si_{0.500}$	<u>−17.43</u>			MnSi	[18,36]
$Mn_{11}Si_{19}$ (120)	C	$Mn_{0.367}Si_{0.633}$	−9.52				
Liquidus Minimum	=	$Mo_{0.017}Si_{0.983}$					
Mo_3Si (8)	NC	$Mo_{0.750}Si_{0.250}$	−0.66				
Mo_5Si_3 (16/32)	C	$Mo_{0.625}Si_{0.375}$	−1.06				
$MoSi_2$ (6)	C	$Mo_{0.333}Si_{0.667}$	<u>−2.24</u>	$MoSi_2$	$MoSi_2$	$MoSi_2$	[18,37–40]
Liquidus Minimum	=	$Nb_{0.050}Si_{0.950}$					
Nb_5Si_3 (32)	C	$Nb_{0.625}Si_{0.375}$	−4.86				
$NbSi_2$ (9)	C	$Nb_{0.333}Si_{0.667}$	<u>−6.90</u>	$NbSi_2$	$NbSi_2$	$NbSi_2$	[18,39]

Cont...

System	Congruency	Composition	$\Delta H'$ kJ(mol.at.)$^{-1}$	EHF Model	Zhang Ivey	Observed Phases	Ref
Liquidus Minimum	=	$Ni_{0.535}Si_{0.465}$					
Ni_3Si (4)	NC	$Ni_{0.750}Si_{0.250}$	−26.54				
Ni_5Si_2 (43)	C	$Ni_{0.714}Si_{0.286}$	−31.68				
Ni_2Si (6/12)	C	$Ni_{0.667}Si_{0.333}$	−37.64	Ni_2Si	Ni_2Si	Ni_2Si	[18,41–49]
Ni_3Si_2 (80)	NC	$Ni_{0.600}Si_{0.400}$	−40.30				
NiSi (8)	C	$Ni_{0.500}Si_{0.500}$	−39.43	NiSi			
$NiSi_2$ (12)	NC	$Ni_{0.333}Si_{0.667}$	−20.44				
Liquidus Minimum	=	$Pd_{0.845}Si_{0.155}$					
Pd_5Si (24)	NC	$Pd_{0.833}Si_{0.167}$	−27.16				
Pd_9Si_2 (44)	NC	$Pd_{0.818}Si_{0.182}$	−26.68				
Pd_3Si (16)	NC	$Pd_{0.750}Si_{0.250}$	−23.87		Pd_3Si		
Pd_2Si (9)	C	$Pd_{0.667}Si_{0.333}$	−19.99	Pd_2Si		Pd_2Si	[18,39,34,51,52]
PdSi (8) [b]	C	$Pd_{0.500}Si_{0.500}$	−8.12				
Liquidus Minimum	=	$Pt_{0.770}Si_{0.230}$					
Pt_3Si (16)	NC	$Pt_{0.750}Si_{0.250}$	−33.95				
Pt_7Si_3 (–) [c]	NC	$Pt_{0.700}Si_{0.300}$	−33.58				
Pt_2Si (6)	C	$Pt_{0.667}Si_{0.333}$	−32.91	Pt_2Si	Pt_2Si	Pt_2Si	[51,53–55]
Pt_6Si_5 (22)	NC	$Pt_{0.545}Si_{0.455}$	−28.39				
PtSi (8)	C	$Pt_{0.500}Si_{0.500}$	−25.76				
Liquidus Minimum	=	$Ta_{0.010}Si_{0.990}$					
$Ta_{4.5}Si$ (–)	C	$Ta_{0.818}Si_{0.182}$	−0.33				
Ta_3Si (–)		$Ta_{0.750}Si_{0.250}$	–				
Ta_2Si (12)	C	$Ta_{0.667}Si_{0.333}$	−0.61				
Ta_5Si_3 (32)	C	$Ta_{0.625}Si_{0.375}$	−0.67				
$TaSi_2$ (9)	C	$Ta_{0.333}Si_{0.667}$	−0.97	$TaSi_2$	$TaSi_2$	$TaSi_2$	[18,39]
Liquidus Minimum [d]	=	$Ti_{0.160}Si_{0.840}$					
Ti_3Si (32)	NC	$Ti_{0.750}Si_{0.250}$	−11.31				
Ti_5Si_3 (16)	C	$Ti_{0.625}Si_{0.375}$	−18.53			Ti_5Si_3	[32,58,66–69]
Ti_5Si_4 (36)	NC	$Ti_{0.556}Si_{0.444}$	−23.33				
TiSi (8)	NC	$Ti_{0.500}Si_{0.500}$	−25.15			TiSi	[18,32,58,69,63–65,70–73]
$TiSi_2$ (24)	C	$Ti_{0.333}Si_{0.667}$	−27.36	$TiSi_2$	$TiSi_2$	$TiSi_2$	[18,34,58,66,67,63–65,57,59–6
Liquidus Minimum	=	$V_{0.030}Si_{0.970}$					
V_3Si (8)	C	$V_{0.750}Si_{0.250}$	−1.81				
V_2Si (–)		$V_{0.667}Si_{0.333}$	–				
V_5Si_3 (32)	C	$V_{0.625}Si_{0.375}$	−2.78				
VSi_2 (9)	C	$V_{0.333}Si_{0.667}$	−3.62	VSi_2	VSi_2	VSi_2	[18,39,34,74]
Liquidus Minimum	=	$W_{0.010}Si_{0.990}$					
W_5Si_3 (16/32)	C	$W_{0.625}Si_{0.375}$	−0.27				
W_3Si_2 (–)		$W_{0.600}Si_{0.400}$	–				
WSi_2 (6)	C	$W_{0.333}Si_{0.667}$	−0.93	WSi_2	WSi_2	WSi_2	[18,39,40,28,75]
Liquidus Minimum	=	$Zr_{0.100}Si_{0.900}$					
Zr_4Si (–)		$Zr_{0.800}Si_{0.200}$	–				
Zr_2Si (12)	NC	$Zr_{0.667}Si_{0.333}$	−10.48				
Zr_5Si_3 (16)	NC	$Zr_{0.625}Si_{0.375}$	−11.52				
Zr_3Si_2 (10)	NC	$Zr_{0.600}Si_{0.400}$	−12.83				
Zr_5Si_4 (36)	C	$Zr_{0.556}Si_{0.444}$	−14.00				
ZrSi (8)	NC	$Zr_{0.500}Si_{0.500}$	−15.48				
$ZrSi_2$ (12)	NC	$Zr_{0.333}Si_{0.667}$	−15.93	$ZrSi_2$	$ZrSi_2$	$ZrSi_2$	[18,23]

[a] This phase is sometimes referred to as $ErSi_{1.7}$[166]. [b] A recent publication [167] shows that this phase is probably only stable above 824°C. [c] Also referred to as Pt_5Si_2 or $Pt_{12}Si_5$ [16]. [d] Ti has another lowest eutectic point at the same temperature (1330°C) for a composition of 14 at % Si [16].

6.7.2 Comparison of the Zhang and Ivey Model to the EHF model

The EHF model is based on both kinetics and thermodynamics. It uses the liquidus minimum and heats of formation to predict phases. The Zhang and Ivey model uses maximum release rates for phase prediction.

The Zhang and Ivey model has many restrictions as to when it can be used. Only those systems in which the Zhang and Ivey model can be applied are listed. The EHF model is more successful in predicting first phase formation in the given 15 systems. This model is also not limited to these few (only 15 silicides). It does not have as many restrictions on applicability as the Zhang and Ivey model. It can be applied not only to silicides, but also to germanides as well as to metal-metal systems.

It is also well known that non-congruent phases of the silicides do not nucleate readily and are skipped. The Zhang and Ivey model does not take this into account. The Walser-Bene [2], Effective Heat of Formation (EHF) [11, 8] and Statistical models will be compared to each other, as they are the only models which make definite and unambiguous predictions regarding first phase formation. Although these models appear to have a lot in common, if their success in correctly predicting first phase formation is used as criterion, a careful analysis will reveal fundamental differences between them.

6.7.3 Comparison of W-B to EHF model

It should be no surprise that the W-B and EHF models agree on a large number of predictions, since it can be shown that the EHF model will generally predict the same phase as will be selected by the W-B model. This observation stems from the following: In general, the EHF for a particular phase will be the most negative at effective concentrations close to the compound concentration. If the heats of formation of two compound phases on both sides of the liquidus minimum (in many cases the lowest-temperature eutectic) are approximately the same, the phase closest in concentration to the liquidus minimum will have the most negative EHF and will

therefore be predicted by the EHF model. But this is exactly the selection rule applied by the W-B model.

In order to compare the EHF and W-B models we replace the lowest-temperature eutectic in the W-B model with the liquidus minimum for those systems where either no eutectic exists (eg. Al-V) or the lowest-temperature eutectic is not at the concentration of the liquidus minimum (eg. Au-Ga). There are **18** systems for which it was necessary to use this extended form of the W-B model and such cases will be superscripted by the symbol †. This allows a comparison of **84** binary systems for which we have found both sufficient thermodynamic data and experimental observations.

The general agreement in predictions by the two models is clearly revealed in **Table 6.2**. This table lists **50** binary systems where the EHF model and the W-B model predict the same first phase and that prediction is confirmed experimentally. Both models apply the same restriction of congruency in the case of the Si-metal and Ge-metal systems. In the metal-metal systems "phase skipping" is not predicted, as both congruent and non-congruent phases are expected to nucleate.

The agreement between the W-B and EHF models must necessarily be limited since the W-B unlike the EHF model does not make direct use of thermodynamic quantities. The EHF model combines both kinetics and thermodynamics by taking into account the effective concentration at the growth interface and the heats of formation of the relevant phases in a quantitative manner. This feature of the EHF model highlights differences between the two models.

In the rules for phase prediction by the EHF model the experimental uncertainties in thermodynamic quantities are also acknowledged. This is done by choosing an arbitrary 5% window [8] in the EHF values wherein it is no longer possible to uniquely predict a single phase. Instead it is argued that from a thermodynamic-kinetic viewpoint, there is not much to choose between such phases. The W-B phase prediction rules are designed to predict one first phase, but it is inherent to the EHF model, that certain systems will exhibit competing phases with very little to choose between them from a thermodynamic-kinetic point of view. **Table 6.3** lists those **13**

TABLE 6.2: COMPARISON BETWEEN W-B AND EHF MODELS. Binary systems for which there is complete agreement between experimentally observed first phase formation and the predictions of both the Walser-Bené and Effective Heat of Formation models.

System	First Phase	References	System	First Phase	References
Ag-Al	Ag_2Al	[108]	Cu-Sb	Cu_2Sb	[100]
Ag-Ga	Ag_3Ga	[98]	Cu-Si	$Cu_{19}Si_6$	[18]
Ag-In	$AgIn_2$	[98]	Cu-Sn	Cu_6Sn_5	[98,101]
Ag-Sn	Ag_3Sn	[98,99]	Er-Si	Er_3Si_5	[18,28]
Al-Co	Co_2Al_9	[113–115]	Fe-Si	FeSi	[18,29]
Al-Cr	Cr_2Al_{13}	[108,115–117]	Ge-Hf	Hf_5Ge_3	[80]
Al-Cu	$CuAl_2$	[4,118–123]	Ge-Mn	Mn_5Ge_3	[80]
Al-Hf†	$HfAl_3$	[114,127,128]	Ge-Ni	Ni_5Ge_3	[78,80,91]
Al-Nb†	$NbAl_3$	[130–135]	Ge-Pt	Pt_2Ge	[78,79]
Al-Ni	$NiAl_3$	[113,136–138]	Ge-Rh	RhGe	[80]
Al-Ta†	$TaAl_3$	[113–115,145]	Ge-Ti	Ge_3Ti_5	[78]
Al-Ti†	$TiAl_3$	[113–115,127,146–148]	Hf-Si	HfSi	[18,32,33]
Al-Zr†	$ZrAl_3$	[114,128,147]	Mg-Si	Mg_2Si	[34]
Au-Ga†	$AuGa_2$	[152]	Mo-Si	$MoSi_2$	[18,38–40,173]
Au-In†	$AuIn_2$	[152–156]	Nb-Si	$NbSi_2$	[18,39]
Au-Nb†	Au_2Nb	[157]	Os-Si	Os_2Si_3	[18,50]
Au-Sb	$AuSb_2$	[152]	Pb-Pd	Pb_2Pd	[98]
Ca-Si	Ca_2Si	[17]	Pb-Pt	Pb_4Pt	[99]
Co-Ge	Co_5Ge_3	[80,81]	Pd-Si	Pd_2Si	[18,39,34,51,52]
Co-Si	Co_2Si	[18,20,23,174–176]	Pt-Si	Pt_2Si	[51,53–55]
Cr-Si	$CrSi_2$	[3,18,23–27]	Si-Rh	RhSi	[18,56]
Cu-Ge	Cu_3Ge	[82]	Si-Ta	$TaSi_2$	[18,39]
Cu-Mg	$CuMg_2$	[100]	Si-V	VSi_2	[18,39,34,74]
Cu-Pd†	Cu_3Pd	[98,100]	Si-W	WSi_2	[18,39,40,28,75]
Cu-Pt†	Cu_3Pt	[100]	Si-Y	Y_3Si_5	[18,28]

† Denotes binary systems where the lowest-temperature eutectic is not the liquidus minimum.

systems for which the W-B and EHF models both predict the correct experimentally found first phase, but the EHF model predicts more than one phase.

The EHF model does not contend that when the $\Delta H'$ values of phases are close together they must necessarily be observed as a first phase. The model rather predicts that those phases have almost equal chances to form from a thermodynamic-kinetic viewpoint. Because the W-B model can only predict one first phase, it fails to indicate the possibility that other phases might, from a thermodynamic point of view, form just as readily.

It is interesting to note from **Table 6.3** that for

TABLE 6.3: COMPARISON BETWEEN W-B AND EHF MODELS. Binary systems for which the W-B and EHF model predict the same first phase, but the EHF also predicts other phases. The $\Delta H'$ values have been calculated at the concentration of the liquidus minimum of the binary system. For systems where the liquidus minimum coincides with the melting point of one of the elemental compounds, an arbitrary effective concentration of 98 at.% of the element with the lowest melting point is taken. The phases for which the $\Delta H'$ values are underlined are those, which have been found experimentally to form first. The number of atoms per unit cell are given in brackets behind each phase.

System	Congruency	Composition	ΔH^o kJ(mol.at.)$^{-1}$	$\Delta H'$ kJ(mol.at.)$^{-1}$	EHF	W-B	Observed Phases	Ref
Liquidus Minimum	=	$Al_{0.980}Mo^{\dagger}_{0.020}$						
$AlMo_3$ (8)	NC	$Al_{0.250}Mo_{0.750}$	−50	−1.33				
Al_8Mo_3 (22)	C	$Al_{0.727}Mo_{0.273}$	−49	−3.59				
Al_4Mo (30)	NC	$Al_{0.800}Mo_{0.200}$	−37	−3.70				
Al_5Mo (12)	NC	$Al_{0.833}Mo_{0.167}$	−32	−3.84	Al_5Mo			
$Al_{12}Mo$ (26)	NC	$Al_{0.923}Mo_{0.077}$	−15	−3.90	$Al_{12}Mo$	$Al_{12}Mo$	$Al_{12}Mo$	[115,129]
Liquidus Minimum	=	$Al_{0.920}Pd_{0.080}$						
$AlPd_2$ (12)	C	$Al_{0.333}Pd_{0.667}$	−85	−10.19				
AlPd (26)	C	$Al_{0.500}Pd_{0.500}$	−92	−14.72				
Al_3Pd_2 (5)	NC	$Al_{0.600}Pd_{0.400}$	−83	−16.60	Al_3Pd_2		Al_3Pd_2	[138,177]
Al_3Pd (-)	NC	$Al_{0.750}Pd_{0.250}$	−52	−16.64	Al_3Pd		Al_3Pd	[114]
Al_4Pd (90)	NC	$Al_{0.800}Pd_{0.200}$	−40	−16.00	Al_4Pd	Al_4Pd	Al_4Pd	[113,140]
Liquidus Minimum	=	$Al_{0.980}V^{\dagger}_{0.020}$						
Al_8V_5 (52)	NC	$Al_{0.615}V_{0.385}$	−35.4	−1.84				
Al_3V (8)	NC	$Al_{0.750}V_{0.250}$	−24.3	−1.94	Al_3V		Al_3V	[126,146,149]
$Al_{23}V_4$ (54)	NC	$Al_{0.857}V_{0.143}$	−14.3	−1.93	$Al_{23}V_4$			
Al_7V (104)	NC	$Al_{0.875}V_{0.125}$	−12.1	−1.94	Al_7V			
$Al_{10}V$ (176)	NC	$Al_{0.909}V_{0.091}$	−8.8	−1.93	$Al_{10}V$	$Al_{10}V$	$Al_{10}V$	[126,149]
Liquidus Minimun	=	$Al_{0.980}W^{\dagger}_{0.020}$						
Al_4W (30)	NC	$Al_{0.800}W_{0.200}$	−10.4	−1.04	Al_4W			
Al_5W (12)	NC	$Al_{0.833}W_{0.167}$	−9.0	−1.08	Al_5W			
$Al_{12}W$ (26)	NC	$Al_{0.923}W_{0.077}$	−4.0	−1.04	$Al_{12}W$	$Al_{12}W$	$Al_{12}W$	[108,150,151]
Liquidus Minimum	=	$Au_{0.159}Pb_{0.841}$						
$AuPb_3$ (32)	NC	$Au_{0.250}Pb_{0.750}$	−1.4	−0.89	$AuPb_3$	$AuPb_3$	$AuPb_3$	[152]
$AuPb_2$ (12)	NC	$Au_{0.333}Pb_{0.667}$	−1.9	−0.91	$AuPb_2$		$AuPb_2$	[99,158]
Au_2Pb (24)	NC	$Au_{0.667}Pb_{0.333}$	−2.4	−0.57				
Liquidus Minimum	=	$Au_{0.063}Sn_{0.937}$						
$AuSn_4$ (20)	NC	$Au_{0.200}Sn_{0.800}$	−9.7	−3.06	$AuSn_4$	$AuSn_4$	$AuSn_4$	[99,152,159–161]
$AuSn_2$ (24)	NC	$Au_{0.333}Sn_{0.667}$	−16.0	−3.03	$AuSn_2$		$AuSn_2$	[152,160,161]
AuSn (4)	C	$Au_{0.500}Sn_{0.500}$	−21.2	−2.67			AuSn	[152,162]
Au_5Sn (6)	NC	$Au_{0.833}Sn_{0.167}$	−10.6	−0.80				
$Au_{10}Sn$ (16)	NC	$Au_{0.909}Sn_{0.091}$	−5.7	−0.40				
Liquidus Minimum	=	$Au_{0.980}Ti^{\dagger}_{0.020}$						
$AuTi_3$ (8)	C	$Au_{0.250}Ti_{0.750}$	−46.2	−1.23				
AuTi (4)	C	$Au_{0.500}Ti_{0.500}$	−71.5	−2.86				
Au_2Ti (6)	C	$Au_{0.667}Ti_{0.333}$	−58.5	−3.51	Au_2Ti			
Au_4Ti (10)	NC	$Au_{0.800}Ti_{0.200}$	−36.1	−3.61	Au_4Ti	Au_4Ti	Au_4Ti	[107,157,165]
Liquidus Minimum	=	$Au_{0.940}Zr^{\dagger}_{0.060}$						
$AuZr_3$ (8)	C	$Au_{0.250}Zr_{0.750}$	−66.4	−5.31				
$AuZr_2$ (6)	NC	$Au_{0.333}Zr_{0.667}$	−86.8	−7.81				
Au_4Zr_5 (-)	C	$Au_{0.444}Zr_{0.556}$	−106.4	−11.49				
$Au_{10}Zr_7$ (34)	NC	$Au_{0.588}Zr_{0.412}$	−108.6	−15.82				
Au_2Zr (6)	C	$Au_{0.667}Zr_{0.333}$	−96.8	−17.42				
Au_3Zr (8)	C	$Au_{0.750}Zr_{0.250}$	−76.4	−18.34	Au_3Zr			
Au_4Zr (20)	NC	$Au_{0.800}Zr_{0.200}$	−61.6	−18.48	Au_4Zr	Au_4Zr	Au_4Zr	[157]

Cont...

System	Congruency	Composition	ΔH^* kJ(mol.at.)$^{-1}$	$\Delta H'$ kJ(mol.at.)$^{-1}$	EHF	W-B	Observed Phases	Ref
Liquidus Minimum	=	$Cu_{0.011}In_{0.989}$						
$Cu_{11}In_9$ (20)	NC	$Cu_{0.550}In_{0.450}$	−0.75	−0.015	$Cu_{11}In_9$	$Cu_{11}In_9$	$Cu_{11}In_9$	[100]
$Cu_{16}In_9$ (6)	NC	$Cu_{0.640}In_{0.360}$	−0.74	−0.013	$Cu_{16}In_9$			
Cu_9In_4 (-)	NC	$Cu_{0.692}In_{0.308}$	−0.69	−0.011	Cu_9In_4			
Liquidus Minimum	=	$Cu_{0.17}Zn^{\dagger}_{0.983}$						
$CuZn_4$ (2)	NC	$Cu_{0.200}Zn_{0.800}$	−4.1	−0.35	$CuZn_4$	$CuZn_4$	$CuZn_4$	[98]
Cu_5Zn_8 (-)	C	$Cu_{0.385}Zn_{0.615}$	−7.5	−0.33	Cu_5Zn_8			
Liquidus Minimum	=	$Ni_{0.535}Si_{0.465}$						
Ni_3Si (4)	NC	$Ni_{0.750}Si_{0.250}$	−37.2	−26.54				
Ni_5Si_2 (43)	C	$Ni_{0.714}Si_{0.286}$	−42.3	−31.68				
Ni_2Si (6/12)	C	$Ni_{0.667}Si_{0.333}$	−46.9	−37.64	Ni_2Si	Ni_2Si	Ni_2Si	[18, 41–43, 45–49, 178]
Ni_3Si_2 (80)	NC	$Ni_{0.600}Si_{0.400}$	−45.2	−40.30				
NiSi (8)	C	$Ni_{0.500}Si_{0.500}$	−42.2	−39.43	NiSi		NiSi	[179–182]
$NiSi_2$ (12)	NC	$Ni_{0.333}Si_{0.667}$	−29.3	−20.44				
Liquidus Minimum	=	$Pd_{0.020}Sn_{0.980}$						
$PdSn_4$ (20)	NC	$Pd_{0.200}Sn_{0.800}$	−30.3	−3.03	$PdSn_4$	$PdSn_4$	$PdSn_4$	[105]
$PdSn_3$ (32)	NC	$Pd_{0.250}Sn_{0.750}$	−38.0	−3.04	$PdSn_3$			
$PdSn_2$ (24)	NC	$Pd_{0.333}Sn_{0.667}$	−50.3	−3.02	$PdSn_2$			
PdSn (8)	NC	$Pd_{0.500}Sn_{0.500}$	−68.3	−2.73				
Pd_3Sn_2 (6)	NC	$Pd_{0.600}Sn_{0.400}$	−69.6	−2.32				
Pd_2Sn (12)	NC	$Pd_{0.667}Sn_{0.333}$	−64.9	−1.95				
Pd_3Sn (4)	NC	$Pd_{0.750}Sn_{0.250}$	−53.3	−1.42				
Liquidus Minimum	=	$Ru_{0.170}Si_{0.830}$						
Ru_4Si_3 (28)	?	$Ru_{0.571}Si_{0.429}$	−33.3	−9.91				
RuSi (8)	C	$Ru_{0.500}Si_{0.500}$	−32.4	−11.02	RuSi			
Ru_2Si_3 (40)	C	$Ru_{0.400}Si_{0.600}$	−25.6	−10.88	Ru_2Si_3	Ru_2Si_3	Ru_2Si_3	[18, 50]

† Denotes binary systems where the lowest-temperature eutectic is not the liquidus minimum.

5 of these systems (Al-Pd, Al-V, Au-Pb, Au-Sn and Ni-Si) there is indeed more than one experimentally found first phase. One such example is the Pd-Al system where both the W-B and the EHF model predict $PdAl_4$ as the first phase and this is confirmed experimentally **[113, 140]**.

This is the phase closest in composition to the lowest-temperature eutectic, which for this system is at $Al_{0.92}Pd_{0.08}$ (see **Fig. 6.4**, bottom).

There are however two other experimentally found first phases viz. $PdAl_3$ **[114]** and Pd_2Al_3 **[138, 177]**. The EHF model predicts correctly all three experimentally observed first phases. This arises from the fact that the effective heats offormation of these phases lie close to each other (within 5%) as can be seen from the EHF diagram (top) in **Fig. 6.4** and from **Table 6.3**. Why are all three found as first phases? As far as the system is concerned a slight variation in experimental parameters (such as impurities) can easily swing the system from one first phase to the other. Such effects are readily accommodated by the EHF model.

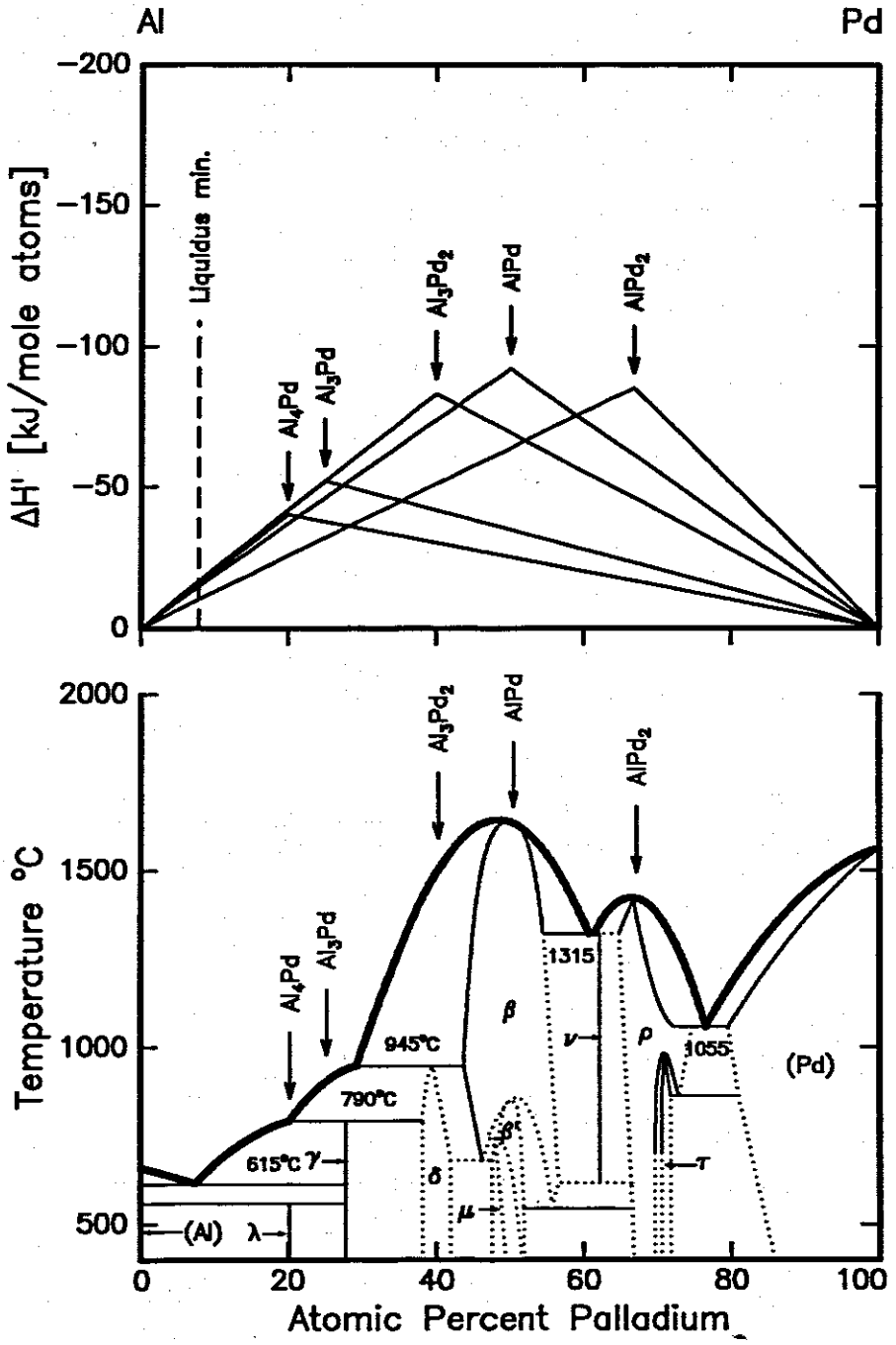

FIGURE 6.4: Diagram showing effective heats of formation versus atomic % in the Al-Pd system. Triangles represent energy released as a function of concentration for different phases. It is clear that at a concentration corresponding to the liquidus minimum, there is not much difference between $\Delta H'$ values for the three phases, Pd_2Al_3, $PdAl_3$ and $PdAl_4$. These are indeed phases that have been found experimentally to form first. The W-B model only predicts $PdAl_4$.

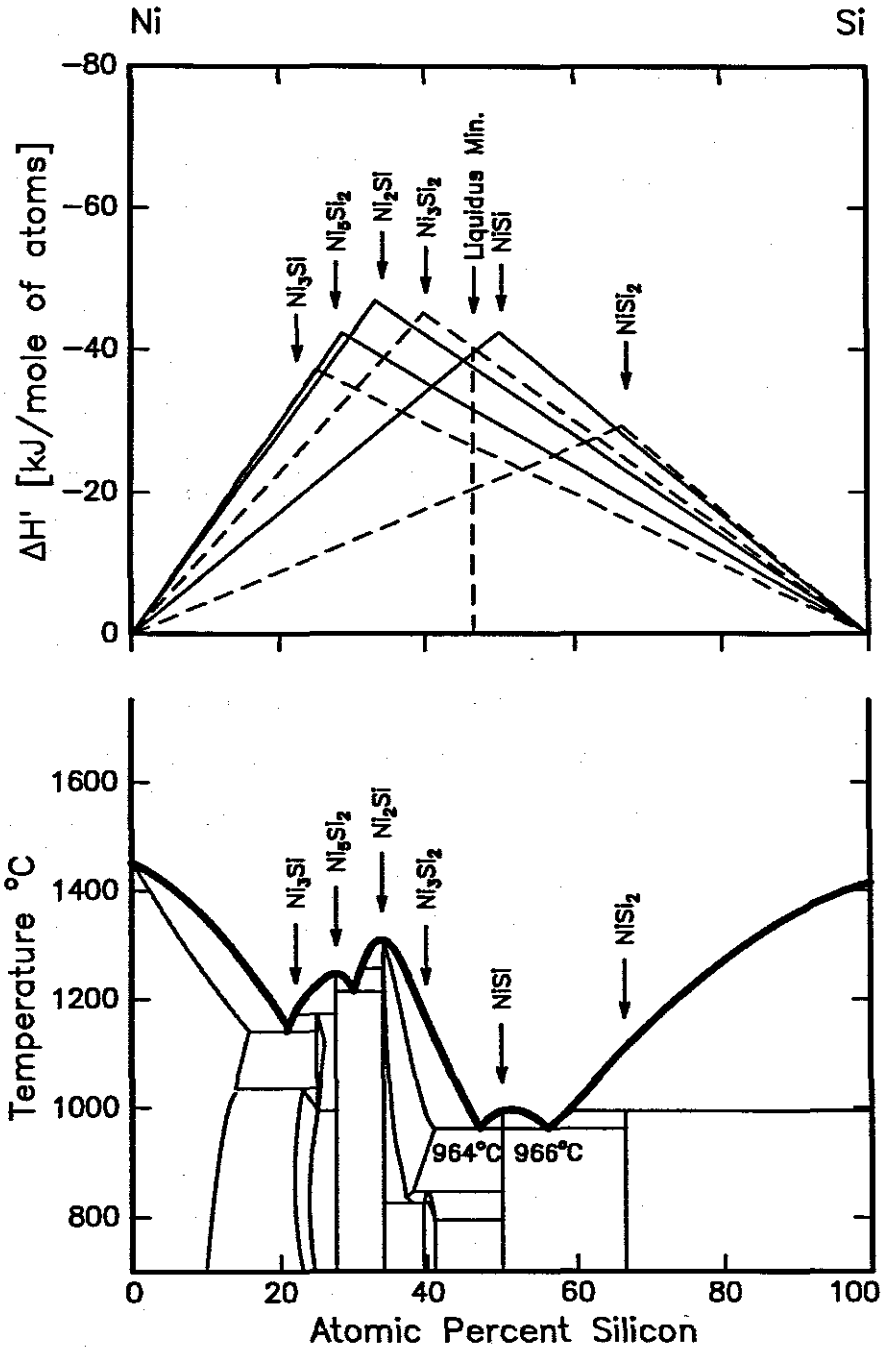

FIGURE 6.5: In the Ni-Si system the EHF model predicts both NiSi and Ni_2Si. Though Ni_3Si_2 would yield the largest effective heat of formation, it is non-congruent and will have difficulty in nucleating. Experimental evidence shows that both NiSi and Ni_2Si form first. The W-B model predicts only Ni_2Si.

Fig. 6.5 illustrates the thermodynamic-kinetic situation for the Ni-Si system. At an effective concentration of 47 at.% Si Ni_3Si_2 has the most negative $\Delta H'$ of -40.30 kJ/mol.at. However, this is a non-congruently melting phase and is not expected to nucleate readily at a moving reaction interface. For this reason the EHF triangulation for the non-congruently melting phases, Ni_3Si_2 and $NiSi_2$, have been drawn with dashed lines (see **Fig. 6.5**, top). This leaves the two congruently melting phases NiSi and Ni_2Si which have effective heats of formation of -39.43 and -37.64 kJ/mol.at respectively (see **Table 6.3**). Although, NiSi has the most negative EHF the value for Ni_2Si lies within 5% and the EHF model therefore predicts that there is thermodynamically not much to choose between the two. The Ni-Si system is, to our knowledge, the only metal-covalent system where the W-B model has to make use of the higher melting temperature criterion (see W-B rule for metal-covalent systems, section 6.2). The congruently melting phase which is closest in composition to the lowest-temperature eutectic is NiSi, however Ni_2Si is predicted [4] since the eutectic lies between NiSi and Ni_2Si and the latter has the highest melting temperature (see **Fig. 6.5**, bottom). Ni_2Si has always been regarded as the first phase to form and is indeed the dominant growing first phase in thin-film Ni-Si interactions [18, 41–43, 45–49, 178]. However, there are many recent reports that NiSi is indeed the first phase to nucleate [179–182], but does not grow beyond a thickness of about 15 nm [179]. Clearly this competitiveness is reflected by the EHF values, while the W-B model has much difficulty in explaining the experimental observations.

There are also other cases where the W-B model fails completely to predict the correct first phase and they are listed in **Table 6.4**.

Consider, for example, the Au-Al system, which is of considerable importance in semiconductor device metallurgy and has been the subject of much attention [109–112]. The Au-Al phase diagram shows five stoichiometric compounds namely Au_4Al, Au_5Al_2, Au_2Al, AuAl, and $AuAl_2$ (see **Fig. 6.6**, bottom).

There is some uncertainty regarding first phase formation as certain measurements show that Au_5Al_2 and Au_2Al start to grow simultaneously [110] while

TABLE 6.4: COMPARISON BETWEEN W-B AND EHF MODELS. Binary systems for which the EHF model correctly predicts the first phase and the W-B model does not. The $\Delta H'$ values have been calculated at the concentration of the liquidus minimum of the binary system. For systems where the liquidus minimum coincides with the melting point of one of the elemental compounds, an arbitrary effective concentration of 98 at.% of the element with the lowest melting point is taken. The phases for which the $\Delta H'$ values are underlined are those, which have been found experimentally to form first. The number of atoms per unit cell are given in brackets behind each phase.

System	Congru-ency	Composition	$\Delta H°$ kJ(mol.at.)$^{-1}$	$\Delta H'$ kJ(mol.at.)$^{-1}$	EHF	W-B	Observed Phases	Ref
Liquidus Minimum	=	$Al_{0.220}Au_{0.780}$						
Al_2Au (8)	C	$Al_{0.667}Au_{0.333}$	−31.4	−10.36				
AlAu (8)	NC	$Al_{0.500}Au_{0.500}$	−37.2	−16.37				
$AlAu_2$ (12)	C	$Al_{0.333}Au_{0.667}$	−30.1	−19.88	$AlAu_2$		$AlAu_2$	[110]
Al_2Au_5 (-)	NC	$Al_{0.286}Au_{0.714}$	−26.4	−20.31	Al_2Au_5		Al_2Au_5	[109–112]
$AlAu_4$ (20)	NC	$Al_{0.200}Au_{0.800}$	−18.6	−18.14		$AlAu_4$		
Liquidus Minimum	=	$Al_{0.991}Fe_{0.009}$						
$AlFe_3$ (16)	NC	$Al_{0.250}Fe_{0.750}$	−22	−0.26				
Al_2Fe (18)	NC	$Al_{0.667}Fe_{0.333}$	−25	−0.68	Al_2Fe			
Al_5Fe_2 (-)	C	$Al_{0.714}Fe_{0.286}$	−22	−0.69	Al_5Fe_2		Al_5Fe_2	[124]
Al_3Fe (102)	NC	$Al_{0.750}Fe_{0.250}$	−19	−0.68	Al_3Fe	Al_3Fe		
Al_6Fe (28)	M	$Al_{0.857}Fe_{0.143}$	−11	−0.69	Al_6Fe		Al_6Fe	[125]
Liquidus Minimum	=	$Al_{0.950}Gd_{0.050}$						
$AlGd_2$ (12 or 32)	NC	$Al_{0.333}Gd_{0.667}$	−49	−3.68				
Al_2Gd_3 (20)	NC	$Al_{0.400}Gd_{0.600}$	−58	−4.83				
AlGd (2 or 16)	NC	$Al_{0.500}Gd_{0.500}$	−68	−6.80				
Al_2Gd (24)	C	$Al_{0.667}Gd_{0.333}$	−65	−9.75				
Al_3Gd (8)	NC	$Al_{0.750}Gd_{0.250}$	−54	−10.80	Al_3Gd	Al_3Gd		
Al_4Gd (20)	NC/M	$Al_{0.800}Gd_{0.200}$	−44	−11.00	Al_4Gd		Al_4Gd	[126]
Liquidus Minimum	=	$Au_{0.980}V^{\dagger}_{0.020}$						
AuV_3 (4)	NC	$Au_{0.250}V_{0.750}$	−20.0	−0.53				
Au_2V (12)	NC	$Au_{0.667}V_{0.333}$	−22.5	−1.35	Au_2V		Au_2V	[157]
Au_4V (10)	NC	$Au_{0.800}V_{0.200}$	−13.7	−1.37	Au_4V	Au_4V		
Liquidus Minimum	=	$Au_{0.020}Zn^{\dagger}_{0.980}$						
$AuZn_8$ (2)	NC	$Au_{0.111}Zn_{0.889}$	−8.5	−1.53	$AuZn_8$	$AuZn_8$		
Au_2Zn_9 (-)	NC	$Au_{0.182}Zn_{0.818}$	−14.0	−1.54	Au_2Zn_9			
$AuZn_3$ (32)	NC	$Au_{0.250}Zn_{0.750}$	−19.0	−1.52	$AuZn_3$		$AuZn_3$	[152]
Au_4Zn_9 (-)	C	$Au_{0.308}Zn_{0.692}$	−22.7	−1.47	Au_4Zn_9			
Au_4Zn_5 (-)	NC	$Au_{0.444}Zn_{0.556}$	−27.6	−1.24				
AuZn (2)	C	$Au_{0.500}Zn_{0.500}$	−27.7	−1.11				
Au_5Zn_3 (16)	NC	$Au_{0.625}Zn_{0.375}$	−24.1	−0.77				
Au_3Zn (32)	NC	$Au_{0.750}Zn_{0.250}$	−16.8	−0.45				
Au_4Zn (-)	NC	$Au_{0.800}Zn_{0.200}$	−13.4	−0.34				
Liquidus Minimum	=	$Pt_{0.330}Ti_{0.670}$						
$PtTi_3$ (8)	C	$Pt_{0.250}Ti_{0.750}$	−69.8	−62.35		$PtTi_3$		
PtTi (4)	C	$Pt_{0.500}Ti_{0.500}$	−111.5	−73.59	PtTi		PtTi	[107]
Pt_5Ti_3 (32)	C	$Pt_{0.625}Ti_{0.375}$	−101.8	−53.75				
Pt_3Ti (16)	NC	$Pt_{0.750}Ti_{0.250}$	−80.0	−35.20				
Pt_4Ti (-)	C	$Pt_{0.800}Ti_{0.200}$	−58.7	−24.21				
Pt_8Ti (18)	NC	$Pt_{0.889}Ti_{0.111}$	−32.3	−11.99				

† Denotes binary systems where the lowest-temperature eutectic is not the liquidus minimum.

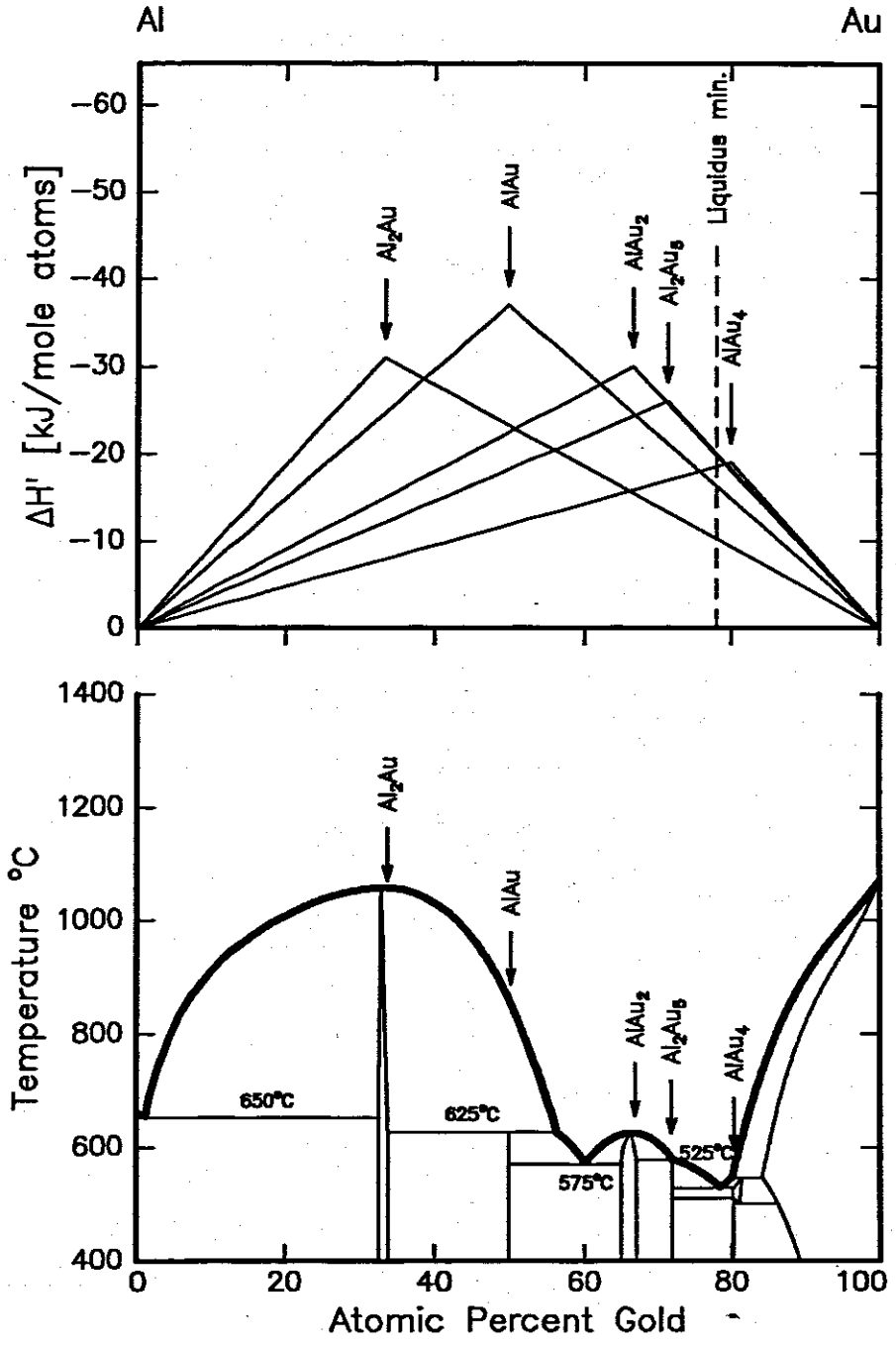

FIGURE 6.6: An effective heat of formation diagram for the Au-Al binary system. The diagram shows that at the concentration of the lowest eutectic effective heats of formation of the phases Au_2Al and Au_5Al_2 are the most negative and are close to each other. These are indeed experimentally found first phases. The W-B model predicts Au_4Al, which has never been found to form first.

others have found only Au_5Al_2 to be the first phase to form [109, 111, 112]. When using the EHF model to predict first phase formation we see that there is from a thermodynamic-kinetic point of view hardly any difference between Au_5Al_2 and Au_2Al formation (see EHF diagram in **Fig. 6.6** and **Table 6.4**). At the composition of the lowest eutectic ($Au_{0.780}Al_{0.220}$) the $\Delta H'$ value for Au_5Al_2 is -20.31 kJ(mol.at.)$^{-1}$ and -19.88 kJ(mol.at.)$^{-1}$ for Au_2Al (see **Table 6.4**). This difference is negligible and differences in experimental conditions could thus favour formation of one or the other. This is confirmed by experimental results [109–112]. The formation of both Au_5Al_2 and Au_2Al as found by Campisano *et al.* [110] is probably due to small variations in the effective concentrations laterally along the growth interface due to, for instance, impurities. If conditions are exactly identical along the entire growth interface, formation of only one phase would be expected. The first phase nucleated in metal-metal thin-film reactions according to the W-B rule is the phase immediately adjacent to the low-temperature eutectic in the binary phase diagram. If we look at the Au-Al binary phase diagram (bottom, **Fig. 6.6**) we see that the predicted first phase according to this rule is Au_4Al. Not only does the EHF model correctly predict that formation of Au_4Al is not favoured ($\Delta H' = -18.14$) compared to Au_5Al_2 ($\Delta H' = -20.31$), but it also gives a quantitative explanation for the experimental finding of either Au_5Al_2 [109, 111, 112] or both Au_5Al_2 and Au_2Al [110]. The W-B model predicts Au_4Al which has never been found as a first phase.

The liquidus minimum in the Pt-Ti system is not well defined (see **Fig. 6.7**, top) with two minima within approximately 10°C of one another at 16 and 33 at.% Pt.

If we compare the predictions of the EHF to those of the W-B rules for these values of the liquidus minima it is obvious that the W-B predicts $PtTi_3$ for both cases. This is not the experimentally observed first phase. At a liquidus minimum lying of 33 at.% Pt the EHF model correctly predicts first phase formation of PtTi (see **Table 6.4**). Only by taking the concentration at the reaction interface into account can these results be explained.

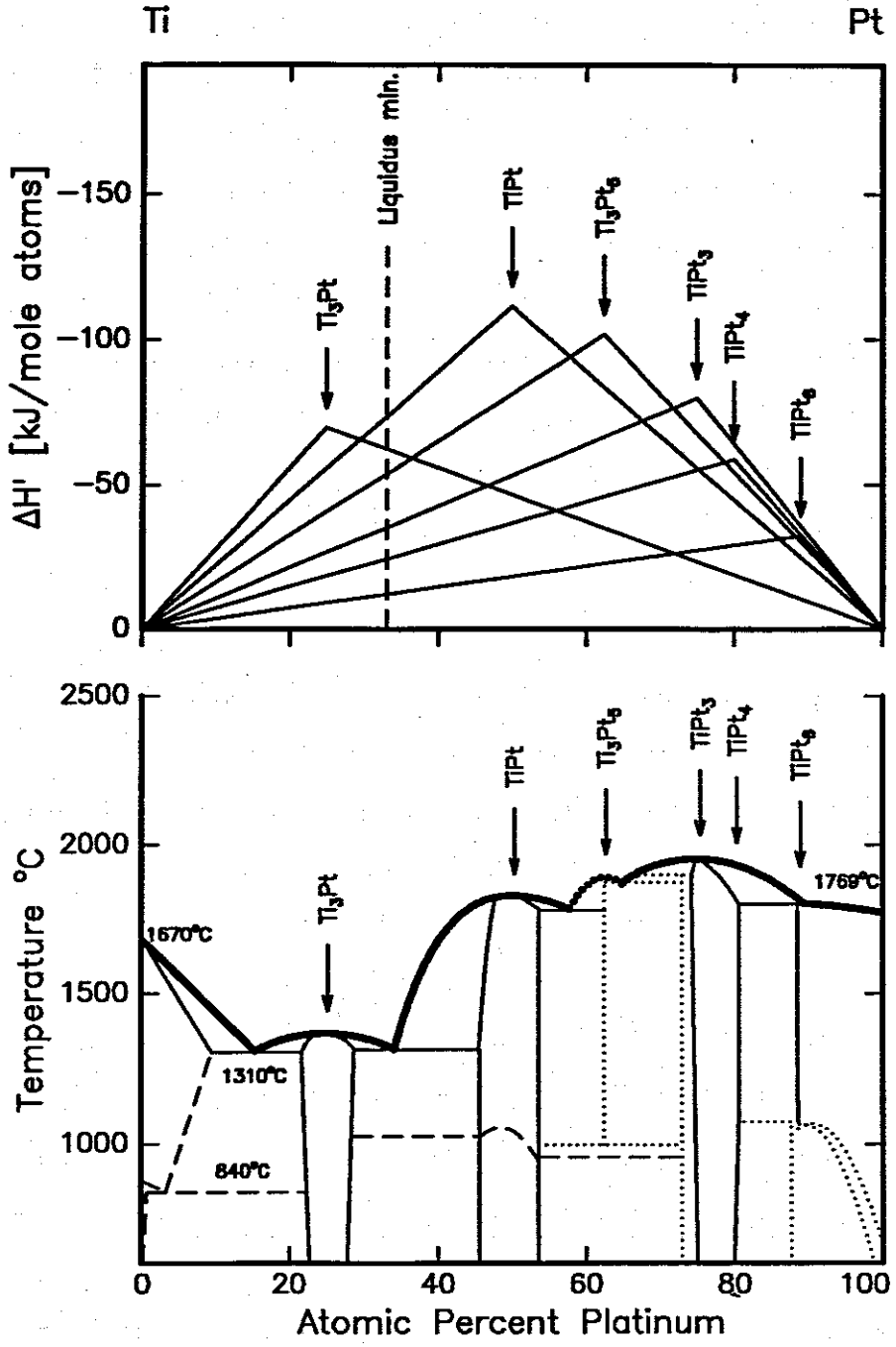

FIGURE 6.7: There is uncertainty as regards the liquidus minimum of the Pt-Ti system. If it is taken to be at 33 atomic % Pt the EHF model correctly predicts PtTi as the first phase. The W-B model always predicts $PtTi_3$ regardless which liquidus minimum is chosen.

To illustrate the differences between the EHF model and the W-B model even more clearly, hypothetical liquidus minima have been chosen at 55 atomic % Ti, 30 atomic % Ti, 15 atomic % Ti as well as at 5 atomic % Ti in the Pt-Ti system. **Table 6.5** shows results that would be obtained if both models are used in this hypothetical situation. If the liquidus minimum was at 55 atomic % Ti these two models would agree. At 30 atomic % Ti the EHF model would predict Pt_5Ti_3, but the W-B model would give Pt_3Ti as a first phase (a phase which is nearer to a hypothetical liquidus minimum in composition). For a liquidus minimum situated at 15 atomic % Ti the EHF model would predict two phases, namely Pt_3Ti and Pt_4Ti, showing that thermodynamically there is not much to choose from between the two phases (see **Fig. 6.8**).

The models would completely disagree the W-B model would predict a phase nearest in composition to the hypothetical liquidus minimum at 15 atomic % Ti, namely Pt_3Ti. At 5 atomic % Ti the models would agree in predicting Pt_8Ti as a first phase. The EHF model would, however, in addition also predict Pt_4Ti and Pt_3Ti. Not just one phase nearer in composition to the liquidus minimum as is the case with the W-B model. It is known that in some systems up to three phases have been found experimentally to form first (e.g. Pd-Al system).

6.7.4 Comparison of the Statistical model to the EHF model

Both models use thermodynamic quantities to make predictions about phase formation. The EHF model uses atomic concentration of reacting species at the liquidus minimum of a binary system as well as heats of formation to make its predictions. On the other hand the statistical model uses probabilities of atoms to meet in the correct ratio to form a phase. As in the EHF model, these probabilities are calculated at the liquidus minimum of a binary system. The stability of phases against breaking into constituent parts is estimated in the statistical model using activation energies of diffusion and in cases where covalent bonds are involved also activation energies of rotation. When these activation energies are not available, the model predicts phases using only meeting probabilities.

TABLE 6.5: COMPARISON BETWEEN W-B AND EHF MODELS. Prediction of first phase formation in the Pt-Ti system; according to the Walser-Bené and Effective Heat of Formation model for different hypothetical values of the liquidus minimum.

System	Composition	$\Delta H'$ kJ(mol.at.)$^{-1}$	EHF Model	W-B Model
Liquidus Minimum	$Pt_{0.160}Ti_{0.840}$			
$PtTi_3$		−44.67	$PtTi_3$	$PtTi_3$
PtTi		−35.68		
Pt_5Ti_3		−26.06		
Pt_3Ti		−15.61		
Pt_4Ti		−11.74		
Pt_8Ti		−5.81		
Liquidus Minimum	$Pt_{0.330}Ti_{0.670}$			
$PtTi_3$		−62.35		$PtTi_3$
PtTi		−73.59	PtTi	
Pt_5Ti_3		−53.75		
Pt_3Ti		−32.20		
Pt_4Ti		−24.21		
Pt_8Ti		−11.99		
Liquidus Minimum	$Pt_{0.450}Ti_{0.550}$			
$PtTi_3$		−51.19		
PtTi		−100.35	PtTi	PtTi
Pt_5Ti_3		−73.30		
Pt_3Ti		−43.90		
Pt_4Ti		−33.02		
Pt_8Ti		−16.35		
Liquidus Minimum	$Pt_{0.700}Ti_{0.300}$			
$PtTi_3$		−27.92		
PtTi		−66.90		
Pt_5Ti_3		−81.44	Pt_5Ti_3	
Pt_3Ti		−68.29		Pt_3Ti
Pt_4Ti		−51.36		
Pt_8Ti		−25.43		
Liquidus Minimum	$Pt_{0.850}Ti_{0.150}$			
$PtTi_3$		−13.96		
PtTi		−33.45		
Pt_5Ti_3		−40.72		
Pt_3Ti		−43.90	Pt_3Ti	
Pt_4Ti		−43.35	Pt_4Ti	
Pt_8Ti		−30.88		Pt_8Ti
Liquidus Minimum	$Pt_{0.950}Ti_{0.050}$			
$PtTi_3$		−4.65		
PtTi		−11.15		
Pt_5Ti_3		−13.57		
Pt_3Ti		−14.63	Pt_3Ti	
Pt_4Ti		−14.43	Pt_4Ti	
Pt_8Ti		−14.55	Pt_8Ti	Pt_8Ti

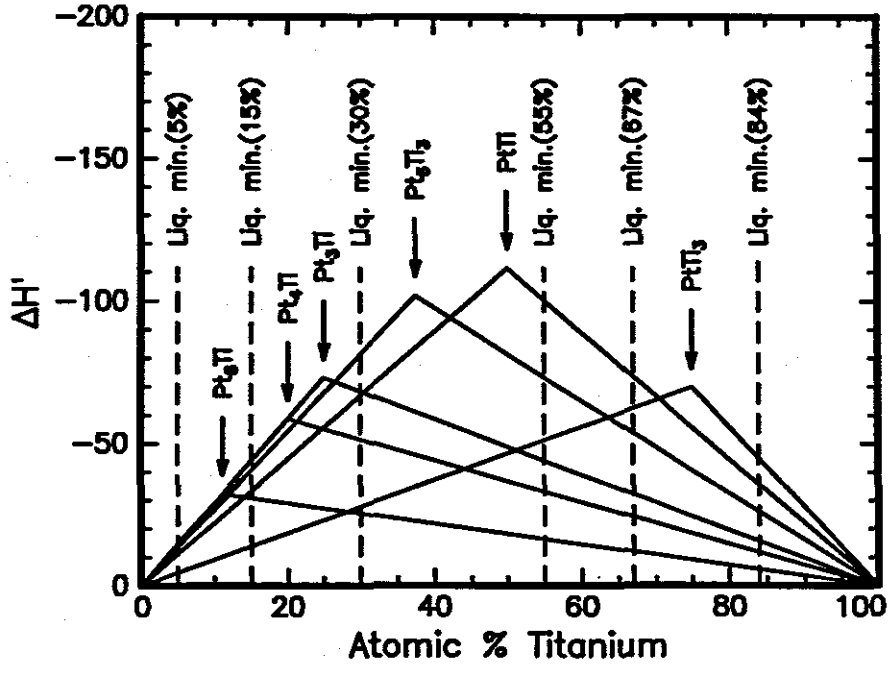

FIGURE 6.8: A graph showing hypothetical liquidus minima in the Pt-Ti system.

If only meeting probabilities are used, the Statistical model will agree completely with the Walser-Bene model. Under this condition, as far as phase predictions are concerned a comparison of the Statistical model to the EHF model will be exactly similar to the comparison of the Walser-Bene model to the EHF model.

There are striking similarities between the EHF model and the Statistical model. Meeting probabilities which are vertically normalised (i.e. normalised such that they add to unity at all atomic % B) can be used to calculate that fraction of heat produced during phase formation. These *fractional heats* are very similar to effective heats of formation as given by the EHF model.

$$f = \text{fractional heats} = P_{A_pB_q}\Delta H^\circ \tag{6.68}$$

where it is understood that meeting probabilities are vertically normalised and trivial cases of atoms of element A meeting atoms of A (or those of B meeting B) are taken into account. To find fractional heats, heats of formation are multiplied by the meeting probability normalised vertically (this is described fully in chapter 5). The heat of formation for the phase Nb_2Al is -25kJ/mole.at. The meeting probability for this phase at 40 at. % is 0.51, (see **Fig. 5.9**) therefore a fractional heat of 12.75kJ/mole.at. is obtained. **Table 6.6** lists and compares these predictions between the two models for four systems chosen at random.

The predicted first phase according to the statistical model in the Ni-Si system is NiSi with a fractional heat of -9.3kJ(mol.at.)$^{-1}$ as it is the congruent phase with the most negative fractional heat. This is not the only observed first phase. The other observed first phase is Ni_2Si. The difference between the fractional heats of these congruent phases is less than 10%. The EHF model also predicts correctly both observed first phases. In the Pd-Sn system the statistical model predicts $PdSn_4$ as the first phase. This is the experimentaly observed first phase. The phase with the next largest fractional heat is $PdSn_3$. The difference between its fractional heat and that of the first phase is 61%, and it is therefore not expected to be found together with the first phase. In the Pt-Ti system the phase $PtTi_3$ is predicted by the statistical model as a first phase. It has however never been found to occur first.

TABLE 6.6: Fractional heats produced during solid state interaction according to the Statistical model. Predicted phases are shown for both models. For the statistical model predicted phases are the ones with the largest fractional heats at the liquidus minimum of each binary system.

System	Congruency	Composition	f-heats kJ(mol.at.)$^{-1}$	$\Delta H'$ kJ(mol.at.)$^{-1}$	EHF	Stat.	Observed Phases	Ref
Liquidus Minimum	=	$Al_{0.220}Au_{0.780}$						
Al_2Au (8)	C	$Al_{0.667}Au_{0.333}$	−0.24	−10.36				
AlAu (8)	NC	$Al_{0.500}Au_{0.500}$	−2.22	−16.37				
$AlAu_2$ (12)	C	$Al_{0.333}Au_{0.667}$	−6.47	−19.88	$AlAu_2$		$AlAu_2$	[110]
Al_2Au_5 (-)	NC	$Al_{0.286}Au_{0.714}$	−7.02	−20.31	Al_2Au_5	Al_2Au_5	Al_2Au_5	[109–112]
$AlAu_4$ (20)	NC	$Al_{0.200}Au_{0.800}$	−5.97	−18.14				
Liquidus Minimum	=	$Ni_{0.535}Si_{0.465}$						
Ni_3Si (4)	NC	$Ni_{0.750}Si_{0.250}$	−4.4	−26.54				
Ni_5Si_2 (43)	C	$Ni_{0.714}Si_{0.286}$	−6.1	−31.68				
Ni_2Si (6/12)	C	$Ni_{0.667}Si_{0.333}$	−8.4	−37.64	Ni_2Si		Ni_2Si	[18, 41–43, 45–49, 178]
Ni_3Si_2 (80)	NC	$Ni_{0.600}Si_{0.400}$	−9.7	−40.30				
NiSi (8)	C	$Ni_{0.500}Si_{0.500}$	−9.3	−39.43	NiSi	NiSi	NiSi	[179–182]
$NiSi_2$ (12)	NC	$Ni_{0.333}Si_{0.667}$	−3.6	−20.44				
Liquidus Minimum	=	$Pd_{0.020}Sn_{0.980}$						
$PdSn_4$ (20)	NC	$Pd_{0.200}Sn_{0.800}$	−1.1	−3.03	$PdSn_4$	$PdSn_4$	$PdSn_4$	[105]
$PdSn_3$ (32)	NC	$Pd_{0.250}Sn_{0.750}$	−0.43	−3.04	$PdSn_3$			
$PdSn_2$ (24)	NC	$Pd_{0.333}Sn_{0.667}$	−0.070	−3.02	$PdSn_2$			
PdSn (8)	NC	$Pd_{0.500}Sn_{0.500}$	-8.1×10^{-4}	−2.73				
Pd_3Sn_2 (6)	NC	$Pd_{0.600}Sn_{0.400}$	-3.2×10^{-5}	−2.32				
Pd_2Sn (12)	NC	$Pd_{0.667}Sn_{0.333}$	-2.9×10^{-6}	−1.95				
Pd_3Sn (4)	NC	$Pd_{0.750}Sn_{0.250}$	-1.1×10^{-7}	−1.42				
Liquidus Minimum	=	$Pt_{0.330}Ti_{0.670}$						
$PtTi_3$ (8)	C	$Pt_{0.250}Ti_{0.750}$	−33.2	−62.35		$PtTi_3$		
PtTi (4)	C	$Pt_{0.500}Ti_{0.500}$	−32.7	−73.59	PtTi		PtTi	[107]
Pt_5Ti_3 (32)	C	$Pt_{0.625}Ti_{0.375}$	−11.8	−53.75				
Pt_3Ti (16)	NC	$Pt_{0.750}Ti_{0.250}$	−2.3	−35.20				
Pt_4Ti (-)	C	$Pt_{0.800}Ti_{0.200}$	−0.8	−24.21				
Pt_8Ti (18)	NC	$Pt_{0.889}Ti_{0.111}$	−0.1	−11.99				

The phase PtTi is the one that has been found experimentally to occur first. The difference between the fractional heats of $PtTi_3$ and PtTi is (as can be seen from the table) only 1.5%. It is therefore not surprising that PtTi is found as a first phase. It is however difficult to explain why $PtTi_3$ is not found as a first phase. The EHF model correctly predicts only PtTi as a first phase. Using this model it is possible to explain why $PtTi_3$ is not found as a first phase. The difference between the effective heat of the phase PtTi and that of $PtTi_3$ is more than 15%. This is large.

6.8 Summary and conclusion

There are many models that have been formulated to explain phase formation phenomena in thin solid films. None of them agree completely with the experimental measurements. The very first model, that of Walser and Bene, though only empirical in nature is a good attempt at predicting phase formation. It identifies important parameters like atomic concentration at the eutectic of the binary system and notes the role of congruency during phase formation in metal-silicon systems. This makes the Walser-Bene model to be reasonably successful. The Walser-Bene model is not as successful as the EHF model in predicting first phase formation.

The Gosele and Tu kinetic model is well formulated. It gives a good description as to why all phases are found in bulk (*bulk case*) couples and why not all of them are found simultaneously in thin film couples (*thin-film case*). The cases of diffusion-controlled growth as contrasted to interface controlled growth are well explained and used to show why at times grown layer thicknesses are proportional to time while at other times they are proportional to the square root of time. The model is based on the existence of interfacial reaction barriers. The existence of these barriers is however questionable. This is a weakness in the model. The model also fails to predict the first phase and its prediction of phase sequence is at best flimsy. Its equations are unwieldy and difficult to handle. It fails badly to identify important parameters in phase formation.

The Zhang and Ivey kinetic plot model is badly formulated. A quick glance

at the two expressions

$$X_i^i = \frac{n_d}{n^* + (\frac{m_i}{n_i})n^*} \tag{6.69}$$

and

$$Q = \frac{X_i^i}{(X_i^N)^{n_i}(X_i^M)^{m_i}} \tag{6.70}$$

where n_d is the number of defects and other symbols have their usual meaning, shows that if one puts $n_d = 0$ then Q=0. Zhang and Ivey go on to take a logarithm of Q in subsequent expressions ! It may of course be argued that no crystal is perfect, but one can subdivide it such that the sections one is dealing with are perfect crystals (or simply it is locally perfect on the atomic scale), and then one has the same problem as before, a logarithm of zero. This is mathematically wrong, unless we are mistaken (something we doubt). The model also fails to identify important parameters which play a major role in phase formation. The model is also very restrictive in its use. Major diffusers must be known and it deals only with silicides.

The EHF model defines an effective heat of formation $\Delta H'$, which is concentration dependent and has a linear dependency on the concentration of the limiting element at the growth interface. In this way the model combines thermodynamics and kinetics. Unlike the Walser and Bené rules [2, 4] which are rather empirical, the EHF model makes direct use of thermodynamic data. Both models do however make use of the liquidus minimum as a measure of the concentrations of the elements which interact at the growth interface. The EHF model in effect gives a quantitative reason for the relatively large margin of success the Walser and Bené rules have in predicting first phase formation.

In this work a comparison between the two models show that four categories of systems are found.

1. Of the **84** comparable systems there are **50** listed in **Table 6.2** where both models predict the same first phase found experimentally.

2. Though the W-B model has merit in first phase prediction it does not match the EHF model in its ability to combine thermodynamics and kinetics. This enables the EHF model to show when the situation at a growing interface is

such that a slight variation in experimental parameters may lead to more than one first phase. **Table 6.3** lists the **13** systems where both predict the correct experimentally found first phase, but the EHF model shows that there are, from a thermodynamic point of view, phases which are just as likely to form. Indeed, in **5** of these systems (Al-Pd, Al-V, Au-Pb, Au-Sn and Ni-Si) there is more than one experimentally observed first phase.

3. There are also **6** cases where the W-B model fails completely to predict the first phase and the EHF correctly predicts the thermodynamic-kinetic situation. These are listed in **Table 6.4.**

4. In the remaining **15** systems both the W-B and EHF models have difficulty in predicting the correct first phase. The reasons for this have been discussed in greater detail in ref. **[8]** and a short summary will only be given here. In **8** cases the liquidus minimum is not well-defined (Au-Cd, Au-Cu, Cr-Pt, Cu-Ti, Cu-Zr, Gd-Si, Ge-Pd and Ti-Si), in **3** cases non-congruent phases are formed first (Ge-Zr, Mn-Si and Si-Zr), in **2** cases metastable phases not indicated on the phase diagrams are found and the remaining **2** cases can be explained by nucleation difficulties (Pt-Al) and impurity effects (Pd-Ti).

Although many models and rules have been formulated for predicting compound phase formation during solid state interaction in thin-film binary systems **[2–6]**, it was only after the Effective Heat of Formation (EHF) model was proposed **[11,12,95,96]** that thermodynamic data such as heats of formation could be directly used to predict first phase formation and subsequent phase formation sequence. Several authors have been unsuccessful in trying to use the heats of formation of compounds to predict first phase formation and phase formation sequence **[109, 183–186]**. The reason for this failure is due to the fact that the concentration of the reactants at the growth interface was not taken into account. Since phase formation at the growth interface is a dynamic non-equilibrium process, the "excess" atoms should be looked upon as being available for formation of the next increment of the compound at the moving interface. Many factors such as impurities, diffusing

species, diffusivity, kinetics, temperature etc., could affect the concentration, but apparently the overriding factor is the liquidus minimum of the binary phase diagram. This is the reason why the Walser and Bené rules show good agreement with experiment.

The EHF model only states that formation of the compound phase with the most negative effective heat of formation $\Delta H'$ at a particular effective concentration, will lead to the biggest change in free energy. Such a compound phase may have a barrier to nucleation which may prevent its formation at the moving growth interface. Factors that may affect nucleation include the number of atoms per unit cell, crystal structure, temperature, congruency and directionality of bonding.

The first phase that is observed is sometimes dependent on the measurement technique which is used as phase formation is much more sensitive to impurities at the beginning stages of growth, where impurities at the interface can effect the effective concentrations, thereby affecting which phase might start to form. It is therefore understandable that very sensitive techniques (good depth resolution, eg. cross-sectional TEM with SAD) will reveal different initial phases than less-sensitive techniques such as RBS and X-ray diffraction, for example. Since the EHF model requires one to think in terms of the interaction concentrations, such effects can be accommodated. On the other hand the Walser and Bené rules have difficulty in explaining these results.

The EHF model, unlike the Walser and Bené rules, can also handle phase decomposition or phase formation when the metal is in contact with one of its compound phases, or when two or more compound phases are in contact with each other. Mixing at the interface(s) will always be controlled by the lowest temperature eutectic of the system, even if the eutectic composition does not lie between the compositions of the interacting phases. A general rule has been formulated [8], which can be applied to first phase formation, phase formation sequence and phase decomposition, which states:

> *'Phases will react with each other to form a phase with a composition lying between that of the interacting phases, whose effective heat of for-*

mation, calculated at the concentration closest to that of the liquidus minimum within this composition range, is the most negative.'

The EHF model is applicable not only to thin film systems but also to lateral and bulk diffusion couples. The transition from thin-film growth to bulk is understood by the shifting of the effective concentration at the reaction interface during diffusion-limited growth, until the phase reaches a critical thickness where the effective concentration is in a regime where the EHF of another phase is more negative. In this way phase formation of another phase can start to take place long before one of the original interacting phases are used up. The effect of impurities on phase formation can be explained by the EHF model. It has been shown how either Ni_2Si, NiSi or $NiSi_2$ can be the first phase to form, depending on experimental conditions [187].

It can be stated categorically that no model for prediction of first phase formation or phase formation sequence can be successful if it does not include concentration. The EHF model defines an effective heat of formation $\Delta H'$ which is concentration dependent and has a linear dependency on the concentration of the limiting element. The model actually in this way combines thermodynamics and kinetics. Unlike the Walser and Bené rules [2, 4], which are rather empirical, the effective heat of formation rule makes direct use of thermodynamic data. It in effect gives a quantitative reason for the relatively large margin of success of the Walser and Bené rules.

CHAPTER 7

Summary and Conclusion

There is a general lack of understanding as to what leads to specific compound phases nucleating at interfaces during solid-state interaction. There have been several articles dealing with this problem mainly due to the role thin films play in integrated circuit technology. In the field of micro-elelectronics they provide ohmic or rectifying contacts to silicon or germanium devices, barriers to interdiffusion, unreactive and stable overlayers, interconnects, etc. Many questions however still remain concerning the initial stage of the interfacial phase formation and the temperature range as well as sequence in which the binary compounds are formed at the interface during processing.

Phase characterisation of samples was done by means of Rutherford Backscattering Spectrometry (RBS) and X-ray Diffraction (XRD). These techniques are described in chapter 2. Chapter 3 deals with germanium-metal systems and first phase formation for the Ti-Ge, Pd-Ge, Zr-Ge, Fe-Ge, and Cr-Ge systems are summarized in **Table 7.1**. The experimentally found first phase in the Ti-Ge system is Ti_6Ge_5, while the phase predicted by the EHF model is Ti_5Ge_3. Other groups have found Ti_5Ge_3 as a first phase [78]. It is however interesting to note that some researchers have also reported first phase formation of Ti_6Ge_5 which is a non-congruent phase with an effective heat of formation more negative than the most negative congruent phase. Pd_2Ge was found experimentally to be the first phase in the Pd-Ge system.

TABLE 7.1: Observed first phase formation and predicted first phase in metal-germanium systems using the Effective Heat of Formation model. In the case of the Fe-Ge and Cr-Ge systems, a value for ΔH^{trans} of 15kJ/mole.at. was used. In other cases the usual value 25kJ/mole.at. was used. The predicted phases are the congruent phases with the most negative $\Delta H'$ at the concentration of the liquidus minimum. The underlined phases are the phases found to form first in this investigation.

System	Liq. Min. (at.% Ge)	Predicted Phases	Observed Phases	Ref.	Congruency	$\Delta H°$ kJ(mol.at.)$^{-1}$	$\Delta H'$ kJ(mol.at.)$^{-1}$
Cr	85		Cr_5Ge_3	[90]	NC	−19.1	−4.6
			$\underline{Cr_{11}Ge_8}$	This work	NC	−19.4	−5.0
		CrGe [a]			NC	−18.4	−5.5
Fe	75	FeGe	$\underline{FeGe}$	This work	NC	−14.0	−7.0
Ni	67	Ni_5Ge_3	$\underline{Ni_5Ge_3}$ [c]	This work [80,78,91]	C	−22.3	−11.77
Pd	64 [d]	PdGe	—		C	−51.4	−37.01
			$\underline{Pd_2Ge}$	This work [80,78,83]	C	−45.3	−24.45
Ti	89	Ti_5Ge_3	Ti_5Ge_3	[78]	C	−59.4	−10.45
			$\underline{Ti_6Ge_5}$	This work [84]	NC	−64.3	−12.98
Zr	98.7	Zr_5Ge_3	—		C	−83.0	−1.73
			$\underline{ZrGe}$ [e]	This work	NC	−95.8	−2.49

[a] Effective heats of formation of CrGe, $Cr_{11}Ge_8$ and $Cr_{11}Ge_{19}$ within 10% of each other. [b] No congruent phases. [c] This phase was previously referred to as Ni_2Ge [80,78,91]. [d] Liquidus Minimum not well defined as there are two lowest eutectics (30 at.% Pd and 81 at.% Pd) which have approximately the same temperatures (725°C and 760°C). [e] Only slightly non-congruent ($\Delta T = 20$°C).

Several other groups also find Pd_2Ge as the first phase to form [78, 80, 83]. From the Pd-Ge phase diagram it is clear that the liquidus minimum and therefore the effective concentration is not well defined in this system due to two eutectics at 36 and 81 at. % Pd (see **Fig. 8** of [8]) which have similar temperatures. The more Pd-rich eutectic (760°C) tends to favour Pd_2Ge formation. The EHF model predicts PdGe as a first phase and the apparent discrepancy between experiment and theory can be expected because of the reasons given. In the Zr-Ge system, ZrGe was observed experimentally to form first (see **Table 7.1**). The EHF model however predicts Zr_5Ge_3 first phase formation. ZrGe is probably formed because it is only slightly non-congruent, with a small temperature difference ΔT ($\simeq$20°C) between the peritectic point and the liquidus curve. Furthermore, it has a more negative $\Delta H'$ value than the predicted Zr_5Ge_3 phase.

In the Fe-Ge system FeGe was found experimentally to be the first phase, whic agrees with the EHF model prediction. Of the three forms of FeGe, FeGe(c) was found at the lowest temperature, followed by FeGe(m) at a higher temperature and finally by FeGe(h). That FeGe(c) should occur at lower temperatures agrees with Pearson [87]. The order of occurence of the other two phases in our results is however reversed. This is not surprising because ours is a thin film case whereas Pearson's is a bulk case. The phase sequence found experimentally for the case Fe<Ge, was FeGe followed by $FeGe_2$. For the case Fe$\simeq$Ge, it was FeGe followed by $FeGe_2$. The phase sequence found for the case Fe>Ge was FeGe followed by Fe_5Ge_3.

In the Cr-Ge system $Cr_{11}Ge_8$ was found experimentally to be the first phase. The EHF model predicts CrGe as a first phase. Lundberg *et.al.* found Cr_5Ge_3 as a first phase [90]. It is however interesting to note that according to the EHF model there is thermodynamically not much to choose between CrGe and $Cr_{11}Ge_8$. Effective heats of formation of these phases calculated at the liquidus minimum of this system are within 10% of each other (see **Table 7.1**) and thermodynamic quantities are usually not known with accuracies of better than 10%. The phase sequence observed experimentally for Cr-Ge for the case Cr<Ge was $Cr_{11}Ge_8$, CrGe and then $Cr_{11}Ge_{19}$. For the case Cr>Ge, the sequence found was $Cr_{11}Ge_8$, Cr_5Ge_3

followed by Cr_3Ge.

In chapter 4 nucleation and phase skipping in germanides was investigated. In some germanide systems, e.g. Co-Ge and Pt-Ge, it has been found that non-congruent phases nucleate first, when their effective heats of formation are much more negative than those of congruent phases in the same binary system [8]. Notable exceptions are Hf-Ge, Ni-Ge and Ti-Ge [8]. Because of this it was decided to anneal Ni-Ge and Ti-Ge samples at low temperatures, thereby lowering the velocity of the growth interface, thus giving all phases more time to nucleate. A phase with a more negative $\Delta H'$ could be expected to form first, even if it is non-congruent. In the Ni-Ge system NiGe has the most negative effective heat of formation. After annealing samples belonging to this system for 2 days at about 115°C Ni_5Ge_3 was found to be the first phase. This is the phase also found when annealing at higher temperatures for shorter periods [78,80,91]. In the Ti-Ge system annealing at lower temperatures did not result in any observable phase formation. Only after annealing at about 400°C for 1 day could any interaction be detected. This temperature was found to be close to the normal temperature (450°C) at which phases begin to form in this system (see chapter 3). The phase found to form first is Ti_6Ge_5, which is the same phase found for short anneals. Reducing the anneal temperature will however not only result in a lower velocity for the interface, but will also reduce mobility of the atoms. If the decrease in atomic mobility is less than the decrease in interfacial velocity then the phases we sought to nucleate (NiGe and $TiGe_2$) would have had a larger likelihood to form at lower temperatures. The fact that these phases do not form first at lower temperatures suggests that atomic mobilities in the two systems (Ni-Ge and Ti-Ge) are reduced at a higher rate (or at least at the same rate) than is the reduction of interfacial velocities.

In chapter 5 the question of phase formation has for the first time been approached from a statistical point of view. This model uses elementary probability theory to predict phases that form in a thin film reaction couple. In a thin film couple made up of element A and B, it is assumed that all atomic % concentrations are present at the interface. The activation energy for diffusion of element A is

expected to vary with concentration(also that of B). If activation energies are averaged over both A and B, and a curve of atomic concentration versus average activation energy is drawn, a minimum of this curve should correspond roughly to the liquidus minimum of the binary system A-B. Note that the activation energy is proportional to the melting point of a solid [97]. Atoms of A are mixing with those of B at the interface. The rate at which this intermixing takes place should be greater at that concentration which correspond to the liquidus minimum of the binary system. In this concentration more attempts are being made by atoms to form compound phases as compared to other concentrations where the intermixing rate is lower.

Atoms must meet in a specific ratio in order to form a particular compound phase A_sB_q. This meeting probability is calculated for all compound phases as given by the equilibrium phase diagram, for all atomic concentrations. In order to calculate the meeting probability, the same cluster of atoms, of both A and B must be chosen for each phase. This allows a fair comparison to be made between different phases. To form a compound phase A_sB_q for example, of chosen cluster $s+q=N$, the probability of meeting in the correct ratio to form this phase is,

$$P^m_{A_sB_q}(x) = c(100-x)^s x^q \tag{7.1}$$

where c is a normalisation constant. There are two ways of normalising this probability function, an equal area normalisation,

$$\int_0^{100} P^m_{A_sB_q}(x)dx = 1 \tag{7.2}$$

or a vertical normalisation, where it is required that meeting probabilities of all compound phases in a given system should add up to unity at each and every atomic concentration,x. The equal areas normalisation can be used where only a comparison of meeting probabilities is required. It however has no justification on physical grounds. It is much easier to perform mathematically. The vertical normalisation has merit because it means that for a given number of atoms, making up a specific concentration x, considering all compound phases, the probability that a compound phase(s) will form is unity(a certainty). This however need to be

qualified. Meeting of atoms in atomic ratios that do not coincide with correct ratios for phase formation is neglected. It is assumed that atoms do not remain in these configurations for any appreciable length of time. If physical variables(temperature, strain, stress, etc) preclude the formation of a particular compound phase, then this compound phase should not be included in the normalisation. As a result of this, the probability of meeting to form a phase depends on other phases that may form, i.e. are there other channels that may take up atoms, anchor them thus removing them from intermixing ?

A compound phase will not be detected as having formed if it breaks up into it's constituent parts as soon as it forms. The probability that the i-th atom of compound phase A_sB_q will change position inside a solid of A_sB_q is

$$exp(-\frac{E_i}{kT}) \tag{7.3}$$

The probability that it will remain in position is

$$1 - exp(-\frac{E_i}{kT}) \tag{7.4}$$

where E_i is the activation energy of diffusion of the i-th atom in the chosen cluster making up A_sB_q. If clusters of N atoms are being considered, then the probability that in a single cluster no atom leaves the cluster through diffusion is,

$$\prod_{i=1}^{N}[1 - exp(-\frac{E_i}{kT})] \tag{7.5}$$

Because of a lack of values of activation energies for each atom in a lattice site, one may use average activation energies, of A diffusing in A_sB_q and of B diffusing in A_sB_q. For the case of metals interacting with other metals, the probability that a compound phase A_sB_q will form at any atomic concentration of B, x is:

$$P^{ms}_{phase}(x) = P^{m}_{A_sB_q}(x)\prod_{i=1}^{s,q}[1 - exp(-\frac{E^A_i}{kT})][1 - exp(-\frac{E^B_i}{kT})] \tag{7.6}$$

The first compound phase predicted is the one with the largest probability of forming at a value of x corresponding to the liquidus minimum of the binary system, A-B. For cases where interaction is between metal atoms and atoms which form directional bonds (Ge or Si), the probability that spatial electronic configurations have proper

orientations must be taken into account. Let the probability that one atom of either Si or Ge has proper orientation be $P_{orient.}$. Then the probability that all atoms in a cluster have proper orientation is

$$P^{tot.}_{orient.} = (P_{orient.})^q \tag{7.7}$$

Metal atoms do not count. Let the activation energy for rotation of the i-th atom of B (Ge or Si) in a cluster be E^r_i. The probability that once bonded the atoms won't break free from their bonds through rotations is:

$$\prod_{i=1}^{q}[1 - exp(-\frac{E^r_i}{kT})] \tag{7.8}$$

The probability that a compound phase A_sB_q will form, where B is covalent (either Si or Ge) will form is:

$$P^{msr}_{phase}(x) = P^{m}_{A_sB_q}(x)P^{tot.}_{orient.}(x)\prod_{i=1}^{N,q}[1 - exp(-\frac{E_i}{kT})][1 - exp(-\frac{E^r_i}{kT})] \tag{7.9}$$

It is interesting to note that the form of the equation describing probability for linear motion is similar to that of rotational motion. The probabilities also depend on temperature and concentration, something which is quite desirable.

Because activation energies (both of diffusion and rotation) are not readily available, phase prediction has been based only on probabilities of atoms to meet in the correct ratio to form phases. In spite of this lack of experimental data correct predictions could be made in 68 metal-metal, Si-metal and Ge-metal systems.

The model may be further developed to explain solid-state kinetics. If x_b is assumed to be the amount of the mixture at the growth interface, and $x_{A_sB_q}$ is the amount of compound phase that is forming, then the rate at which it is forming is:

$$\frac{dx_{A_sB_q}}{dt} = a_{A_sB_q}x_b - b_{A_sB_q}x_{A_sB_q} \tag{7.10}$$

Similar equations may be written for other phases, and are then solved simultaneously. The value of the rate constants a and b is

$$a_{A_sB_q} = \nu_o P^{mv}_{A_sB_q}(x)P^{tot.}_{orient.}(x)\prod_{i=1}^{N,q}[1 - exp(-\frac{E_i}{kT})][1 - exp(-\frac{E^r_i}{kT})] \tag{7.11}$$

$$b_{A_sB_q} = \nu_o \prod_{i=1}^{N,q} [exp(-\frac{E_i}{kT})][exp(-\frac{E_i^r}{kT})] \tag{7.12}$$

It is seen from these rate equations that they will describe a non-equilibrium situation only if the concentration x is changing with time. This change in concentration is governed by the diffusion equation.

Fractional heats are given by

$$f = \text{meeting probability X heat of formation} \tag{7.13}$$

In chapter 6 the most important models that deal with phase formation are discussed and compared to each other.

Walser-Bene Model

This model [2] was initially formulated to predict first phase nucleation in silicon-metal planar interfaces. In these systems it is well known that non-congruently melting phases are skipped during phase formation. This was attributed to a higher energy barrier associated with a large rearrangement in short range order required to go from a liquidlike short range order to a crystalline short range order for non-congruent states contrasted to the much smaller change in short range order associated with conguently melting states. The phase nucleated should therefore be congruent and closest in atomic concentration to the initial eutectic composition. In a case where two congruently melting phases existed on both sides of the eutectic, the most stable compound, as indicated by the higher melting temperature, is expected to form first. The following rule was therefore formulated for predicting phases in silicon-transition metal planar interfaces [2].

" The first compound nucleated in planar binary reaction couples is the most stable congruently melting compound adjacent to the lowest-temperature eutectic on the bulk equilibrium phase diagram."

The rule was later generalised as a metal-covalent rule for phase selection. It also applies to transition-metal metal germanium systems. It was extended to metal-metal systems by relaxing the requirement that the first phase that forms needs to be congruently melting [2]:

"The first phase nucleated in metal-metal thin-film reactions is the phase immediately adjacent to the low temperature eutectic in the binary phase diagram"

The Walser-Bene rule is succesful in predicting first phase formation many Si-metal, Ge-metal and metal-metal systems. The basic understanding of the problem (e.g. why first phases form first) of phase formation at interfaces is however lacking.

Gosele and Tu Model

The Gosele and Tu model [5] describes phase formation using principally the phenomenon of diffusion. The model is well formulated mathematically. Conditions under which thicknesses grow linearly with time and those when they are not linear with time are discussed by defining critical thicknesses. The model contrasts very well the bulk case (where all phases are usually grow simultaneously) and the thin film case (where phases usually grow one at a time). The model introduces the concept of interfacial reaction barriers, but these are not well explained. It is difficult to understand the physics behind interfacial reaction barriers. It is said that they lead to the absence of some phases in thin films. Why do they not lead to the absence of the same phases in bulk couples? The model cannot predict first phases and phase sequence. It neglects to make use of parameters that have been shown to play a significant role in phase formation. These are atomic concentration corresponding to the liquidus minimum and congruency [2, 11] as well as heats of formation [11, 12, 8, 95, 96].

Zhang and Ivey Model

In this model [172] solid state reactions in thin film metal-silicon diffusion couples are described. The model is restricted only to cases where one of the species (called a moving reactant) diffuses faster than the other species considered. Relative Maximum Release rates (RMR rates) and Semiquantitative Reaction Process plots (SRP plots) are used to predict phases (see Chapter 6 and Zhang and Ivey [172]). This model is too restricted in its use. No good reasons are given why it cannot be used on metal-metal systems. It is not explained how to use the model if a major diffuser in one phase is not a major diffuser in another phase of the same system. The model does not take into account important parameters like atomic concentration

at the growth interface, congruency and heats of formation [8, 11, 12, 95, 96].

Effective Heat of Formation Model

The EHF model was formulated for predicting compound phase formation in metal-metal, Ge-metal and Si-metal thin film reaction couples. It uses thermodynamic data such as heats of formation to predict first phase formation and subsequent phase formation sequence. The model combines heats of formation and concentration of the reactants at the growth interface. Heats of formation are calculated as a function of concentration according to the formula: [11–15]

$$\Delta H' = \Delta H^{\circ} \times \left(\frac{\textit{effective concentration limiting element}}{\textit{compound concentration limiting element}} \right) \tag{7.14}$$

where $\Delta H'$ and ΔH° are expressed in kJ per mole of atoms. To form a phase the two elements must be available in a specific ratio (the effective concentration) and when forming a specific compound the elements will be consumed in the compound ratio. If the effective concentration of a specific element is less than it's concentration in the compound to be formed, then that element is the limiting element (e.g. if the effective concentration is 20% of element A, at the growth interface, and the compound to be formed is AB in an A-B system, then A is the limiting element. The compound concentration of A is 50%). It is assumed in this model that a single phase grows at a time on the interface. The excess atoms are available for the next phase formation in cases where effective concentration does not match the compound concentration. Factors such as impurities, diffusing species, kinetics, temperature, etc. may affect the effective concentration. The effective concentration is assumed to be at that concentration which corresponds to the liquidus minimum of the binary system as determined from the phase diagram. The reason for this choice is that mobility is proportional to the melting point of a solid. In systems where the minimum of the liquidus coincides with the melting point of one of the elements, an arbitrary effective concentration of 98 atomic % of the element with the lowest melting point is taken.

According to this model, that compound phase whose formation will lead to the most negative effective heat of formation ΔH', should be the one that forms. Such a compound may however have a barrier to nucleation which may prevent its for-

mation. Factors influencing nucleation are given in an excellent review by Pretorius *et. al.*[8]: Metal-metal phases are known to nucleate readily whereas non-congruent phases of the silicides and the germanides have difficulty in nucleating. The larger the temperature difference ΔT between the peritectic point and the liquidus for non-congruent phases of the silicides, the more difficult it will be for a phase to nucleate. Germanium lies somewhere between the metals and the silicides, therefore its behaviour should reflect this fact [8]. There are cases in germanides where non-congruent phases are known to form first (e.g. CoGe, Pt_3Ge_2, Ti_6Ge_5, FeGe, etc.). The rule for predicting first phase formation, which combines the effects of atomic concentration, heats of formation and factors related to the nucleation of phases in silicides is [8] :

"The first compound to form during metal-silicon interaction is the congruent phase with the most negative effective heat of formation ($\Delta H'$) at the concentration of the liquidus minimum of the binary system"

If the system does not have congruent phases then the phase with the phase with the most negative effective heat of formation should form first. For metal-metal systems the model drops the restriction of non-congruency [8] :

"The first compound phase to form during metal-metal interaction is the phase with the most negative effective heat of formation ($\Delta H'$) at the concentration of the liquidus minimum of the binary system"

Germanides occupy a position between that of the silicides and metal-metal systems. The model does not drop the restriction of congruency entirely in germanides. The rule for first phase formation in germanides is [8]:

"The first phase nucleated in metal-germanide interaction is either the congruent phase or the non-congruent phase with the most negative effective heat of formation at the liquidus minimum of the binary system."

The EHF model is very successful in predicting first phases. It could predict first phases correctly in more than 90 phases at the last count.

The EHF model can also predict phase formation sequence in binary thin film couples. If in a system A-B, the thickness of film A is much more than that of

B, after first phase formation, the effective concentration will move towards the direction of the thicker film,viz. A. The second phase will therefore be next A-rich phase. Rules governing nucleation apply. The second phase will grow untill the first phase is completely consumed. This process continues with subsequent phases richer in the unreacted element forming untill the most A-rich phase is formed. If B>>A, then the opposite will happen, i.e. phases which are ever richer in B will form after the first phase, until the most B-rich phase is formed. A rule for phase formation sequence for silicides according to the EHF model is [8] :

"After first phase silicide formation,in Si-metal and Ge-metal systems the effective concentration moves in the direction of the remaining element and the next phase to form at the growth interface is the next phase richer in the unreacted element, which has the smallest temperature difference ΔT between the peritectic(or peritectoid) point and the liquidus. (ΔT= 0 for congruent phases)."

For metal-metal systems the rule for phase formation sequence is: *"After first phase formation in metal-metal binary systems, the next phase to form at the interface between the compound phase and the remaining element is the next phase richer in the unreacted element, which has the most negative effective heat of formation."*

It is possible to have two compound phases in contact with each other, or a compound phase in contact with an unreacted element (Si, Ge or metal). A general rule that can be applied for predicting first phase formation, phase formation sequence as well as phase decomposition may be stated as follows:

"Phases will react with each other to form a phase with a composition lying between that of the interacting phases, whose effective heat of formation, calculated at the concentration closest to that of the liquidus minimum within this composition range, is the most negative."

Fractional heats defined in the Statistical model bear close resemblance to effective heats of formation of the EHF model. Comparison between the Statistical model and the EHF model is similar to the comparison between the Walser-Bene model and the EHF model. When the EHF model was compared to the Walser-Bene model four categories of systems were found.

- In 53 of the 84 binary systems on which the models were tested, complete agreement was found between experimental observations and model predictions. This is due to the fact that both models make use of the liquidus minimum and if the heats of formation of compounds close to the liquidus minimum are approximately the same the compound with the most negative EHF value will be the one closest to the liquidus minimum.

- In the second category both models predict the correct experimentally found first phase, but the EHF model shows that there are, from a thermodynamic point of view, several phases which are just as likely to form. In 6 (Al-Pd, Al-V, Au-Pb, Au-Sn, Ni-Si and Si-Ti) of these 14 systems there is more than one experimentally observed first phase.

- In this category there are 7 cases (Al-Au, Al-Cd, Al-Fe, Al-Gd, Au-V, Au-Zn and Pt-Ti) where the Walser-Bene model fails completely to predict the first phase, while the EHF model correctly predicts first phase formation.

- The last category contains 15 systems where both the Walser-Bene and the EHF model have difficulty in predicting the correct first phase. In five of these cases the liquidus minimum (and therefore the effective concentration at the growth interface) is not well defined and the models therefore cannot be expected to predict phase formation correctly. The remaining cases can be explained in terms of nucleation difficulties.

The EHF model only states that formation of the compound phase with the most negative effective heat of formation at a particular effective concentration, will lead to the biggest change in free energy. Such a compound may have a barrier to nucleation which may prevent its formation at the moving growth interface. Factors that may affect nucleation include the number of atoms per unit cell, crystal structure, temperature, congruency and directionality of bonds in the phase being formed.

The EHF model unlike the Walser-Bene rules, can also handle phase decomposition or phase formation when the metal is in contact with one of its compound

phases, or when two or more phases are in contact with each other. Mixing at the interface will always be controlled by the liquidus minimum of the system, even if it does not lie between the compositions of the interacting phases.

The EHF model unlike the W-B rules is applicable not only to thin film systems but also to lateral and bulk diffusion couples. The transition from thin-film growth to bulk is understood in terms of a change of the effective concentration at the reaction interface during diffusion-limited growth. When the growing phase reaches a critical thickness where the effective concentration has decreased to such an extent that the efective heat of formation of another phase is more negative, formation of such a phase can start to take place long before one of the original interacting phases are used up. The effect of impurities and diffusion barriers on phase formation can also be explained by the EHF model by considering their effect on the effective concentration.

The EHF model defines an effective heat of formation which is concentration dependant and has a linear dependancy on the concentration of the limiting element. The model in this way combines thermodynamics and kinetics for predicting phase formation at interfaces.

APPENDIX

*Definitions of some of the symbols used in the statistical model**.

- $P^{m}_{A_sB_q}$ meeting probabilities which are normalised such that the area under their curves add up to unity.

- $P^{mv}_{A_sB_q}$ meeting probabilities which are such that when added for all phases of a given binary system, sum up to unity at any atomic %.

- $P^{stab}_{A_sB_q}$ probability that none of the atoms belonging to a cluster will break free from the cluster or stability probability.

- P^{ms}_{phase} probability to form a compound phase based on both meeting probability and stability probability.

- P_{orient} probability that a single covalent atom is properly orientated for bonding.

- $P^{tot.}_{orient}$ probability that all covalent atoms in a cluster are properly orientated for bonding.

- P^{msr}_{phase} probability to form a phase based on meeting probability, stability probability and rotational probability.

- P^{mvr}_{phase} probability to form a phase based on stability and rotations only (does not include stability against diffusional and rotational cluster breaking agitations).

**Symbols other than those used in the statistical model are described in original papers where these models are derived.*

References

[1] C.R.M. Grovenor, *Micro Electronic Materials* (Adam-Hilger, Briston, Philadelphia, 1989).

[2] R.M. Walser and R.W. Bené, Appl. Phys. Lett. **28**, 624 (1976).

[3] B.Y. Tsaur, S.S. Lau, J.W. Mayer, and M.-A. Nicolet, Appl. Phys. Lett. **38**, 922 (1981).

[4] R.W. Bené, Appl. Phys. Lett. **41**, 529 (1982).

[5] U. Gösele and K.N. Tu, J. Appl. Phys. **53**, 3252 (1982).

[6] M. Ronay, Appl. Phys. Lett. **42**, 577 (1983).

[7] O. Kubaschewski and C.B. Alcock, *Metallurgical Thermochemistry* (Pergamon Press, Oxford, 1979), p. 268.

[8] R. Pretorius, T.K. Marais, and C.C. Theron, Mater. Sci. Eng. R **10**, 1 (1993).

[9] A.R. Miedema, P.F. de Châtel, and F.R. de Boer, Physica **100B**, 1 (1980).

[10] G.V. Kidson, J. Nucl. Mater. **3**, 21 (1961).

[11] R. Pretorius, MRS Proc. **25**, 15 (1984).

[12] R. Pretorius, Vacuum **41**, 1038 (1990).

[13] R. Pretorius, R. de Reus, A.M. Vredenberg, and F.W. Saris, Materials Letters **9**, 494 (1990).

[14] R. Pretorius, R. de Reus, A.M. Vredenberg, and F.W. Saris, J. Appl. Phys. **70**, 3636 (1991).

[15] R. Pretorius, T.K. Marais, and C.C Theron, Materials Science Reports (1993).

[16] T.B. Massalski, *Binary Alloy Phase Diagrams*, 1st ed. (American Society for Metals, Metal Park, OH, 1986).

[17] J.F. Morar and M. Wittmer, Phys. Rev. B **37**, 2618 (1988).

[18] G. Ottaviani, Thin Solid Films **140**, 3 (1986).

[19] G.J. Van Gurp and C. Langereis, J. Appl. Phys. **46**, 4301 (1975).

[20] S.S. Lau, J.W. Mayer, and K.N. Tu, J. Appl. Phys. **49**, 4005 (1978).

[21] G.J. van Gurp, D. Sigurd, and W.F. van der Weg, Appl. Phys. Lett. **29**, 159 (1976).

[22] G.J. van Gurp, W.F. van der Weg, and D. Sigurd, J. Appl. Phys. **49**, 4011 (1978).

[23] A.P. Botha and R. Pretorius, Thin Solid Films **93**, 127 (1982).

[24] E.G. Colgan, B.Y. Tsaur, and J.W. Mayer, Appl. Phys. Lett. **37**, 938 (1980).

[25] C.J. Bedeker, S. Kritzinger, and J.C. Lombaard, Thin Solid Films **141**, 117 (1986).

[26] A. Martinez, D. Esteve, A. Guivarc'h, P. Auvray, P. Henoc, and G. Pelous, Solid State Electron **23**, 55 (1980).

[27] A.P. Botha, R. Pretorius, and S. Kritzinger, Appl. Phys. Lett. **40**, 412 (1982).

[28] J.E. Baglin, F.M. d'Heurle, and C.S. Petersson, Appl. Phys. Lett. **36**, 594 (1980).

[29] S.S. Lau, J.S. -Y. Feng, J.O. Olowolafe, and M.-A. Nicolet, Thin Solid Films **25**, 415 (1975).

[30] R.D. Thompson, B.Y. Tsaur, and K.N. Tu, Appl. Phys. Lett. **38**, 535 (1981).

[31] K.N. Tu, R.D. Thompson, and B.Y. Tsaur, Appl. Phys. Lett. **38**, 626 (1981).

[32] H. Kato and Y. Nakamura, Thin Solid Films **34**, 135 (1976).

[33] J.F. Ziegler, J.W. Mayer, and C.J. Kircher, J. Appl. Phys. **44**, 3851 (1973).

[34] W.K. Chu, S.S. Lau, J.W. Mayer, H. Muller, and K.N. Tu, Thin Solid Films **25**, 393 (1975).

[35] L. Zhang and D.G. Ivey, J. Mater. Res. **6**, 1518 (1991).

[36] K.E. Sundstrom, S. Petersson, and P.A. Tove, Phys. Solid State **A20**, 653 (1973).

[37] O.B. Loopstra, W.G. Sloof, Th. H. de Keijser, E.J. Mittemeijer, S. Radelaar, A.E.T. Kuiper, and R.A.M. Wolters, J. Appl. Phys. **63**, 4960 (1988).

[38] J. Baglin, F. d'Heurle, and S. Petersson, Appl. Phys. Lett. **33**, 289 (1978).

[39] J.E.E. Baglin, F.M. d'Heurle, W.N. Hammer, and S. Petersson, Nucl. Instr. and Meth. **168**, 491 (1980).

[40] P.R. Gage and R.W. Bartlett, Trans. Metall. Soc. AIME **232**, 832 (1965).

[41] K.N. Tu, G. Ottaviani, U. Gösele, and H. Föll, J. Appl. Phys. **54**, 758 (1983).

[42] K.N. Tu, W.K. Chu, and J.W. Mayer, Thin Solid Films **25**, 403 (1975).

[43] J.O. Olowolafe, M.-A. Nicolet, and J.W. Mayer, Thin Solid Films **38**, 143 (1976).

[44] D.M. Scott and M.-A. Nicolet, Nucl. Instr. and Meth. **182/183**, 655 (1981).

[45] D.J. Coe and E.H. Rhoderick, J. Phys. D: Appl. Phys. **9**, 965 (1976).

[46] W.K. Chu, H. Krautle, J.W. Mayer, H. Muller, M.- A. Nicolet, and K.N. Tu, Appl. Phys. Lett. **25**, 454 (1974).

[47] R. Pretorius, C.L. Ramiller, S.S. Lau, and M.-A. Nicolet, Appl. Phys. Lett. **30**, 501 (1977).

[48] K.N. Tu, E.I. Alessandrini, W.K. Chu, H. Kraütle, and J.W. Mayer, Jap. J. Appl. Phys. **Suppl. 2**, 669 (1974).

[49] V. Koos and H.G. Neumann, Phys. Stat. Solidi **A29**, K115 (1975).

[50] F.M. d'Heurle, Thin Solid Films **151**, 41 (1987).

[51] R. Pretorius, C.L. Ramiller, and M.-A. Nicolet, Nucl. Instr. and Meth. **149**, 629 (1978).

[52] G.A. Hutchins and A. Shepala, Thin Solid Films **18**, 343 (1973).

[53] K.N. Tu, Appl. Phys. Lett. **27**, 221 (1975).

[54] A. Hiraki, M.-A Nicolet, and J.W. Mayer, Appl. Phys. Lett. **18**, 178 (1971).

[55] H. Muta and D. Shinoda, J. Appl. Phys. **43**, 2913 (1972).

[56] W.K. Chu (private communication).

[57] R.W. Bower and J.W. Mayer, Appl. Phys. Lett. **20**, 359 (1972).

[58] J.S. Maa, C.J. Lin, and J.H. Lin, Thin Solid Films **64**, 439 (1979).

[59] R. Beyers and R. Sinclair, J. Appl. Phys. **57**, 5240 (1985).

[60] I.J.M.M. Raaijmakers, A.H. Reader, and P.H. Oosting, J. Appl. Phys. **63**, 2790 (1988).

[61] J.C. Hensel, J.M. Vandenberg, F.C. Unterwald, and A. Maury, Appl. Phys. Lett. **51**, 1100 (1987).

[62] A. Guldan, V. Schiller, A. Steffan, and P. Balk, Thin Solid Films **100**, 1 (1983).

[63] L.S. Hung, J. Gyulai, J.W. Mayer, S.S. Lau, and M.-A. Nicolet, J. Appl. Phys **54**, 5076 (1983).

[64] R. Butz, G.W. Rubloff, T.Y. Tan, and P.S. Ho, Phys. Rev. B **30**, 5421 (1984).

[65] D. Levy, J.P. Ponpon, A. Grob, J.J. Grob, and R. Stuck, Appl. Phys. A **38**, 23 (1985).

[66] K. Shenai, P.A. Piacente, N. Lewis, G.A. Smith, M.D. McConnell, and B.J. Baliga, J. Vac. Sci. Tecnol. B **6**, 1728 (1988).

[67] C. Queniset, R. Naslain, and P. Demoney, Surf. Interface Anal. **13**, 123 (1988).

[68] C.X. Dexin, H.B. Harrison, and G.K. Reeves, J. Appl. Phys. **63**, 2171 (1988).

[69] C.C. Hsu, Y.X. Wang, S.D. Yin, B.Q. Li, M.R. Ji, and J.X. Wu, J. Vac. Sci. Technol. A 5, 1402 (1987).

[70] S.P. Murarka and D.B. Fraser, J. Appl. Phys. 51, 342 (1980).

[71] C.A. Pico and M.G. Lagally, J. Appl. Phys. 64, 4957 (1988).

[72] R.J. Nemanich, R.T. Fulks, B.L. Stafford, and H.A. Vander Plas, J. Vac. Sci. Technol. A 3, 938 (1985).

[73] C.S. Wei, J. Van der Spiegel, and J. Santiago, J. Vac. Sci. Technol. A 3, 2259 (1985).

[74] P.A. Psaras, M. Eizenberg, and K.N. Tu, J. Appl. Phys. 56, 3439 (1984).

[75] J.A. Borders and J.N. Sweet, in *Applications of Ion Beams to Metals*, edited by S.T. Picraux, E.P. EerNisse, and F.L. Vook (Plenum Press, New York, 1974).

[76] J.J. Rosenberg, IEEE Trans. Electron Devices 30, 1602 (1983).

[77] J.C. Bean, in *Proceedings of the First International Symposium on Si Molecular Beam Epitaxy*, edited by J.C. Bean (Electrochemical Society, Pennington, NJ, 1985).

[78] E.D. Marshall, C.S. Wu, C.S. Pai, D.M. Scott, and S.S. Lau, MRS Proc. 47, 161 (1985).

[79] Y.F. Hsieh and L.J. Chen, J. Appl. Phys. 63, 1177 (1988).

[80] M. Wittmer, M.-A. Nicolet, and J.W. Mayer, Thin Solid Films 42, 51 (1977).

[81] Y.F. Hsieh, L.J. Chen, E.D. Marshall, and S.S. Lau, Appl. Phys. Lett. 51, 1588 (1987).

[82] S.Q. Hong, C.M. Comrie, S.W. Russell, and J.W. Mayer, J. Appl. Phys. 70, 3655 (1991).

[83] Y.F. Hsieh and L.J. Chen, Thin Solid Films 162, 295 (1988).

[84] O. Thomas, S. Delage, F.M. d'Heurle, and G. Scilla, Appl. Phys. Lett. 54, 228 (1989).

[85] M.G. Grimaldi, L. Wielunski, M.-A. Nicolet, and K.N. Tu, Thin Solid Films 81, 207 (1981).

[86] L.R. Doolittle, Nucl. Instr. and Meth. B 4, 344 (1985).

[87] P. Villars and L.D. Calvert, *Pearson's Handbook of Crystallographic Data for Intermetallic Phases* (American Society for Metals, Metal Park OH, 1989).

[88] W.G. Moffat, *The Handbook of Binary Phase Diagrams* (Genium Pubishing Corporation, New York, 1984) – updated as issued.

[89] G. Ottaviani, C. Canali, G. Ferrari, R. Ferrari, G. Majni, M. Prudenziati, and S.S. Lau, Thin Solid Films 47, 187 (1977).

[90] M. Ostling N. Lundberg and F.M. d'Heurle, Appl. Surf. Sc **53**, 126 (1991).

[91] Y.F. Hsieh, L.J. Chen, E.D. Marshall, and S.S. Lau, Thin Solid Films **162**, 287 (1988).

[92] *Electronic Thin Film Science for Electrical Engineers and Scientists* (Macmillan Publishing Company, New York, 1992).

[93] F.M. d'Heurle, J. Mater. Res. **3**, 167 (1988).

[94] R. Pretorius, C.C. Theron, T.K. Marais, and H.A. Ras, Materials Chemistry and Physics (accepted for publication - 1993).

[95] R. Pretorius, R. de Reus, A.M. Vredenberg, and F.W. Saris, Mater. Lett. **9**, 494 (1990).

[96] R. Pretorius, A.M. Vredenberg, F.W. Saris, and R. de Reus, J. Appl. Phys. **70**, 3636 (1991).

[97] A.M. Brown and M.F. Ashby, Acta Metallurgica **24**, 1088 (1980).

[98] V. Simić and Ž. Marinković, J. Less-Common Met. **95**, 259 (1983).

[99] K.N. Tu and R. Rosenberg, Jap. J. Appl. Phys. **Suppl. 2**, 633 (1974).

[100] Jian Li, J. Strane, S.W. Russell, S.T. Hong, J.W. Mayer, T.K. Marais, C.C. Theron, and R. Pretorius, J. Appl. Phys. **70**, 2810 (1991).

[101] K.N. Tu, Acta Met. **21**, 347 (1973).

[102] J.L. Liotard, D. Gupta, P.A. Psaras, and P.S. Ho, J. Appl. Phys. **57**, 1895 (1985).

[103] C. Apblett, D. Muira, M. Sullivan, and P.J. Ficalora, J. Appl. Phys. **71**, 4925 (1992).

[104] A.E. Gershinskii, A.A. Khoromenko, and E.I. Cherepov, Phys. Status Solidi **A31**, 61 (1975).

[105] K.N. Tu, Material Letters **1**, 6 (1982).

[106] J. Baglin, F. d'Heurle, and S. Zirinsky, J. Electrochem. Soc. **125**, 1854 (1978).

[107] T.C. Tisone and J. Drobek, J. Vac. Sci. Technol. **9**, 271 (1972).

[108] Y. Fujino, S. Yamaguchi, H. Naramoto, and K. Ozawa, Nucl. Instr. and Meth. **218**, 691 (1983).

[109] G. Majni, C. Nobili, G. Ottaviani, M. Costato, and E. Galli, J. Appl. Phys. **52**, 4047 (1981).

[110] S.U. Campisano, G. Foti, E. Rimini, S.S. Lau, and J.W. Mayer, Phil. Mag. **31**, 903 (1975).

[111] G. Majni, G. Ottaviani, and E. Galli, J. Crystal Growth **47**, 583 (1979).

[112] J.M. Vandenberg and R.A. Hamm, J. Vac. Sci. Technol. **19**, 156 (1981).

[113] J.K. Howard, J.F. White, and P.S. Ho, J. Appl. Phys. **49**, 4083 (1978).

[114] J.K. Howard, R.F. Lever, P.J. Smith, and P.S. Ho, J. Vac. Sci. Technol. **13**, 68 (1976).

[115] E.G. Colgan and J.W. Mayer, J. Mater. Res. **4**, 815 (1989).

[116] M.B. Chamberlain, J. Vac. Sci. Technol. **16**, 339 (1979).

[117] J.K. Howard, W.K. Chu, and R.F. Lever, in *Ion Beam Surface Layer Analysis*, edited by O. Meyer, G. Linker, and F. Kapeller (Plenum Press N.Y., 1976).

[118] H.T.G. Hentzell, R.D. Thompson, and K.N. Tu, J. Appl. Phys. **54**, 6923 (1983).

[119] A.E. Gershinskii, B.I. Fomin, E.E. Chorepov, and F.L. Edelman, Thin Solid Films **42**, 269 (1977).

[120] S.U. Campisano, E. Costanco, and F. Scaccianoce, Thin Solid Films **52**, 97 (1978).

[121] J.M. Vandenberg and R.A. Hamm, Thin Solid Films **97**, 313 (1982).

[122] K. Rajan and E.R. Wallach, J. Cryst. Growth **49**, 297 (1980).

[123] J.A. Rayne, M.P. Shearer, and C.L. Bauer, Thin Solid Films **65**, 381 (1980).

[124] S.R. Teixeira, F.L. Freire, and I.J.R. Baumvol, Appl. Phys. **A 53**, 481 (1989).

[125] A. Csanády, J.R. Gunter, P.B. Barna, and J. Mayer, Thin Solid Films **167**, 203 (1988).

[126] M. Eizenberg, R.D. Thompson, and K.N. Tu, J. Appl. Phys. **53**, 6891 (1982).

[127] H.C.W. Huang and M. Wittmer, MRS Proc. **25**, 157 (1984).

[128] R.F. Lever, J.K. Howard, W.K. Chu, and P.J. Smith, J. Vac. Sci. Technol. **14**, 158 (1977).

[129] M. Kitada and N. Shimizu, J. Mater. Sci. **19**, 1339 (1984).

[130] R.K. Ball and A.G. Todd, Thin Solid Films **149**, 269 (1987).

[131] K.R. Coffey, L.A. Clevenger, K. Barmak, D.A. Rudman, and C.V. Thompson, Appl. Phys. Letters **55**, 852 (1989).

[132] R. Bormann, H.U. Krebs, and A.O. Kent, in *Advances in Cryogenic Engineering*, edited by A.F. Clarke and R.P. Reed (Plenum Press, New York, 1986).

[133] Yoonsoon Im and Jr. J.W. Morris, J. Appl. Phys. **64**, 3487 (1988).

[134] K. Barmak, K.R. Coffey, D.A. Rudman, and S. Foner, J. Appl. Phys. **67**, 7313 (1990).

[135] J.M. Vandenberg, M. Hong, R.A. Hamm, and M. Gurvitch, J. Appl. Phys. **58**, 618 (1985).

[136] E.G. Colgan, M. Nastasi, and J.W. Mayer, J. Appl. Phys. **58**, 4125 (1985).

[137] J.E.E. Baglin and F.M. d'Heurle, in *Ion Beam Surface Layer Analysis*, edited by O. Meyer, G. Linker, and F. Kapeller (Plenum Press N.Y., 1976).

[138] U. Köster, P.S. Ho, and M. Ron, Thin Solid Films **67**, 35 (1980).

[139] E.G. Colgan, J. Appl. Phys. **62**, 2269 (1987).

[140] M. Nastasi, L.S. Hung, and J.W. Mayer, Appl. Phys. Lett. **43**, 831 (1983).

[141] E.G. Colgan, J. Appl. Phys. **62**, 1224 (1987).

[142] S.P. Murarka, I.A. Blech, and H.J. Levinstein, J. Appl. Phys. **47**, 5175 (1976).

[143] E. Ma and M.-A. Nicolet, Phys. Stat. Sol. **A110**, 509 (1988).

[144] X.A. Zhao, E. Ma, H.Y. Yang, and M.-A. Nicolet, Thin Solid Films **153**, 379 (1987).

[145] J.-W. Liaw, Y.-C. Liu, J.-S. Maa, W.-S. Hsu, W.-J. Shen, and S.K. Hsiung, Ts'ai Liao K'o Hsueh **12**, 36 (1980).

[146] K. Nakamura, S.S. Lau, M.-A. Nicolet, and J.W. Mayer, Appl. Phys. Lett. **28**, 277 (1976).

[147] M. Wittmer, F. LeGoues, and H.-C.W. Huang, J. Electrochem. Soc. **132**, 1450 (1985).

[148] J. Tardy and K.N. Tu, Phys. Rev. **B32**, 2070 (1985).

[149] T.G. Finstad, G. Salomonsen, N. Norman, and J.S. Johannessen, Thin Solid Films **114**, 271 (1984).

[150] I. Krafesik, J. Gyulai, C.J. Palmström, and J.W. Mayer, Appl. Phys. Lett. **43**, 1015 (1983).

[151] G.J. van Gurp, J.L.C. Daams, A. van Oostrom, L.J.M. Augustus, and Y. Tamminga, J. Appl. Phys. **50**, 6915 (1979).

[152] Ž. Marinković and V. Simić, J. Less-Common Met. **115**, 225 (1986).

[153] T.G. Finstad, T. Andreassen, and T. Olsen, Thin Solid Films **29**, 145 (1975).

[154] V. Simić and Ž. Marinković, Thin Solid Films **41**, 57 (1977).

[155] J. Bjøntegaard, L. Buene, T. Finstad, O. Lønsjø, and T. Olsen, Thin Solid Films **101**, 253 (1983).

[156] Y. Hasumi, J. Appl. Phys **58**, 3081 (1985).

[157] E.G. Colgan and J.W. Mayer, J. Mater. Res. **2**, 28 (1987).

[158] C. Weaver and L.C. Brown, Philos. Mag. 8, 1379 (1963).

[159] B. Hugsted, L. Buene, T. Finstad, O. Lønsjø, and T. Olsen, Thin Solid Films 98, 81 (1982).

[160] J.M. Vandenberg and R.A. Hamm, in *Proc. Symp. on Thin Film Interfaces and Interactions*, edited by J.E.E. Baglin and J.M. Poate (Electrochemical Society, Princeton, NJ, 1980).

[161] S. Nakahara, R.J. McCoy, L. Buene, and J.M. Vandenberg, Thin Solid Films 84, 185 (1981).

[162] L. Buene, H. Falkenberg-Arell, and J. Taftø, Thin Solid Films 65, 247 (1980).

[163] T.C. Tisone and S.S. Lau, J. Appl. Phys 45, 1667 (1974).

[164] C.A. Christou and H. Day, J. Appl. Phys. 44, 3386 (1973).

[165] J.M. Poate, P.A. Turner, and W.J. DeBonte, J. Appl. Phys. 46, 4275 (1975).

[166] J.A. Knapp and S.T. Picraux, Appl. Phys. Lett. 48, 466 (1986).

[167] H.C. Baxi and T.B. Massalski, Journal of Phase Equilibria 12, 349 (1991).

[168] T.K. Marais, E. Taylor, O.M. Ndwandwe, B. Spoelstra, and R. Pretorius, Nucl. Instr. and Meth. B 85, 183 (1994).

[169] M. Hansen and K. Anderko, *Constitution of Binary Alloys*, 2nd ed. (Genium Publishing Corporation, New York, 1986).

[170] L. Zhang and D.G. Ivey, J. Appl. Phys. 71, 4314 (1992).

[171] C.V Thompson, J. Mater. Res. 7, 367 (1992).

[172] L. Zhang and D.G. Ivey, Thin Solid Films 245, 234 (1994).

[173] O.B. Loopstra, W.G. Sloof, Th. H. De Keijser, E.J. Mittemeijer, S. Radelaar, A.E.T. Kuiper, and R.A.M. Wolters, J. Appl. Phys. 63, 4960 (1988).

[174] G.J. van Gurp and C. Langereis, J. Appl. Phys. 46, 4301 (1975).

[175] G.J. van Gurp, D. Sigurd, and W.F. van der Weg, Appl. Phys. Lett. 29, 159 (1976).

[176] G.J. van Gurp, W.F. van der Weg, and D. Sigurd, J. Appl. Phys. 49, 4011 (1978).

[177] E.G. Colgan, J. Appl. Phys. 62, 2269 (1987).

[178] D.M. Scott and M-A. Nicolet, Nucl. Instr. Meth. 182, 655 (1981).

[179] R. Mattheis and D. Hesse, Phys. Stat. Sol. (a) 109, 217 (1988).

[180] P.K. John, A.C. Rastogi, B.Y. Tong, and X.W. Wu, Can. J. Phys. 65, 1037 (1987).

[181] P.K. John, H. Frohlich, A.C. Rastogi, and B.Y. Tong, Thin Solid Films **164**, 481 (1988).

[182] A.C. Rastogi, P.K. John, and B.Y. Tong, Phys. Rev. B **37**, 8308 (1988).

[183] K.N. Tu, G. Ottaviani, R.D. Thompson, and J.W. Mayer, J. Appl. Phys. **53**, 4406 (1982).

[184] E.G. Colgan, J. Appl. Phys. **62**, 1224 (1987).

[185] R.W. Bené, J. Appl. Phys. **61**, 1826 (1987).

[186] J.W. Mayer and S.S. Lau, *Electronic Material Science: For Integrated Circuits in Si and GaAs* (Macmillan, New York, 1990).

[187] R. Pretorius, C.C. Theron, T.K. Marais, and H.A. Ras, Mater. Chem. Phys. **36**, 31 (1993).